University of Southampton

Development of a Dispenser Printer to Realise Electroluminescent Lamps on Fabrics

by

Marc de Vos

A thesis submitted for the degree of

Doctor of Philosophy

in the

Faculty of Physical Sciences and Engineering

School of Electronics and Computer Science

University of Southampton

United Kingdom

August 2016

Abstract

Dispenser printed electroluminescent (EL) lamps on fabric have been investigated and a functional dispenser printed prototype that outperforms the commercial equivalent is presented. The state of the art in dispenser printing and screen-printing is considered and existing patents and prototype devices reviewed. No examples of printed electroluminescent lamps on fabric were found therefore providing an opportunity for novel work to be produced.

A simulation model of the dispenser printer was developed, allowing the best performing dispense pressure for a defined ink to be found. An experimental method for identifying a suitable dispense pressure was also compared to the simulation. The results showed that the experimental method offered the same results more quickly, so an experimental approach was selected.

The ability to print complex shapes was developed, enhancing the usefulness of the technology for a commercial application. A requirement for maintaining a constant separation between the substrate and the dispenser nozzle was discovered and this capability was integrated to allow the printing of complex shapes in a continuous print mode. Many displacement sensors were reviewed and a selection were tested before the Keyence LK-G10 was selected. The results from the Keyence profiles were validated against a commercial profilometer and the University of Southampton systen was found to fail to measure the transparent conducting layer although it could measure the transparent interface which the other displacement sensors could not.

Phosphor and transparent conducting layers were investigated and optimised solutions for different use scenarios such as different lamp colours are identified. The route the dispenser nozzle takes to fill a defined area with ink was investigated. The results recommended the rectilinear pattern at 70% density as the best performer out of five infill patterns tested.

Novel dispenser printed EL lamps on fabric were demonstrated. The dispenser printed EL lamps were compared to University of Southampton screen-printed and commercial screen-printed EL lamps. The results showed the dispenser printed EL lamps outperformed the commercial lamps and had comparable performance to the University of Southampton screen-printed EL lamps.

Acknowledgements

I would like to express my sincere gratitude to my supervisors John Tudor and Russel Torah. Without their continuing support this project would not have been possible. I am also grateful to the EU FP7 CREATIF project for the funding I received during the past three years and the research facilities provided by the School of Electronics and Computer Science at the University of Southampton.

I would like to thank my parents for the support they have always given me and would like to dedicate this thesis to them.

Table of Contents

List of Figures

List of Tables

List of Abbreviations

EL	Electroluminescent
TFEL	Thin-film electroluminescent
TFACEL	Thin-film alternating current electroluminescent
LED	Light emitting diode
OLED	Organic light emitting diode
FDM	Fused deposition modelling
ITO	Indium tin oxide
PVDF	Polyvinylidene fluoride
GTP	Global Tungsten and Powders Corporation
PET	Polyethylene terephthalate
PDMS	Polydimethylsiloxane
QD	Quantum Dot
UoS	University of Southampton
PEDOT:PSS	Poly(3,4-ethylenedioxythiophene) polystyrene sulfonate

1. Introduction

1.1. Introduction

Dispenser printing is a new additive manufacturing process for smart fabrics that has a number of commercial applications due to its advantages over previously developed printing techniques such as inkjet or screen printing. The benefits of dispenser printing fall into three main categories:

- A dispenser printer has the ability to print a wide range of inks both in terms of ink viscosity and particle size within the ink. The user is able to select a suitable nozzle diameter to suit the ink, meaning viscosities in the range 1 mPa.s to 300 Pa.s can be printed. This capability provides an advantage over other direct write technologies, such as inkjet, that can only print ink with viscosities below 0.1Pa.s [1].
- The print design can be easily changed when dispenser printing as stencils, screens, or masks are not required. This capability is particularly appealing in prototyping applications where designs that were typically screen-printed can now be quickly tested and altered without waiting for screen production. As a rapid prototyping process, dispenser printing reduces production time as it is a direct write technology – meaning ink is only deposited in the areas required. Direct write technology also reduces environmental impact through reduced ink usage and, being non-contact, allows printing on complex geometries such as curved moulded plastic.
- The inks used in dispenser printing are compatible with industrial mass production print processes such as roll-to-roll or rotogravure printing. It is therefore known that the prototype will work if mass produced as the same inks can be used. This is an advantage over inkjet printing where the inks are not normally compatible with mass production printing techniques.

Electroluminescent (EL) lamps, while not a new technology, have seen a recent increase in interest due to their robust nature [2, 3]. They offer a low power, thin, and robust light source that can be entirely constructed using printable materials. Combining dispenser printing with EL lamps potentially offers the ability to print a range of light sources in varying colours and shapes. The work in this project is undertaken as part of the CREATIF project [4]. CREATIF is an EU funded Framework 7 project “providing the creative and cultural industries with state of the art printed smart fabrics and collaborative design software”[4].

The thesis starts with a review of relevant literature in Chapter 2 covering EL devices and a number of print processes. Chapter 3 investigates the best method to identify the print parameters; modelling and an experimental method are tested and compared. In Chapter 4 the development of dispenser hardware is then considered. The work covers additions such as a laser displacement sensor to automatically profile the substrate surface and new positioning stages plus controller to allow interpolated movements. Chapter 5 covers software improvements and control software development to investigate two different print deposit methods: droplet and continuous mode. Chapter 6 describes the electroluminescent devices that have been produced and assesses the improvements in quality as the dispenser printer has been improved over the course of the PhD. Overall conclusions are presented in Chapter 7.

1.2. Research Objectives

- Develop a method to quickly identify acceptable dispenser printing parameters for an ink.
- Develop the software and hardware of the dispenser printer to maintain a constant separation distance between the nozzle and substrate.
- Develop software to control the dispenser printer to print an EL lamp in any shape that may be required by a designer.
- Identify the best algorithm for the print head to follow when filling a continuous shape with ink.
- Dispenser print high quality EL lamps onto fabric with brightness equivalent to a commercial screen-printed EL lamp.

1.3. Statement of Novelty

- First dispenser printed EL lamps.

  This thesis demonstrates the first use of dispenser printing to fabricate EL lamps. Dispenser printing has previously only been demonstrated on devices with upto three layers, while an EL lamp has five or six layers representing a significantly greater challenge to print. In order to achieve this a number of improvements to the dispenser printing process have been made, these are discussed below. The difficulty was further increased by selecting fabric as the substrate.

- Development of Z-height tracking for the dispenser printer.

  A technology to maintain a separation distance between the dispenser nozzle and the substrate was developed. The process makes much larger prints possible as the errors in the flatness of the printing plate and moving stages can be taken into account and corrected for. This work is the first demonstration of this technology.

- Development of an optimised bus bar design.

  A novel optimised bus bar design has been developed, modelled using finite element analysis and tested using the dispenser printer. The design avoids a bus bar connection around the perimeter of the EL lamp allowing much smaller lamps to be printed as the emitting area is not covered by a bus bar connection. The design was demonstrated using a screen-printed EL watch display with very small EL lamps that would not have been possible before.

- Custom control software to continuously print complex shapes.

  Software was developed that is capable of interpreting CNC machine G-code and converting it to be suitable for use with a dispenser printer. The software controls the moving stages and also controls when the dispenser pneumatic controller is enabled.

- Evaluation of the effect of the infill pattern on print quality when continuously printing.

  Five infill patterns were tested on four commonly used shapes across three densities and the best compromise between coverage, surface roughness, layer thickness and print speed was selected. The development reduces the surface roughness of the printed layer allowing more complex devices with more layers to be dispenser printed.

1.4. Publications Arising From This Thesis

- R. Torah, K. Yang, Y. Wei, Y. Li, M. de Vos, S. Beeby, and J. Tudor. *Screen and inkjet printed electronics on fabrics – the next generation of E-textiles*. In *Plastic Electronics Conference.* 2013. Dresden, Germany (Conference).
- M. de Vos, R. Torah, S. Beeby and J. Tudor. *Functional Electronic Screen-printing – Electroluminescent Lamps on Fabric*. In *Eurosensors Conference.* 2014. Brescia, Italy (Conference).
- M. de Vos, R. Torah, and J. Tudor. *A Novel Pneumatic Dispenser Fabrication Technique for Digitally Printing Electroluminescent Lamps on Fabric*. In *Design, Test, Integration & Packaging of MEMS/MOEMS Conference*. 2015. Montpellier, France (Conference).
- M. de Vos, R. Torah, and J. Tudor. *The effect of infill patterns on the print quality of dispenser printed electronic ink*. In *Electronics Letters Journal*. 2015 (Letter).
- M. de Vos, R. Torah, and J. Tudor. *Dispenser Printed Electroluminescent Lamps on Textiles for Smart Fabric Applications.* In *Smart Materials and Structure Journal.* 2016 (Journal Paper).
- R. Torah, Y. Wei, Y. Li, K. Yang, M. de Vos, S. Beeby, and J. Tudor. *The development of Screen, Inkjet and Dispenser printing techniques for smart fabric applications*. In *CIMTEC 2016 – 7th Forum on New Materials Conference.* 2016. Perugia, Italy (Conference).
- M. de Vos, R. Torah, M. Glanc-Gostkiewicz, and J. Tudor. *A Complex Multilayer Screen-Printed Electroluminescent Watch Display on Fabric.* In *IEEE Journal of Display Technology*. 2016 (Journal Paper - Submitted).
- M. de Vos, R. Torah, and J. Tudor. *Optimum Infill Algorithms to Achieve a Uniformly Dispenser Printed Electronic Ink*. In *The International Journal of Advanced Manufacturing Technology*. 2016 (Journal Paper - Submitted).

2. Literature Review

2.1. Introduction

The emergence of devices that combine light emitting electronics with everyday fabric has seen increasing interest in recent years [5-7]. Fabric is appealing as a substrate as it has formed a fundamental part of our lives for hundreds of years. If electronics can be successfully used with fabrics, it offers the opportunity to fully integrate electronics into people's lives.

An important aspect of electronics is communicating information to a user and to fulfil this requirement light emitting displays are often used. A proposed solution to incorporate light emitting displays into smart fabrics utilises electroluminescent (EL) displays. EL lamps are visible in mobile phone keypads, watches, aeronautical and automotive instrumentation, and advertising panels [8].

Alternating current electroluminescence was first observed by George Destrau in 1936 [9]. The effect was found in ZnS powders meaning the term 'electroluminescent' has often been used to describe thick-film AC powder EL lamps. Since the initial discovery, a number of other types of electroluminescent devices have been developed, including inorganic thin-film AC EL (TFACEL), inorganic semiconductor based EL (such as LEDs), and organic semiconductor EL (such as OLEDs). For the purposes of this thesis the term 'EL lamp' will be used to describe thick-film AC powder EL lamps.

The attraction of EL displays for smart fabrics is primarily based around their simple device structure and their durable properties once fabricated. During fabrication EL devices require no controls on the surrounding atmosphere like those imposed by OLEDs, and after fabrication they are very durable due to their thicker layers [10]. They also offer new possibilities for fabric decoration in wearable technology, creating interest from clothing designers.

Clothing designers have previously woven thin EL light emitting wires into fabric. However, this approach faces issues with high manufacturing costs and connecting to the fibres in an unobtrusive manner [11]. The best results so far using the EL wire approach have produced an 8 x 8 matrix display, with each pixel measuring 35 mm x 35 mm [11]. This prototype is shown in Figure 1 below. A further alternative approach is to attach small LEDs to fabric, however these reduce the flexibility of the fabric and cannot be classified as a truly flexible display due to the rigid LEDs [12]. LEDs also generate heat, making technologies like EL attractive to clothing designers as they emit minimal heat.

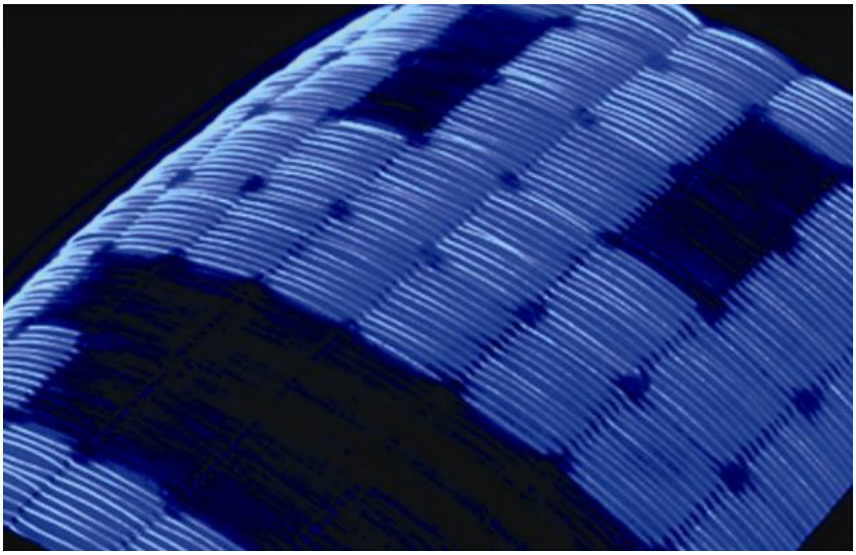

Figure 1. *Image showing prototype of 8 x 8 pixel matrix display using woven light emitting fibres (Image from [11])*

Dispenser printing allows the fabrication of uniform films of functional inks. In this thesis the dispenser printer uses a pneumatic controller attached to an ink filled syringe. This work focuses around dispenser printing EL lamps onto fabric and, once achieved, optimising the shapes, quality, brightness, and size that can be printed.

In this chapter the relevant literature is reviewed, grouped under printing technology and electroluminescence. The two printing techniques used in this thesis, screen-printing and dispenser printing, are discussed highlighting the differences between them. The theory of electroluminescence is then explained along with the state of the art on a variety of substrate types.

2.2. Relevant Printing Technology

2.2.1. Requirements to Print Prototypes onto Fabric

This thesis focuses on developing a printer optimised for low volume prototype production of printed electronics on fabric. The dispenser printer in this thesis will not compete with high volume production printers due to its single nozzle and the modest budget for the project. Printed electronics offers an alternative to traditional electronic manufacturing techniques and creates new possibilities in terms of flexibility and incorporation onto fabric.

The essential requirements for the new printer are:

- Wide range of printable inks in terms of ink viscosity and particle size to enable inks compatible with mass production print techniques to be used.
- Easy to change the print design.

A fast print speed and low cost are also desirable parameters to consider when selecting a print technology.

The majority of smart fabrics produced in the literature make use of either screen-printing or inkjet printing [13]. They are well established technologies with modern screen-printing being developed in

the 1910s and inkjet being developed in the 1950s. Both of these technologies are reviewed in greater detail below. A newer technology first published by G. Vozzi in 2002 is dispenser printing [14]. 3D printing is also considered separately at the end of this chapter as the deposition method used is most similar to dispenser printing.

Figure 2 shows a series of comparisons of screen-printing, inkjet, and dispenser printing. They show a simply hierarchy for each of the print methods comparing the range of acceptable ink viscosities, ease of print design change, print speed and low volume print cost. The aim is to give context as to where dispenser printing will fit in the general fabric printing market.

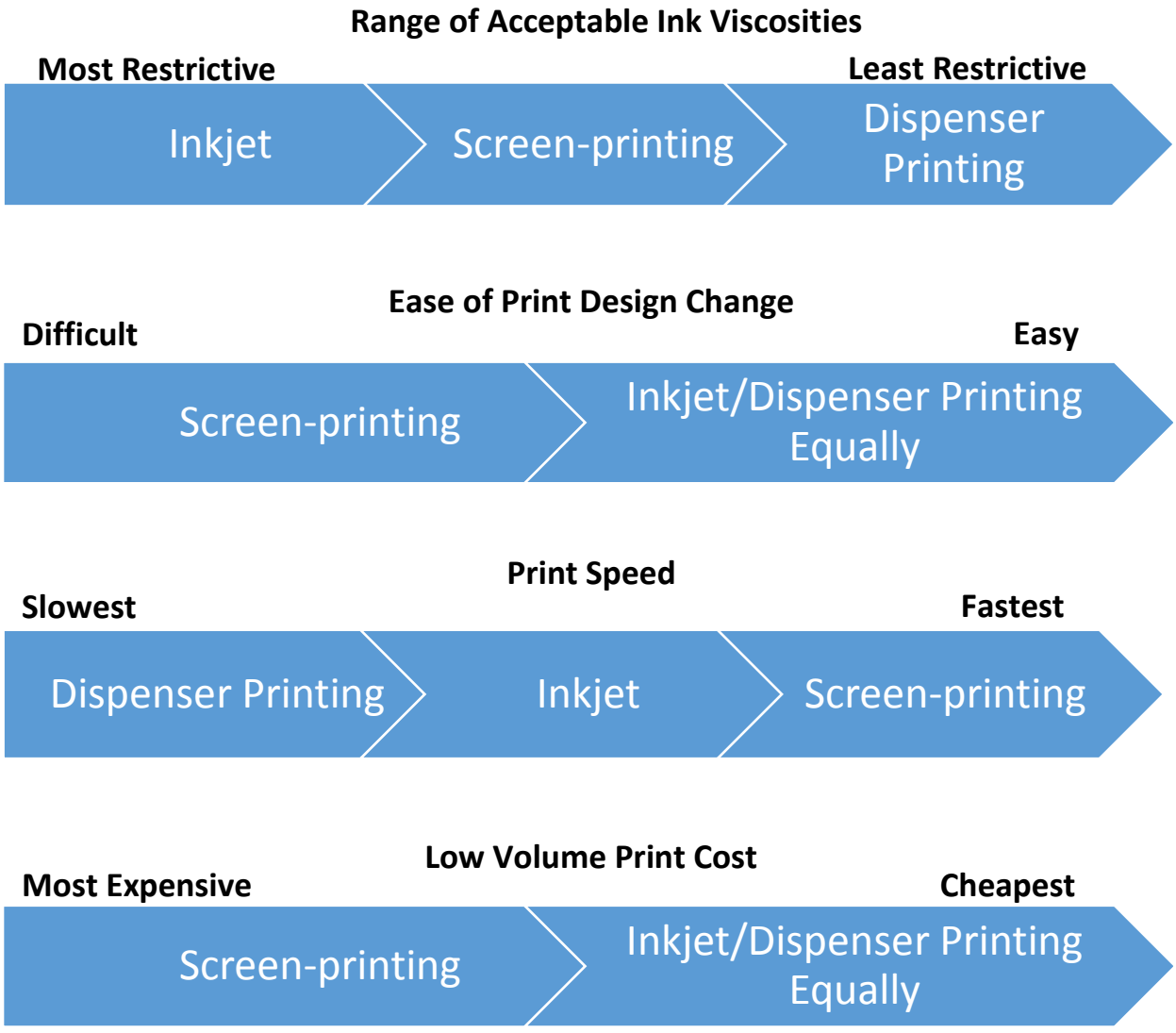

Figure 2. *A comparison of screen-printing, inkjet and dispenser printing when considered in terms of print speed, low volume print cost, and range of acceptable ink viscosities (data from [15]).*

The acceptable ink viscosities comparison for inkjet was based on work by Calvert describing inkjet printers with a maximum viscosity of 0.1Pa.s [1]. The screen-printing viscosity range was defined in the literature as 1-50Pa.s [16]. The value for dispenser printing was estimated based on this research to be 1

mPa.s to 300 Pa.s. The ease of print design change is based on a typical prototyping process involving three design revisions and the associated development time and cost. The print speed comparison was produced by comparing a single printer using each technology. The single printer was assumed to be a finished product, so the print speed for dispenser printing was estimated and may end up being higher as the technology is still being developed. The low volume print cost comparison was made for production volumes of one or two units and included all associated setup costs for each technology.

2.2.2. Screen-Printing

Screen-printing is particularly suited to mass production when incorporated into a 'roll-to-roll' system; a type of printer that automates the printing process into a cylindrical drum for continuous printing [17]. Screen-printing deposits a film of paste in a desired pattern, defined by the screen, with a controlled thickness. The paste is deposited through a mesh reinforced stencil, called a screen, using a rubber squeegee to apply a downwards force onto the paste. The process of screen printing is a multi-stage process consisting of the following steps:

1. Paste is spread over the screen held just above the substrate.
2. A squeegee applies pressure to the screen and moves across the design forcing paste through the screen in the desired pattern onto the substrate below.
3. The screen is removed leaving the film of paste on the substrate.

Step number 2 is shown in detail in Figure 3 below, highlighting that the screen has a maintained 'snap-off distance' above the substrate, with contact between the screen and substrate only being made where the squeegee touches. This is a key requirement to maintain a high quality print as it prevents the paste bleeding outside the desired print area.

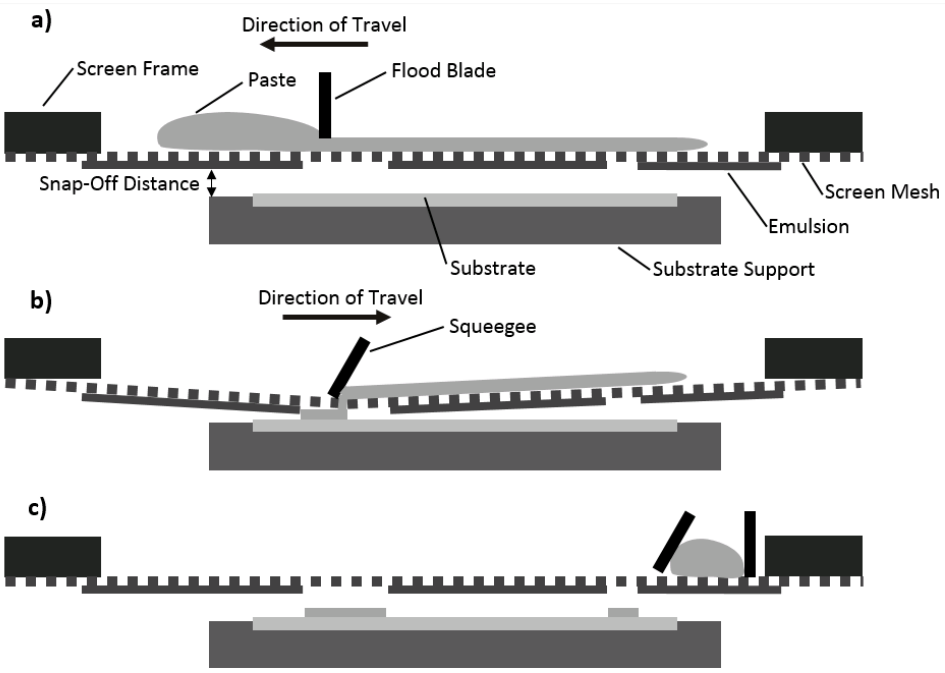

Figure 3. *Image showing a squeegee being moved across a screen forcing paste through, highlighting that a snap off distance is maintained*

Screen-printing offers many methods to control the print thickness and quality, particularly the screen, paste, squeegee, substrate, printing process and printing machine [18]. A full list of controls is shown in Figure 4.

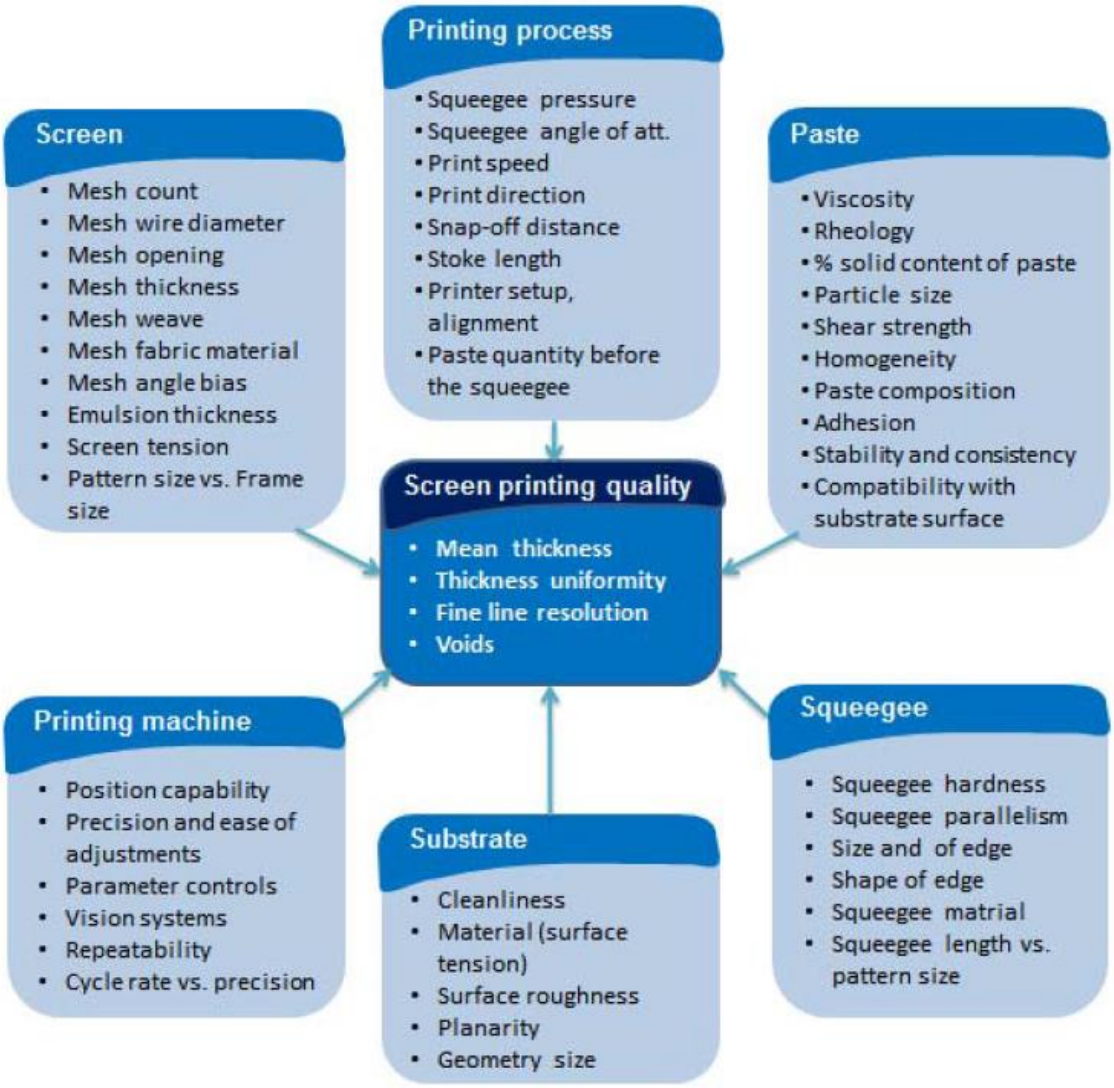

Figure 4. *Factors that influence print quality when screen-printing (Image from [19]).*

In this work, screen-printing is used to initially evaluate new pastes. The more establish process helps to remove errors caused by printing and provides a reference point for subsequent dispenser printing [20-22].

Screen-printing for non-electronic applications does not usually require resolutions under 100 µm, so the printing process has been adapted to provide the higher resolutions required in electronics. The current state of the art in terms of screen-printing resolution was demonstrated by Numakura with 30 µm wide conductive silver tracks printed with 30 µm spacing onto polyimide film [23]. This high resolution printing performance was achieved through a series of tests to optimize the silver paste

viscosity and screen parameters. Soukup et al. demonstrated ultra-thin gold tracks which were printed at a minimum of 0.16 µm layer thickness through optimisation of "squeegee pressure, hardness, angle, printing speed and direction, flooding, and snap off distance" [24]. It is worth noting that these scales approach the practical limits of the printing pastes. For example Numakura showed that resistance of the 30 µm width silver tracks was approximately 10 times that of similar tracks printed at 200 µm width. The results by Namakura show a non-linear relationship between resistance and dimensions as the 30 µm track volume is only 6.7 times smaller. Based on these results all test patterns produced for screen-printing in this research will have tracks in excess of 200 µm in width to maintain a low resistance over the length of the track.

The non-linear relationship between resistance and dimensions implies there are other factors affecting the resistivity. Work presented by Wargo proposes a concept they call "print efficiency", which is a measure of "how well the intrinsic conductivity of the printed conductor is utilised"[25]. The quality of the print is the primary factor affecting print efficiency, which is defined in Equation 1.

$$\xi = \frac{\rho_{minimum}}{\rho_{measured}} \qquad \textit{Equation 1}$$

$\xi - Print\ efficiency$

$\rho_{minimum} - Theoretical\ minimum\ resistivity\ of\ printed\ paste$

$\rho_{measured} - Measured\ resistivity\ of\ printed\ sample$

Examples cases, showing how variations in print efficiency occur, are shown in Figure 5 below. The material shown represents a printed conductive paste.

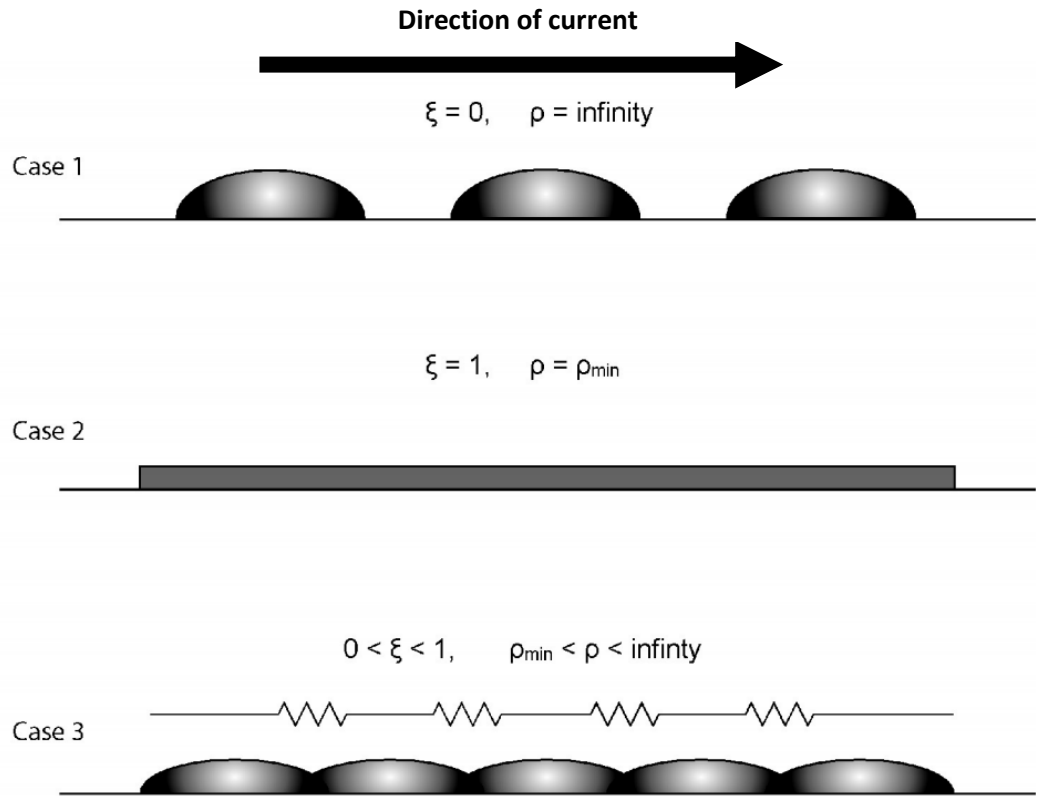

Figure 5. *Example cases showing how variations in print efficiency occur when printing a conductive paste (image from [25]).*

Figure 5 shows an extremely poor print quality in Case 1, an ideal print quality in Case 2, and an expected print quality for practical devices in Case 3. In Case 1 the conductor has been deposited in small droplets which are not connected, this can occur if a very small snap off distance is used with a viscous paste. The small snap off distance causes the screen mesh to separate the deposited ink, and the high viscosity of the ink prevents it from flowing into the voids. Print efficiency is 0 in Case 1 and the resistivity is infinite.

Case 2 shows an ideal uniform print that is not achievable in a practical device due to general errors that will always be present in the printing process such as slight paste variations. In this case the print efficiency is 1 and the resistivity matches the measured theoretical resistivity of the paste.

Case 3 shows a typical printed conductor in a practical device. The figure shows variations in thickness along the track which will affect the measured resistivity. The work by Numakura on very narrow tracks, described earlier, could be affected by print efficiency. The non-linear resistance measurements related to dimensions could be caused by a decrease in print efficiency on the very narrow tracks compared to the wider tracks.

The print efficiency equation can equally be applied to dispenser or any other type of printed silver tracks and is used later in this thesis to analyse the quality of printed tracks with different print parameters.

2.2.3. Inkjet Printing

Inkjet printing is a well-established technology and was first used for production printing colours onto textiles in 2003 and is now used to print around 200 million linear meters per year [26]. The process works by ejecting ink through a very small (normally <500 nm) nozzle. As the ink is ejected it forms droplets that can range from 20 μm to 1 mm in diameter, however typically they are around 150 μm in diameter.

There are two main techniques used to create the pressure pulse required to eject the ink: thermal bubble or piezoelectric. Thermal bubble works by including a small heater in the ink reservoir by the nozzle. A pulse of current is applied, boiling the ink and creating a vapour bubble, forcing a droplet of ink from the nozzle. The piezoelectric method includes a small piezoelectric transducer next to the nozzle. The transducer deforms when a voltage is applied, increasing the pressure in the nozzle and forcing a droplet of ink out. The piezoelectric technology is more commonly used for printing functional inks as there is "no risk of thermal degradation of the ink" [27].

The process is limited by its slow speed relative to industrial screen or rotogravure printing technologies. Attempts to increase the speed have been successful using additional print heads, with the La Rio printer by MS Industry achieving a record of 8100 square meters per hour [26]. While this is a similar speed to industrial screen-printing equipment, the cost is significantly higher due to the number of individual print heads that must be produced. A similar technique, using multiple print heads, could be used to increase the speed of dispenser printing.

There have been previous attempts to inkjet print EL devices, however they have been unable to print a functioning phosphor layer which is essential for an EL lamp. The particles used in the phosphor layer for a typical EL thick film AC EL lamp have a diameter of 20 to 40 μm. The maximum particle size for most inkjet printers is 200 nm, and as shown recently by Angelo et al, it is impossible to inkjet print these phosphor particles [28]. Attempts to reduce the particle size were unsuccessful as they reduced the luminosity of the particles causing the overall device luminance to be undetectable to the human eye. For this reason the process is not considered further in this work.

2.2.4. 3D Printing (Fused Deposition Modelling)

Fused Deposition Modelling (FDM) is a type of 3D printing similar to dispenser printing, in that it additively deposits material onto a substrate, using multiple layers to form 3D structures. However, the materials used are significantly different, with the majority of budget FDM printers using ABS plastic or similar thermoplastics as 3D printing is aimed towards producing relatively large 3D structures compared to dispenser printing. The print processes also differ, with FDM printers typically using a solid filament that is heated and melted in a nozzle before being printed. The pressure to eject the melted plastic is created by further filament being inserted into the nozzle. The technique was patented in the late 1980s and commercialised by Stratasys in 1990 [29]. The patent has since expired leading to the wide adoption of this printing technology.

Some 3D printers use a different process that utilises syringes and pastes similar to dispenser printing, however the pressure required to eject the paste is created by a mechanical plunger being moved. Only one major manufacturer uses this technology (Fab@Home [30]), as it requires external curing equipment compared to the ambient cooling used by the FDM technique. While the applications of 3D printing are different from dispenser printing, it shares aspects such as the control software which could be used to save development time.

2.2.5. Dispenser Printing

Dispenser printing is a rapid additive manufacturing process, with which a variety of electrically functional inks can be printed. Being a direct write technique, it offers the ability to rapidly change the design without the requirement for additional masks or screens. Dispenser printing utilises an ink filled syringe, attached to a dispenser controller using polyurethane tubing. The controller provides pressurised air at a set pressure, via the supply tube, for a specified amount of time to dispense the ink from the syringe. The syringe and nozzle components are shown in Figure 6 below.

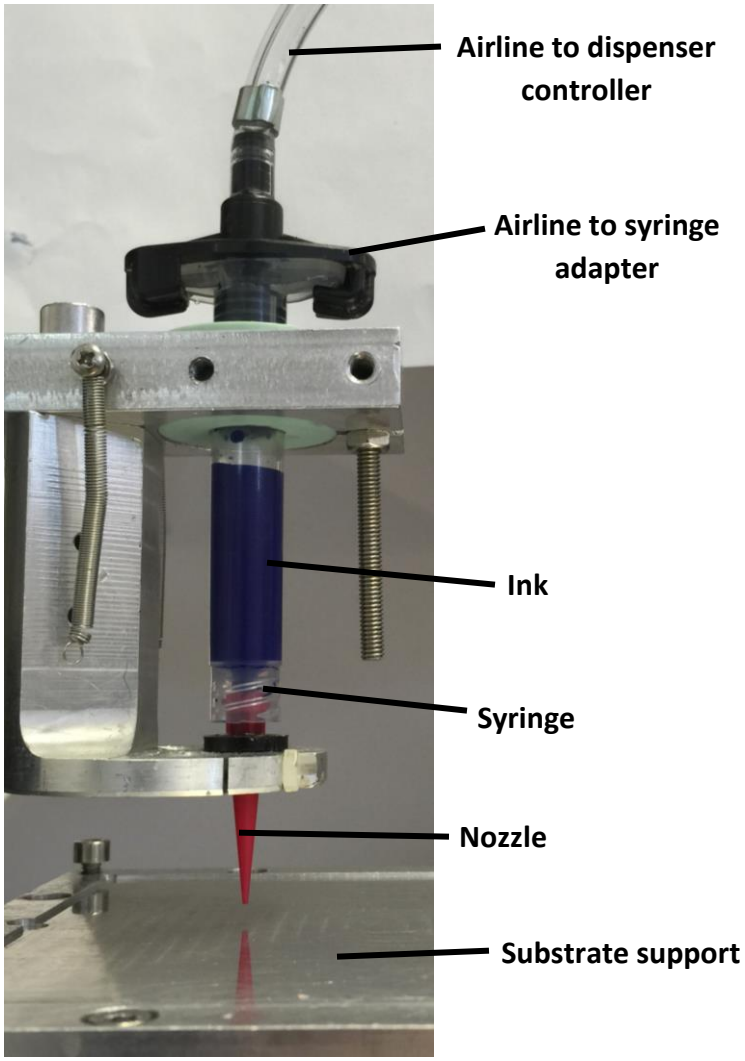

Figure 6. *Image showing the key components around the syringe in a dispenser printer.*

The deposited materials, known as 'inks' to differentiate them from screen-printing pastes, are mostly functional particles dispersed in a binder to achieve a suitable viscosity for printing (1 mPa.s-300 Pa.s depending on the nozzle used) and sufficient substrate adhesion after curing. However, all screen-printing pastes can also be dispenser printed making the fabrication method compatible with existing screen-printing manufacturing processes. This is essential for mass production. As dispenser printing is an additive process wasted ink is kept to a minimum and time is only spent printing ink in the desired areas.

The ability to change the design rapidly is appealing in prototyping applications and dispenser printing can use more viscous materials (< 300 Pa.s) than other direct write technologies such as inkjet (< 20 mPa.s) allowing higher functional material concentrations. Figure 7 below highlights the process differences between dispenser and screen-printing for a series of conductive tracks. The advantages

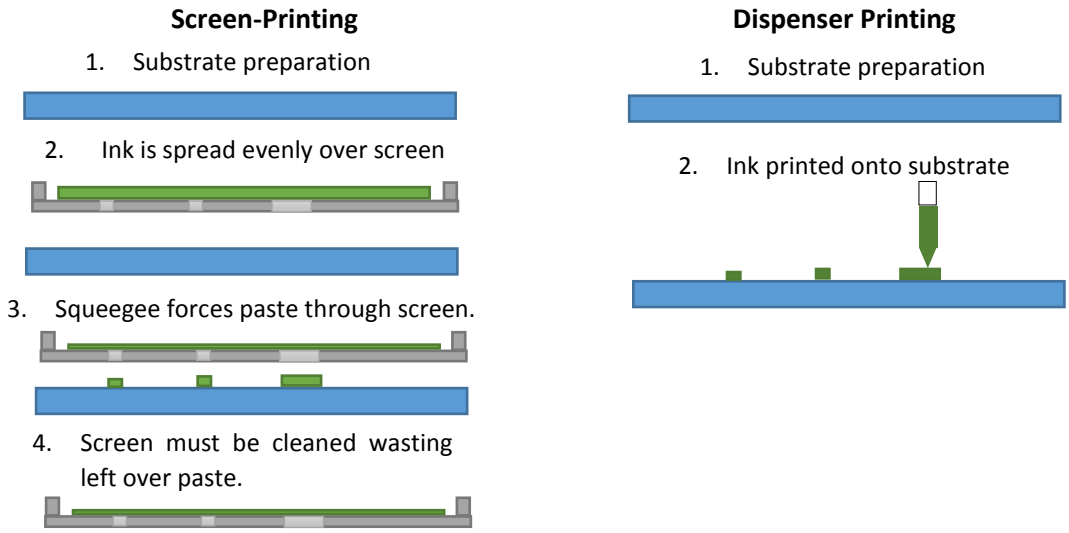

Figure 7. *Comparison of printing process for screen-printing (left) and dispenser printing (right).*

make dispenser printing attractive to industries where ink costs are high and production volumes are low or where the print design often changes.

A number of mechanisms can be used to force the ink from the syringe such as: mechanical piston, Archimedes screw and pneumatic pressure. An example of an Archimedes screw type dispenser if the 'eco-Pen' from Intertronics [31]. The datasheet suggests that liquids with viscosities up to 7,000,000 mPas can be dispensed, although it gives no minimum viscosity. Deposits of as little as 1nL are possible with the smallest head. This work will focus on pneumatic dispensers, which operate by forcing ink stored in a syringe through a nozzle using pulses of pressurised air. Pneumatic dispensers were selected by the CREATIF project funding this work and were already purchased when the thesis was started. The dispenser printer used in this work was bespoke using a commercially available Nordson Ultimus V dispenser controller [32]. Complete pneumatic dispenser printers are also available such as the bioplotter [33].

In pneumatic dispensers, a vacuum pressure is applied to the syringe when not printing to prevent ink

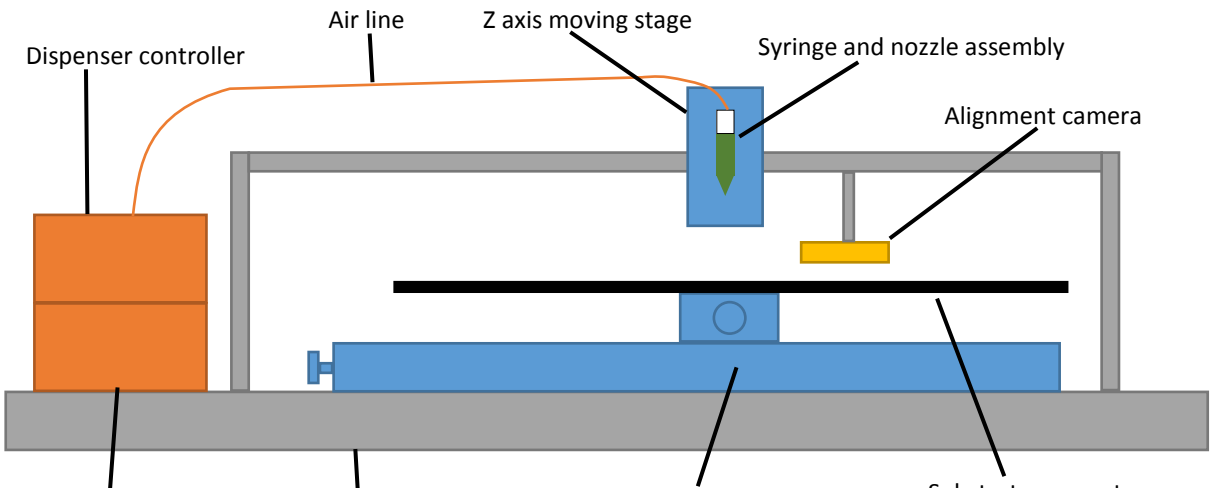

Figure 8. *Diagram showing the key components in a time pressure dispenser printer.*

being erroneously dispensed. The dispense pressure, dispense duration and vacuum pressure can be adjusted using the dispenser controller. The syringe or substrate is mounted on an XYZ moving stage depending on the setup. The X and Y stage movement is controlled to deposit ink in the desired area of the substrate. The Z stage is controlled to maintain a defined Z height above the substrate across a varying surface topology, allowing substrates to be curved or uneven. A diagram showing the components in a typical dispenser printer is shown in Figure 8 below.

In a dispenser printer, the main parameters that can be varied to alter the amount of deposited ink are the dispense pressure, print speed, nozzle to substrate separation distance, and the type of nozzle. Typically, the dispense pressure is varied while the other parameters are kept constant to avoid an excessive number of variables. The dispense pressure is normally set to a value between 10 and 110 kPa based on the results from a process described in chapter 3.

The print speed depends on the movement stages of the printer and the speed at which they can reliably move without causing problems with the motors. A faster print speed will mean less ink deposited in a defined area. The nozzle to substrate separation distance is the distance between the bottom of the nozzle and the substrate underneath. If the distance between them is too low or they are in contact, then less ink will be deposited onto the substrate. None of the literature specifies this distance so in this work a value of 220 µm was found experimentally and used for all samples.

The selected nozzle can also impact the dispensed volume for set print parameters. The correct nozzle choice depends on the required print resolution and the desired ink flow rate. The three key factors that affect the flow rate are the diameter of the tip of the nozzle, the length of the nozzle and whether it's a tapered or straight nozzle. A narrower nozzle diameter, or longer nozzle, or a straight nozzle will all result in a lower flow rate if other parameters are kept the same. Figure 9 below highlights a range of the available nozzles suitable for use with the dispenser printer. The needle nozzles produce the narrowest tracks, however they are more sensitive to particle size and are more prone to blocking than the tapered nozzles.

Figure 9. *Examples of types of available nozzles, from left: 250 µm tapered, 50 µm tapered, 100 µm ¼ inch needle, 100 µm 1-inch needle.*

Significantly less information is available about the state of the art in dispenser printing as it is still a developing research field. One paper by Wright et al. suggested their dispenser printer was able to print 50 µm wide tracks with printed layer thicknesses ranging from 10 µm – 200 µm [34]. The small tracks described by Wright et al. describe the smallest dispenser printed feature sizes that have been published. However, Wright et al. gave no details on the ink, substrate, or performance of the printed layer for these thin tracks. The ink used will have a significant impact on the minimum track widths that can be printed as the maximum particle size will dictate the nozzle diameter that must be used.

Dispenser printing was first published by G. Vozzi in 2002 targeted towards the application of tissue engineering [14]. The paper describes biomaterial inks ejected through a 20 µm glass nozzle by a pressure controlled air source. The nozzle is kept fixed while an XY position bed is moved underneath. Dispenser printing has since been shown in 2010 to be a promising technology for rapidly producing printed batteries; an example by Ho et al produced a prototype zinc microbattery with a discharge capacity of 0.98 mA h cm^{-2} and an energy density of 1.2 mW h cm^{-2} [35]. The use of dispenser printing to fabricate flexible batteries highlights the potential of the technology to produce self-contained all printed electronic systems. In late 2013 an EngD thesis from S. Raja was published that showed a range of printed antennas and demonstrating a communications antenna printed onto the wing of an unmanned aerial vehicle [36]. Further to this dispenser printing has been used to fabricate thermoelectric energy generators in 2014. The work by Chen et al. produced a generator producing a power of 10.5 µW at 61.3 µA and 171.6 mV [37]. While the generated power is low, it highlights the range of materials that can be dispenser printed resulting from the relatively large nozzle diameters and range of acceptable viscosities.

Dispenser printing has been demonstrated as a versatile prototyping tool by Wright et al. [34] as well as the work described above; however the technology still has to overcome issues including maintaining a separation distance between the nozzle and substrate, particularly over large areas of movement.

2.3. Electroluminescence State of the Art

"Electroluminescence is the non-thermal conversion of electrical energy into luminous energy"[38]. Electroluminescence has been researched for many years with the first work being carried out in 1936 by Georges Destriau [9] and there are early patents dating back to 1960 [39]. Since these early devices significant work has advanced the technology to the commercial devices seen today. Two examples of commercial EL displays can be seen in Figure 10. The image on the left in Figure 10 was produced using large screen-printed EL sheets on a plastic substrate that were then cut to size. The image on the right in Figure 10 was produced using rotogravure printing as the panels were mass produced. In the following sections, recent advances will be reviewed that provide the basis for dispenser printed EL lamps on fabric.

Figure 10. *Examples of commercial EL displays. Left: "All the Time in the World" installation at Heathrow Airport (Image from [40]). Right: Engine parameter panel from Planar Displays (Image from [41]).*

2.3.1. Potential Approaches to Electroluminescent Lamps

As described in 2.1, there are many different types of electroluminescent lamp. Four of the most common types are shown in Figure 11 with a description of the typical characteristics from [42]. The two thin-film lamps are not possible to produce using the printing techniques covered in this thesis as the layers are typically less than 1 µm thick. The thin-film lamps are also unsuited to fabrics as the weave of a fabric can produce changes in substrate height of up to 100 µm. This far exceeds the thickness of the thin-film device so would cause reliability issues. Of the two thick-film devices, the AC device clearly outperforms the DC device in terms of half-life and luminous efficiency. Therefore, in this work the AC thick-film type of lamp was used for all devices and is referred to throughout simply as an 'EL lamp'.

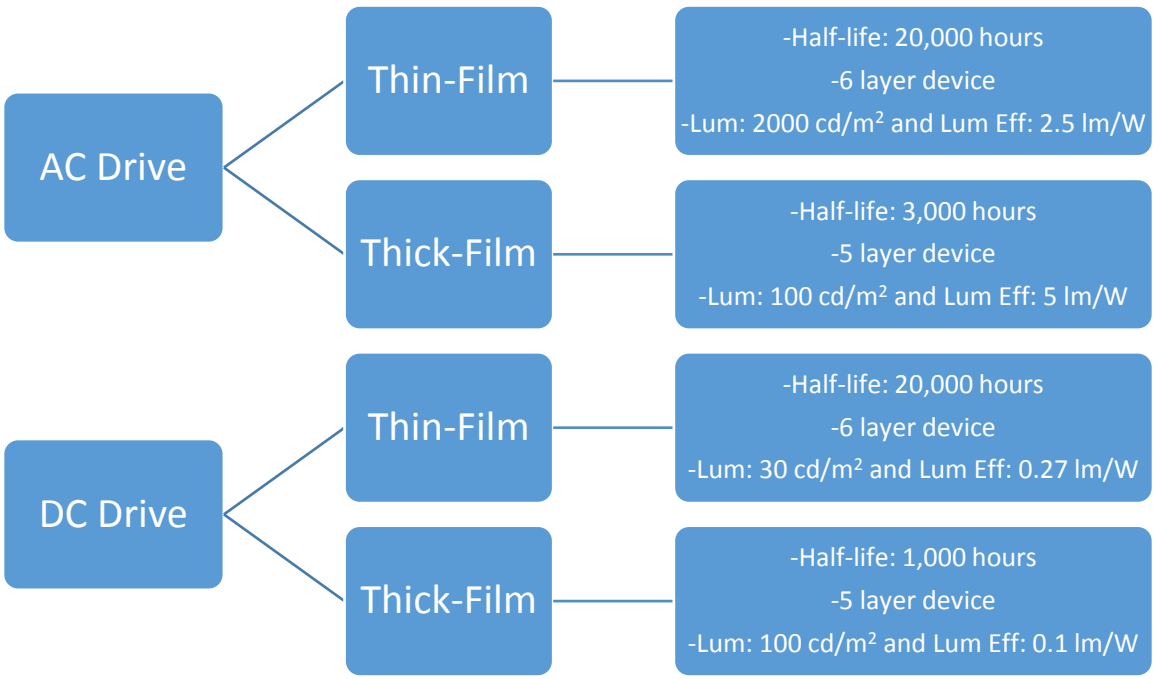

Figure 11. *Characteristics of four types of electroluminescent lamp (based on data from [42]).*

2.3.2. Principles and Structure of AC Electroluminescent Lamps

The emitted light from an EL lamp is the product of radiative recombination of electron hole pairs. The electron hole pairs are created through one of two processes;

1) Semiconductor materials are excited by the impact of high energy electrons.
2) PN junctions are formed by doping semiconductor materials with donor/acceptor materials.

The EL lamps in this work operate via the second of these processes. For the remainder of this research, these semiconductors are referred to as 'phosphors'. The first process is only suitable for very thin EL device structures (typically around 1 µm [42]), as it is only in these thin devices that the field strength over the phosphor layer is strong enough to excite the electrons to a high enough energy level. As described previously the thin film AC EL lamps are not suitable for this work.

The second process, involving doped semiconductors (commonly Zinc Sulphide – ZnS), is most commonly used in printed EL lamps. As the ZnS is doped with donor/acceptor materials the EL lamps function with lower field strengths (typically 10^6 – 10^7 V/m [42]), meaning the overall device can be in the order of 100 to 200 µm thick. This thicker device is more suitable to current printing technologies and all EL devices in this work will operate using the second emission process described above.

A typical structure for a dispenser or screen-printed EL device on an opaque substrate is shown as a cross-section view in Figure 12 and a top view in Figure 13. The same structure would be used for thin film AC lamps, however the layers would be much thinner and high performance transparent conductors, such as Indium Tin Oxide (ITO), would be used. ITO is not compatible with screen or dispenser printing as it needs to be printed in layers less than 120 nm thick to maintain transparency. ITO is also very expensive and becomes brittle once deposited, making it unsuitable for use on flexible substrates.

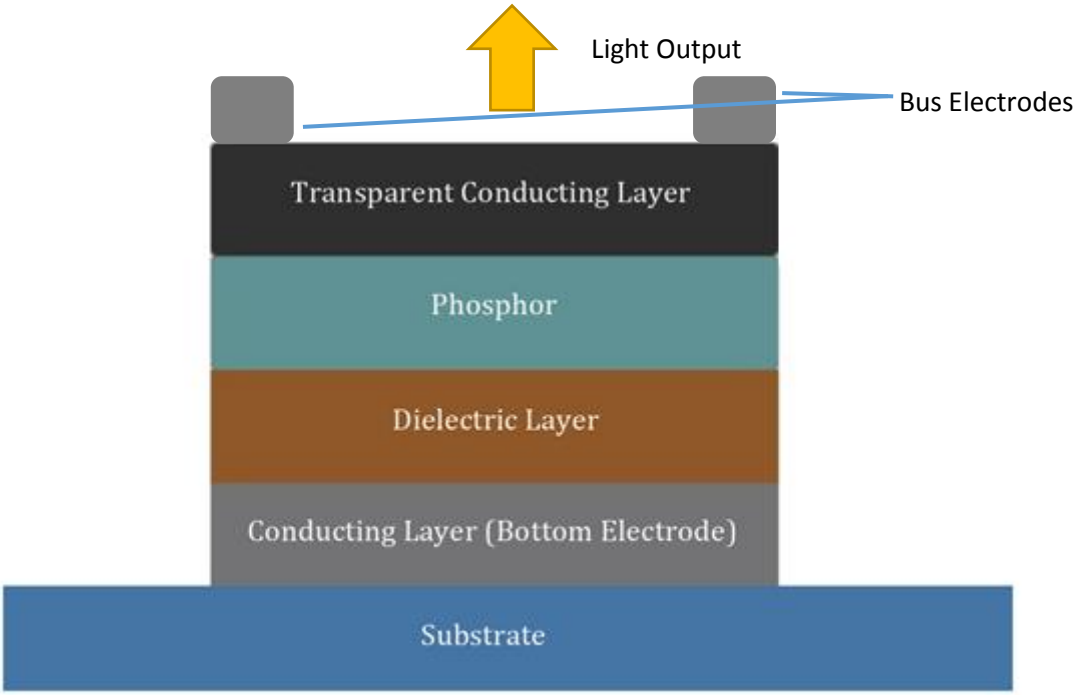

Figure 12. *Cross-sectional view of a Thick-film EL lamp structure on an opaque substrate.*

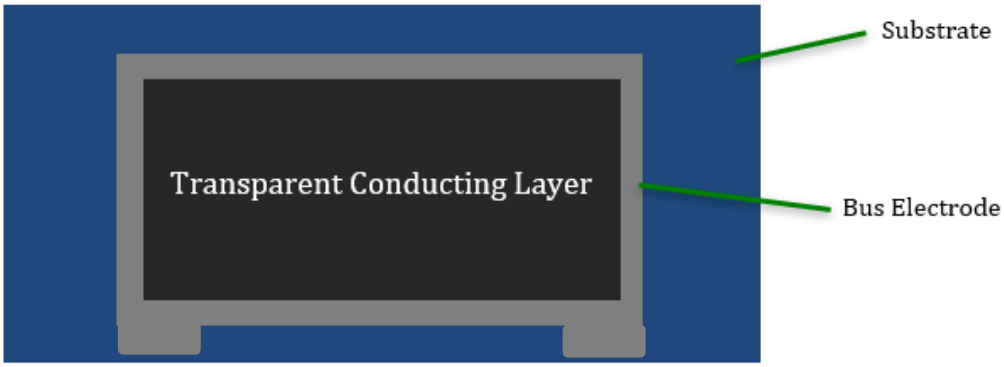

Figure 13.*Thick-film EL lamp structure on an opaque substrate viewed from the top.*

The aim of the multi-layer construction is to provide a capacitor structure, with a phosphor layer in the centre. A dielectric layer is required to prevent short circuits between the electrodes and increase the potential field strength across the phosphor layer to reduce the chance of dielectric breakdown. One of the electrodes must be transparent to allow light to efficiently escape the capacitor structure. The device comprises five individually deposited layers:

- Bottom electrode layer – provides the bottom opaque side of the capacitor structure; should be low resistance (<10 Ω) [9].
- Dielectric layer – prevents short circuits across the capacitor structure and acts as a light reflector, should be able to maintain an electric field of 10^7 V/m [9].

- Phosphor layer – the phosphor emits light under the influence of an alternating electric field and the brightness depends on emission colour, however a good green-blue phosphor should have a luminance >15 cd/m^2 at 150 V_{peak}, 400 Hz driving voltage [43].
- Transparent electrode layer – provides an even distribution of charge across the phosphor layer and allows light to pass through. The resistance should be as low as possible, a typical resistance value of a good commercial printable transparent conductor would be <500 Ω [9].
- Top/Bus electrode layer – provides connection to the top electrode and is usually printed with the same material as the bottom electrode.

2.3.3. Materials for AC-Electroluminescent Lamps

A typical device structure has already been shown in Figure 12 highlighting the multiple layers required to form an EL lamp. The first printed layer in the structure shown is a conducting layer, forming the bottom electrode of the capacitor structure. As no light passes through this layer, opaque conductors are typically used. The conductivity of the material is important as it affects the homogeneity of the charge across the electrode, which in turn controls whether uniform visible light is produced. Typically silver inks are used due to their high conductivity and low temperature processing, although these pastes are expensive and suffer from electromigration [9]. Alternatives are carbon or aluminium inks, although carbon has relatively low conductivity, and aluminium requires high temperatures for processing. The bottom electrode material is usually also used to form the bus top electrode connecting the driver to the transparent conductor.

The next printed layer in the structure shown in Figure 12 is a dielectric layer. Typically Barium Titanate ($BaTiO_3$) inks have been used for this layer due to their high dielectric constant of 2000-3000 at room temperature [44]. The inks perform well with a particle size under 1 µm [9]. An alternative technique is to combine the dielectric and phosphor layers by dispersing phosphor particles in a transparent polymer binder with high dielectric constant [9]. This approach adds complication in identifying a suitable transparent polymer binder with a high dielectric constant, and ensuring the phosphor particles are small. One example shows polyvinylidene fluoride (PVDF) based inks can produce a dielectric constant of around 50 at room temperature [45], making it suitable for use as a phosphor binder. Devices with a combined phosphor and dielectric layer are also more prone to short circuits, as it is difficult to ensure a constant dielectric thickness due to the inclusion of phosphor particles.

Phosphor is usually printed as a separate layer on top of the dielectric in the structure described for flexible opaque substrates. Almost all devices utilise ZnS phosphors doped with acceptor/donor materials. Table 1 provides a summary of the common dopants and the emission colour they produce.

Table 1. *Table comparing common ZnS dopants against the visible emission colour they produce (data from [42]).*

Zns:Dopant	Peak Wavelength (nm)	Colour Approximation
ZnS:Cu,Cl	450	Blue
Zns:Cu,Al	540	Green
ZnS:Cu,Mn,Cl	590	Green/Yellow
ZnS:Cu	690	Orange/Red

Phosphor inks are readily available from manufacturers such as DuPont [46], or alternatively individual EL phosphor particles can be purchased from Global Tungsten and Powders Corporation (GTP) [43]. Both phosphor particles and inks are available in a range of brightness levels, with the compromise being a shorter lifetime for a higher brightness. The brightness and lifetime options available are dependent on the colour of the phosphor. As an example the green phosphor is available in brightness options of 53 cd/m^2, 74 cd/m^2, or 82 cd/m^2, with half-lives of 3600, 2600, or 2500 hours respectively [43]. A drawback of current EL phosphors is the lack of a white emitting phosphor. Currently, white light has to be produced using a combination of blue and orange phosphors, which has a very limited lifetime as the blue phosphor deteriorates faster than the orange, quickly leading to a colour shift towards orange. An alternative method utilises green EL phosphor with a red fluorescing dye on top, however these devices have shown low brightness and poor efficiency [47].

A printed transparent conductor forms the top electrode of the EL lamp and, as with the bottom electrode, a high conductivity is important to distribute the charge evenly. As the light must pass through this layer, transmittance is also an important characteristic. A low transmittance reduces the perceived brightness and also can distort the colour if only parts of the spectrum pass through the conductor. Traditionally ITO has been used for this layer, but as previously discussed, ITO is difficult to print and is expensive. Conductive polymers are currently the only feasible alternatives, primarily PEDOT:PSS is being produced and sold commercially. Research is being carried out on alternative solutions, such as using fine grids of silver, referred to as silver nano-wires, to transport the charge [48], or using graphene to form a transparent conductive sheet in solar cells [49].

2.3.4. Summary of Printed Electroluminescent Lamps

2.3.4.1. Printed Electroluminescent Lamps on Rigid Substrates

Early demonstrations of printed EL devices in the 1990s were on rigid glass substrates. These demonstrators used Indium Tin Oxide (ITO) as the transparent conductor; however the glass substrates were pre-patterned with ITO using a non-printing based method. The ITO is usually sputtered onto the glass; the devices use a combination of manufacturing processes and cannot claim to be fully printed.

The device structure for an opaque substrate is shown in Figure 12, however devices on transparent substrates, such as ITO coated glass, are able to use an alternative structure where light is emitted through the substrate. Figure 14 shows the device structure for a hybrid printed EL lamp on a transparent rigid substrate.

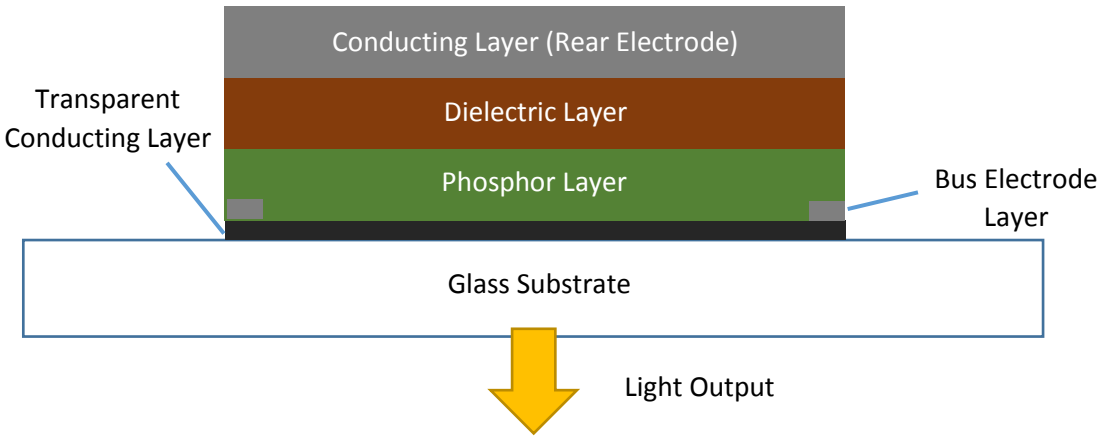

Figure 14. *Cross-sectional view of a thick-film EL lamp structure for a transparent rigid substrate.*

Printed EL devices on rigid substrates from Heikenfeld et al in 2001 show screen-printing as a viable method [50]. Their work demonstrated small EL lamps screen-printed onto glass substrates for vehicle displays. The samples had the bottom conductor and transparent conductor split into tracks to enable individual pixels to be controlled. There is also a partially inkjet printed device [51] by Bharathan et al. The device used a sputtered ITO film, followed by a spin coated phosphor layer and then an inkjet printed transparent conducting layer. The devices by Bharathan et al. are shown in Figure 15 below. The lamps are rigid due to the glass substrate and the transparent conducting layer and bus electrode layer are swapped. This is because the glass substrates are sputtered with ITO first, as this layer cannot be added after the other layers are printed.

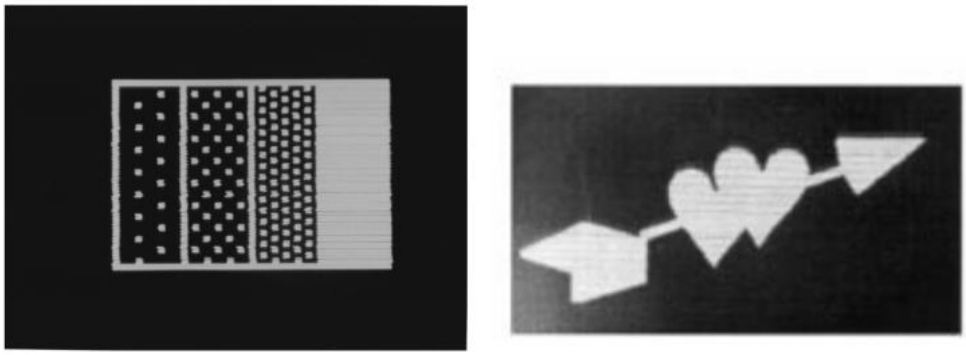

Figure 15. *Examples of inkjet printed EL lamps onto glass (Image from [51])*

2.3.4.2. Printed Electroluminescent Lamps on Flexible and Stretchable Substrates

As described in section 2.3.2, EL lamps require a transparent conductive layer to form the capacitor structure and still allow light out. Sputtered ITO polyethylene terephthalate (PET) film is commonly used to form this layer because it is transparent, highly conductive, and PET is readily available with ITO already sputtered onto it. ITO is usually limited to sputtering deposition due to its brittleness, meaning it can only be used in very thin layers (typically 120 nm) and is therefore not suitable for printing. Examples of flexible EL lamps partially screen-printed onto PET can be seen in Figure 16 [52]. The device structure is as shown in Figure 14. In this structure light is transmitted through the PET, and the PET was sputtered with ITO meaning it is not a fully printed device.

Figure 16. *Example of flexible EL display in a tablecloth (Image from [52])*

The design provides a good example of printed EL of a flexible substrate, however the design faced issues with lamp control as well as connector design. Gaver et al. described facing issues with reliability and that the majority of their 10 samples "burnt out" before testing began. They did not give details of the EL pastes used or layer thicknesses so the cause is not identified. The design also had to include a large ribbon cable that affected the device aesthetics. The rigid support with the ribbon cable can be seen in Figure 17 below.

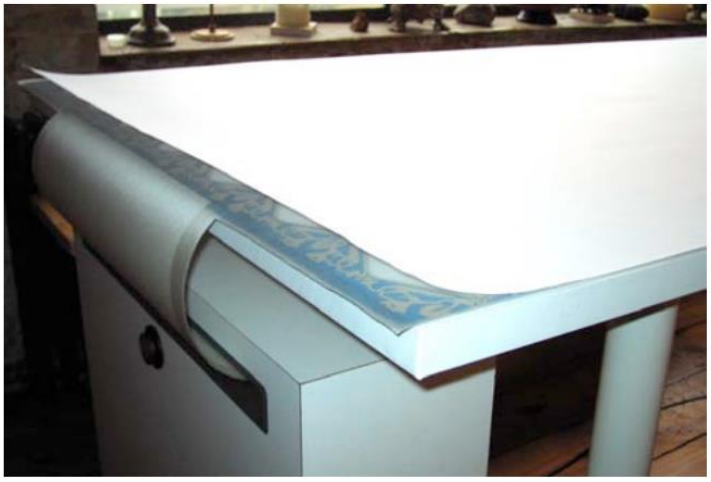

Figure 17. *The ribbon cable in a rigid support at the edge of the 'History Tablecloth' (Image from [52])*

More recent developments in the EL lamp field have been on stretchable flexible non-fabric substrates. Initial work conducted by Wang et al. involved polydimethylsiloxane (PDMS) spray coated with silver nanowires to form a transparent conducting material [3]. A ZnS:Cu phosphor mixed with liquid PDMS was then spun onto the silver nanowire coated PDMS forming a complete EL lamp. The device survived a strain of up to 100% and can be seen in Figure 18. This work was then furthered by Larson et al. who

produced an ‘electroluminescent skin’ that was even more stretchable and was demonstrated in blue, green and orange [2].

Figure 18. *PDMS based stretchable EL lamp by Larson et al. (Images from [2])*

2.3.4.3. Printed Electroluminescent Lamps on Fabric Substrates

There have been few examples of printed EL devices onto fabric substrates, and some of the examples claiming to have achieved this have used methods outside of typical printing processes. The majority of devices printed onto fabric use synthetic fabric, such as woven PET, as this largely avoids the issues of surface roughness faced when printing onto fabrics which are more suitable for clothing. The devices therefore have limited applications as many consumers are not willing to wear clothing made of fabric with plastic based fibres. An example presented by Hu et al. [7] uses the structure shown in Figure 14. However the researchers replace the ITO with a semi-transparent conducting PEDOT:PSS layer so the layer can be inkjet printed. The substrate is a woven fabric, however the yarns are made of transparent PET, making the fabric transparent with a plastic feel.

Work presented by Sloma et al. [6] presents a screen-printed EL lamp on paper and fabric substrates using a similar structure to that shown in Figure 12. Instead of a PEDOT:PSS layer they use a semi-translucent conductor made from carbon nanotubes and graphene platelets. The devices suffer from reliability issues particularly on the fabric substrates and during bending. The issues arise from printing the silver electrode directly onto a woven substrate, creating an uneven surface for the subsequent printed layers.

A patent by Park et al. [53] for Kolon Glotech Inc related to printed EL lamps on fabric claims invention rights to the device structure shown in Figure 19**.** , although no prototypes or devices have been publicly announced or made commercially available at the time of writing.

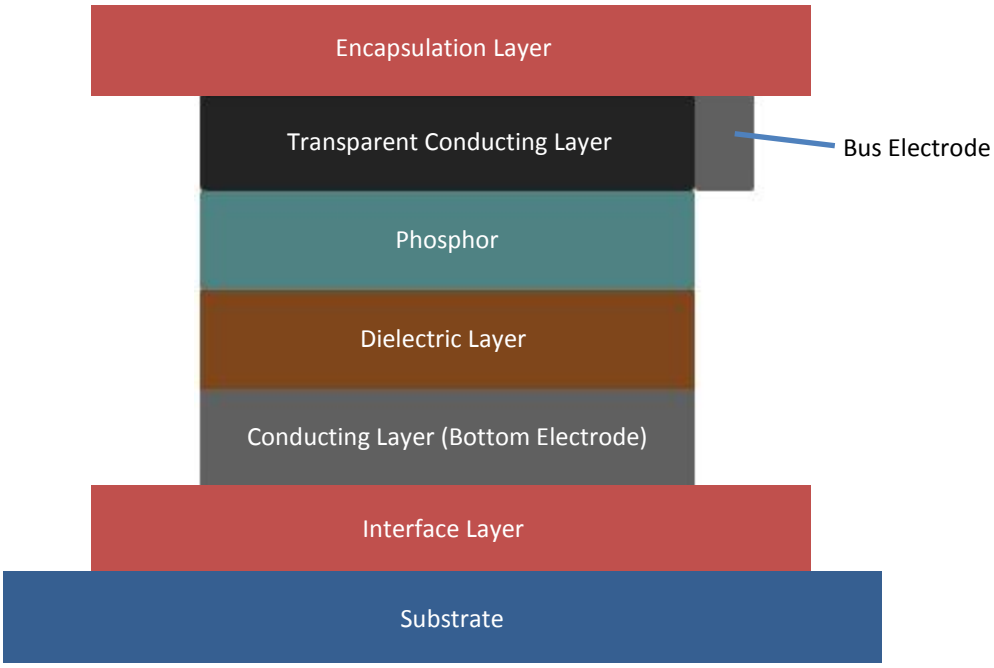

Figure 19. *Thick-film EL lamp structure for opaque fabrics as patented by Park et al. [53].*

The structure includes an interface layer designed to smoothen the woven fabric surface. A top encapsulation layer is also included, protecting the device from environmental damage (moisture) as well as protecting users from the high voltage (>100 V A.C.) electrodes. The deposition method mentioned throughout the patent is listed simply as "printing" and no further details are given. There are no publications from Kolon Glotech relating to this and no prototypes or news reports relating to this could be found. However, utilising a bottom interface layer and top encapsulation layer has also been researched at the UoS using screen printing [54] proving that the concept is viable.

A second patent relating to the production of EL lamps was published in 2012 by Hochschule Niederrhein [55]. The patent covers the production of the structure shown in Figure 7 and Figure 14, it also makes reference to a large range of substrates include plastic and woven fabrics. The production methods listed cover many printing techniques includes "screen-printing and digital printing", although there is no specific definition of digital printing.

2.3.4.4. Printed Electroluminescent Lamps with Quantum Dots

Recently with the revived interest in EL lamps, efforts have been made to improve the colour range available. Due to the limited range of phosphors the majority of bright EL lamps (>50 cd/m^2) are either blue, green-blue, or orange. There are very few bright 'true' green or red EL phosphors available and efforts to improve the colour range have been mostly unsuccessful [9]. An alternative approach is to print a bright dark blue EL lamp, and then print quantum dots (QDs) onto the EL lamp. The QDs act as optical down-converters and absorb the blue light, transforming it into either green or red light depending on the diameter and material of the QD. This approach was first demonstrated by Wood et al and acted as a proof of concept [56]. Wood et al's paper reproduced in Figure 20 shows the emission of the blue EL lamp as well as the absorption and emission spectrums of the green and red QDs. This approach offers designers of EL lamps on fabric a potentially much greater range of available colours.

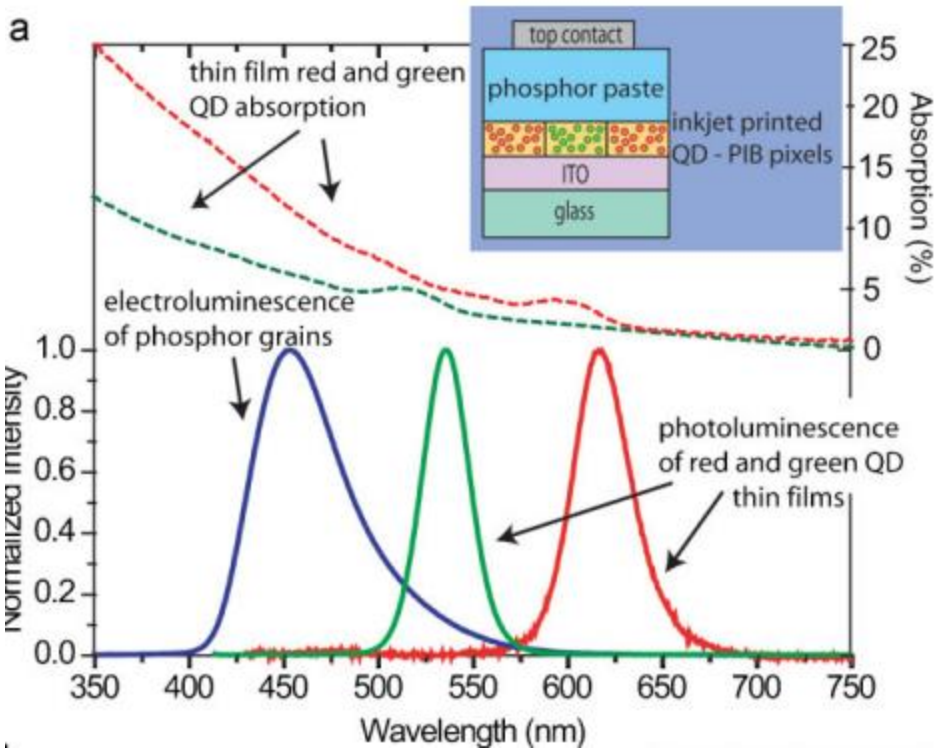

Figure 20. *Emission spectrum of a blue EL lamp and absorption and emission spectrums for red and green QDs. Top cross-section shows the structure used by Wood et al. (Image from Wood et al. [56])*

2.4. Conclusions

The work in this chapter has considered dispenser printing compared to screen-printing, finding it has the advantages of an easily changeable design and wide ink viscosity range. A technique previously used to assess the quality of screen-printed layers will be used to characterise the finished dispenser devices. The screen-printing literature review also showed that although some printing techniques can print very narrow tracks (30 µm width), the performance is significantly affected with resistance in this case being 10 times higher compared to a 200 µm track.

Screen-printing is a more established printing method and will be used when characterising new materials to provide a reference point for the subsequent dispenser printed devices. The review of inkjet printing showed it is not suitable for use in this research due to the ink limitations. While 3D printing is targeted towards building much larger 3D structures, it was identified as utilising similar control software. The control software that splits a 3D object into individual print layers with a tool path will later be investigated to be used to save development time on the dispenser printer.

Based on the literature review dispenser printing was selected to be used as the main printing technology for this research. A pneumatic dispenser will be used combined with XYZ moving stages. Initially, a smaller printer known as the ‘G1’ printer will be used until a larger more capable ‘G2’ printer is built.

There has been very little research published in the field of dispenser printing, and none printing EL lamps, making it an exciting and novel area to investigate. The limited publications on dispenser printing

showed the narrowest track that had been printed was 50 μm wide, however an earlier review on screen-printing had already shown that the resistance of tracks increases non-linearly with a decrease in dimensions. Therefore, it was decided that all tracks would be in excess of 200 μm wide to avoid high resistances.

Literature shows that EL lamps have been researched since 1936; however little work has been published on printed EL lamps and no working demonstrations could be found on non-plastic woven fabric substrates. Combining EL lamps with dispenser printing is a novel approach offering the possibility of flexible light sources on fabric without the restrictions imposed by screen-printing.

A review of the materials used in EL lamps showed that work can be performed in optimising the layer thickness. Areas to investigate include a full characterisation of commercially available colours and the performance of transparent conducting materials. The commercial phosphor particles were shown to be optimised for either brightness or long lifetime. For this research the phosphor particles optimised for brightness will be used.

More recent publications show a revival in research into EL lamps due to their robust nature. Two areas that have received particular attention are EL lamps on stretchable substrates and EL lamps with printed QDs on top to significantly improve the range of colours. The second of these areas could in future be combined with this research to create a full colour display on woven fabric.

3. Improved Dispenser Printing Parameters

3.1. Introduction

Dispenser printing has many factors that can affect the amount and characteristics of the ejected ink. Factors such as nozzle to substrate separation distance and print speed are kept constant to simplify the print process and typically only the dispense pressure is varied. Throughout this work different inks will be printed and a reliable method to identify a suitable dispense pressure is required. The method should be as fast as possible to allow more time to be spent printing and should use as little ink as possible to reduce wastage.

In this chapter two methods to find a suitable dispense pressure are considered:

- An experimental only method that involves printing a test pattern at different pressures with a visual inspection to identify the best parameters to use.
- A COMSOL simulation of the dispenser printer to estimate a flow rate. A target flow rate for each constituent ink required to fabricate an EL lamp has already been identified via experimentation. The results from the model can be compared to these values to define the relevant printer settings for new materials.

3.2. Experimentally Identifying Dispense Parameters

In order to identify a suitable dispense pressure, a range of typical dispense pressures will be tested to identify the best performing dispense pressure to +/- 1 kPa. Finding the settings experimentally has the advantage of being simple and requiring no knowledge of the properties of the ink you are printing. However, it has the disadvantage of using up ink in the testing process and can be time consuming given the number of adjustable parameters.

In this section, an interface ink and a silver ink are tested to identify a suitable dispense pressure. For all tests a substrate to nozzle separation distance of 220 µm and a print speed of 10 mm/s were used to ensure only the dispense pressure changes are causing the changes seen in the printed layers. The print speed was tested later chapter 4.2.2 and 10 mm/s was found experimentally to give repeatable high quality prints. As discussed previously in chapter 2.2.5 the nozzle to substrate separation distance can reduce flow rate if the nozzle comes into contact with the substrate so a value of 220 µm was found experimentally to be sufficient to avoid this happening.

3.2.1. Experiment Design

The majority of dispenser inks used in this thesis can be printed with a dispense pressure of between 10 and 110 kPa. To identify the best performing dispense pressure a test print will be completed while the pressure is varied after each print over pre-defined values. A process to identify the best dispense pressure was developed that will give the best dispense pressure to the accuracy described earlier without having to complete a print with every pressure value between 10 and 110 kPa. The process is described in Figure 21 below and involves initially printing 60 kPa (in the middle of 10 and 110 kPa). A visual inspection of the sample is completed and then the user can decide whether a higher or lower print pressure is required. The visual inspection process looks for ink that has bled significantly suggesting too much ink, or a track that has broken up as not enough ink was deposited. This process is

described later in this chapter. The process of testing the middle of the possible range of pressures continues for prints 1-4 as shown below. After this a series of three values are tested for prints 5-7 and one of these three values will be the best performing dispense pressure setting. The experimental process could miss sharp peaks in performance between the final test dispense pressure, however the movement stage accuracy and nozzle to substrate height variations are such that these errors will far exceed any lost performance from a dispense pressure accurate to +/- 1 kPa.

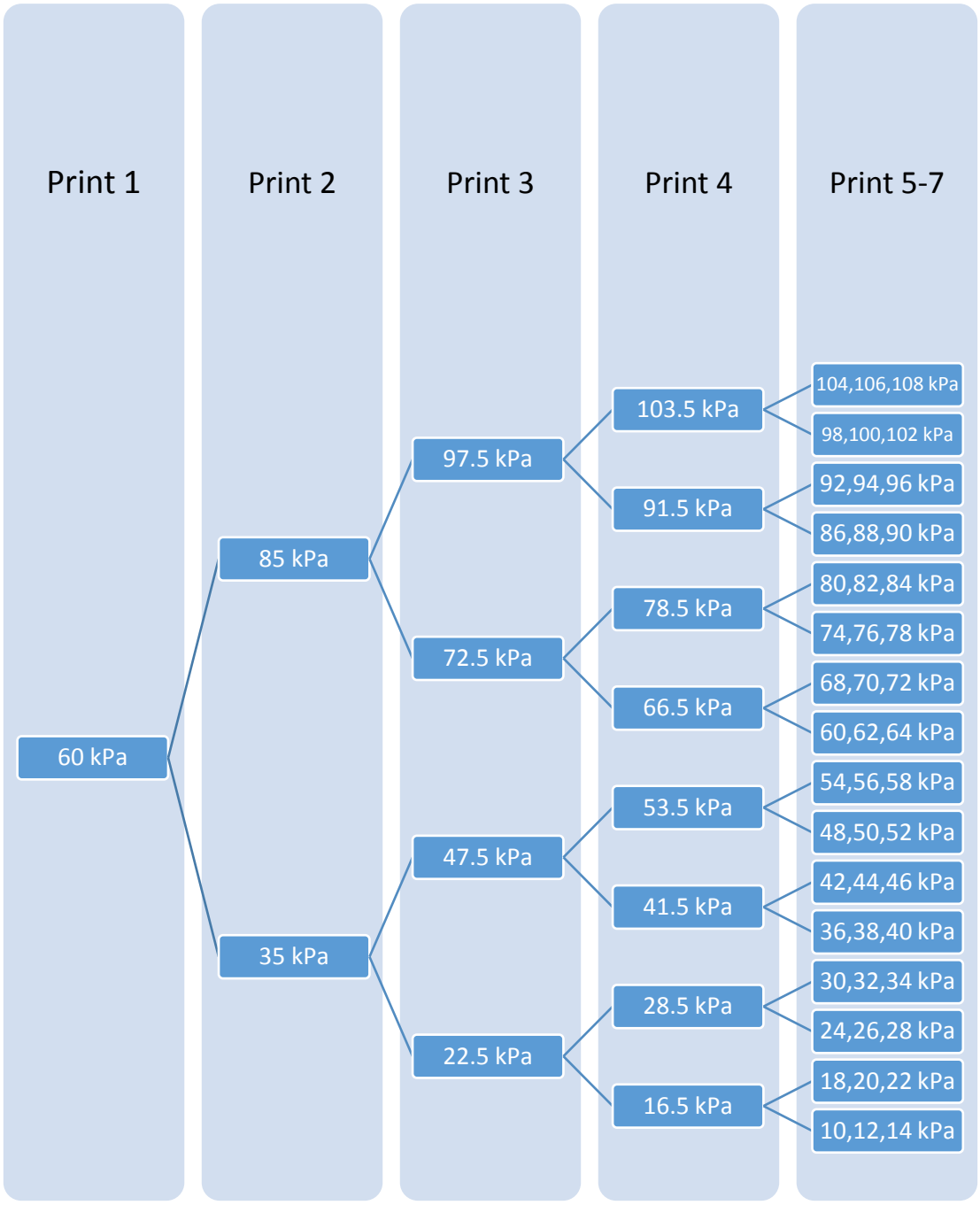

Figure 21. *Flow diagram showing the process to identify the best dispense pressure experimentally.*

The test print pattern consists of five 50 mm tracks printed for each pressure. Using the latest dispenser software, developed as part of this thesis, it is possible to upload a 'multi-layer' design that pauses the printer between each layer. This is usually to allow the user to change the ink in the syringe and adjust the print height, however in this case these parameters will be kept constant and the dispense pressure will be changed. The print pattern is shown in Figure 22 below. It shows the five tracks that will be printed for a single dispense pressure, each track is 50 mm long, approximately 0.3 mm wide and have 5 mm spacing between them, meaning a single pass of the print head for each track. The width is approximate as the nozzle is 0.25 mm diameter but the ink will bleed after deposition depending on how much ink was deposited. A total of seven of the patterns shown in Figure 22 are printed to identify a suitable dispense pressure.

Figure 22.*Drawing showing the print pattern to be used for each dispense pressure to be tested.*

After each of the first four prints the user will have to decide whether the dispense pressure was too high or low, and then decide which is the best print of the final three layers. This decision will be made after a visual inspection of the five printed tracks. Figure 23a below shows an example of a printed silver ink track with a dispense pressure that is too low. As can be seen the track has started to break up as the ink flow rate cannot maintain a continuous stream of ink at that print speed. Figure 23b shows tracks printed with a suitable dispense pressure. The tracks have straight edges and a uniform diameter along the entire length. The tracks in Figure 23c show a print with too high dispense pressure. The excess ink has created a very thick track that has quickly bled away from the defined track creating a non-uniform diameter.

As a further measure to determine whether the dispense pressure was too high or low, a quantitative approach of measuring the variation in line thickness can be used. An example is shown in Figure 23a where the variation is 0.18 mm between the widest and narrowest points on the line, this measurement can be easily found using a digital microscope. The aim is to minimise this variation as much as possible, and when correctly set a value of 0.02mm or below is expected.

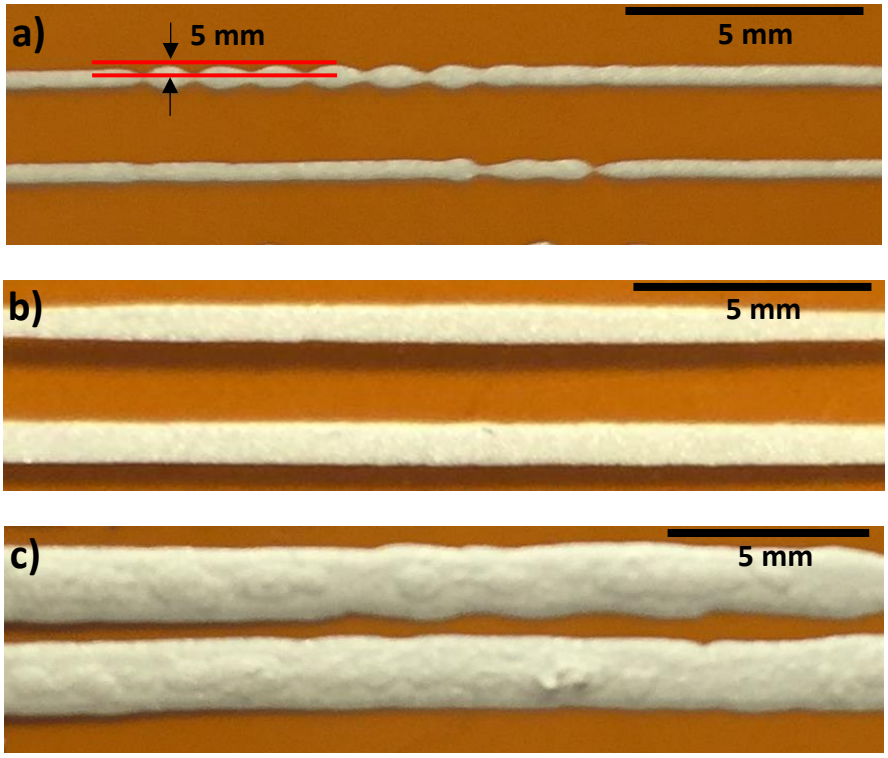

Figure 23. *Printed silver ink tracks with a pressure of in a) 10 kPa (too low), b) 20 kPa (ok), c) 80 kPa (too high).*

3.2.2. Results

Two materials, interface and silver ink, were printed onto Kapton polyimide file to demonstrate the process of finding a dispense pressure. Kapton was selected as the substrate as it is smooth and does not absorb the ink, allowing for an accurate comparison to be made. The process described in 3.2.1 was used to identify the best performing dispense pressure for both materials. The settings found were then used to print the first two layers of an EL lamp (interface with silver on top) to demonstrate the settings were correct.

As explained earlier, the setting used in Table 2 below were kept constant for all tested dispense pressures for both materials. Table 3 shows the results of the dispense pressure tests for the interface and silver inks with the results of the visual inspection after each print. Table 4 shows details of the tests on the silver ink along with a picture from each printed layer highlighting why the pressure was deemed to be too high or too low. The results show that the best dispense pressure for interface ink is 100 kPa and for silver ink is 20 kPa.

Table 2. *Constant nozzle separation and stage speed chosen for the dispense pressure testing with interface and silver ink.*

Nozzle to Substrate Separation Distance	Dispenser Stage Movement Speed
220 µm	10 mm/s

Table 3. *Results from the dispense pressure testing with interface and silver inks.*

Print Number	Layer Details	Interface Ink	Silver Ink
1	Print Pressure (kPa)	60	60
	Result	Too low	Too high
2	Print Pressure (kPa)	85	35
	Result	Too low	Too high
3	Print Pressure (kPa)	97.5	22.5
	Result	Too low	Too high
4	Print Pressure (kPa)	103.5	16.5
	Result	Too high	Too low
5	Print Pressure (kPa)	98	18
	Result	Too low	Too low
6	Print Pressure (kPa)	100	20
	Result	Ok	Ok
7	Print Pressure (kPa)	102	22
	Result	Too high	Too high

Table 4. *Description and image of a printed silver track for each print number highlighting the justification for whether the pressure was too high or low.*

Layer and Description of Print	Image of Printed Track from Layer
Print 1 – Too high pressure as the track has quickly bled away from path.	
Print 2 – Too high pressure, similarly the edge of the track is non uniform due to excess ink.	
Print 3 – Too high pressure, similar to layers 1 and 2.	
Print 4 – Too low pressure as the low flow rate caused a small break in three of the tracks.	
Print 5 – Too low pressure. Reduced effect compared to layer 4 and only in one track but could cause problems on larger prints.	
Print 6 – Ok pressure. Track appears uniform.	
Print 7 – Slightly too high pressure. Slight bleeding and uneven edge.	

This experimental procedure takes approximately 10 minutes to complete and therefore quickly identifies suitable printer settings to achieve the desired print quality. To demonstrate that these dispense pressures work with a practical device, a test print was carried out. The test print included four shapes using a dispense pressure of 100 kPa. Two of the shapes were then printed with a silver layer on top, as they would be in the target EL lamp application. The samples were printed onto a woven fabric as opposed to the Kapton tested on earlier to demonstrate the inks on a substrate that would be used in the target EL lamp application. The fabric represents a more challenging substrate as the ink is more prone to bleeding or being absorbed if an incorrect amount of ink is deposited. The results are shown in

Figure 24 below and show all layers were successfully printed without excessive bleeding or sections missing due to incorrect dispense pressure.

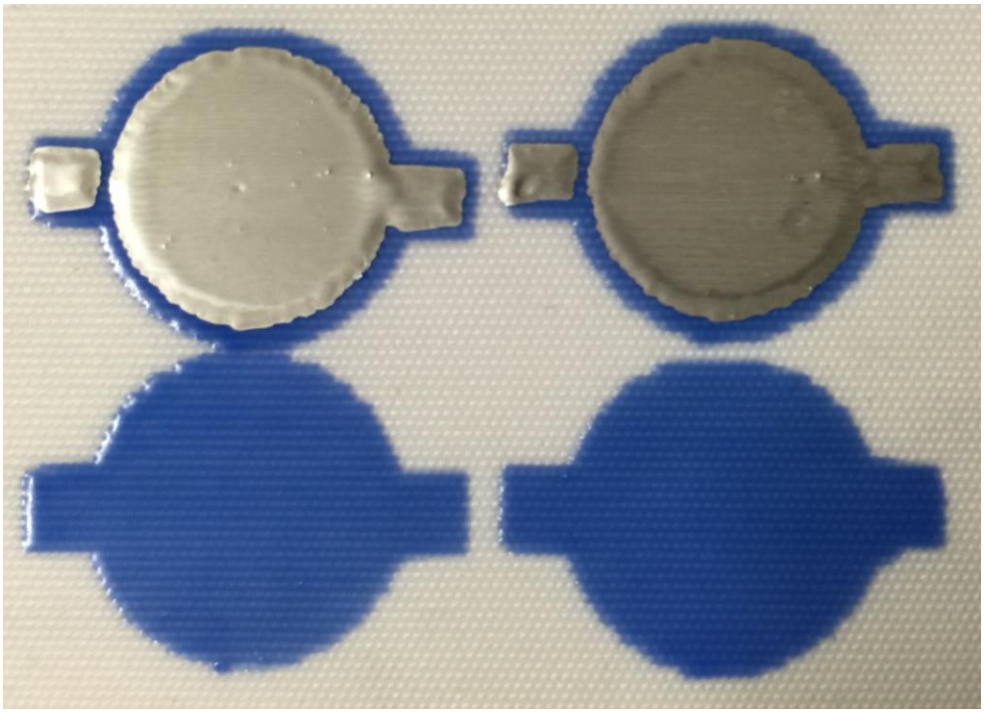

Figure 24. *Image showing four printed samples of interface, two of which are printed with a silver layer on top to demonstrate the dispense pressures found experimentally.*

3.3. Modelling a Pneumatic Dispenser Printer Syringe

An alternative method to identify a suitable dispense pressure is to use a finite element model to determine the flow rate in relation to a specific dispense pressure. The model could automatically try different dispense pressures until a flow rate closest to the defined target flow rate is found. Building a model allows variations of the dispense pressure to be tested without wasting material on practical print tests. The disadvantage of using a model is it requires exact material parameters, such as viscosity, surface tension, and density, to be known. These parameters are often not available from the manufacturers, meaning the time consuming process of measuring them must be undertaken.

COMSOL Multiphysics finite element modelling software was used to build the model as it actively supports fluid flow simulations and offers an easier to use interface than ANSYS, the only other major competitor. The work in this section focuses on building and testing the model, by way of a comparison with a real world system.

The final procedure for identifying a suitable dispense pressure will be based on a flow rate found from a single set of experiments as described in the previous section. The process of finding the optimum flow rate is described in greater detail later in this chapter. Once the target flow rate for the silver or interface layer has been found, different materials could then be modelled that would require different dispense pressures to achieve the same flow rate. The same target flow rate could only be used if the ink needed to be the same thickness.

3.3.1. Model Geometry

In a dispenser printer the dispenser controller is programmed to produce controlled pulses of air at a desired pressure for a desired duration. The dispenser controller is connected to the syringe using a flexible piece of tubing. The syringe has a nozzle attached and contains an amount of ink with air filling the remainder of the syringe. The nozzle is positioned to have an air gap underneath, allowing the ink to escape the nozzle onto the substrate.

The model is simulated from the exit of the dispenser controller to the substrate surface. The model includes the compression of air in the tubing between the dispenser controller and syringe. The movement of the ink after contact with the substrate is not currently considered as it does not affect the flow rate of the ink through the nozzle and adds to the simulation time. The syringe is initially considered to be half full as this was found to be the most common case during initial prints for this thesis. The size of the syringe and nozzle is based on physical measurements taken from the syringe (Intertronics 3cc), and nozzle (Intertronics SmoothFlow 250 µm tip) used for all work in this thesis. The Intertronics syringe and nozzle parts are shown in Figure 25(a) below, and the model based on these parts is shown below in Figure 25(b). The model includes an area defined as the “air gap under the nozzle”, this is to define the area of air under the nozzle that the ink moves in. If it was left undefined it would be modelled as a vacuum and would be inaccurate.

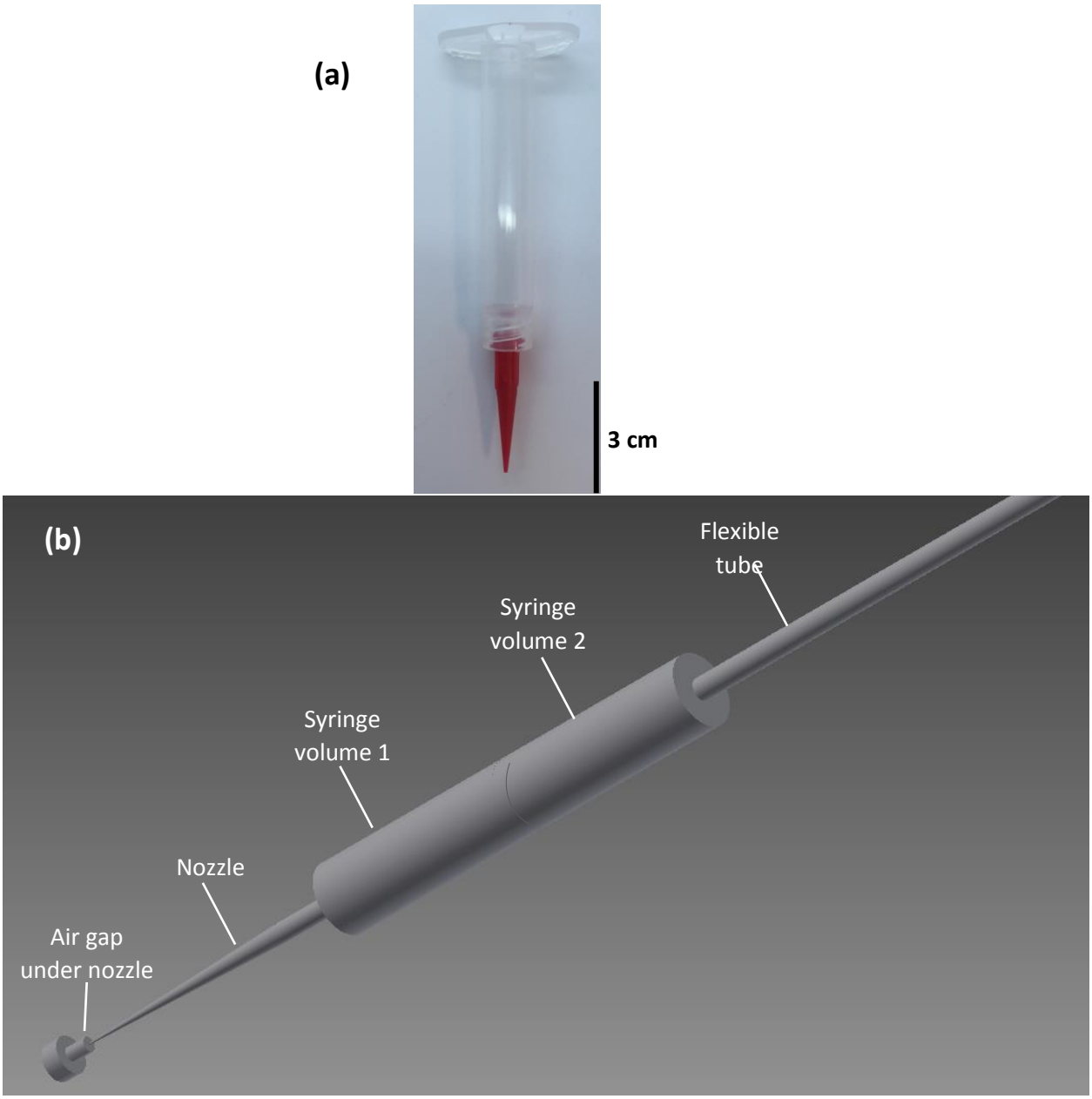

Figure 25. (a) Intertronics 3cc syringe and Intertronics SmoothFlow 250 µm tip. The COMSOL model is based on these parts as they are most commonly used when dispenser printing. (b)Model geometry based on the measurements taken from the physical parts. Syringe volume 2 and the flexible tube are filled with air, and syringe volume 1 and the nozzle are filled with ink. The flexible tube is 91 cm (3 ft) long so not fully shown.

To reduce solution time an axisymmetric 2D model will be used in COMSOL, where the centre line of the cylinder is used as the line of symmetry to be rotated around. Modelling in 2D significantly reduces the computational load and yields identical results in models such as that shown in Figure 25 where a symmetry can be identified.

3.3.2. Theories Defining the Model and Initial Conditions

After the model geometry was established, a series of variables were defined that would govern the behaviour of the model. A variable called 'inlet' was defined that gave a pulse from 0 to 1 for a desired

period of time. The slope could be controlled to represent the time taken to pressurise the syringe. The time taken to pressurise represents the time take to change the pressure of physical volume of air in the syringe (approximately $1.6e^{-6}m^3$) from atmospheric to the defined pressure. The pressurisation does not happen instantly as there is a maximum flow rate through the narrow tube leading to the syringe. An estimate of 2ms was used in the model as this value was found experimentally using an in line pressure sensor plugged into a National Instruments ADC. The test was repeated 3 times giving an average of 1.96ms so an estimate of 2ms was used in the model. The 'inlet' variable was multiplied by a 'set_pressure' variable in Pascals to give the absolute inlet pressure profile.

The interfaces between the ink and air must be defined so the model can correctly predict the fluid flow. An initial interface is defined between the ink and air halfway along the syringe; a second interface is defined between the ink in the nozzle and the air underneath. The Laminar Two-Phase Flow, Level Set method in COMSOL Multiphysics was selected to track the fluid interface. COMSOL offers a second option called Laminar Two-Phase Flow, Phase Field however the description states that while it solves faster it is much less accurate so it was not used for this work. The initial position of the ink and air in the model is shown in Figure 26 below. COMSOL displays the image inverted, however it has no effect

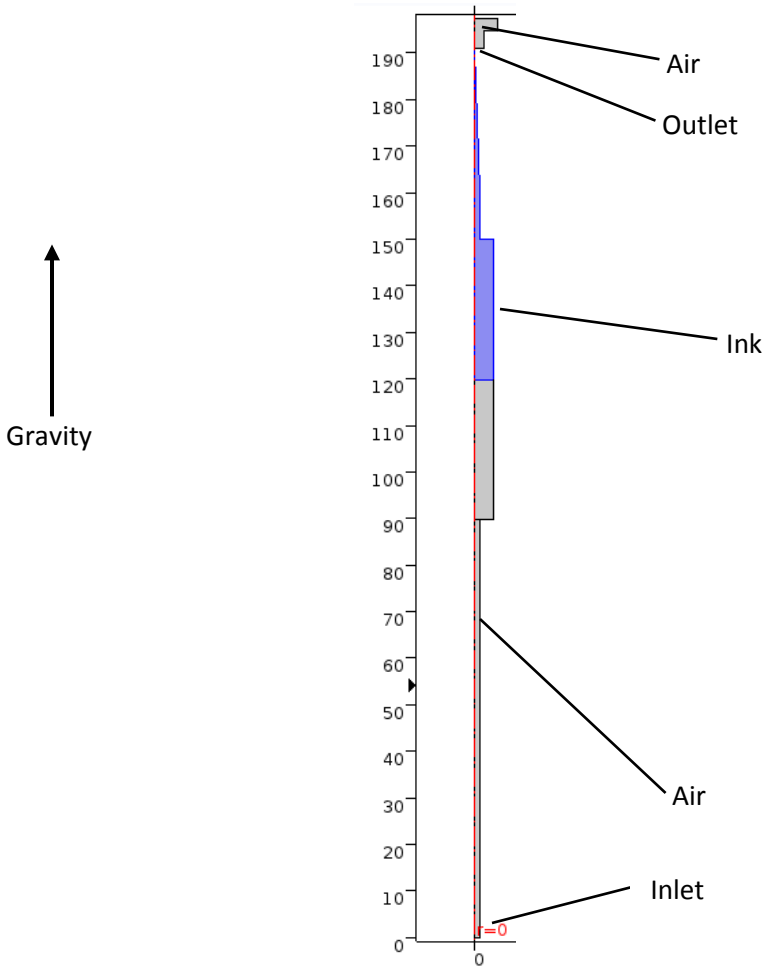

on the output as gravity is applied in the correct direction.

Figure 26. *Model geometry as shown in COMSOL, showing the boundaries between ink and air. The full length of the flexible tube is not shown (continues below 0).*

The material properties for air are set by COMSOL, whereas the ink's properties can be varied to simulate any dispenser ink. The surface tension, density, and dynamic viscosity are required for the ink, as well as the temperature for the overall system. A temperature of 21˚C was used as it was the average temperature of the room during printing.

Gravity is applied in the positive Y direction as shown in Figure 26. The inlet and outlet are also defined in the figure. The simulation tracks the boundaries of the ink during the simulation time, meaning droplet formation can be seen.

The model is defined into a number of points using a mesh and the size of the mesh is selected using descriptive words such as 'coarse' or 'fine'. A fine mesh was used for the majority of the model, which should give sufficient resolution to track the fluid movement. Around the nozzle tip an 'extremely fine' mesh was defined to accurately track the fluid flow on the boundary. The fine mesh around the nozzle is shown in Figure 27 below. COMSOL offers an option for adaptive mesh refinement, whereby the mesh is capable of moving during the simulation to track points of interest that appear. The feature was not used as it increased simulation time from around ten minutes to over three hours. The requirement for the model is based on the idea that it shortens the testing times for an ink to identify suitable dispensing parameters. If each simulation takes over three hours and multiple simulations are required to identify the best parameters then it devalues the model. The effect of the adaptive mesh refinement was enabled and the output compared to a simulation with it disabled. With the adaptive mesh refinement enabled the flow rate was 0.5% higher so the effect was assumed to be minimal.

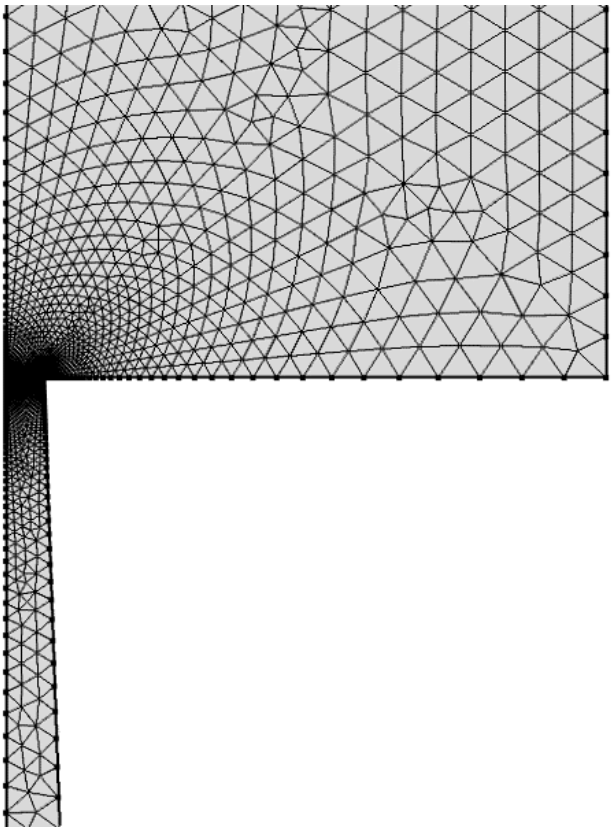

Figure 27. *Image showing the mesh geometry around the nozzle outlet. A much finer mesh has been used to track the fluid interface accurately.*

To calculate the best dispense pressure the flow rate through the nozzle had to be calculated. A boundary was defined in COMSOL along the bottom of the nozzle where the ink is ejected into the air. A continuous integration was calculated during the simulation along this boundary, meaning the total volume of dispensed ink could be found. An alternative method to identify the flow rate was tested where the volume of the ink was calculated at the end of the simulation. The method works by measuring the volume of the ink droplet at the end of the nozzle. However, the method described that measures the ink as it exits the nozzle was found to be the fastest to solve and the different methods had less than a 1% difference between the results. COMSOL engineers also advised that on some ink simulations the method that measures the volume of the formed droplet could be inaccurate due to the small volume size. Therefore, the first method where the volume is calculated using a continuous integration was used for all tests.

3.3.3. Calculating the Target Ink Flow Rate

The model will try different dispense pressures until a target flow rate is reached. The process described in Figure 21 will be followed to reduce the number of computations that have to be performed. To test the model these target flow rates had to be found for the interface and silver inks tested in this chapter. The target flow rates for the inks were found using the best performing dispense pressure found in 3.2.2. Once these target flow rates have been found they could be used to identify the dispense pressure for other interface or silver inks. To avoid minor errors during printing affecting the result, a series of 120 50 mm long tracks were printed onto each piece of Kapton polyimide film. Five individual

samples were produced with 120 tracks on each. Kapton was selected as the sample due to its smooth surface and because it doesn't absorb the ink. The dispenser printer settings are shown in Table 5 below.

Table 5. *Dispenser printer settings for model validation tests with interface and silver ink.*

Ink	Dispense Pressure	Vacuum Pressure	Print Speed	Nozzle to Substrate Separation Distance
Interface	100 kPa	1.1 kPa	10 mm/s	220 µm
Silver	20 kPa	1.1 kPa	10 mm/s	220 µm

Each Kapton piece was weighed before and after printing the ink. The interface ink was cured in a UV box for two minutes and the silver ink was cured at 120°C for 10 minutes. The samples were also weighed after curing to see how much of the mass was lost through evaporation. The results are shown in Table 6 below.

Table 6. *Measured masses of samples printed with interface for model validation tests.*

Ink	Sample Number	Mass of Wet Ink (g)	Mass of Dry Ink (g)
Interface	1	0.130	0.127
	2	0.135	0.131
	3	0.134	0.130
	4	0.133	0.130
	5	0.134	0.130
	Average	**0.133**	**0.1296**
Silver	1	0.542	0.432
	2	0.527	0.415
	3	0.511	0.394
	4	0.563	0.454
	5	0.517	0.406
	Average	**0.532**	**0.420**

The five samples are very closely grouped for the interface ink with a standard deviation of the wet ink masses of 4.4×10^{-4}. There is more variance in the silver ink results (standard deviation of 6.7×10^{-3}) as the ink has silver particles that occasionally partially block the nozzle before clearing. The silver ink also loses significantly more mass during curing than the interface. This is due to the solvent used in thermally curable inks that evaporates during curing compared with the solvent used in UV curable inks that also performs the role of a photo-initiator for the polymerisation process and is therefore mostly consumed during curing. Using the results in Table 6 and the printer settings described earlier, it is possible to calculate the volume of ink dispensed and the flow rate of the dispenser. The results are shown in Table 7 below.

Table 7. *Summary of calculations to identify the printed track volume and dispenser flow rate.*

Ink	Average Mass of 120 Printed Tracks (g)	Average Mass of Single Printed Track	Average Volume of Single Printed	Dispense Time for Single Printed Track	Dispenser Flow Rate (nL/s)

		(mg)	Track (nL)	(s)	
Interface	0.133	1.11	972	5.30	183.4
Silver	0.532	4.43	2007	5.30	378.7

The flow rate for both inks were found. The model can be entered with these target flow rate and the user will follow the process in Figure 21, comparing the flow rate after each simulation against the target flow rate and then finding the next dispense pressure depending on whether the flow rate was higher or lower than the target. In future this process could be automated within COMSOL.

3.3.4. Measuring Ink Characteristics

In order to accurately model the behaviour of the ink the shear viscosity, surface tension and density of the ink had to be measured. The measurement process is discussed in detail below for the interface ink. The same process was followed for the silver ink and the results for both are shown together at the end of this section.

The viscosity was measured using a Brookfield CAP 1000+ viscometer, which is a cone and plate system with a fixed rotation speed of 10rpm. Multiple measurements were taken with each sample of the interface ink; each measurement was an average taken over a 60 second period. The interface ink used spindle 3 (~20mPa.s to 80mPa.s) and the silver ink used Spindle 1 (~2mPa.s to 10mPa.s). The time between measurements can be altered as some materials show thixotropic properties, meaning the measured viscosity reduces if tests are conducted with no delay compared to a 60 second delay. To check whether the interface responded in this way, samples were measured using no delay between measurements and with a 60 second delay between measurements. The results are shown in Figure 28 below. The error was calculated by measuring a calibration fluid five times and calculating the standard deviation to identify the error inherent within the measurements.

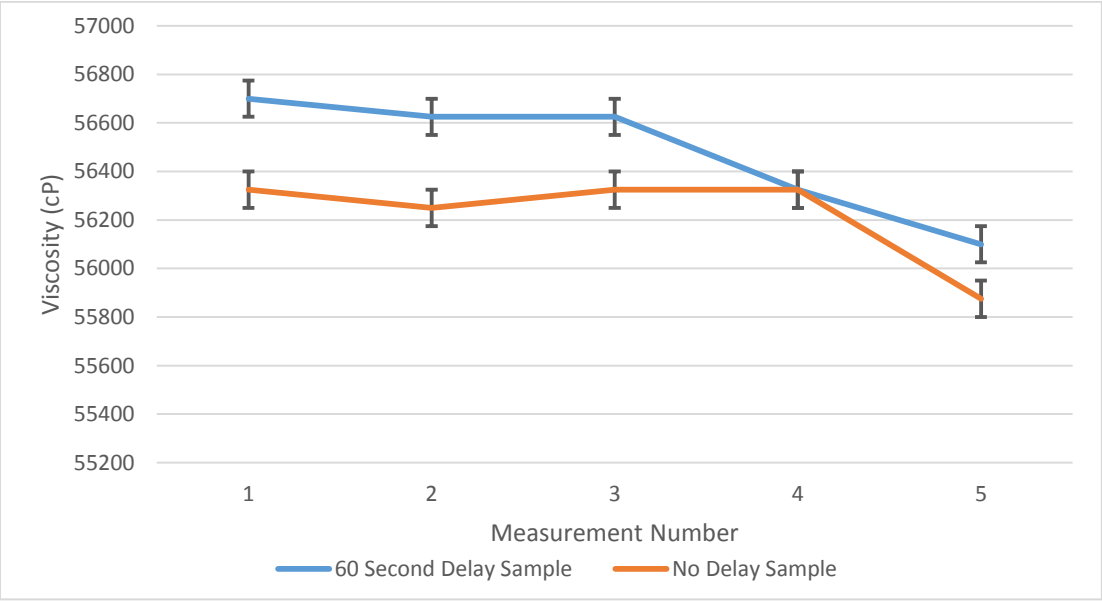

Figure 28. *The viscosity of interface paste when measured with a 60 second delay between measurements, compared to the viscosity when measured with no delay between measurements*

The results show that both the sample with the 60 second delay between measurements and the sample with no delay between measurements had a viscosity that declined during the measuring process. The sample with the 60 second delay declined 600cP compared to 450cP for the sample without the delay. This is the opposite of the expected effect, as most printing inks are thixotropic, meaning the longer the material undergoes a shear stress the lower the viscosity. The most likely explanation is a slight measurement error from the viscometer and that that the 60 second delay makes no measurable difference to the results. The overall effect of a lower viscosity as more measurements are taken was expected as the material gradually spreads over the measurement plates and thins meaning less material is in between the measurement plates. In these tests no delay will be used between measurements to reduce the testing time.

Five separate samples of the interface paste were measured using the 'no delay' method. Each sample had an initial measurement taken that was discarded, followed by five further measurements. The initial measurement is not accurate as the paste has not fully coated the disc of the viscometer. A test was conducted and confirmed there was a full coating of the disc after a single 60 second period of movement.

Each of the five samples had five measurements taken; an average of all the first measurements was calculated, followed by an average for all the second measurements, this continued to an average for the fifth and final measurement. The results are shown in Figure 29 below.

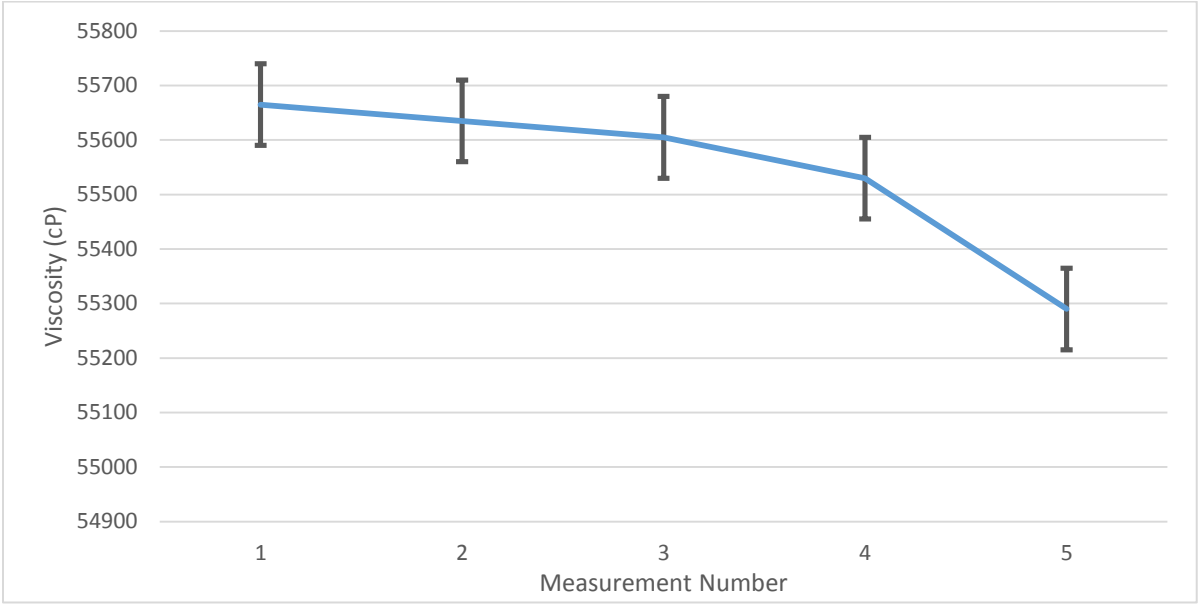

Figure 29. *Average viscosity of five samples of interface ink measured five times each.*

The results show a slight reduction in viscosity after each measurement. For the model the average of the first measurements will be used. The first measurement is closest to the conditions the ink will be experiencing in the dispenser as it will not have been moving significantly prior to being ejected from the nozzle. The average of the first measurements for the interface ink is 55700cP.

The surface tension was measured using a KRUSS DSA30 drop shape analyser. The ink was loaded into a syringe and the maximum amount of ink was ejected from the syringe to form a large droplet at the tip

of the needle without the droplet falling. The equipment then calculates the surface tension from the shape of the droplet. This process was repeated five times and an average was taken. The measured average surface tension is 5.94 N/m for the interface ink.

The density was measured using Ohaus Voyager Pro scales. A syringe was zeroed on the scales and then filled with 3 ml of ink and measured. This test was repeated five times and averaged. To verify the measurement process the test was repeated with water. The measured density of the interface was 1.142 g/ml.

These measurement processes were repeated for the silver ink. As with the interface ink no significant difference was observed between the viscosity measurement with a 60 second delay and without it. As with the interface, an average of the first measurements was used to determine for viscosity. A summary of the measured material properties is shown in Table 8 below. These values were then used in the model to simulate how the respective ink will behave.

Table 8. *Summary of the measured interface and silver ink properties.*

Ink	Viscosity (cP)	Surface Tension (mN/m)	Density (g/ml)
Interface	55,665	5.94	1.142
Silver	6,450	33.51	2.209

3.3.5. Validating the Model

To validate the model and show that it can accurately identify a suitable dispense pressure to +/-1 kPa when given the material properties and a target flow rate, simulations were run on the interface and silver inks discussed in this chapter. If the model is sufficiently accurate, the results should match those found in 3.2.2 and show that 100 kPa and 20 kPa are the best dispense pressure for this specific silver and interface ink.

The simulation results at various pressures defined by the process described previously in Figure 21 are shown in Table 9 below. The simulation was run for 0.15 seconds to reduce simulation time and scaled linearly to 5.3 seconds as this was the time the ink was dispensed for to print a 50 mm line as used in the experimental section. A test simulation run for 5.3 seconds showed a dispensed ink mass with a difference of less than 1% compared to a scaled 0.15 second simulation suggesting a minimal change in accuracy. The simulation returned the simulated dispense mass and flow rate was then calculated from this.

Table 9. *Results from COMSOL simulations on interface and silver inks at various pressures.*

Interface Target Flow Rate = 183.4nL/s			
Set Dispense Pressure (kPa)	**Simulated Dispense Mass in 0.15 seconds (kg)**	**Simulated Flow Rate (nL/s)**	**Decision Result**
60	1.439×10^{-8}	84	Too low
85	2.559×10^{-8}	149	Too low
97.5	3.038×10^{-8}	177	Too low
103.5	3.238×10^{-8}	189	Too high
98	3.088×10^{-8}	180	Too low
100	3.281×10^{-8}	183	Ok

102	$3.488x10^{-8}$	186	Too high
Silver Target Flow Rate = 378.7nL/s			
Set Dispense Pressure (kPa)	**Simulated Dispense Mass in 0.15 seconds (kg)**	**Simulated Flow Rate (nL/s)**	**Decision Result**
60	$3.282x10^{-7}$	991	Too high
35	$2.304x10^{-7}$	695	Too high
22.5	$1.454x10^{-7}$	439	Too high
16.5	$1.017x10^{-7}$	307	Too low
18	$1.126x10^{-7}$	340	Too low
20	$1.272x10^{-7}$	384	Ok
22	$1.362x10^{-7}$	411	Too high

The process of measuring the necessary parameters and completing the simulations for a single ink was approximately two hours. The majority of this time was spent measuring the viscosity as 36 measurements are taken and each takes at least one minute. It is possible that fewer measurements of viscosity could be taken as the values did not vary significantly. I estimate this would reduce the total time to measure and simulate a single ink to approximately one hour.

3.4. Conclusions

The results in this chapter have shown that a usable dispense pressure can be found experimentally by following a structured iterative process of testing various pressures. The dispense pressures found were shown to be usable in a subsequent successful print of both interface and silver layers.

The equivalent finite element model developed in this work is successful as confirmed by both simulations identifying the same dispense pressures for both inks in section 3.2.2. The error between the interface simulation and practical results was negligible (0.2%) and was 1.4% for the silver ink. The slight discrepancy can be attributed to the COMSOL model including some rounding errors at such small flow rates.

The simulation method allows a totally inexperienced user of the printer to identify the correct dispense pressure (+/-1 kPa) in approximately 1 hour. It is therefore recommended that new users of the printer use this method. The simulation method is also suited to very expensive inks, such as some semiconductor inks, that can cost up to £1000 for 5 ml. The model is also useful if a characterised ink needs to be deposited using a different syringe or nozzle. This scenario could be relevant if a larger printer was used where ink syringes are typically 10 ml not 3 ml. The geometry of the model could be quickly updated and simulations could be carried out to find the new dispense pressure to achieve the same flow rate.

The time taken for the simulation method (~1 hour) is still significantly longer than the experimental method (~10 minutes) and the inks are typically <£1000/kg so using a small amount of ink to experimentally find a suitable dispense pressure is not an issue. Therefore, for all further work in this thesis the experimental method will be followed to identify a suitable dispense pressure.

4. Dispenser Printer Hardware Development

4.1. Introduction

In order to print high quality EL lamps, significant development was needed on the dispenser printer. The key aspects of the printer addressed in this Chapter are:

- Characterise the hardware capabilities of the new printer (G2) built for the University of Southampton. These tests analyse the printer's speed and acceleration settings in order to identify the best compromise between print speed and repeatability.
- Add a displacement sensor and validate this by comparing results with a commercial profilometer. The displacement sensor enables a defined distance between the bottom of the nozzle and the substrate to be maintained.
- Analyse the base plate uniformity that could cause errors and attempt to correct. The base plate uniformity is a key source of errors during printing as the height can vary significantly.

4.2. G2 Dispenser Printer Characterisation and Comparison to G1 Dispenser Printer

4.2.1. Introduction

A dispenser printer has a number of key components as shown previously in Figure 8. The components' roles are described in Table 10 below. For each component the equipment used at the UoS is described along with its specifications. The UoS has two dispenser printers, known in this work as G1 and G2. The G1 was built first and is used for the initial part of this work; the G2 is a larger printer with a number of improvements to the moving stage accuracy and speed. The G2 dispenser printer uses a commercially available dispenser controller, with bespoke moving stages and motion controller as specified by the author. The control software for the G2 printer has been entirely developed in LabVIEW as part of this thesis. The G2 is used for the majority of work in this thesis.

Table 10. *Summary of the components in a dispenser printer and their respective specifications for the G1 and G2 printers at UoS.*

Component	Description	Part Parameter	G1	G2
Compressed air source	Provides compressed air through a regulator at 650 kPa.	Part Name	Jun-Air 0F302 compressor	Compressed nitrogen cylinder
Syringe and nozzle	The syringe holds the ink and is connected to the dispenser controller via an airline. The ink is ejected through the nozzle.	Component	Range of syringes from 3 cc to 50 cc, nozzles vary from 1 mm to 5 µm inner diameter producing lines from 2 mm to 10 µm.	Range of syringes from 3 cc to 50 cc, nozzles vary from 1 mm to 5 µm inner diameter producing lines from 2 mm to 10 µm.
3 axis moving stage and controller (data from [57] for G1, and [58] for G2).	Moves the substrate/nozzle to the desired location.	Component	Sigma Koki SHOT-204MS controller with 3 Sigma Koki SGSP 26-50.	Arcus PMX-4EX-SA controller with Arcus NEMA 23 motors. Moving stages by LG Motion.
		Resolution (µm)	2	0.5
		Max Speed (mm/s)	7	50
		XYZ Max Travel (mm)	50	500 (XY), 70 (Z)
		Max Load Mass (Kg)	10	10
Dispenser Controller (data from [59] for G1, and [32] for G2).	Controls the flow of air to the syringe. A pressure can be set for a desired dispense time.	Component	Musashi ML-808 FX COM-CE (range: 20 kPa-800 kPa)	Nordson EFD Ultimus V (range: 0.1 kPa-800 kPa)
		Dispense Pressure Range (kPa)	20-800	0-680
		Minimum Dispense Time (s)	0.01	0.0001
		Vacuum Pressure Range (kPa)	0-20 Digital	0-4.5 Manual
		Max Cycle Rate (cycles/min)	Unknown	600

The G2 dispenser printer software was upgraded as part of the CREATIF project funding this work. The printer offers the following advantages when compared to the G1 printer:

- Larger maximum print area of 45 cm x 45 cm (50 cm x 50 cm movement to allow this), compared to 5 cm x 5 cm movement for the G1.
- Stage movement speeds up to 50 mm/s, compared to 7 mm/s for the G1.
- Improved movement accuracy through use of optical encoder position feedback, compared to no positional feedback on the G1.
- Simultaneous movement of all 3 axes, compared to single axis movement only on the G1.

The G1 and G2 dispenser printers developed at the UoS is shown in Figure 30 and Figure 31 below respectively.

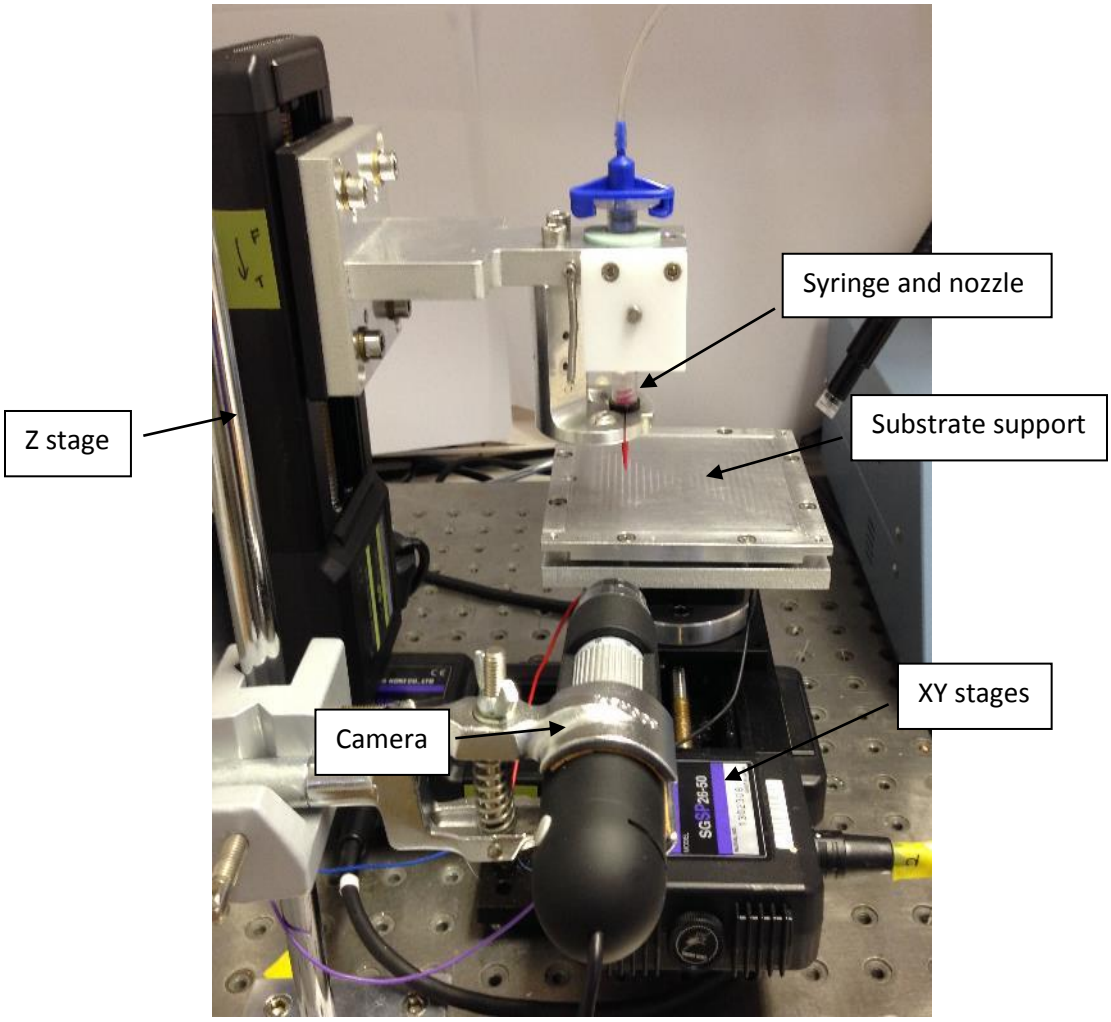

Figure 30. *UoS G1 dispenser printer.*

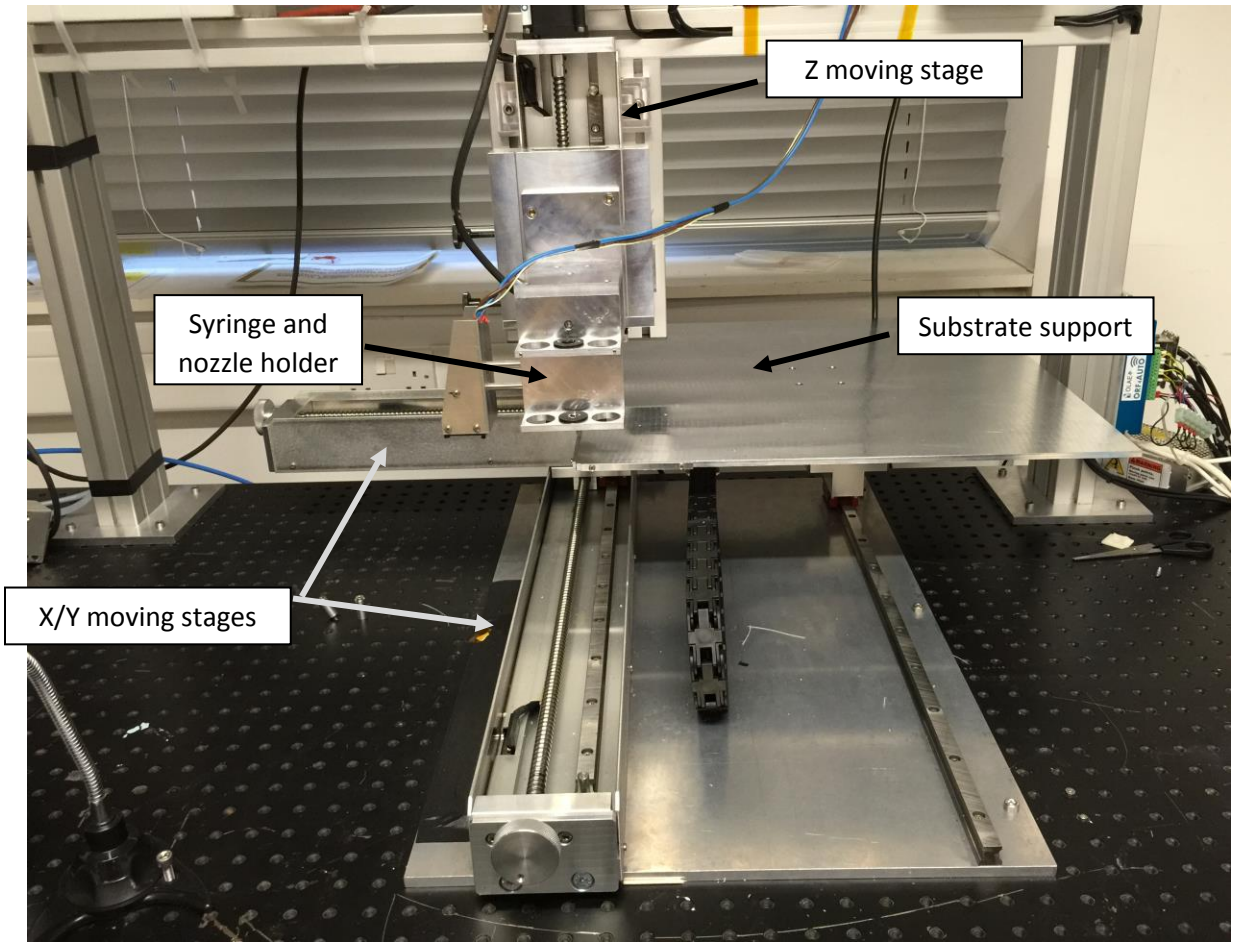

Figure 31. *UoS G2 dispenser printer.*

There are two dispenser printing modes available on both printers - droplet or continuous mode. In droplet mode the nozzle is moved into position and the ink is dispensed for a set period of time; the nozzle is then moved a defined distance and the process repeats. The layer is built up from a series of ink droplets spaced closely together to form a continuous line of ink. Droplet printing has the advantage of being a simple process making stage movement easy to control. However, the process is slower than continuous printing and excessively long print times, of the order of >15 minutes for a 4 x 4 cm filled square, can cause the ink to bleed from the desired pattern.

Continuous printing is where ink is continually dispensed from the nozzle while it is moved to create the desired pattern. The process is approximately 10 times quicker than droplet printing, however, stage control for complex designs can be challenging and requires an advanced motor controller. The motion controller on the G1 can only move 1 axis at a time so to print continuously it must follow a rectangular print patter. The G2 can move all axes continuously so can print any shape or pattern continuously.

Both the G1 and G2 motion controllers utilise a trapezoidal motion profile, whereby a low speed, high speed, and acceleration time are set. An example of a trapezoidal motion profile is shown in Figure 1 below.

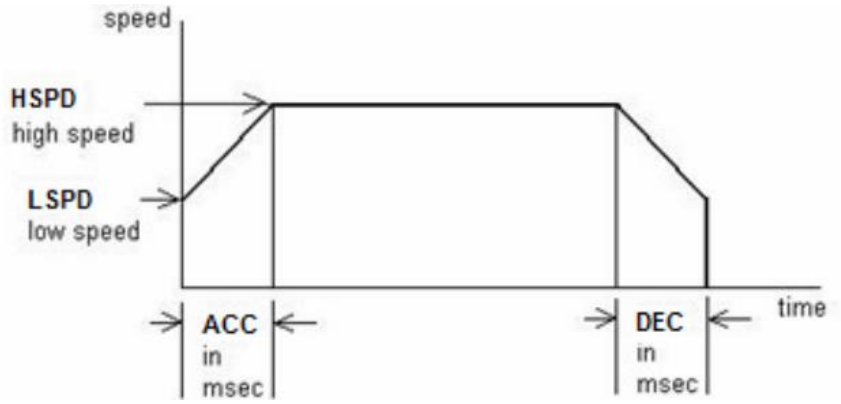

Figure 32. *Example trapezoidal motion profile used on G2 moving stages (Image from [58]).*

The G1 and G2 moving stage settings are shown in Table 1 below. The values are the default values recommended by the respective manufacturers.

Table 11. *G1 and G2 printer moving stage settings*

Parameter	G1	G2
Low Speed	0.1 mm/s	0.5 mm/s
High Speed	7 mm/s	50 mm/s
Acceleration Time	100 ms	300 ms
Calculated Acceleration	69 mm/s^2	165 mm/s^2

In the G2 printer the stages are set to accelerate to high speed over a period of 300ms. It is possible that for small movements the stages never reach their top speed and instead form a triangular motion profile as there is insufficient time to finish accelerating before reaching the desired positon.

Using the data from the G2 settings it can be shown that it takes a displacement of 7.58 mm, with an acceleration time of 300ms, to accelerate to full speed (50 mm/s). The distance to move between points in a typical droplet mode print is 1 mm or lower, therefore the top speed of the G2 stages is not being fully utilised in this print mode. In continuous print mode movements are typically longer than 15 mm so the full speed of the G2 stages is utilised.

The G1 settings show that it takes a displacement of 0.36 mm to reach the top speed of 7 mms^{-1}. For droplet mode prints with an X/Y resolution (distance between the droplets) greater than 0.71 mm the G1 will reach its top speed.

The G2 could make better use of its higher top speed by adjusting the settings of the stages to accelerate over a shorter period of time, however if the acceleration is too fast it could cause the stepper motors to skip, giving unrepeatable results. The datasheet for the moving stages offers no guidance on minimum acceleration time as it depends on the load on the stages, however all the examples in the datasheet use an acceleration time of 300ms. All tests use an acceleration time of 300ms unless otherwise stated.

4.2.2. Printer Speed Tests

A series of tests were developed to see how the max stage speed differences practically affected a dispenser printed device. A practical test gives greater insight than comparing the movement speeds alone as other factors such as the acceleration also affect the overall print time. For the practical print speed tests the syringe was left filled with air to simulate a printing scenario without having to waste ink. The print quality was not considered at this stage.

The droplet print mode was tested first - the dispense time used for all droplet mode tests was 10ms, a typical dispense time used in previous work within the group for the majority of inks in droplet mode. The overall print time was measured using a stopwatch and is therefore only given to the nearest second.

Tests were also carried out in continuous printing mode. So the results are comparable both the G1 and G2 printer followed the same print path. If a real print was taking place, ink would be ejected from the nozzle whilst the stages move in the X direction. The ink deposition would pause while the stages move up in the Y axis, before repeating to print the next row in the X axis. The time taken to complete a print for both printers in both print modes is shown in Table 12. A range of print areas were tested to check if the print time increased linearly with area.

Table 12. *Comparison of G1 and G2 printers in droplet and continuous printing mode.*

	Print Area	**10mm x 10mm**	**20mm x 20mm**	**40mm x 40mm**	**10mm x 10mm**	**20mm x 20mm**	**40mm x 40mm**
Print Mode	**Parameter**	**G1 Droplet**			**G2 Droplet**		
Droplet Mode	X/Y Resolution	X Res: 1 mm, Y Res: 1 mm					
	Dispense Time	10ms					
	Total Number of Droplets	121	441	1681	121	441	1681
	Stage Speed	7 mm/s			50 mm/s		
	Print Time (min:secs)	1:12	4:16	16:13	0:52	3:09	11:57
Continuous Mode	Y Resolution	1 mm					
	Stage Speed	7 mm/s			50 mm/s		
	Time Taken (min:secs)	0:34	1:46	6:10	0:14	0:27	1:05

The results from Table 12 are compared in Figure 33 below to check for linearity.

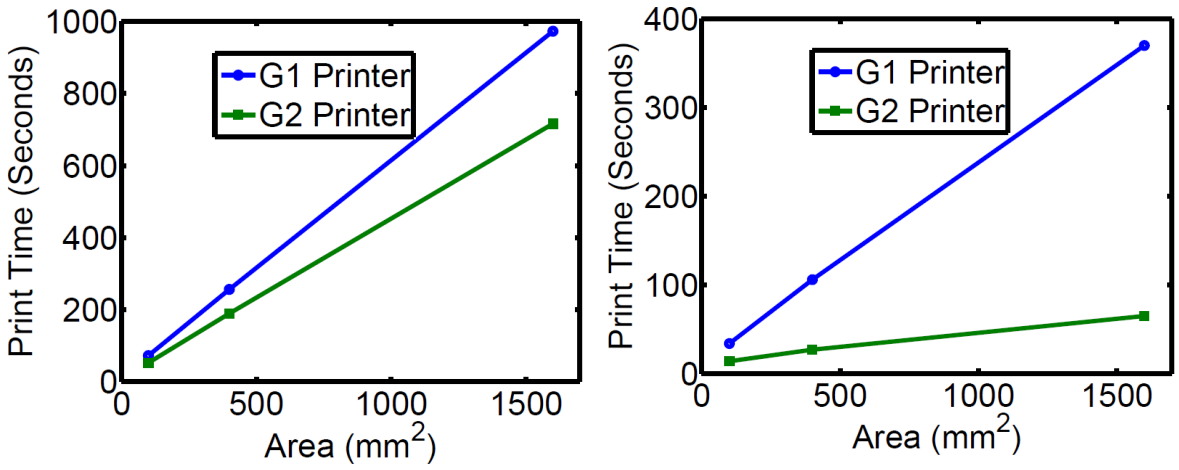

Figure 33. *Comparison of G1 and G2 print times relative to print area in droplet printing mode (left) and continuous printing mode (right).*

The print time for the G1 and G2 printers both increase linearly when using droplet printing mode. In continuous printing mode the print time for the G1 printer also increases approximately linearly. The gradient of the G2 printer plot decreases with a larger area, meaning it does not increase linearly. The decrease in gradient can be attributed to a larger percentage of the print time on each print row being spent at maximum speed for the longer movements of the G2. The effect is less apparent in the results for the G1 as it has a lower top speed and faster acceleration, meaning the majority of the print row is spent at top speed, even for smaller print areas.

The results show that the G2 offers a reduction in print time compared to the G1 in both droplet and continuous printing mode for all print sizes. Table 13 below shows the improvement in print time for the G2 on each of the print modes/sizes.

Table 13. *Print time improvements for the G2 compared to the G1 for all print modes.*

	Droplet Print Mode			**Continuous Print Mode**		
Print Size (mm)	**10x10**	**20x20**	**40x40**	**10x10**	**20x20**	**40x40**
G2 Multiples Quicker than G1	1.4 x	1.4 x	1.4 x	2.4 x	3.9 x	5.7 x

The overall reduction in print time across all print modes and print sizes is primarily caused by the increase in stage speed offered by the G2. In droplet mode the G1 print time improvement multiple remains constant for all print areas. In this mode the larger print areas offered no opportunity for a higher stage speed to be achieved relative to the small areas as the movement distance between droplets was only 1 mm in all tests. This caused the print time improvement multiple to remain constant across all print areas.

In continuous mode the print time improvement multiples increase as the print area increases. The increases are caused by a greater amount of the movement being spent at the top stage speed of 50 mm/s. As previously calculated, the G2 stages take 7.58 mm to accelerate to full speed. With a 40 mm movement this means 62% of the movement is spent at top speed, compared to only 24% with a 20 mm

movement. As the percentage of the movement distance at top speed increases, the improvements in print speed will begin to plateau. The start of this curve can be seen in Figure 34 below.

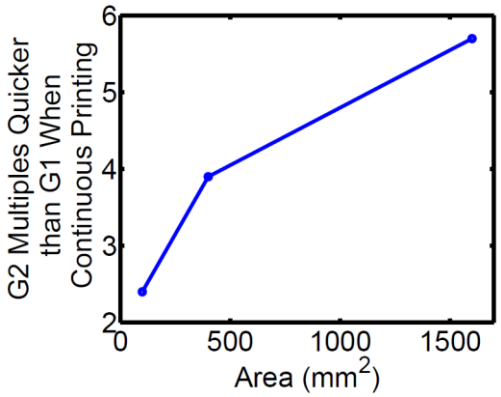

Figure 34. *Comparison of continuous print time improvement for the G2 relative to the G1 against print area.*

The results show that the G2 offers a significant increase in the print speed that should translate into a significantly lower print time. A significant part of the CREATIF project's work focuses on large area prints (50x50 cm) so the speed improvements will be valuable in reducing the time taken to manufacture devices. This is important as if ink is left uncured for an extended period of time then it will bleed away from the defined path.

4.2.3. G2 Printer Acceleration Tests

The acceleration time was altered for a series of X stage movements to test the capability of the G2 printer to perform more demanding movements. The tests were only carried out on the G2 as time spent accelerating on the G2 is much larger as it can achieve higher speeds than the G1. The acceleration time was tested over the range shown in Table 14 below. Each movement was observed for any unusual signs such as the motor skipping or unreasonable vibrations being produced.

Table 14. *Notes from tests on X stage movements with a range of acceleration times on the G2 printer.*

Acceleration Time (ms)	**300**	**200**	**100**	**50**	**25**
Notes	No issues	No issues	No issues	Slight vibrations causing small movements of printing plate.	Large vibrations causing large movements of printing plate.

The results suggest that the G2 printer is capable of moving the X stage with an acceleration time of 100ms without vibration of the printing plate. A series of tests were conducted to compare the print time when using an acceleration time of 200ms and 100ms on the G2 printer. The time taken for each of the acceleration times across a range of print modes and print sizes is shown in Table 15 below. A more accurate, code based, timing solution was developed to measure the print times for continuous printing. Continuous print mode requires more accurate timing due to the short print times, which make

extracting trends from three data points difficult with timing values only given to the nearest second. The timing solution is able to give accurate print times to the nearest millisecond using a computer's internal clock that is accurate far below this level.

Table 15. *Print times for the G2 printer with a range of acceleration times over varying print areas.*

	Droplet Print Mode			Continuous Print Mode		
	10x10 mm	**20x20 mm**	**40x40 mm**	**10x10 mm**	**20x20 mm**	**40x40 mm**
300ms Acceleration Time	0min 52secs	3min 09secs	11min 56secs	0min 11.815secs	0min 25.974secs	1min 3.787secs
200ms Acceleration Time	0min 49secs	2min 56secs	11min 11secs	0min 10.719secs	0min 23.789secs	0min 59.419secs
100ms Acceleration Time	0min 45secs	2min 41secs	10min 12secs	0min 9.518secs	0min 21.418secs	0min 54.750secs

The results from Table 15 show that a shorter acceleration time results in a shorter overall print time. This result was expected as a shorter acceleration time results in a higher acceleration, reducing the overall time required to cover a set distance. Using the equations of motion, it is shown that, when using an acceleration time of 100ms, the G2 printer requires 2.525 mm to accelerate to top speed (50 mm/s). As the resolution is 1 mm for all droplet prints in these tests the motion profile is triangular. The results were plotted to check whether the print time decreases linearly and Figure 35 shows the 40x40 mm droplet printing results. The 40x40 mm results are shown as they demonstrate the trend seen in the other size prints and also because the longer print times (>10 minutes) reduces timing errors.

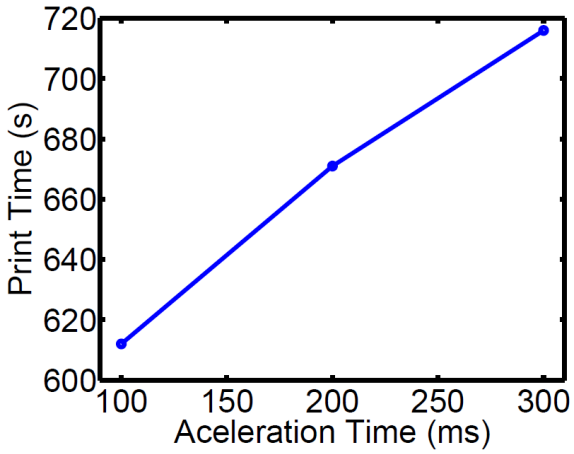

Figure 35. *Comparison of droplet mode print times for a range of acceleration times when printing a 40x40 mm area with the G2.*

The results show that, as the acceleration time decreases, the print time also decreases non-linearly. The pattern shown in Figure 35 was similar for all print sizes in droplet mode. To understand the nonlinear behaviour, the motion profile used for the movement must be considered. An example motion profile is shown in Figure 36 below.

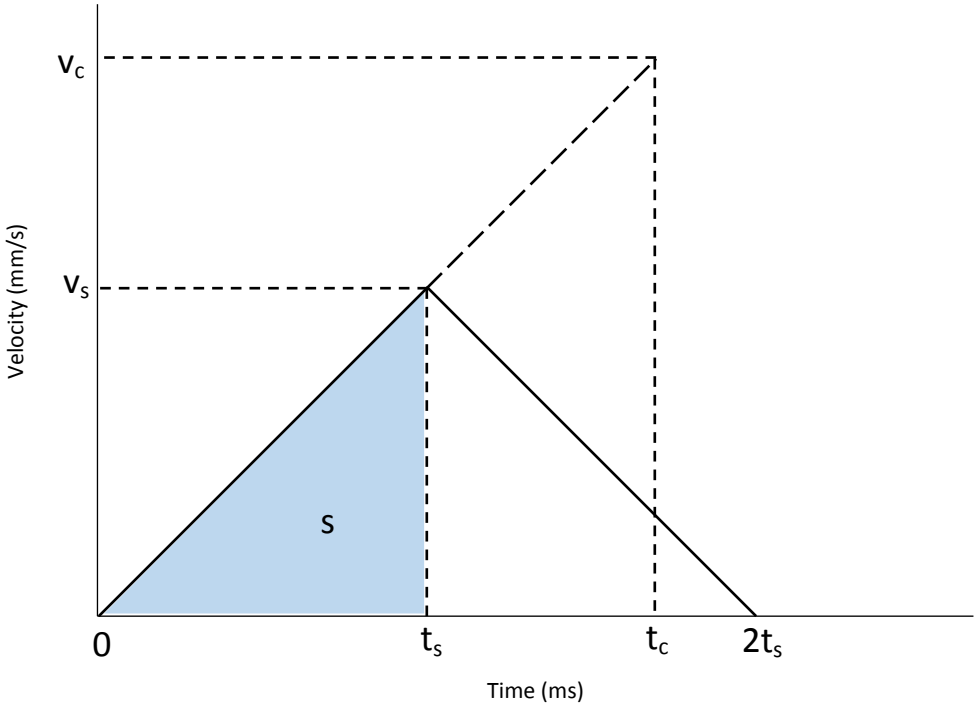

Figure 36. *Example triangular motion profile for the G2 printer in droplet mode.*

The figure shows the following parameters:

t_s = Units: seconds = movement time taken for the acceleration to the desired displacement.

t_c = Units: seconds = time taken for the complete acceleration to the set maximum speed, known as 'acceleration time' in the software.

s = Units: metres = distance travelled during acceleration, equivalent to half of the print resolution in droplet mode.

v_s = Units: metres per second = velocity achieved when desired displacement reached.

v_c = Units: metres per second = maximum velocity to accelerate to, as set by the software.

In order to explain the nonlinear behaviour, the standard equations of motion were used. It is possible to derive the following equation for the movement time (t_s):

$$t_s = \sqrt{2s\,\frac{t_c}{v_c}} \qquad \textit{Equation 2}$$

For the practical tests a displacement (s) of 0.5 mm was used, as this equates to the positive acceleration portion of a 1 mm print resolution. The maximum speed (v_c) used in all tests was 50 mm/s. Using these values gives an equation for the movement time (t_s) of:

$$t_s = \sqrt{0.02 t_c}$$

Equation 3

The plot of Equation 3 is shown in Figure 37 below.

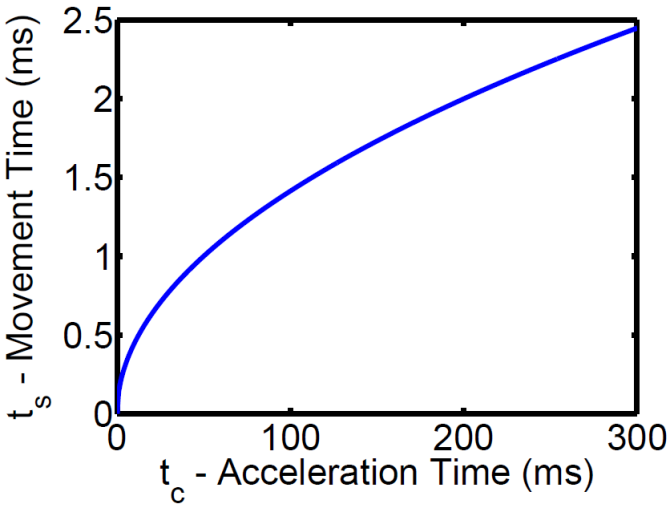

Figure 37. *Equation 9 plotted over a range of acceleration times.*

The non-linear results seen in the previous experiment can be explained by the derived square root relationship. Figure 37 closely matches the results seen over the 100-300ms acceleration time range in the experiment and the derived equation explains the non-linear time response to acceleration changes.

The results from Table 15 were considered for continuous mode printing. The print times for a 40x40 mm area at various acceleration times are shown in Figure 38 below.

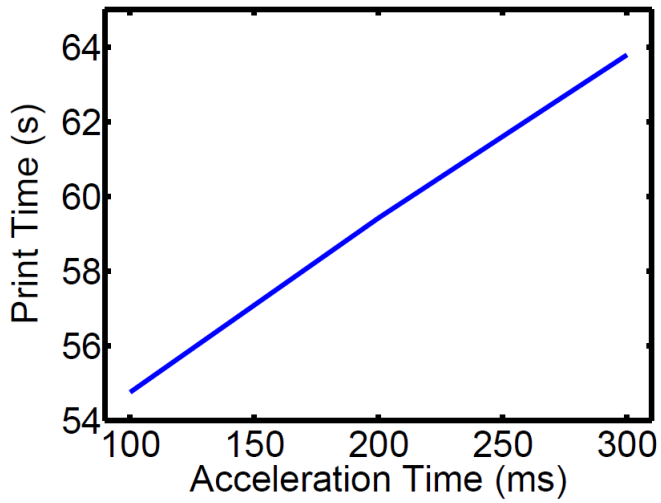

Figure 38. *Comparison of continuous mode print times for a range of acceleration times.*

The results show a linear response of print to acceleration time in continuous printing mode. The results were expected as the motion profile has a trapezoidal shape as opposed to the triangular one seen earlier, meaning the majority of the movement was spent at maximum speed.

The tests have shown that a 100ms acceleration time is the fastest acceleration that can be used on the G2 without causing adverse effects on repeatability. A reduction in acceleration time offers an improvement in overall print time compared to high acceleration times.

4.3. Displacement Sensor and Base Uniformity Investigation

4.3.1. Displacement Sensor Selection

As previously discussed in section 4.1, a displacement sensor is required on the dispenser printer to enable a desired separation distance between nozzle and substrate to be maintained during printing. In operation, the substrate will be profiled prior to printing and the array of measured displacements will then be used to adjust the height of the nozzle as it prints. It is important to select an appropriate displacement sensor that can measure all of the inks that will be printed and then characterise the system against a commercial profilometer.

The dispenser printer integrated with a displacement sensor will allow higher quality printed layers to be produced than would be possible with the printer at Berkeley, University of California [60]. The setup shown by Ho et al. in her thesis shows there is no provision for maintaining a desired separation distance [60]. The lower capability of the printer will significantly limit the size and quality of the printed layers that can be produced for any application because a separation distance between the nozzle and substrate cannot be maintained.

A displacement sensor for use in a dispenser printing application should have a measurement range of at least ±1 mm. This sensing range is required as the total device thicknesses can be up to 400 μm [61]; furthermore the distance between the nozzle and the base plate used to hold the samples is expected to vary by up to 1.5 mm. The variation is caused by the moving stage slides not being perfectly flat and the weight of the printing plate acting as a cantilever on the stages during printing.

A further requirement for the displacement sensor is to have a resolution of equal to or lower than 10 microns. The resolution is required to accurately sense the thinnest printed layer which is the bottom electrode silver layer. The layer is typically 10-15 μm thick.

The displacement sensor will be mounted within 50 mm in X and Y directions of the dispenser nozzle to maximise the area that can be measured by the laser and printed onto with the dispenser on the G2. Size and weight must also be taken into consideration as it must be feasible to mount this on the moving stage that has a maximum load rating of 10 kg. The total mass of the laser head to be mounted near the nozzle should not exceed 5 kg to allow printing and curing heads to also be carried. A small measurement spot is also desirable to allow high resolution profiles of the substrate to be obtained where necessary.

Displacement sensors fall into either contact or non-contact sensing categories. Contact sensors typically rely on a small needle moved over the substrate to sense the displacement [62]. They are used in applications with harsh environmental conditions or sensing displacement of solid objects submerged in liquids. Contact sensors are not suitable for displacement sensing in dispenser printing as the needle could damage previously printed layers. For this reason, contact displacement sensing is not considered further.

A number of non-contact displacement sensing technologies are available. The first technology considered is eddy-current sensors. These sensors operate by applying an AC signal through a coil over the material, the resulting field is measured by a sensor coil. From changes in amplitude and phase a displacement can be calculated. An example eddy current sensor is shown in Figure 39 below.

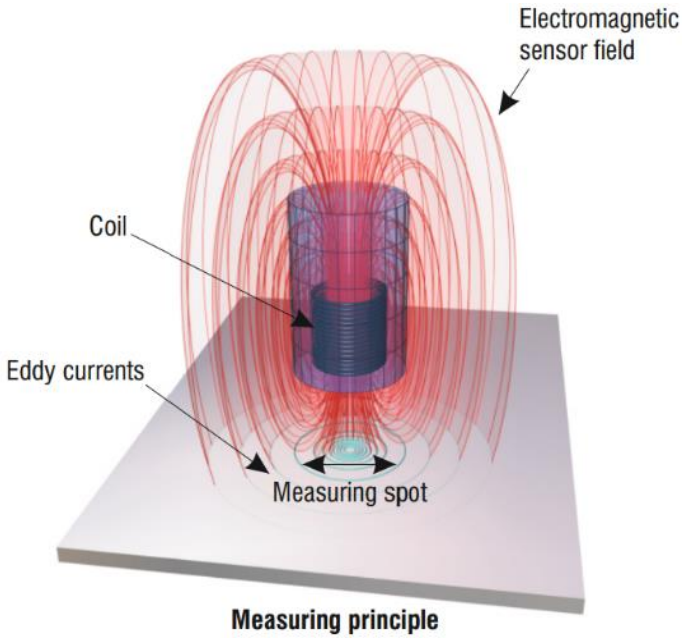

Figure 39. *Example eddy current displacement sensor demonstrating the measuring principle (Image from [63])*

Eddy-current sensors are not suitable for this application as they require the sample to be electrically conductive. As the substrate is commonly a non-conductive fabric, Eddy-current sensors are not considered further. Capacitive sensors also offer non-contact sensing through measuring a change in capacitance between a sensor electrode and substrate electrode. These sensors also require a conductive substrate so are not considered further.

Confocal displacement sensors, which have recently been developed, operate by splitting a white light beam into monochromatic light and focusing it onto the substrate. Only the wavelength in focus on the substrate is sensed by the receiver. Figure 40 below shows the measurement principle.

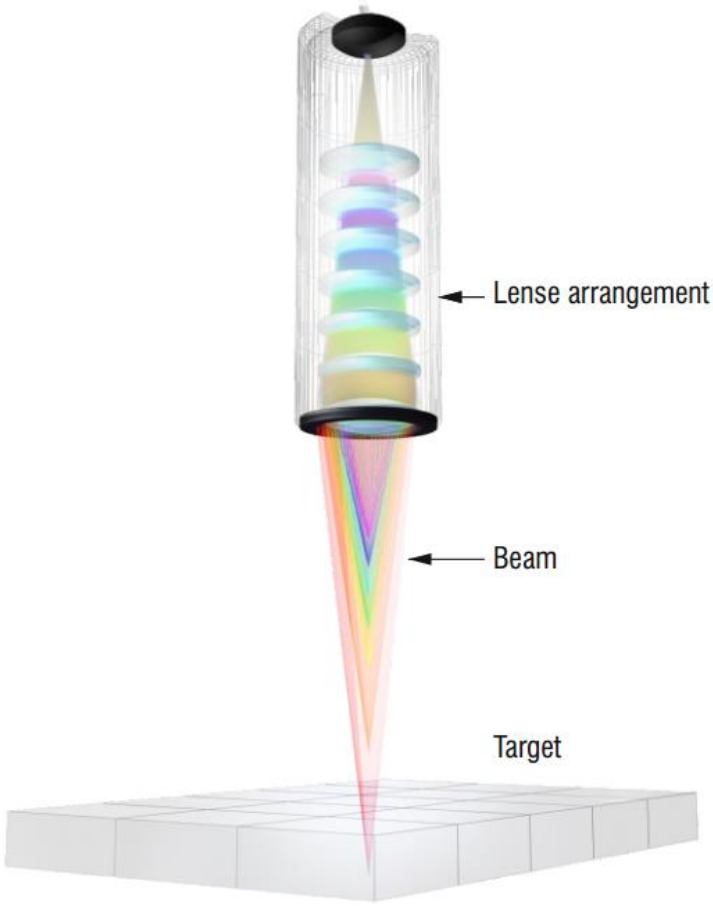

Figure 40. *Example confocal displacement sensor demonstrating the measuring principle (Image from [63])*

Confocal displacement sensors offer excellent resolution down to 10 nm, however they are more expensive than other more traditional optical displacement sensors with similar performance. At this time they are prohibitively expensive to be purchased as part of the project (>£15,000 with external light source) so for this reason they are not included in the practical tests.

Laser triangulation displacement sensors offer a non-contact measurement solution with excellent resolution. Lasers sensors are available with spot sizes down to 20 µm and displacement resolutions can reach 0.02 µm over a 2 mm range. Laser displacement sensors are typically optimised for diffuse or reflective surfaces. The different types of sensors are shown in Figure 41 below.

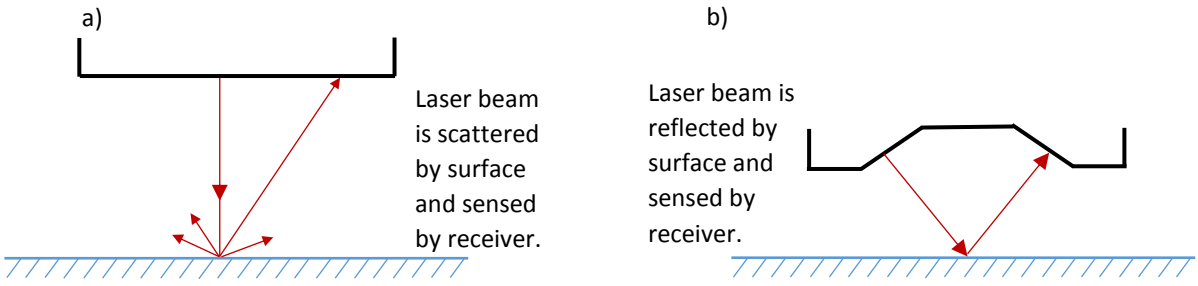

Figure 41. *Laser displacement sensors optimised for a) diffuse surfaces and b) reflective surfaces.*

For a dispensing application both diffuse and reflective surfaces (for example: woven fabric and silver pastes respectively) need to be measured.

To determine suitability, a number of laser triangulation and confocal displacement sensors were tested. Keyence and Micro-Epsilon have been identified as two of the leading companies in the field who are willing to supply sample products to test. A comparison of the suitable laser displacement sensors is shown in Table 16 below.

Table 16. *Comparison of laser triangulation displacement sensors (Data from [64-66])*

Laser Displacement Sensors									
Model	**Optimised For**	**Reference Distance**	**Measuring Range**	**Spot Diameter**	**Resolution**	**Linearity**	**Max Sampling Rate**	**Weight**	**Controller**
Keyence LK-G10	Reflective Surfaces	10 mm	+- 1 mm	20 µm	0.02 µm	+- 0.3 µm	50 kHz	190 g	External – USB
Keyence LK-G32	Diffuse Surfaces	30 mm	+- 5 mm	30 µm	0.05 µm	+- 2.5 µm	50 kHz	280 g	External - USB
Micro Epsilon ILD 2300-2	Diffuse Surfaces	25mm	+- 1 mm	23 µm	0.03 µm	+- 0.3 µm	49 kHz	550 g	Inbuilt – Ethernet, serial or External – USB

LabVIEW software was written to record the output from the displacement sensor in an array and then plot the output on a 3D displacement graph. The laser displacement sensors were tested by profiling a dispenser printed EL lamp. As the laser moves over the EL lamp the material being scanned will vary between interface, silver, dielectric, and semi-transparent conductor (PEDOT:PSS) materials. The sensors were mounted onto the dispenser using custom 3D printed mounts attached to a small manual moving stage allowing the user to zero the sensor before a scan was completed. The displacement sensor on the dispenser is shown in Figure 42.

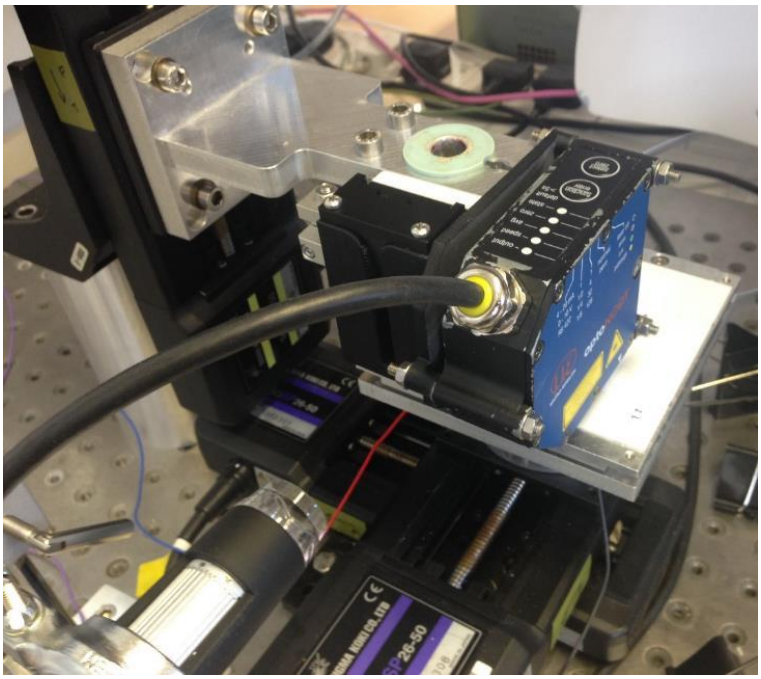

Figure 42. *Micro-Epsilon displacement sensor mounted to the dispenser printer.*

The EL lamp scanned by the Micro-Epsilon laser is not the same sample as the Keyence lasers because they were on loan at different times due to availability. However, they both use identical printed inks and both are dispenser printed onto the same fabric. A scan was completed with each laser and all scans recorded a data point every 0.5 mm in both X and Y directions. The two EL lamps scanned are shown in Figure 43 below.

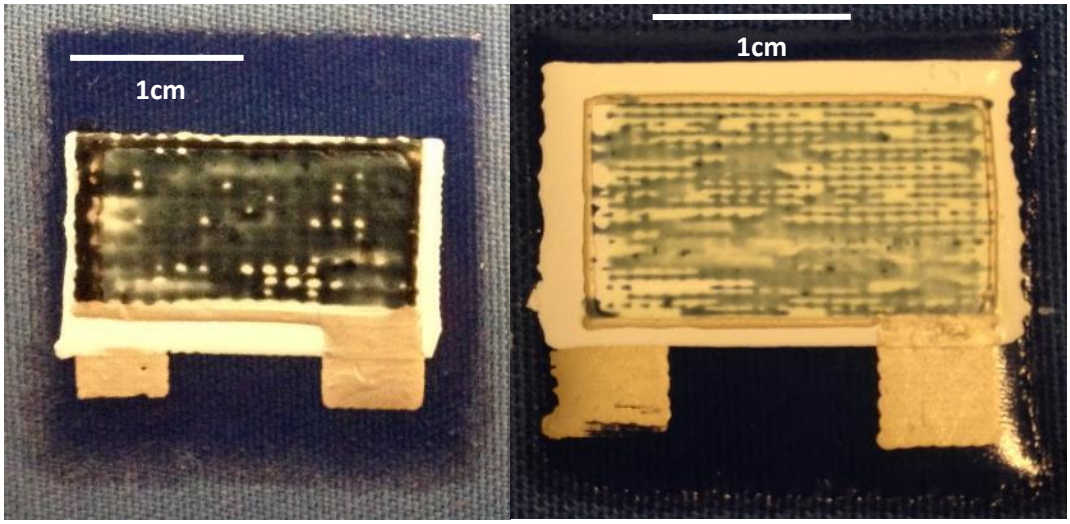

Figure 43. *Dispenser printed EL lamps used to test (left) Keyence LK-G10 and LK-G32 and (right) Micro Epsilon ILD 2300-2*

The 3D graph outputs of the results are shown in Figure 44 to Figure 46.

Interface layer

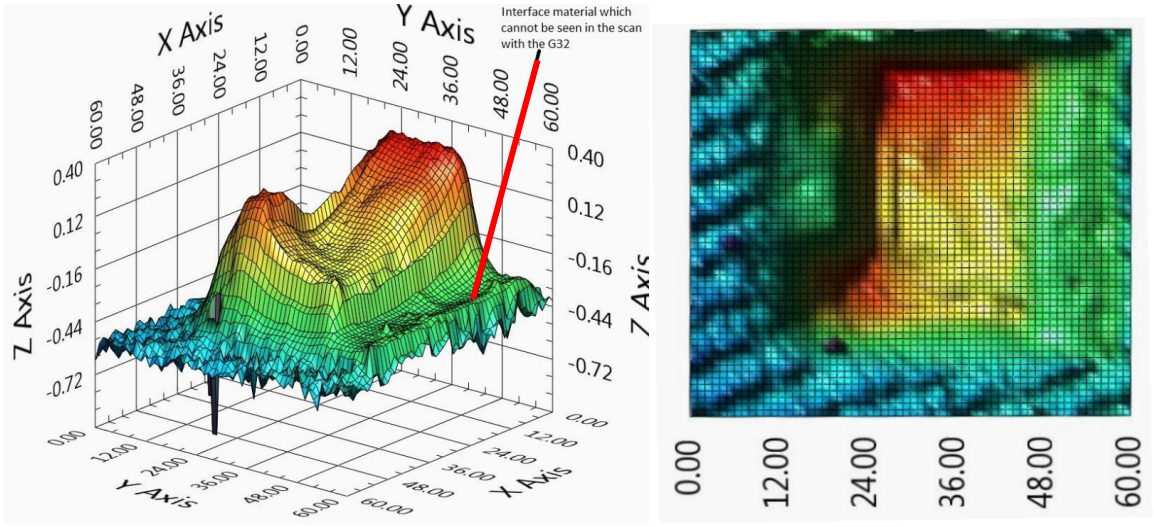

Figure 44. *Profile of EL lamp measured using a Keyence LK-G10 laser displacement sensor - isometric view (left) and top view (right).*

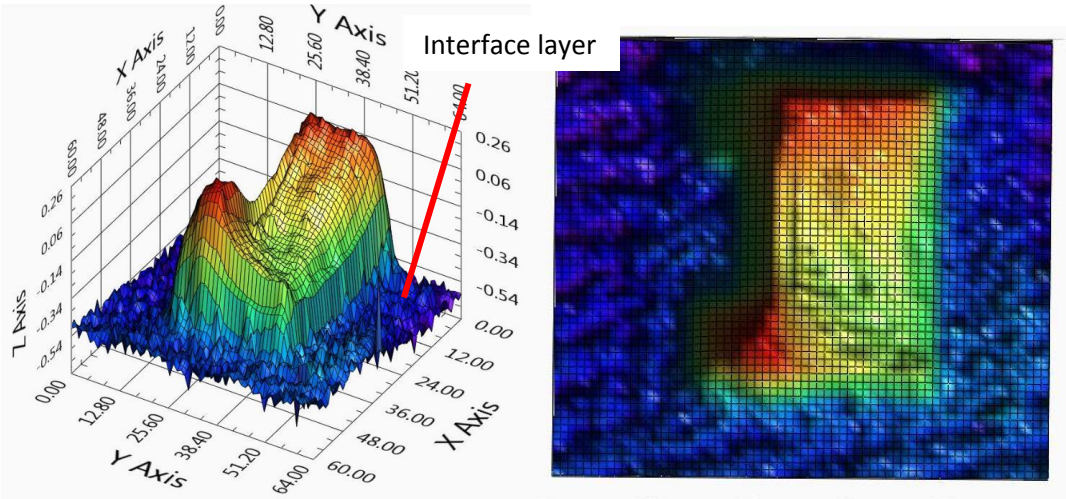

Figure 45. *Profile of EL lamp measuring using a Keyence LK-G32 laser displacement sensor - isometric view (left) and top view (right).*

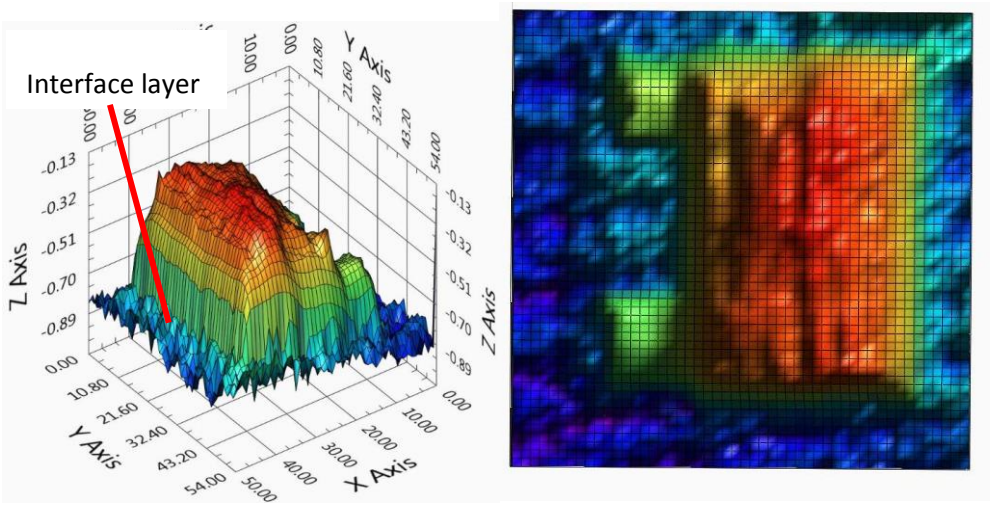

Figure 46. *Profile of EL lamp measured using a Micro Epsilon ILD 2300-2 laser displacement sensor - isometric view (left) and top view (right).*

From the results collected a number of conclusions can be made:

- The Keyence LK-G10 sensor is significantly lighter (300 g) and smaller than the Micro-Epsilon ILD2300 as it has an external controller. It is also 90 g lighter than the Keyence LK-G32. The lighter weight is beneficial as it removes load from the Z-stage, allowing more efficient movements.
- The Keyence LK-G10 has the highest resolution, however all of the sensors tested have a sufficient resolution and no visible difference can be seen in the scans to suggest that the other sensors were disadvantaged by their lower resolution.
- The Keyence LK-G10 correctly sensed the transparent interface layer. The scan for the Micro-Epsilon and G32 sensors did not sense the layer correctly, suggesting the laser had passed through the transparent layer and was sensing the fabric below it. For clarity the layer has been labelled in Figure 44, Figure 45, and Figure 46. Figure 46 shows the highly uneven nature of the scanned surface for the ILD 2300-2, whereas the actual interface surface is smooth at this scale. The interface layer is not visible at all in Figure 45 for the G32 sensor. The problems sensing the interface layer are likely due to the transparent and somewhat reflective nature of the material as seen in Figure 43. The Keyence LK-G10 better senses the interface as it is optimised for reflective surfaces, whereas the other lasers are optimised for diffuse surfaces.
- It is possible to mount the ILD2300 for reflective surfaces by rotating it so the laser angle of approach is 55˚ to the surface. However, it is not optimised for this and the receiver will not be at an ideal angle to receive a reflected laser beam. As another custom mount would have to be made, and the sensor was only on loan for a short period of time, the ILD2300 was not tested in this way.
- Two extreme low points are visible for the Keyence LK-G10 in Figure 44. These are caused by a laser error, due to the returned light level being too low. The likely cause is the laser light falling into the weave of the fabric and because of the shape of the void it is not correctly reflected. The error points will need to be considered by post-processing software to prevent the errors affecting the print.

It is important to correctly sense the interface layer, as it is normally the thickest printed layer at around 50-100 μm. If the laser cannot sense the layer, it could cause the nozzle separation distance to be incorrect, by up to the thickness of the layer.

Based on the conclusions above it was decided to purchase and continue using the Keyence LK-G10 for future work, as the interface layer is printed on many devices, and the Keyence LK-G10 was the only sensor to correctly measure the interface layer thickness. The lightweight and compact design, with the smallest laser spot size are further advantages.

4.3.2. Displacement Sensor Testing and Characterisation

Following the selection of the LK-G10, it was mounted on the G2 printer to create a profilometer which was then compared with a commercial UoS profilometer system, the Alicona Infinite Focus G4G. The Alicona is a non-contact system and was chosen as it is widely used in industry and incorporates quality checking algorithms that ensure reliable results are produced.

A small area of a printed EL lamp was scanned with the G2 profilometer and this was then repeated with the Alicona to compare. A printed EL lamp was chosen as the test sample because it has a multi-layer profile and incorporates a number of materials that some optical profilometers struggle to assess due to their reflectivity or semi-transparent nature. The area chosen for testing includes a white opaque dielectric layer, a reflective silver layer and a semi-transparent PEDOT: PSS conducting layer. The inks printed in each part of the study area are shown in Figure 47 below.

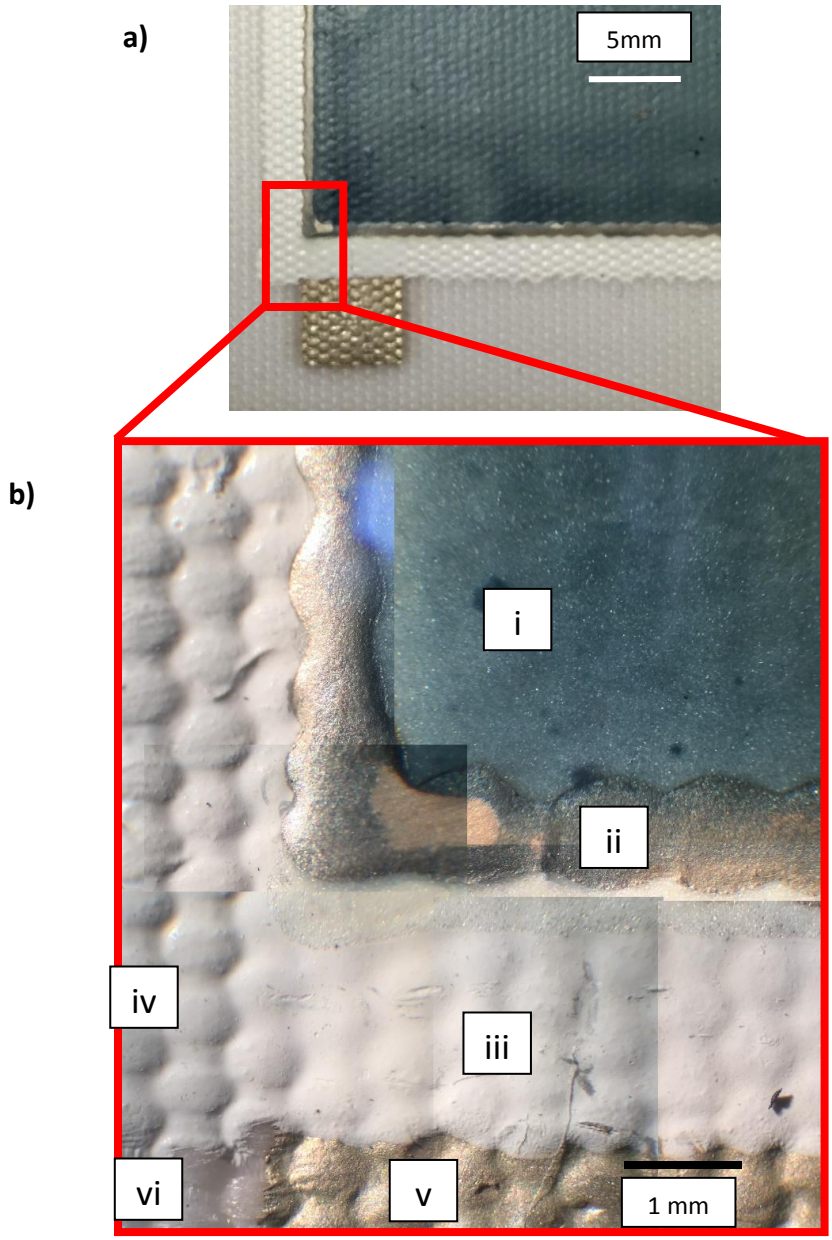

Figure 47. *Images showing the study area for profiling: a) an overview of the larger EL lamp, showing the smaller 6 x 7 mm area that was profiled, b) a detailed view of the 6 x 7 mm profiled area formed by combining multiple individual microscope images causing join lines. At each of the labelled points, the following layers are present, from bottom to top: i) silver, dielectric, phosphor, PEDOT/PSS; ii) silver, dielectric, phosphor, silver, PEDOT/PSS; iii) silver, dielectric; iv) dielectric only; v) silver only; vi) no printed layers exposing the woven polyester substrate.*

The area shown in Figure 47(b) was profiled using the G2 profilometer. Initially the profilometer moving stage settings in Table 17 were used. An X/Y resolution of 0.1 mm is used to generate a high quality profile that will sense fine details such as the fabric weave. A low movement speed of 0.3 mm/s was selected to match the very low X/Y resolution. If a higher speed was used it may cause X/Y movement accuracy to be lost.

Table 17. *G2 profilometer moving stage settings for initial profile.*

X/Y Lateral Resolution	X/Y Movement Speed	Profile Area	Profile Time
0.1 mm	0.3 mm/s	6 x 7 mm	1hr 20min

The output from the G2 profilometer program has been plotted using MATLAB. The aspect ratio on the Z axis has been modified to make the changes in Z displacement more easily visible. The surface graphs can be seen in Figure 48 and Figure 49 below.

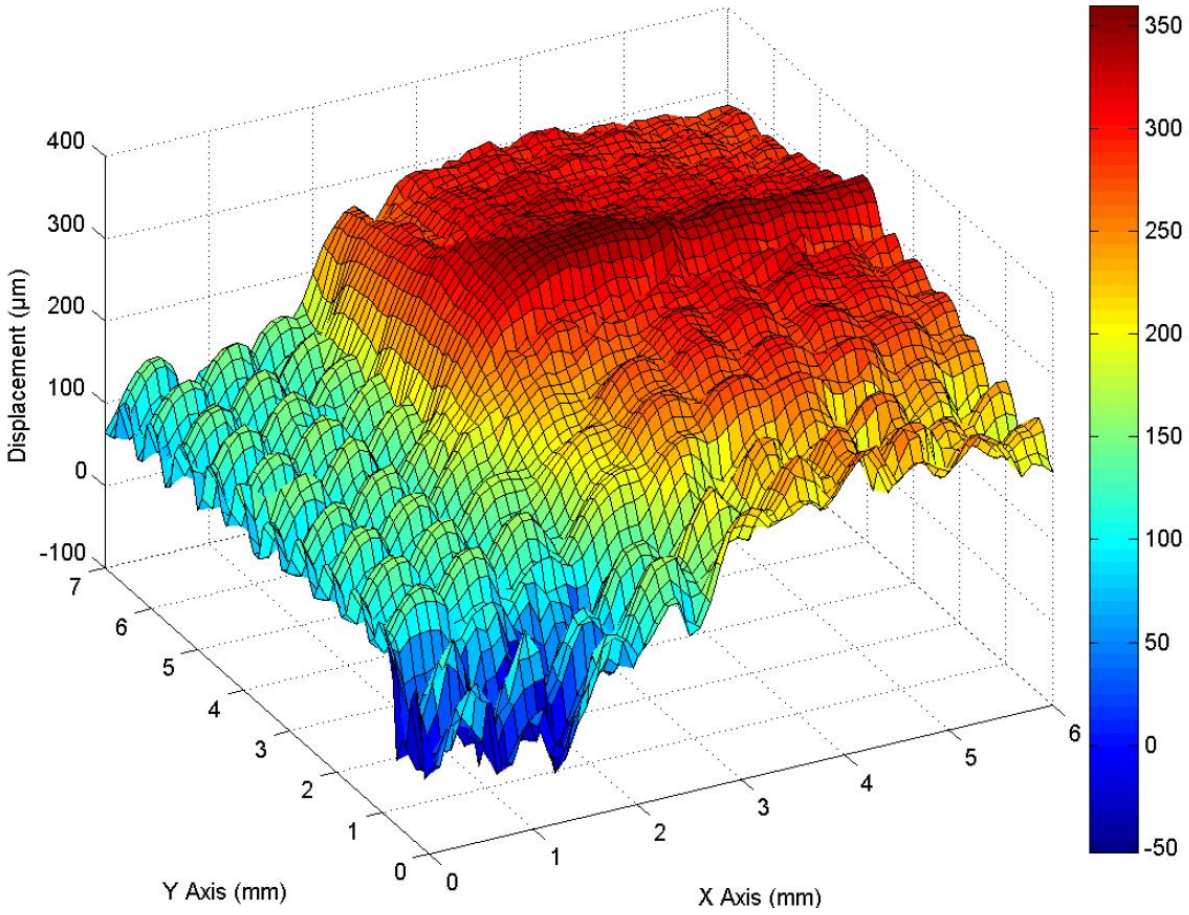

Figure 48. *3D view of the surface profile of the study area using the G2 profilometer with a lateral resolution of 0.1 mm.*

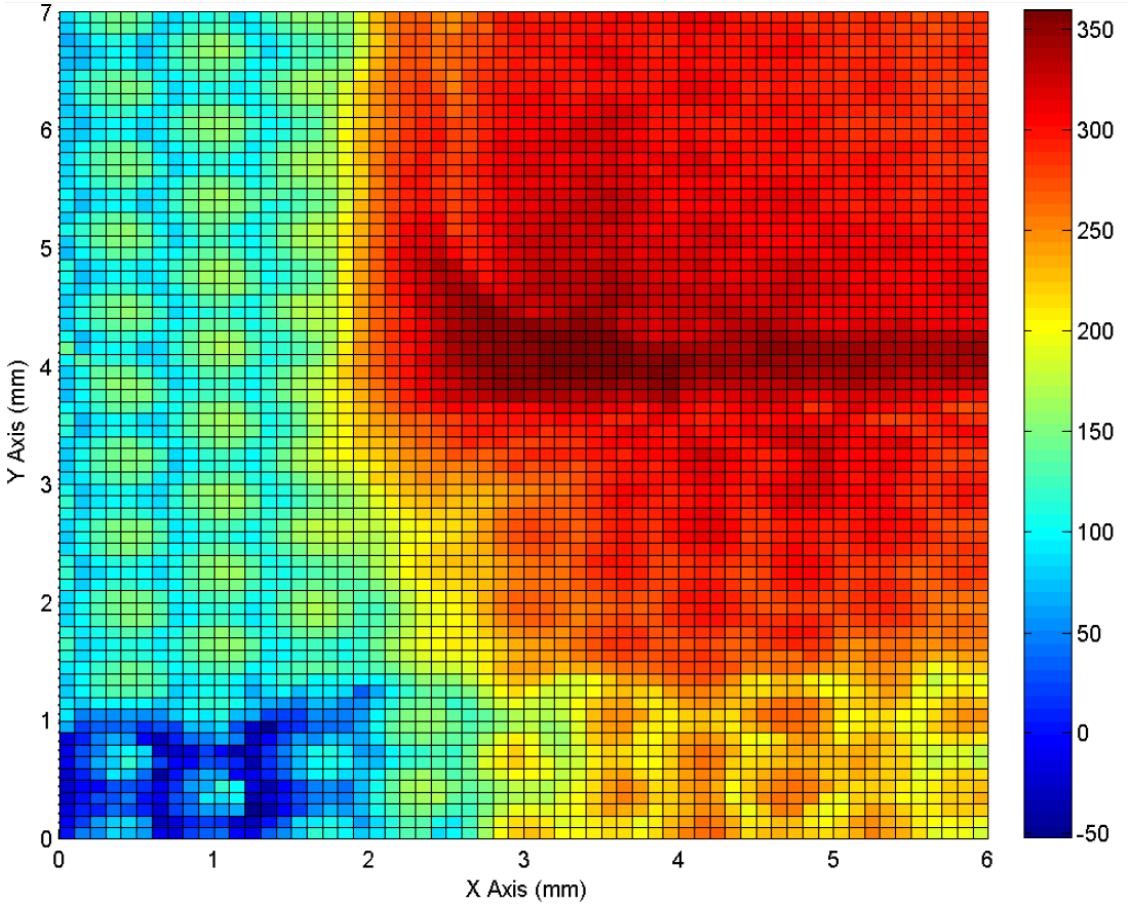

Figure 49. *Top view of the surface profile of the study area using the G2 profilometer with a lateral resolution of 0.1 mm.*

The graphs clearly show the profile of the EL lamp and the features are overall, as expected. The fabric weave, visible in Figure 48 around coordinates (1,5), appears to show a quantisation effect. The angular profile, as opposed to a smooth curve, suggests the lateral resolution used was too low to accurately capture the profile. The rough area in Figure 48 at (0.5,0.5) shows the fabric weave with no printed layers and is very rough with irregularities in the height of the weave. The irregularities suggest inaccurate measurement as the fabric weave should have uniform changes in height at this resolution. The problem in this area could be caused by multiple readings being produced as light is lost and reflected in the woven fabric structure.

A lower lateral resolution results in a higher overall profile resolution, as the steps between data points are reduced. The profile was repeated over the same area with a lower lateral resolution to more accurately capture the shape of the weave. The settings used for this profile are shown in Table 18.

Table 18. *G2 profilometer settings for second profile.*

X/Y Lateral Resolution	X/Y Movement Speed	Profile Area	Profile Time
0.05 mm	0.3 mm/s	6 x 7 mm	5 hr 30 min

The results from the repeated tests with the lower lateral resolution can be seen in Figure 50 and Figure 51.

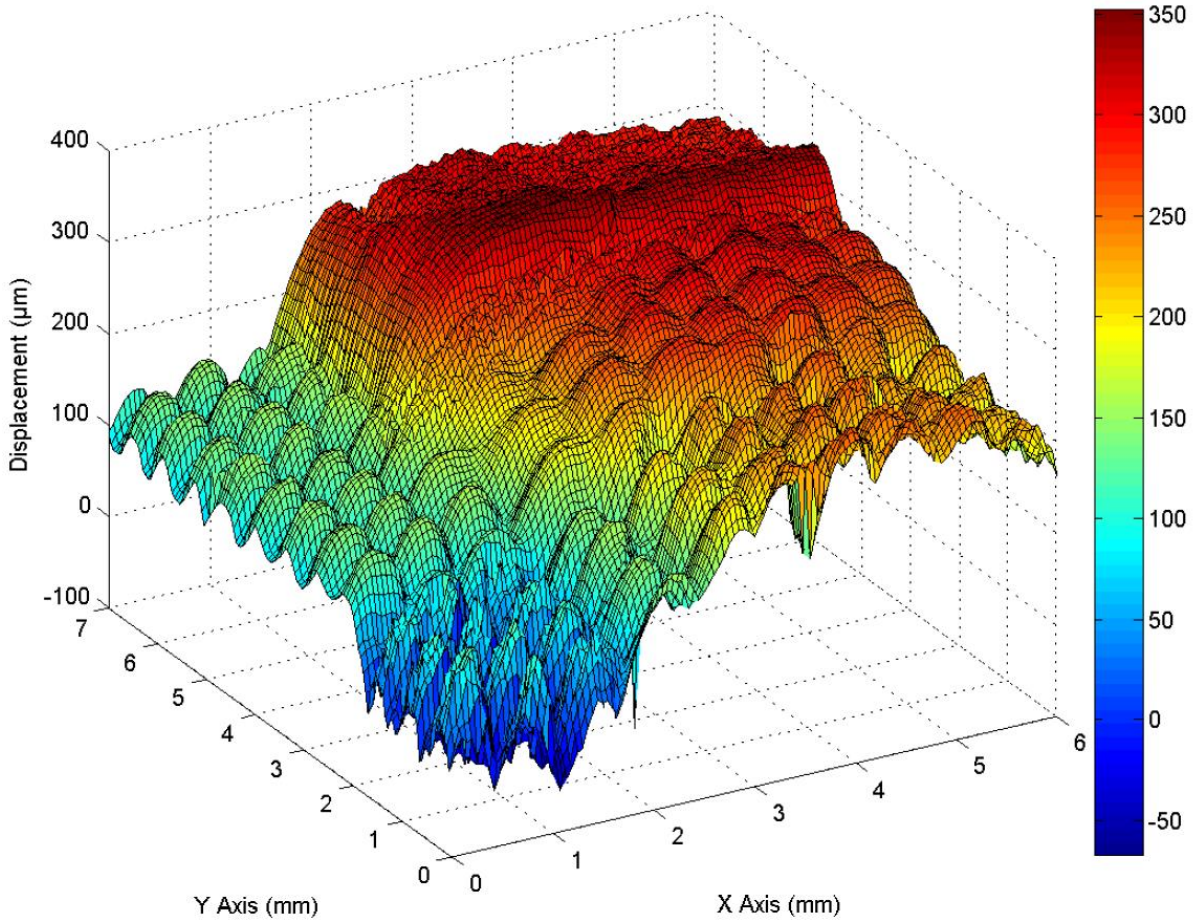

Figure 50. *3D view of the surface profile of the study area using the G2 profilometer with a lateral resolution of 0.05 mm.*

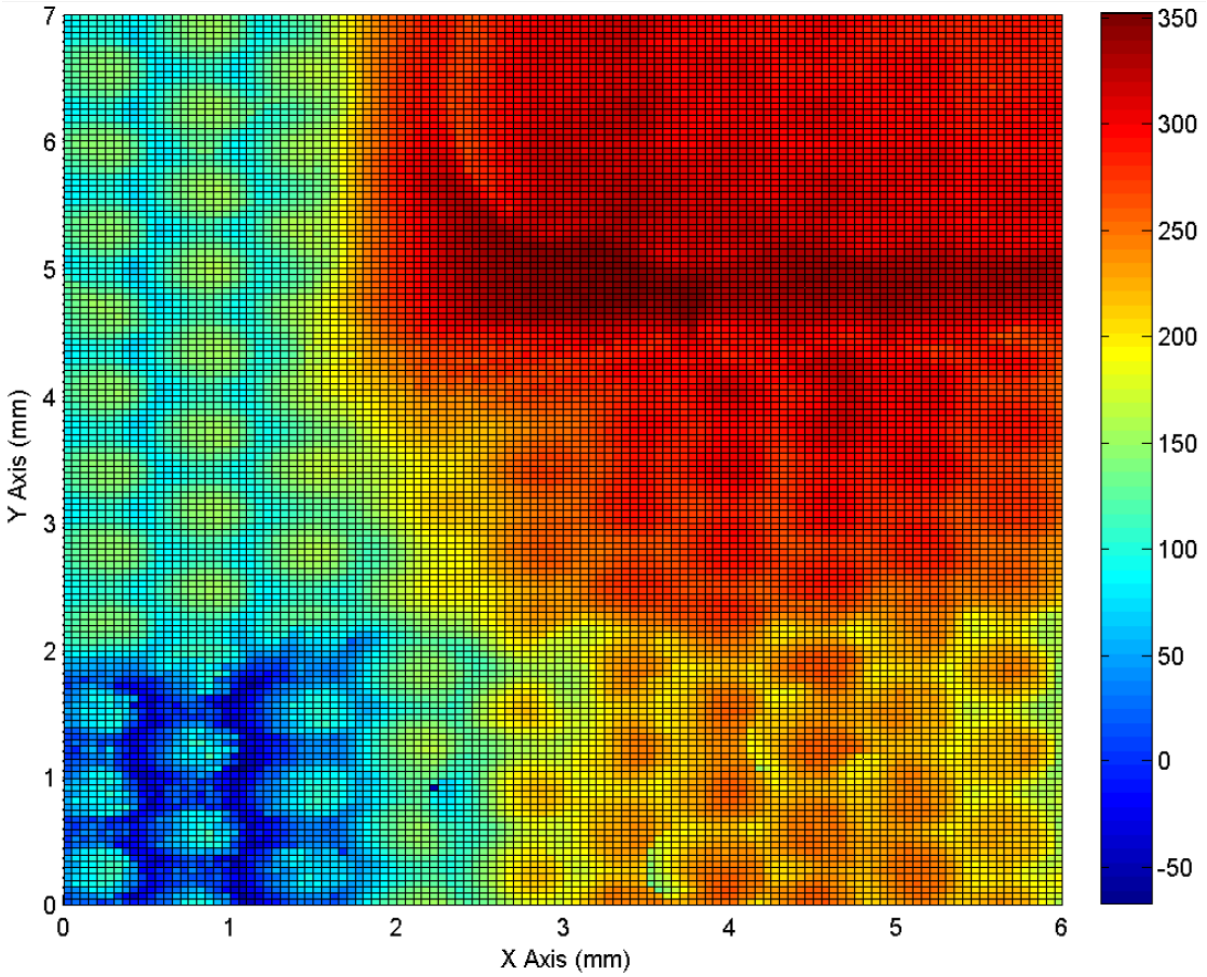

Figure 51. *Top view of the surface profile of the study area using the G2 profilometer with a lateral resolution of 0.05 mm.*

The decreased lateral resolution is visible when viewing the weave in Figure 50. The profile presents a much smoother weave than the previous study using 0.1 mm lateral resolution. Also in Figure 51, a darker point is visible at position (2.2, 0.9), indicating a much lower point than the surrounding area. This point is an erroneous reading, caused by the laser light being scattered by the fabric weave, causing the receiver to record a reading lower than the true value. The point will be replaced with an average value from the surrounding points when the system is used in practise.

The Alicona Infinite Focus G4G was selected for the comparison because it is extremely accurate with a vertical resolution as low as 10 nm depending on the aperture used [67]. The Alicona system uses an aperture to measure the displacement to the surface by slowly altering the Z height of the aperture and recording when each point is in focus. Apertures of 2.5x, 5x, 10x, 50x, and 100x magnification are available, with a greater magnification offering improved vertical resolution with a smaller field of view. The study area is approximately 5.5 x 4.5 mm, meaning the 2.5x magnification aperture must be used to capture the area in a single image. Larger areas can be measured, however this requires multiple images to be taken and 'stitched' together, increasing the profile time and adding unnecessary complication. A slightly larger study area was used for the G2 as it is difficult to accurately start the measurements from exactly the same point. The larger area allows reference points to be identified and a smaller selection

to be used for comparison. Using this aperture, a vertical resolution of 1.33 µm is possible. The vertical resolution for this aperture is not as good as the Keyence LK-G10's resolution of 0.02 µm, however the Alicona has the advantage of quality checking that each reading is accurate to the set resolution and excluding any points which it believes do not match this criterion. The quality filtering process removes erroneous data points by comparing them with the surrounding data. Details of the quality filtering process are not released by Alicona. The LK-G10 has shown that it includes points that are erroneous and these have to be countered by custom built error checking and correction software. The majority of features to be viewed on the EL samples are in excess of 10 µm changes, therefore the difference in resolution should not affect the comparison. The settings shown in Table 19 below were used for the profile using the Alicona.

Table 19. *Alicona Infinite Focus profilometer settings.*

X/Y Lateral Resolution	Vertical Resolution	Aperture	Profile Area	Profile Time
19.571 µm	1.329 µm	2.5x	5.5 x 4 mm	47.92 secs

The results from the tests using the Alicona have been plotted using MATLAB. The aspect resolution for the axes has been corrected to ensure the Alicona results are comparable to the G2 profilometer results. The results are shown in Figure 52 and Figure 53. An image of the study area taken using a microscope is shown in Figure 54 to give context to the observed profile.

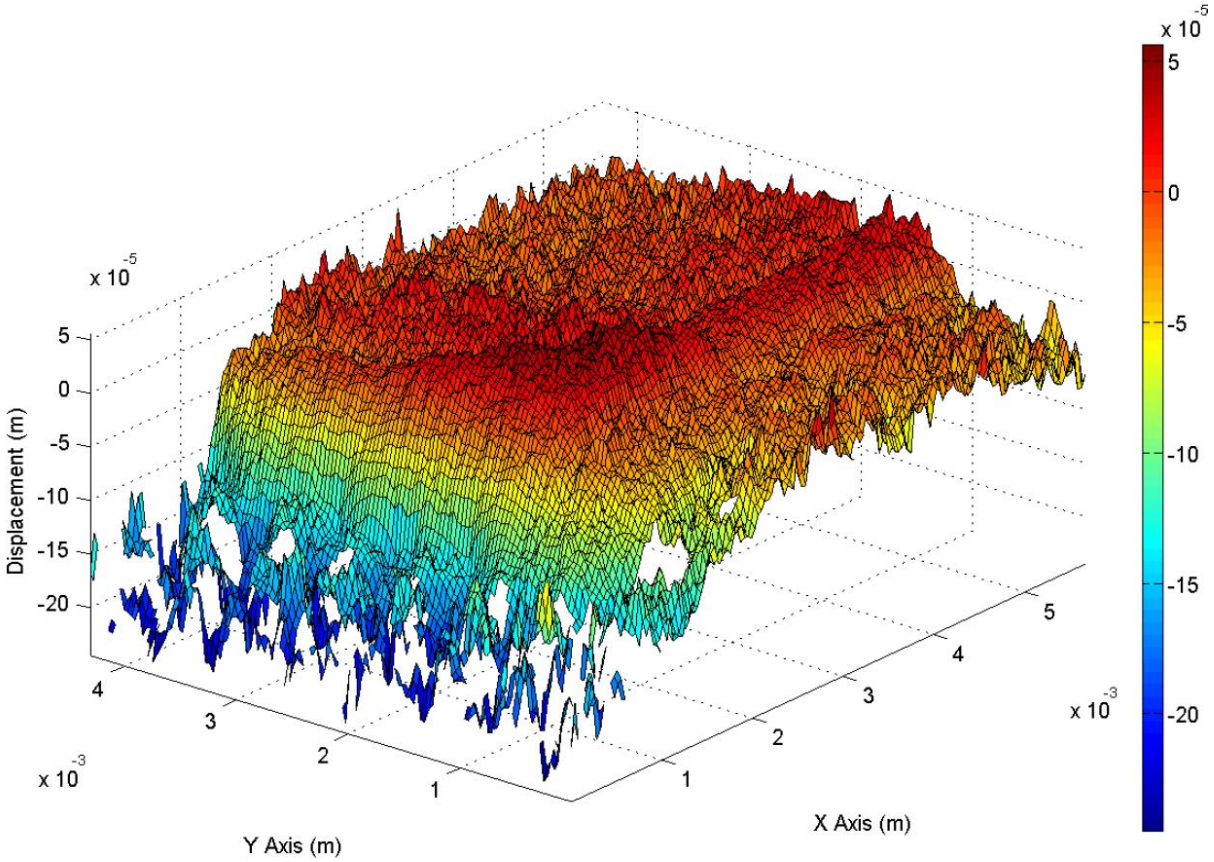

Figure 52. *3D view of the surface profile of the study area using the Alicona profilometer.*

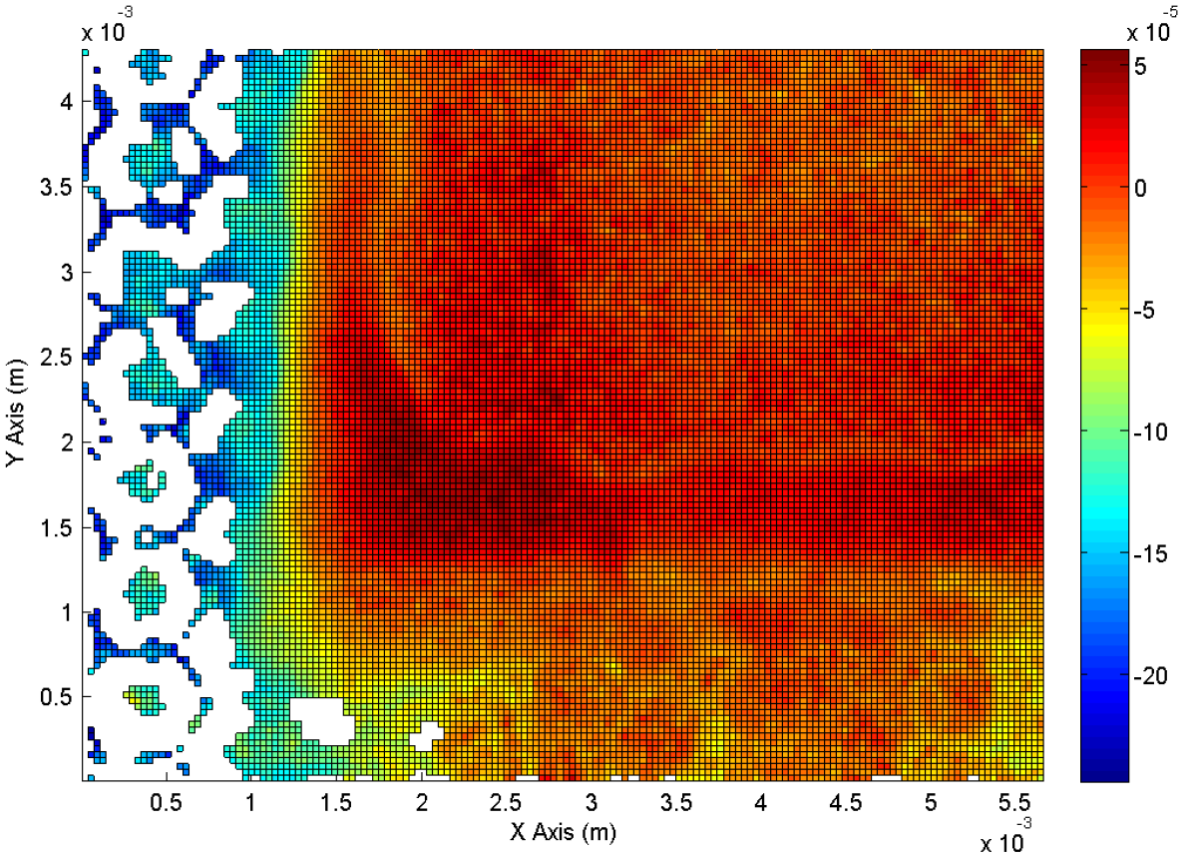

Figure 53. *Top view of the surface profile of the study area using the Alicona profilometer.*

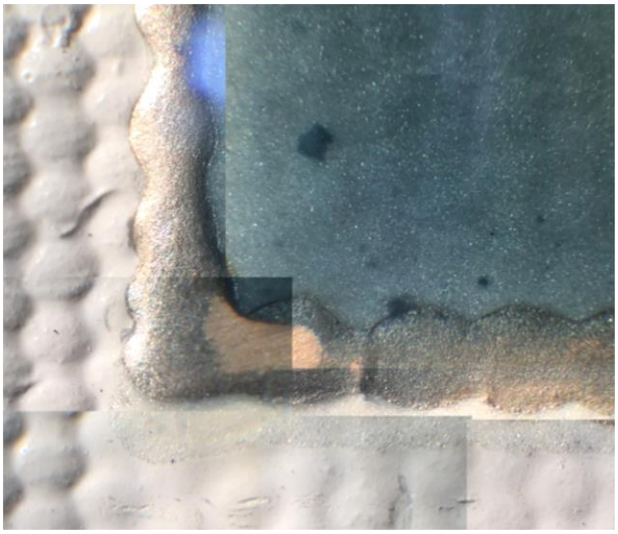

Figure 54. *A detailed microscope view of the 6 x 7 mm profiled area formed by combining multiple individual microscope images causing join lines.*

The results show that a number of points, where the fabric weave is visible, are missing. The data points are not shown as the Alicona post-processing quality filter has found that they are not accurate to the stated vertical resolution. The overall shape of the printed area has been captured and appears to be visually similar to the output from the G2 profilometer.

To compare the output of the G2 profilometer to the Alicona profilometer, a section of the profiles was selected. The comparison area avoids any obvious error points in the G2 output, and also avoids any missing points in the Alicona output. The area covers an area of the EL lamp that is approximately flat in the X direction, and includes a number of height changes in the Y direction. The comparison area is 1 mm wide and covers the height of the profiled areas. The areas were measured at a known X distance from visible features on the sample profile to ensure the selected areas covered the same part of the sample. The selected areas are shown on the profile graphs in Figure 55 and Figure 56 below. The areas appear to be different sizes as the scale is not the same on both figures.

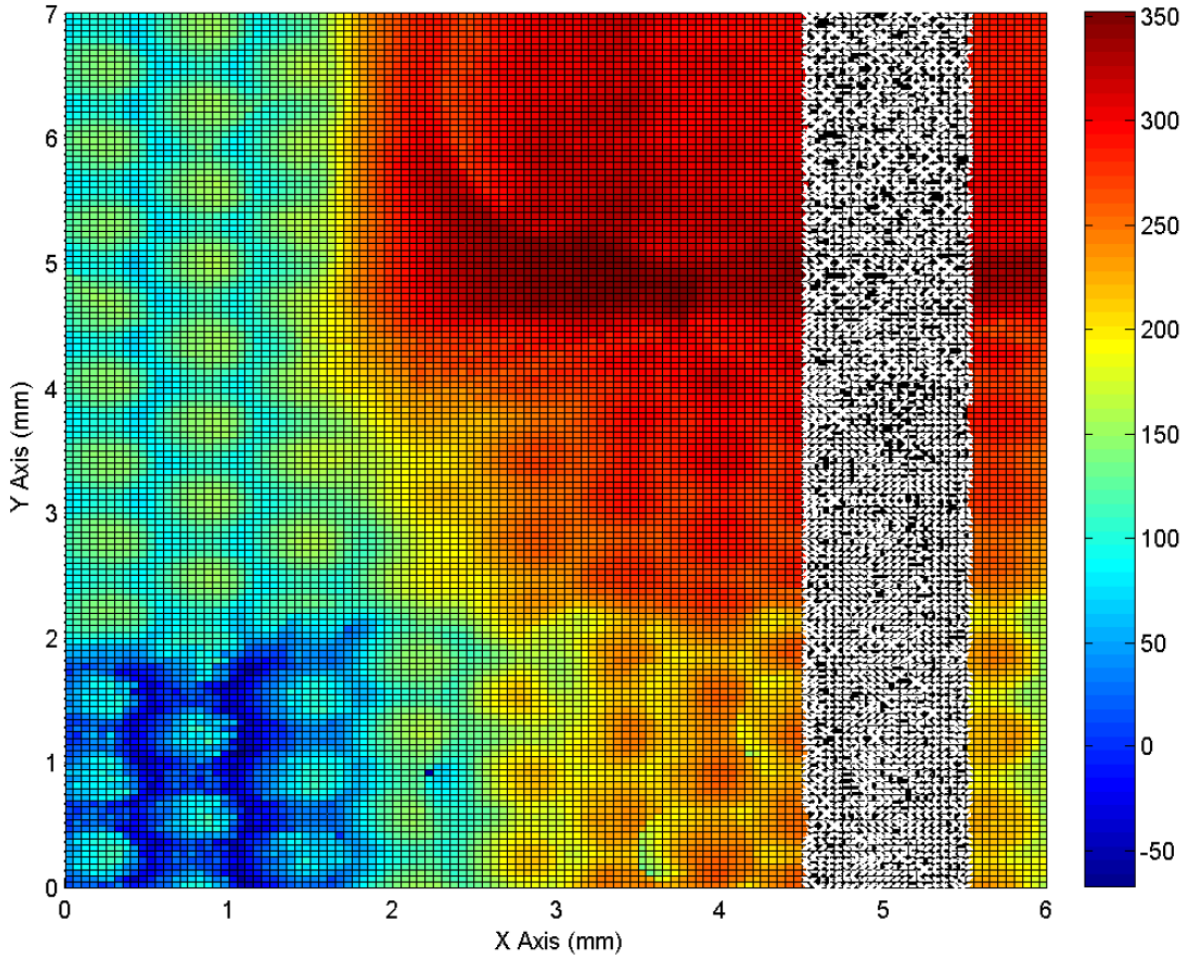

Figure 55. *Selected comparison area on the output from the G2 profilometer with a 0.5 mm lateral resolution.*

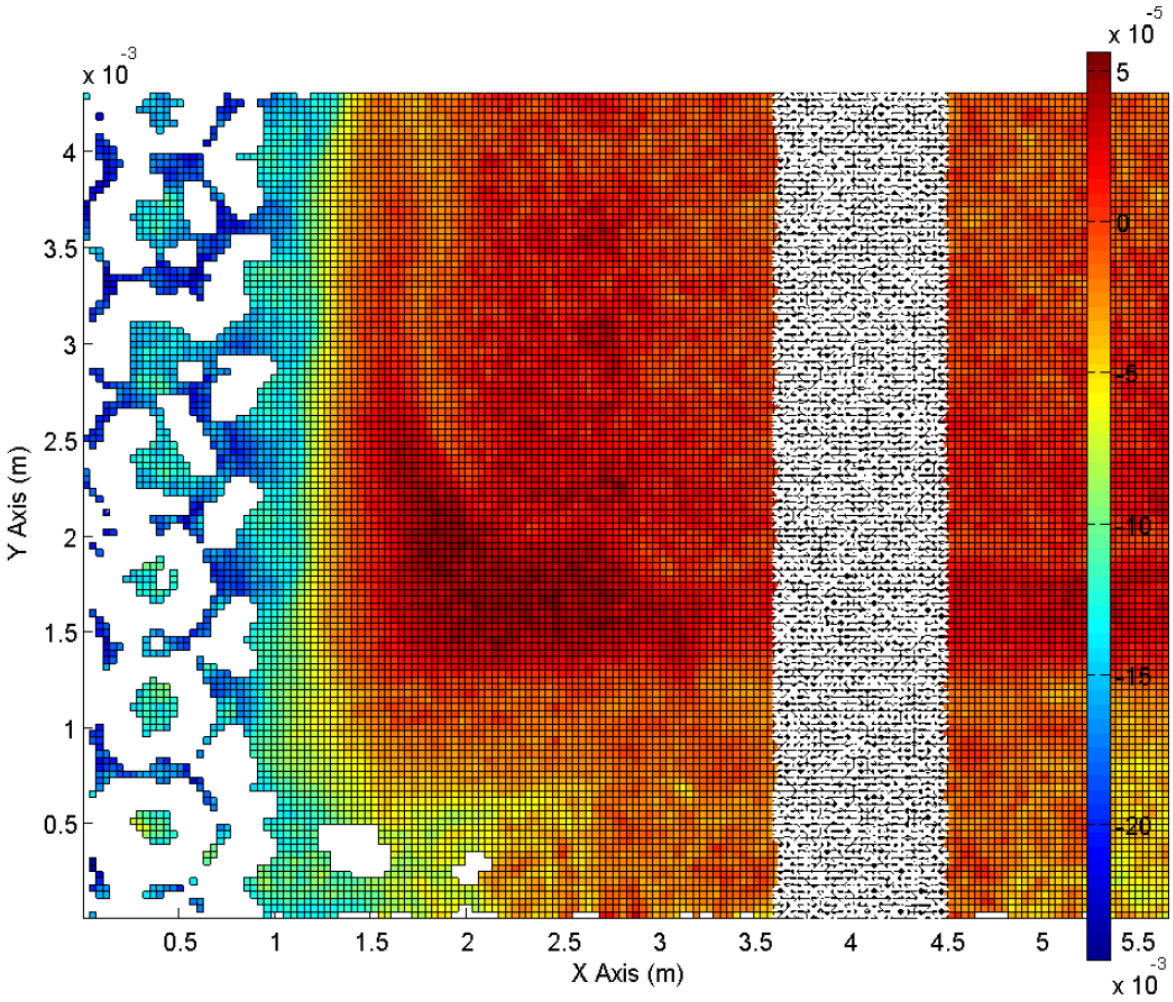

Figure 56. *Selected comparison area on the output from the Alicona Infinite Focus profilometer.*

The data from each profilometer was averaged in the X direction, providing an average displacement for each Y position in the comparison area. The averaging process is a potential source of error as any data showing non-uniformity in the X direction is lost. This error has been minimised by selecting the area that has the smallest variation in displacement across the X axis.

The lateral resolutions of the profilometers are different, therefore an interpolation technique in MATLAB was used to down sample the results from the Alicona profile to match the 0.05 mm lateral resolution of the G2 profile. The original data and the interpolated data are shown in Figure 57 below to highlight the close match of the down sampled data.

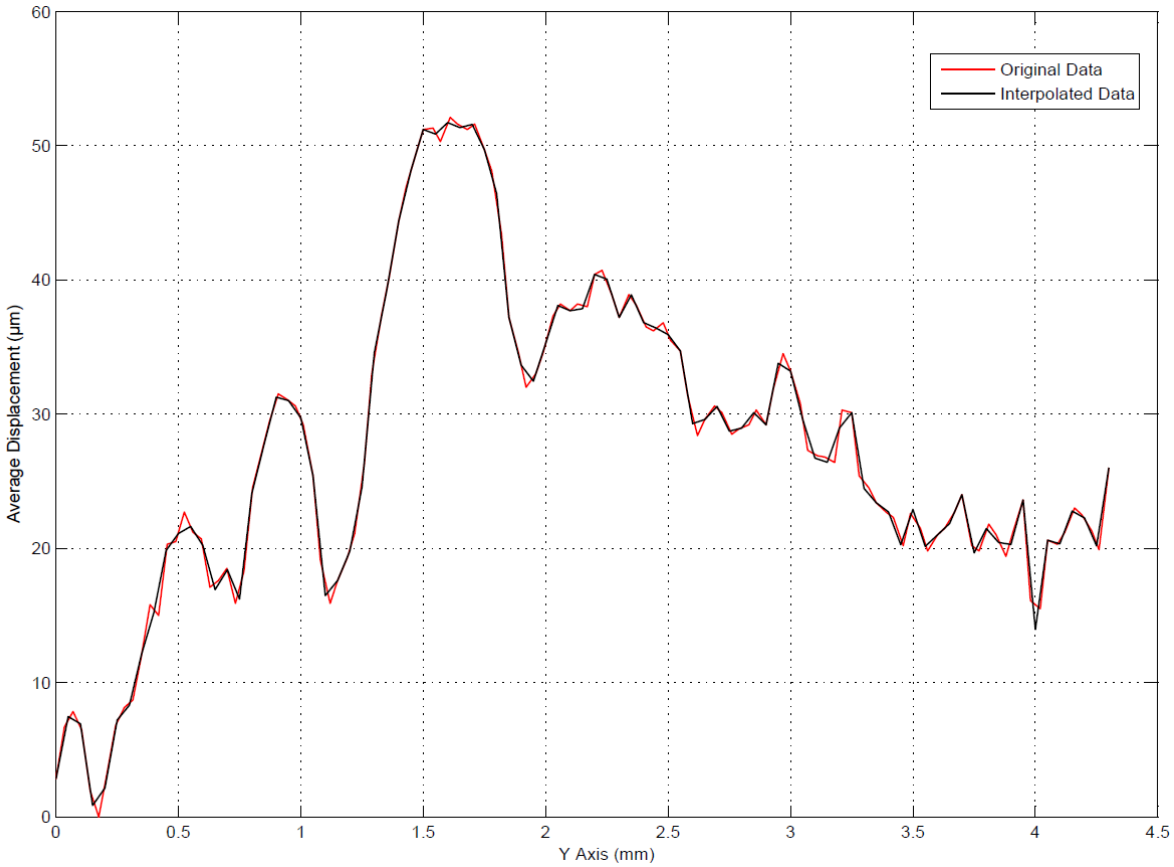

Figure 57. *The original averaged data from the Alicona profilometer is shown, along with the interpolated data that matches the lateral resolution of the G2 profilometer.*

The interpolated Alicona data was plotted on the same axes as the data from the G2. The G2 data is longer in the Y axis as a larger area was profiled, therefore the two sets of data were aligned and then the excess G2 data was removed to allow a like for like comparison. The data alignment process is a further area where errors could be introduced. To mitigate the risk, a large feature was used to align the data – the sharp fall and then significant increase in displacement visible after 1 mm in Figure 57. A graph showing the comparison between the Alicona and G2 data can be seen in Figure 58, along with a microscope image showing the comparison area in Figure 59 below.

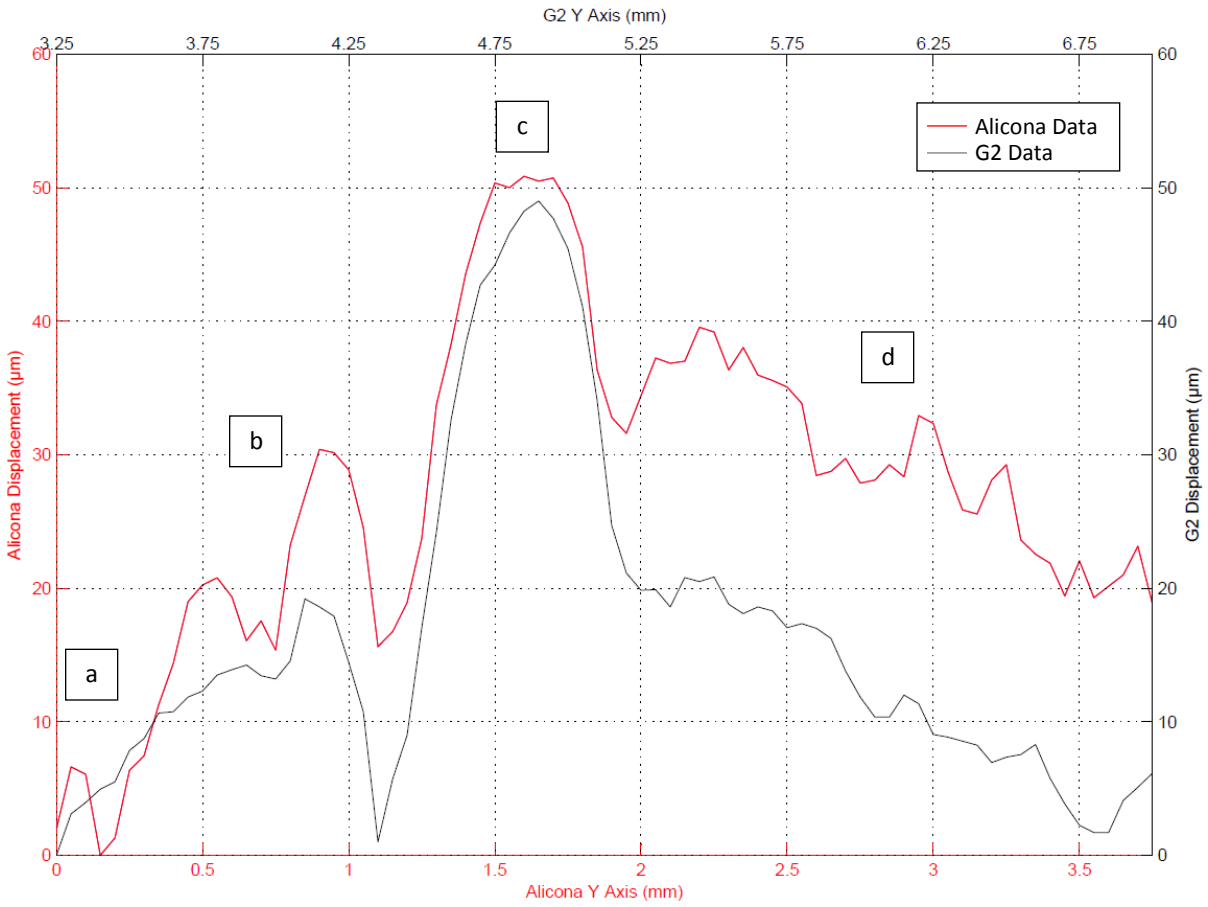

Figure 58. *Comparison of the profile output from the G2 profilometer and the Alicona Infinite Focus profilometer. Areas of the graph have been labelled for discussion purposes.*

The results in Figure 58 have been averaged in the X axis to provide an estimation for comparison. On the graph the data has been aligned in the X axis using notable features on the graph such as the sharp fall between point b) and c). For the Y axis of the graph, alignment data prior to point a) was used where only the dielectric is present. The displacements of the Alicona and Keyence LK-G10 were matched over a period of 1mm to provide a zero for the study area (points a)-d)) and to ensure there was no tilt in the sample causing the discrepancy seen at point d).

The labelled areas show the following printed pastes and features: a) The white dielectric paste only; b) The white dielectric paste with a variable thickness layer of PEDOT:PSS printed on top; c) The white dielectric with a silver track printed on top, covered by a 3 µm layer of PEDOT:PSS; d) The white dielectric paste, with a phosphor paste printed on top, covered by a relatively smooth 15 µm layer of PEDOT:PSS.

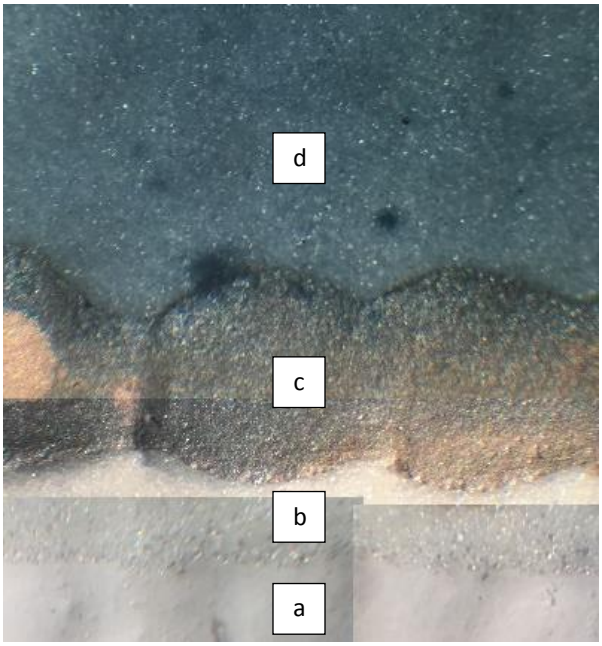

Figure 59. *A microscope image showing the study area, the image is made up of multiple microscope images, causing the join lines. The study area was used as the source of the data in Figure 58, and is labelled with corresponding letters.*

Figure 58 shows a possible match in some areas between the averaged data collected by the G2 profilometer and the Alicona profilometer. The large peak visible in Figure 58 at point c) is caused by a thick silver track being printed for the bus electrode.

The Alicona displacement is noticeably larger at area d) in Figure 58. A possible explanation for this discrepancy is that the Keyence LK-G10 displacement sensor on the G2 is measuring through the semi-transparent PEDOT:PSS layer, whereas the Alicona is measuring the true surface height using its focus based measuring technique. The discrepancies between the data at these points is similar to the expected PEDOT:PSS thicknesses of 3 µm at area b), and 15-20 µm at area d). The PEDOT layer is faintly visible in Figure 59 at the area marked b).

The errors when measuring data from semi-transparent layers is a concern as it could cause the nozzle height to be incorrect by up to 20 µm. However, the PEDOT:PSS layer is the last layer printed for EL lamps, therefore it is unlikely a profile would be needed to maintain a nozzle height for later layers. If a subsequent layer needs to be printed, the overall shape of the PEDOT:PSS layer appears to closely match the shape of the phosphor layer underneath. A temporary solution could be to add an estimated PEDOT:PSS thickness to the profile data and use that for printing.

The graph in Figure 58 shows that the G2 profilometer is within 5 µm of the Alicona data, excluding the area where PEDOT:PSS is printed. A 5 µm accuracy is sufficient for maintaining a nozzle height during printing as the thinnest layer is 10 µm.

The data produced by the G2 profiler includes some erroneous data points. If it proves a problem it is possible to create a ‘maximum expected step height’, whereby changes in height exceeding the value can be marked as error points and averaged out later. This approach would require the user to have

knowledge of the step height on the sample prior to profiling, otherwise they risk averaging out correct data.

4.3.3. Dispenser Printer Base Uniformity Testing

When the nozzle moves over the surface of the substrate without correction, the distance between the nozzle and the substrate will change. One of the major factors that affects how much it changes is the flatness of the substrate holder relative to the Z stage. The two main sources of error are the flatness of the aluminium plate and how much the stages bend as the plate moves.

A surface profile of the aluminium base plate on the G2 printer was taken by driving the plate with the moving stages under a fixed displacement sensor. The measurements were taken using a Keyence LK-G10 laser displacement sensor. The profiler and moving stage settings are shown in Table 20 below.

Table 20: *Profiler and moving stage settings used in all tests.*

Profile Area	X Resolution	Y Resolution	Stage Speed	Acceleration Time
50x50 cm	2 cm	2 cm	30 mms^{-1}	300 ms

The laser has a measurement range of 2 mm; if any results are outside of this range, they are not plotted. This caused some of the graphs to not show the full 50x50 cm of the aluminium base plate as the displacement was more than 2 mm lower than the original starting measurement. Figure 60 below shows the start position of the profiler in the closest left corner; the laser displacement sensor is hidden behind the syringe holder in the picture. Figure 61 shows the final position of the profiler in the far right corner.

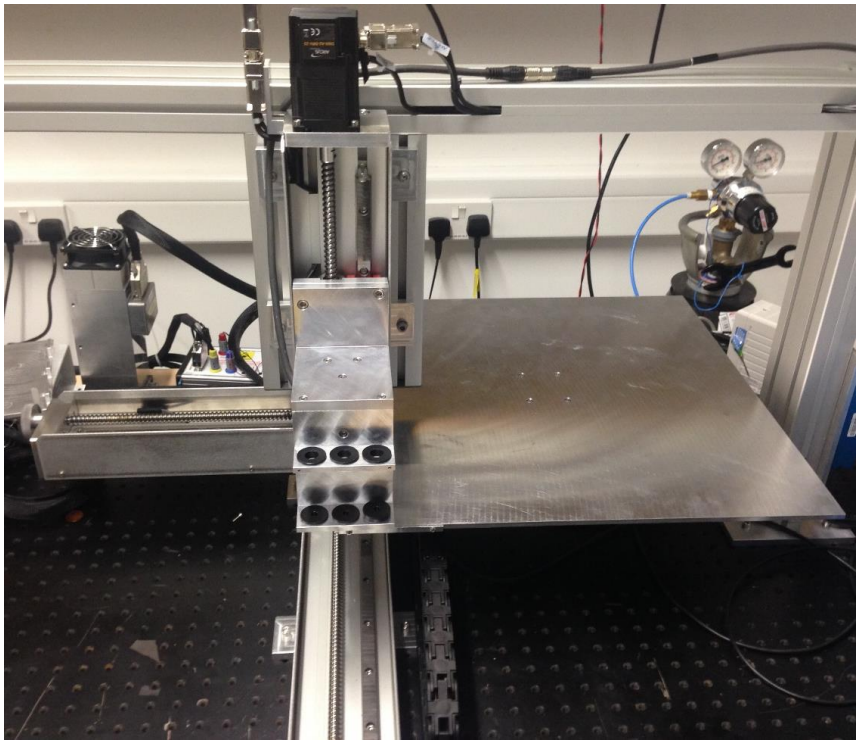

Figure 60. *Start position of the profiler in the closest left corner, representing point (0,0) in later graphs.*

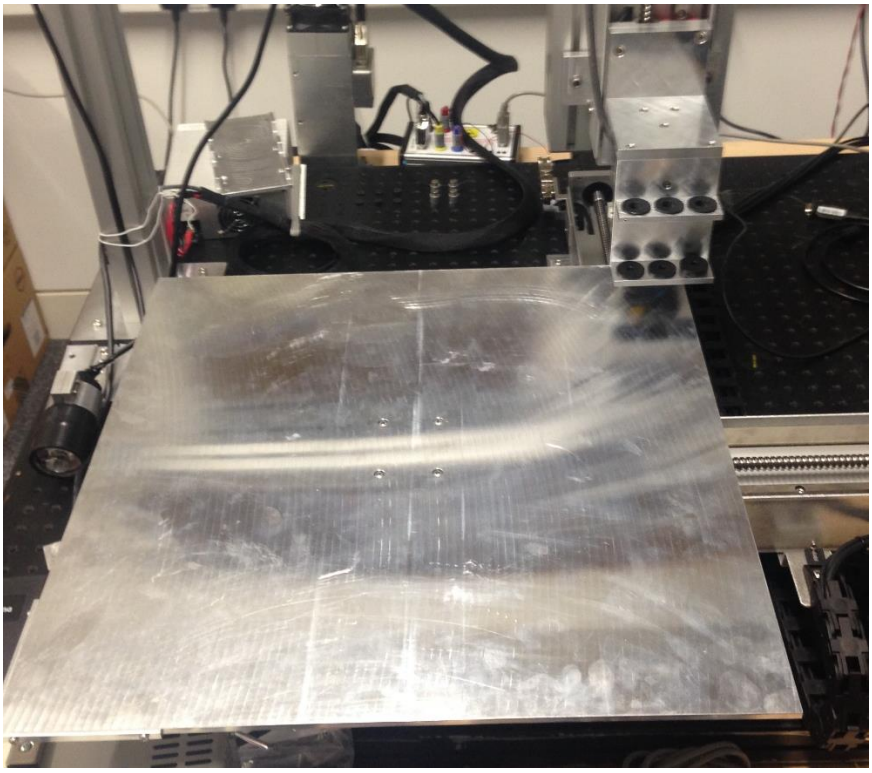

Figure 61. *Final position of the profiler in the furthest right corner, representing point (50,50) in later graphs.*

The results obtained for the base plate, with (0,0) being the closest left side of the printer, are shown in Figure 62 and Figure 63 below.

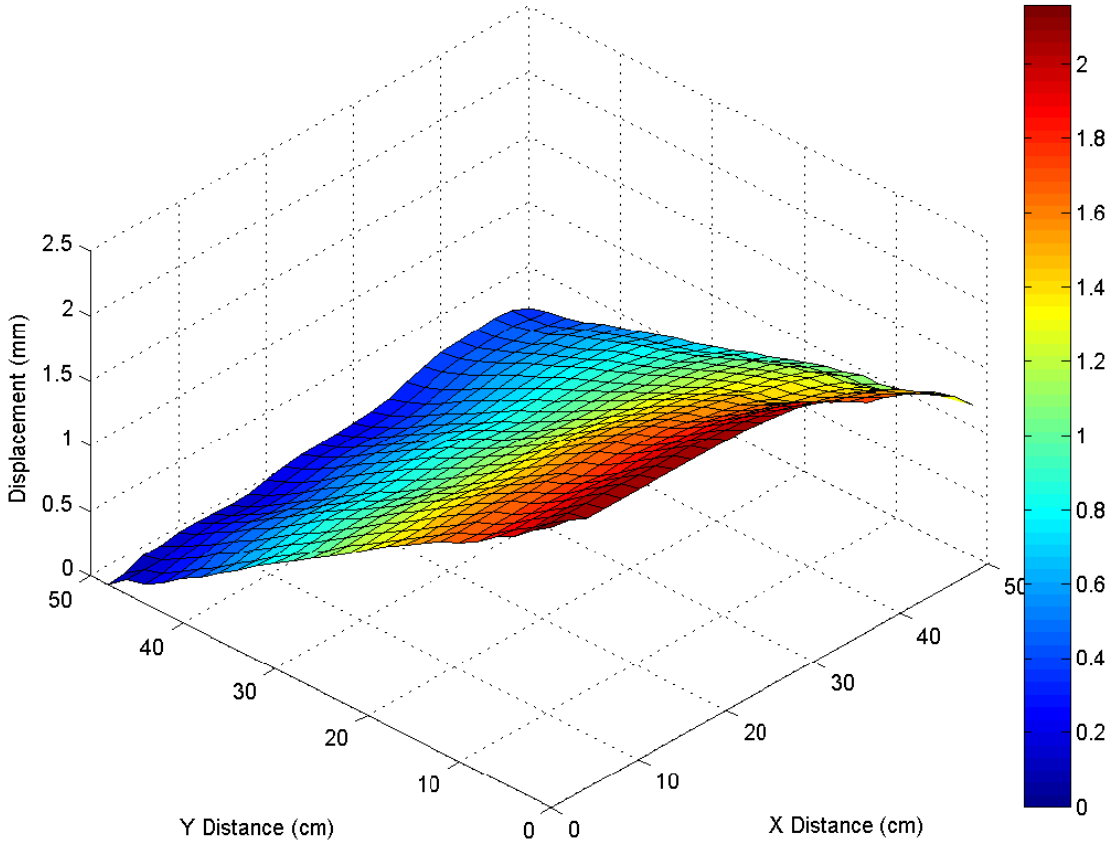

Figure 62. *3D view of the surface profile of the G2 aluminium plate in its original manufacturer's orientation.*

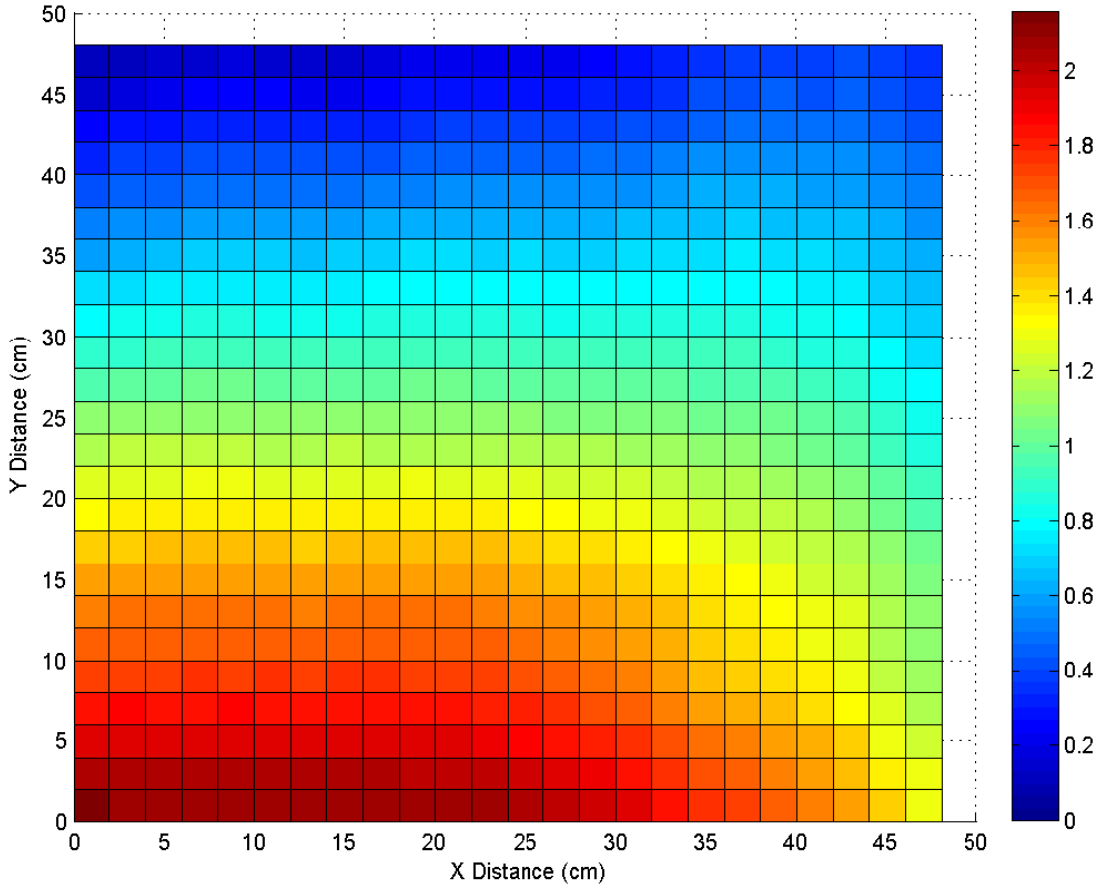

Figure 63. *Top down view of the surface profile of the G2 aluminium plate in the original manufacturer's orientation.*

The results show a change in height across the plate in excess of 2 mm. A variation on this scale will cause significant problems when trying to print large areas even with Z-height tracking. The graph does not determine the cause of the change in height. The base plate was rotated 180° to check whether the aluminium tooling plate, used as the base plate on the printer, was uneven, or if the stages had a bias. A second surface profile was taken, Figure 64 shows a comparison between the two surface profile readings before and after the plate is rotated by 180°.

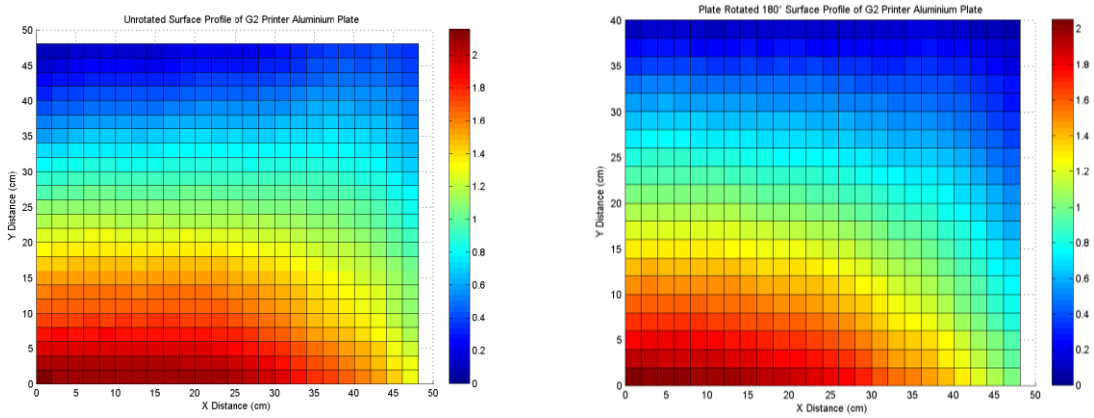

(a) (b)

Figure 64. *Comparison between surface profiles for (a) the original manufacturer's orientation and (b) the plate rotated by 180°.*

From Figure 64, it is possible to draw the following conclusions:

- The original and rotated profiles are very similar – rotating the base plate 180° made little difference to the measured displacements.
- The lack of significant change between Figure 64(a) and Figure 64(b) suggests that the aluminium base plate is relatively flat and it is the moving stage slides that are not flat. After consultation with the manufacturer (LG Motion), they suggested that the ball screws may be tensioned causing them to not lie truly flat.

To correct the ball screw tension, the end caps on both the X and Y stages were loosened and retightened to remove any stress in the ball screw. The surface profile test was repeated and gave identical results.

The printer was returned to LG motion, where the stages were attached to a known flat surface and the surfaces of the stages were skimmed to be flat. The stages were retested using the settings shown in Table 20. The results showed a significant improvement in plate flatness. The largest displacement is 1.249 mm above the lowest displacement on the repaired stages, compared to 2.155 mm for the original stages. A comparison of the original stages' profile and the repaired stages' profile is shown in Figure 65 below.

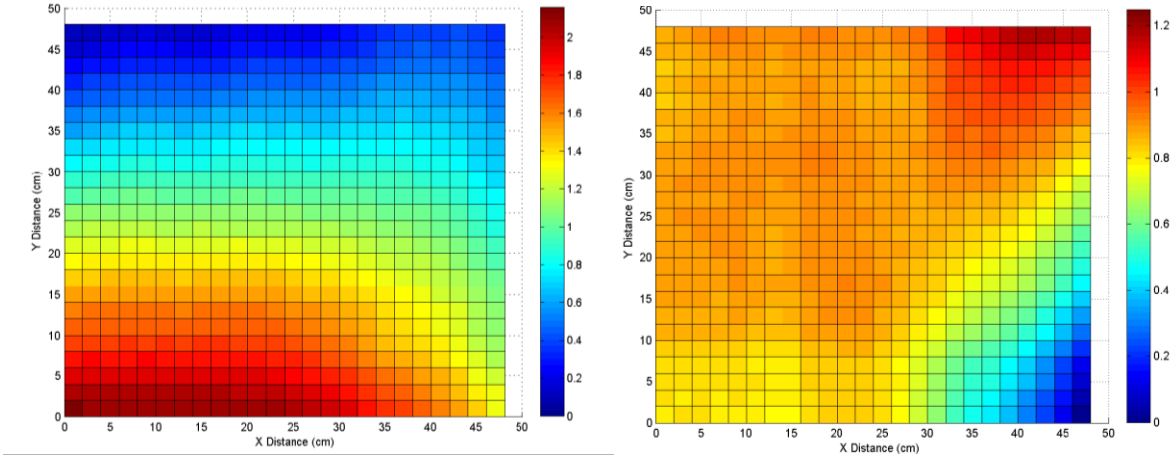

Figure 65. *Comparison between surface profiles for (a) the original stages as supplied and (b) the repaired stages after being skimmed by the manufacturer.*

The profile for the repaired stages show an improvement particularly on the left side where the difference has been reduced to less than 0.1 mm. The profile shown in Figure 65(b) still shows a significant change of 1.25 mm over the Y axis on the right hand side of the plate. The change appears to also be present in Figure 65(a) with a noticeably lower bottom right side and higher top right side. The combined results would suggest that originally there was a non-uniformity in the Y axis stage, which has been repaired.

The remaining non-uniformity shows there is a further problem with the stages. As the remaining error is isolated to two of the corners rather than an entire axis, it is likely to be a complex problem as the stages move. The system was returned to LG Motion where a second moving slide was added as they suspected the weight of the base plate was causing the top stage to tilt when at its extremities. Figure 66 shows the added moving slide on the G2 printer.

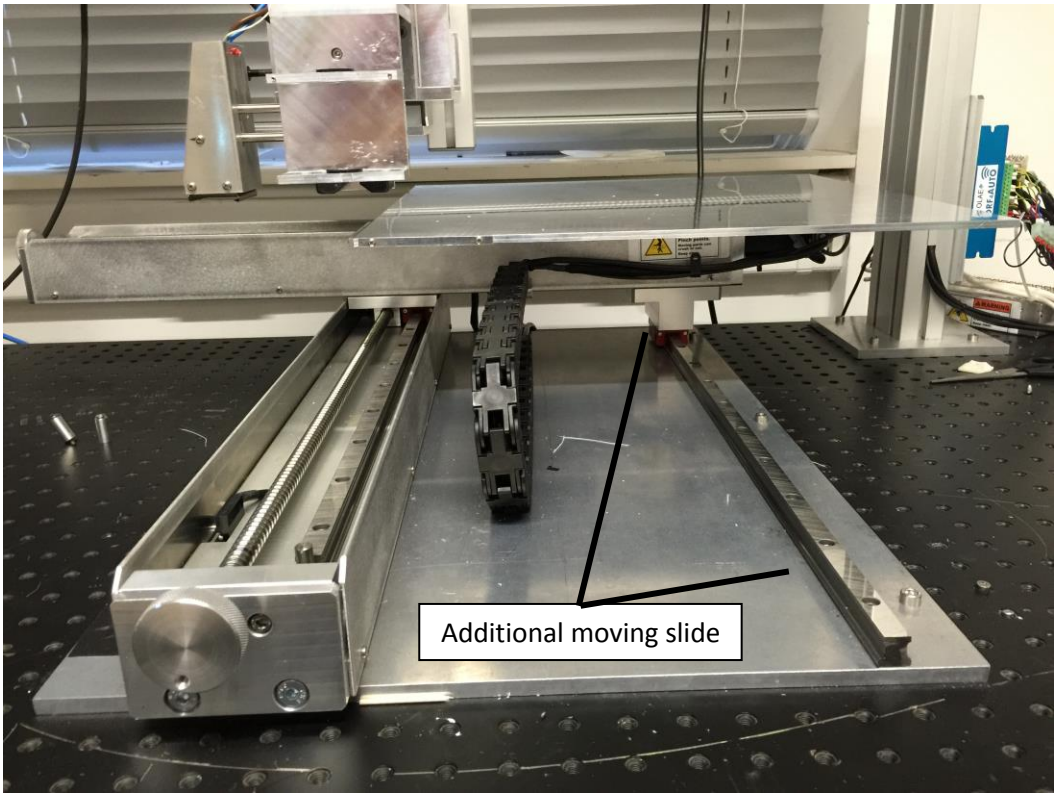

Figure 66. *Image showing the G2 dispenser printer with the additional moving slide.*

The results show that there is still significant variation over the base plate. The highest point is now 1.595 mm higher than the lowest point, compared with 2.155 mm originally, and 1.249 mm after the first set of repairs. The additional slide has in fact made the variation over the plate larger. A possible reason is that the additional and original slide are not exactly aligned, causing a twisting motion as the plate moves. LG Motion advised us that there are no further repairs that can be done, and the error is caused by the tolerance of the materials and extruded aluminium combining to create the variations seen.

In an attempt to further reduce the error, a number of small pieces of 0.2 mm thick sheet metal, known as ‘shims’, were added to the central support of the base plate. The aim was to raise the low areas of the base plate, creating a more even overall surface to print onto. The results from the profile after the shims have been added are shown in Figure 67 and Figure 68 below.

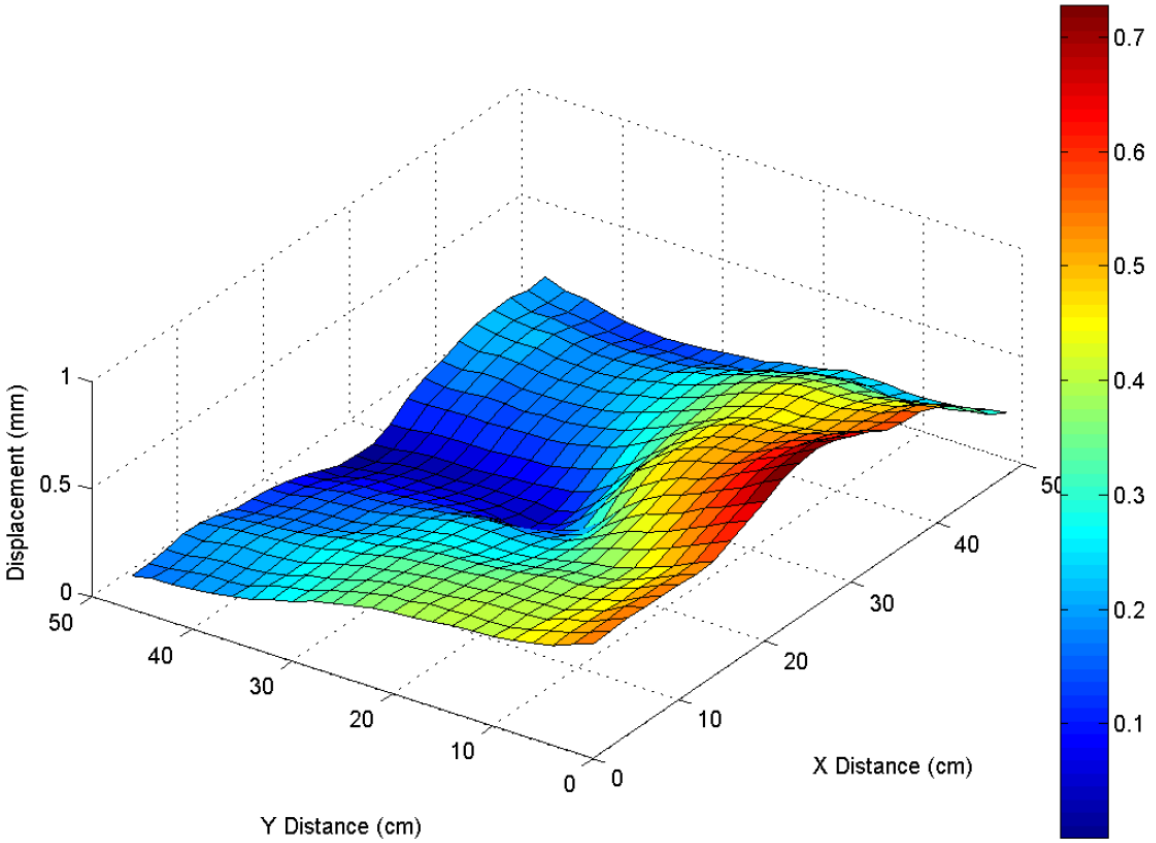

Figure 67. *3D view of the surface profile of the G2 aluminium plate with the shims added to the central support.*

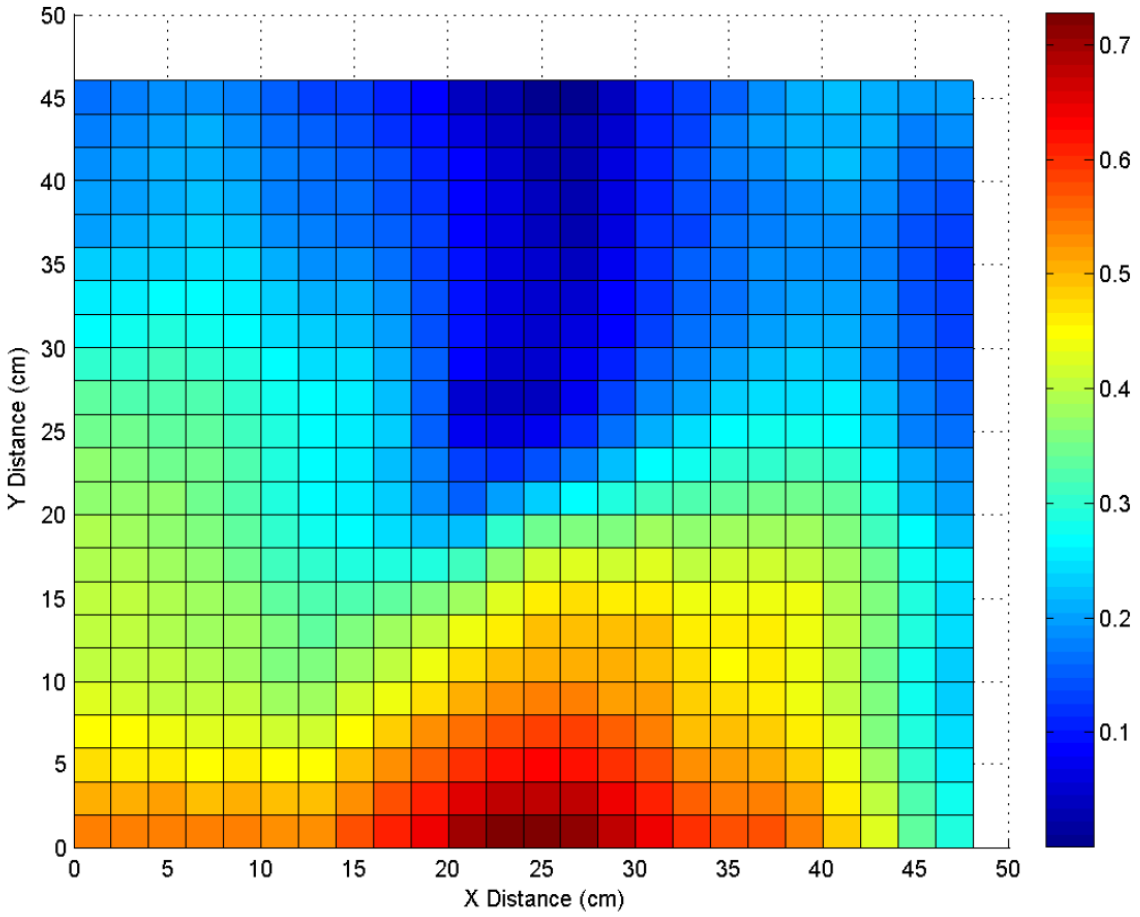

Figure 68. *Top view of the surface profile of the G2 aluminium plate with the shims added to the central support.*

The results show the overall variation from highest to lowest point has been reduced to 0.723 mm, however there are now fewer flat areas to print on. The results therefore highlight the need for z-height tracking when printing on any medium or large size (>10 x 10 cm) area.

A further test was conducted to check the repeatability of the measurements. As the moving stages are moved under the moving stage there is a possibility that positional repeatability issues could cause incorrect displacement measurements. Two measurements of the plate were taken 24 hours apart and then subtracted from one another to work out the error between them. The results are shown in Figure 69 below with the scale in micrometres.

The results show a close match between the two profiles with no measurement point having an error greater than 5µm. Typical separation distances between the nozzle and substrate are 220µm and an error of 5µm from repeatability will not make a different to offset features in the range of 0.5-1.5mm from the uneven printing plate.

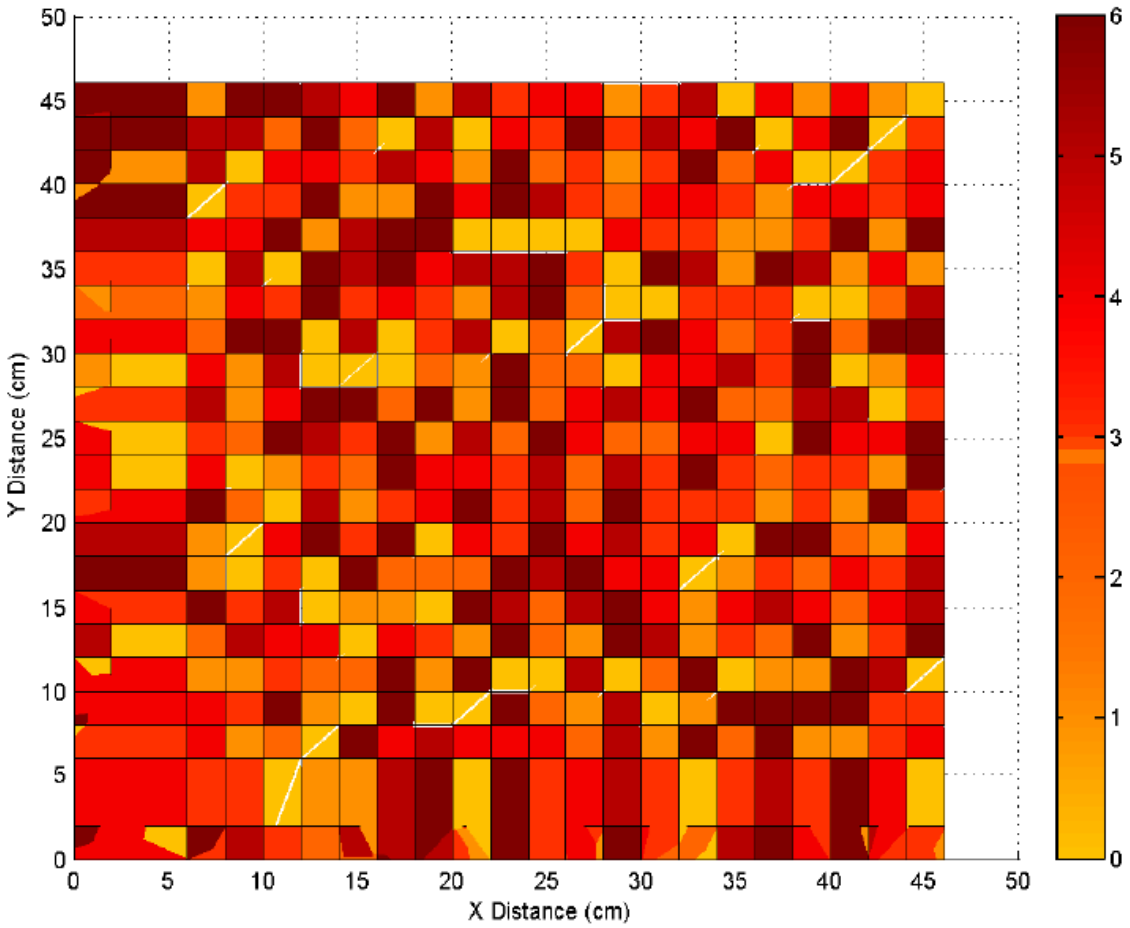

Figure 69. *Top view of difference between two surface profile measured 24 hours apart (Z-Axis key on right in micrometres).*

4.4. Conclusions

The new G2 printer was compared to the existing G1 printer; the results show a significant improvement in print time as a result of the improved movement stages. There was particular improvement when printing in continuous mode, where the G2's higher max speed meant the prints were up to 5.7 times quicker for large area prints. The G2 printer has also been tested to check the response of the printer to variations in print size and acceleration time.

The change in print time of both the G1 and G2 printer to variations in print size were linear for droplet mode printing. The G1 printer also responded linearly to changes in print area for continuous printing, whereas the G2 showed a reducing gradient for larger print areas. The change was attributed to a greater percentage of the total print time being spent at the maximum velocity as the design size is increased. A comparison of the relative improvements for the G2 against the G1 was also conducted. The graph of the relative improvements showed the G2 represents a significant improvement over the G1 for all print areas and that the effect was particularly pronounced for large area designs (>20x20 mm).

Experiments were also conducted to test the effect of variations in acceleration time on the total print time. A nonlinear response for droplet mode printing was seen and explored in depth with relation to the equations of motion. A square root relationship was identified between the movement time and the defined acceleration time. The relationship is caused by the triangular motion profile caused by the short movement distances (1 mm) for droplet printing. The response for continuous mode printing was shown to be linear due to the ideal trapezoidal motion profile used meaning the stages reached maximum speed as desired.

The hardware improvements made on the dispenser printer were then considered. The displacement sensor requirement was addressed and a number of sensing technologies were researched with laser triangulation sensors judged to be the most appropriate to the application. Two models from Keyence (LK-G10 and LK-G32) and two models from Micro-Epsilon (ILD 2300-2 and ILD 1700-2) were trialled. The ILD 1700-2 was withdrawn from testing due to software communication issues and the remainder were tested by attempting to profile a printed EL lamp. The Keyence LK-G10 was the only model to correctly sense the transparent interface layer so was selected for future testing. The laser was then characterised by comparing the results with a commercial profilometer by Alicona. The results and analysis suggested the Keyence LK-G10 sensor was not measuring the semi-transparent PEDOT:PSS layer correctly and was in fact returning the displacement value for the layer underneath.

The base plate uniformity relative to the dispenser nozzle was also measured. A variation of 2.155 mm was recorded over the plate, prompting a series of modifications to be undertaken. After three rounds of modifications the variation over the plate was improved to 0.723 mm. However, the variation is still significant enough to require z-height tracking.

5. Dispenser Printer Software Development

5.1.1. Introduction

In order to print high quality EL lamps a number of software improvements were required. The following areas are addressed in this chapter:

- Modifying the existing droplet mode code available at the start of this thesis on the G1 to work with the better performing Nordson dispenser controller.
- Adding Z-height tracking to the droplet mode control software to maintain a defined separation distance between the nozzle and substrate. Maintaining this distance will result in printed layers with more uniform thickness.
- Writing custom software to allow the G2 printer to dispense ink continuously in any complex shape. This hugely expands the range of devices that can be printed, and is an important feature for the end user where the design appearance is often important
- Adding Z-height tracking software to the continuous complex shape code. As the designs become more complex and larger, the problem of a varying separation distance becomes more pronounced. The result is layers with uneven layer thickness and Z height tracking counters this problem.
- Finding the optimum infill pattern to reduce the surface roughness of the printed layer and improve the print speed.

5.1.2. Dispenser Droplet Mode Control Software Improvements

The dispenser printer at the UoS is controlled through National Instrument's LabVIEW program. The existing software provided at the start of this research used the Musashi ML-808 FX COM-CE dispenser and was not initially compatible with the more advanced Nordson dispenser, meaning only the G1 printer could be used. The G1 printer was only able to print basic rectangular shapes by breaking the design down into individual droplets.

The droplet mode dispensing software requires two developments to allow EL lamps to be produced using either the G1 or the G2. The software requires new code to communicate with the Nordson dispenser controller and the z-axis height tracking capability needs to be developed. The z-tracking software is developed initially for droplet print mode before continuous mode as the software is simpler so easier to test.

New LabVIEW control software was written for the G2 printer, incorporating the all-digital Nordson Ultimus V dispenser controller. Significant work was also undertaken to optimise the communication code on both dispenser printers. The Nordson Ultimus V printer is used for all printed samples in this thesis.

The laser displacement sensor selected earlier (Keyence LK-G10) was used to offer a z-height tracking capability. Z-height tracking could be achieved by real time z-height measurement during printing, or the substrate could be profiled before printing. The real time z-height measurement would require the height directly under the nozzle to be measured in real time. Real-time height measurement during printing would require a bespoke displacement sensor, as there is only a very small (<200 μm) gap underneath the nozzle in which the laser can measure. The laser would have to be offset from the

nozzle and reflect from the area directly under the nozzle, with a receiver positioned to collect the reflected laser. Such a system is complex to build and prohibitively expensive. Because of this it was decided to profile the sample before printing each layer. The results from the profile are stored in a 2D array and then during printing each point is referenced in turn. The z-stage height is adjusted to maintain a desired separation distance.

Further software development was undertaken to incorporate profiler error correction into the code. Figure 70 shows a flow chart highlighting different stages involved when printing with a maintained z-separation.

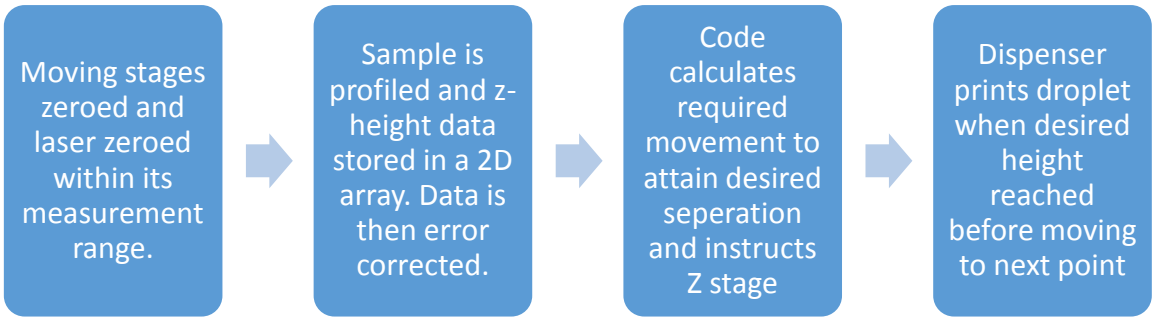

Figure 70. *Flow chart highlighting the different steps involved when printing with a maintained Z separation.*

The error correction is completed after the profiling of the substrate has finished. Each point in the array is checked to see if it falls outside of expected values. Extreme values can sometimes be created if the laser is moved outside of its measurement range or if the level of reflected light is too low. If a point is deemed an 'error point' the previous and following points are averaged and the 'error point' is replaced. The code works similarly for correcting two consecutive 'error points' using nearby values. Replacing error points using nearby averaged values introduces some errors to the profile. However, they are the closest approximation available, and when using typical separation values of more than 100 μm there will be a minimal chance of the nozzle hitting the substrate.

The G1 moving stages are limited to 50 mm of travel in the X and Y directions, whilst the G2 stages have 500 mm of X and Y travel. The laser displacement sensor is mounted next to the dispenser syringe, meaning there is an offset between the point the laser is measuring and the tip of the dispenser nozzle. To compensate, a fixed movement command is given after profiling is completed to move the nozzle to the correct start point. The offset has the drawback of reducing the area that can be profiled and printed and the effect is significant for the smaller G1. The mount for the G1 holds the laser with a 34 mm offset in the X direction meaning the area that can be profiled and printed is only 16 x 50 mm. The profiling and printing areas are shown, highlighting the limited overlap, in Figure 71 below.

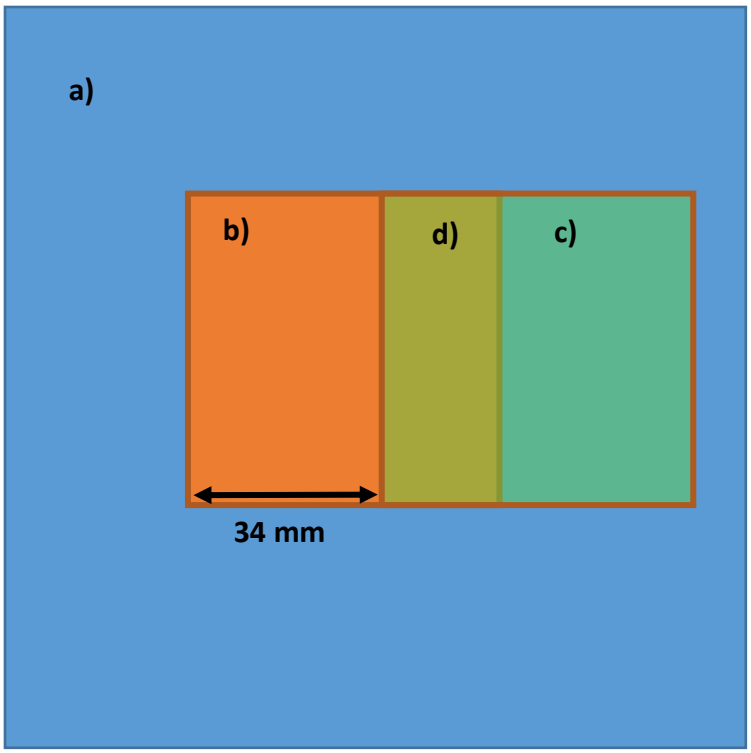

Figure 71. *Image showing a) the overall substrate, b) the print area, c) the profile area, d) the overlap between print and profile areas.*

The z-height tracking feature will not be enabled on the G1 printer as the profile and print overlap is too small to print useful EL lamps. The larger G2 printer has an offset of 43.35 mm in the Y axis between the nozzle and the displacement sensor, meaning the effect is minimal when compared to the 500 mm of travel. The mount was made out of machined 10 mm aluminium tooling plate with a tolerance of +/-0.1 mm and therefore it is possible that there could be a small alignment error between the profiles and the prints. An investigation was conducted into the effect of the droplet mode z-height tracking on layer uniformity and overall print quality.

A series of test rectangles were printed using silver ink onto a fabric substrate. Three of the rectangles were printed with the displacement sensor enabled and three with it disabled. The aim was to evaluate the effectiveness of the displacement sensor in a practical environment. The rectangles were printed with dimensions 70 x 2 mm to show the variation in print quality over a relatively long length. The substrate is a woven polyester fabric, chosen as it is a woven fabric commonly used in architectural applications, and being white it contrasts well with the silver ink.

The printer control software is able to use the displacement sensor with droplet mode printing in rectangular shapes and continuous printing for complex shapes (discussed in 5.1.4). The printer settings are shown in Table 21 below.

Table 21. *Printer settings used in dispenser printing with displacement sensor tests.*

Movement Speed	Print Size	X Resolution	Y Resolution	Dispense Pressure	Vacuum Pressure	Curing
10 mm/s	50 x 2 mm	0.8 mm	0.4 mm	60 kPa	0.8 kPa	120˚C 10 mins

Three rectangles were printed with and without the z-height tracking software enabled. A separation distance of 220 µm between nozzle and substrate was used. When printing using the z-height tracking software, the distance is automatically maintained using the laser displacement sensor. When printing without z-height tracking, the initial height was found using a multimeter and the laser displacement sensor. The point where the nozzle contacts the substrate was checked using conductive tape and a continuity test on a multimeter. The 220m separation distance was then found using the laser displacement sensor to adjust the nozzle height. The printed tracks can be seen in Figure 72 below.

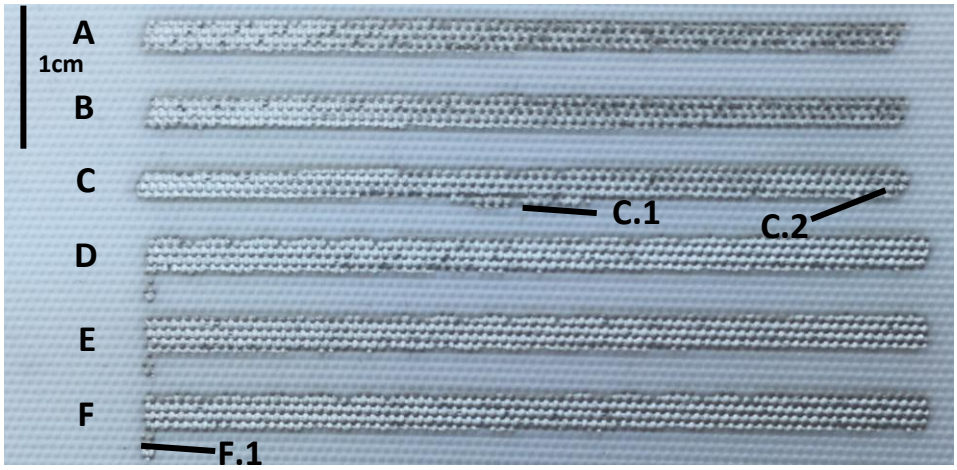

Figure 72. *7 x 1.5 mm printed silver rectangles, samples A, B, C had z-height tracking disabled, samples D, E, F had z-height tracking enabled.*

The tracks appear relatively similar when visually inspected. During printing with the z-height tracking disabled there was significant contact between the nozzle and substrate, causing the nozzle to bend and producing an uneven print. An example of the nozzle bending can be seen in Figure 73 below.

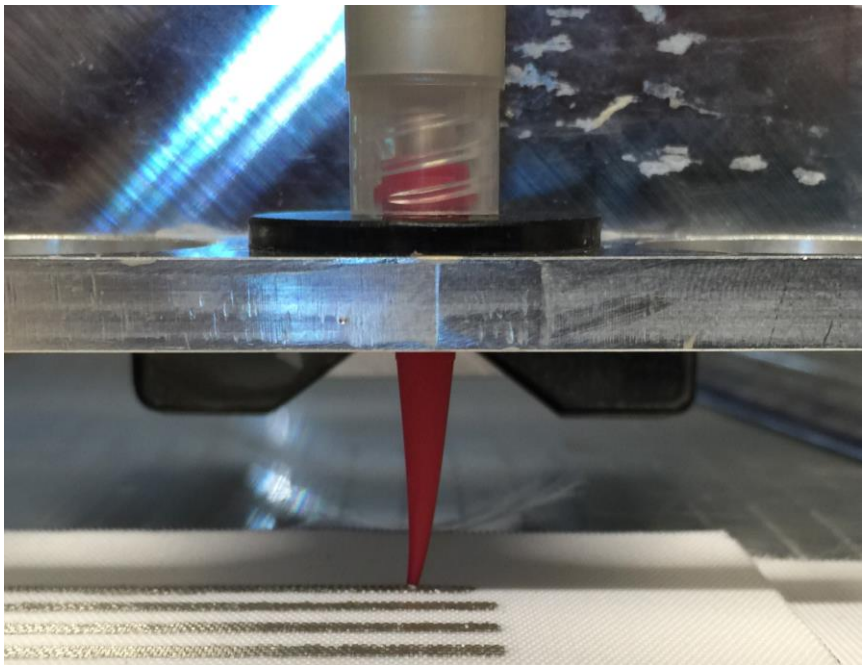

Figure 73. *Dispenser nozzle bending when contacting the substrate when printing without z-height tracking.*

On track C at area C.1 shown in Figure 72, the track can be seen to widen. This is caused by the nozzle contacting the substrate and bending, causing it to move from the desired path. It can also be seen at area C.2 that the rectangles printed without z-height tracking are shorter than those printed with it. This is also caused by the nozzle bending, meaning it did not reach the planned end of the track because it was dragged behind. The small tabs highlighted in F.1 are caused by a timing error in the z-height tracking code that causes the nozzle to lower prematurely, meaning some ink bleeds from the shape. For later prints this error has been removed.

The print quality of the rectangles was judged by testing the resistance over the length of the track. The resistance was measured using a Keithley 2002 Multimeter. The results are shown in Table 22 below.

Table 22. *Results from resistance tests on the samples printed with and without z-height tracking.*

Z-Height Tracking	Sample	Track Resistance (Ω)
Disabled	A	12.80
	B	3.30
	C	1.61
Enabled	D	0.93
	E	0.90
	F	0.91

The resistances of the tracks printed without z-height tracking are all higher than the tracks printed with z-height tracking. The average resistance of those without z-height tracking is 6.4 times higher than the average resistance of the samples printed with z-height tracking. The resistance of samples A, B, and C also varies significantly, showing the print quality is variable and achieving a uniform thickness layer is very difficult.

5.1.3. Continuously Printed Complex Shapes

Both the G1 and G2 dispenser printers were initially limited to printing rectangular shapes. The limitation was imposed as the G1 stage controller is only capable of performing single linear moves one axis at a time, meaning it is impossible to print complex designs using the G1 printer. As part of the CREATIF project, designs are produced by artists which contain curved shapes. To produce these prototypes, the capabilities of the printer must be expanded to print any shape.

The G2 stage controller (Arcus PMX-4EX-SA) is capable of performing buffered linear interpolated moves, which involve sending the controller a series of positions to store in its 36-point buffer. Each position contains an XYZ coordinate and the speed at which the stages should move to that point. Once the moving stages have reached the desired position they automatically start moving to the next position in the buffer. The moving stage controller automatically manages the velocity and acceleration of the individual stages to ensure all coordinate positions are reached.

A new process was developed for creating designs, converting them into paths for the nozzle to follow, and then communicating them to the Arcus stage controller. The process is summarised in Figure 74 below, with the software used for each step and the associated output of that software shown in the orange squares.

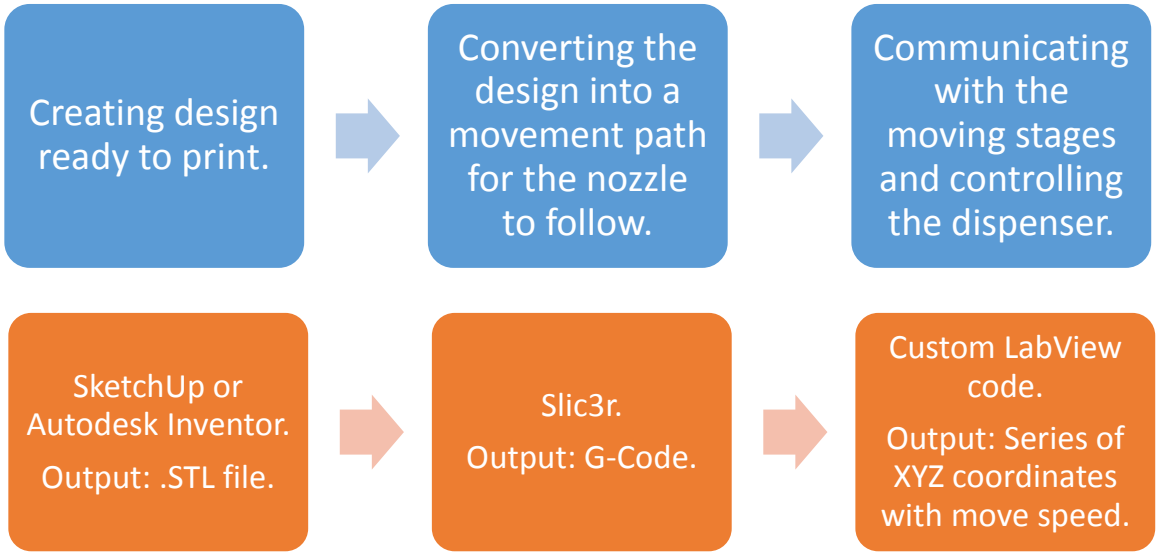

Figure 74. *The blue squares show a summary of the main steps in the software for printing complex shapes. The orange squares show the software used for that process and the associated output from that software.*

For testing, the Sketchup 3D CAD program was used to design the lamps. A commercial logo with many curves was used for testing to show the advancement in printing capability. The logo was loaded into Sketchup and exported as an STL file. The view in Sketchup is shown in Figure 75 below.

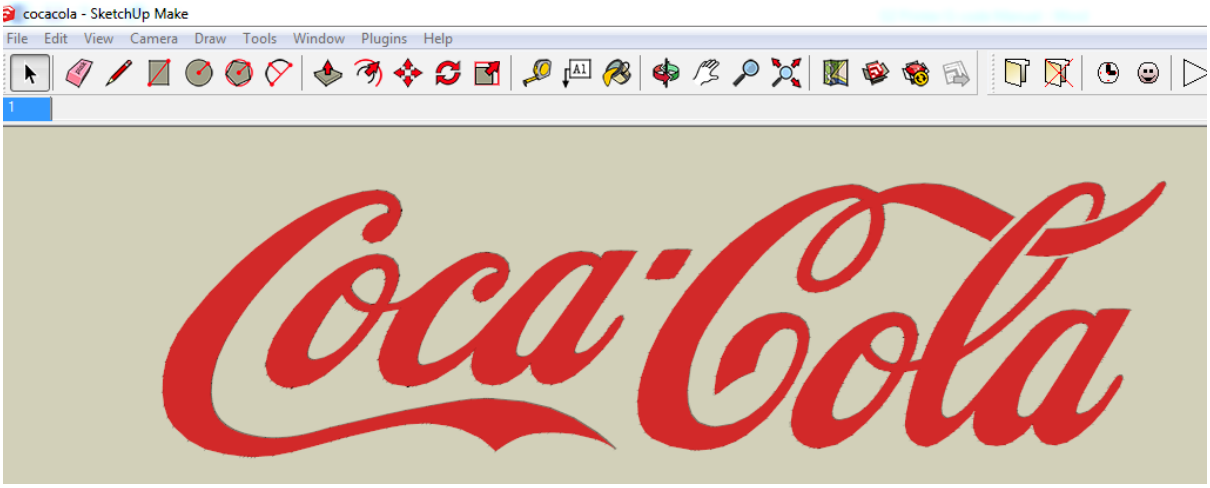

Figure 75. *The commercial Coca Cola logo was used to demonstrate the capability of the printer.*

The exported STL file from Sketchup was loaded into Slic3r [68], an open source tool for converting 3D models into a path for 3D printers to follow. The same principles of interpolated XYZ movement apply for dispenser printing and the tool can be adapted and used for dispensing applications. The software was customised to work with 2D designs by defining each layer to be a specific thickness. Multilayer EL lamps could be produced in the software by stacking the designs in 3D, with each layer having the defined thickness. Slic3r produces a G-code output, which includes a series of XYZ coordinates as required by the stage controller. The route between the points is defined by the infill pattern and a number of different patterns are investigated in the following section.

The last part of the process involves custom software written in LabVIEW that converts the G-code into the correct format for the Arcus stage controller and to control the external Nordson dispenser. This code was developed to accurately control the various components of the dispenser printer.

Dispenser printing is more complex than 3D printing as the nozzle must be lifted when not dispensing to avoid ink being erroneously deposited onto the substrate. The custom software works out the points in the G-code where the nozzle is lifted (e.g. between letters). When it reaches one of these points it creates a command to stop the dispenser pressure and also adds in extra 3D coordinates to lift the nozzle over the area where it is not dispensing. The opposite commands are issued when the software reaches the position to continue dispensing.

Once the G-code is in the correct format for the motion controller, the data points are sent to the stage motion controller. The software must manage the commands it is sending to the stage controller buffer as it is only able to store 36 points at any time. The buffer is constantly monitored to check for free space and extra points are loaded in real time during the print as buffer space becomes available. At the end of the print the nozzle is raised high above the substrate to allow it to be removed without colliding with the nozzle.

When the print is started the zero point is automatically calculated by the software and all XYZ positions are shifted when the user defines the start point. During printing the software controls the stages and the dispenser printer in parallel to ensure a synchronised print. The software is capable of printing multilayer designs and automatically aligning the designs for the different layers. After each layer the Z

axis print height can be reset to consider the thickness of the layer just printed. Support for curing layers was also added as part of the CREATIF project where a UV or thermal print head was passed over the print to cure it in position. The printed test logo can be seen in Figure 76 below that is printed using a transparent polyurethane ink onto Kapton plastic film.

Figure 76. *A transparent polyurethane ink dispenser printed onto Kapton plastic film in a complex shape to demonstrate the printer's improved capability.*

The complexity of this print compared to the simple squares produced before shows a significant improvement in the capabilities of the controller and software for the G2.

5.1.4. Continuously Printed Complex Shapes Utilising the Displacement Sensor

A series of 5 mm width test conductive tracks were printed in continuous mode using silver ink onto a fabric substrate. The tracks were printed using a meander pattern to highlight the improved capabilities over the previous displacement sensor code that could only print rectangles in droplet mode. The Y length of the tracks were 10 cm, 20 cm, and 40 cm, and the length was varied to test the accuracy of the displacement sensor over differing print sizes. For each track length six samples were printed, three using the displacement sensor and three without, meaning a total of 18 samples were printed.

The print settings were the same for both samples with the exception of Z-height tracking being enabled for half the samples. When the displacement sensor profiled the sample for Z-height tracking a Y spacing between sample rows of 10 mm was used. The settings used for all samples are shown in Table 23 below.

Table 23. *Printer settings used with G-code samples with and without the displacement sensor enabled.*

Straight Equivalent Length of Track (cm)	Actual Length of Track (cm)	Nozzle to Substrate Separation Distance at Start (µm)	Print Speed (mm/s)	Dispense Pressure (kPa)	Vacuum Pressure (kPa)	Curing
10	15.7	220	10	22	1.3	120˚c 10 mins
20	31.4					
40	62.8					

The displacement sensor works out the area to profile from the G-code uploaded. A rectangular area is created that covers all of the points in the G-code. The rectangular area is then divided up into continuous lines that are profiled in the X direction. The Y resolution defines the spacing between adjacent X movements. Using the data from the profile, a defined separation distance is then maintained between the nozzle and the substrate.

Kapton polyimide film was used as the substrate to remove any substrate variation affecting the result. The 10 cm, 20 cm, and 40 cm samples are shown in Figure 77.

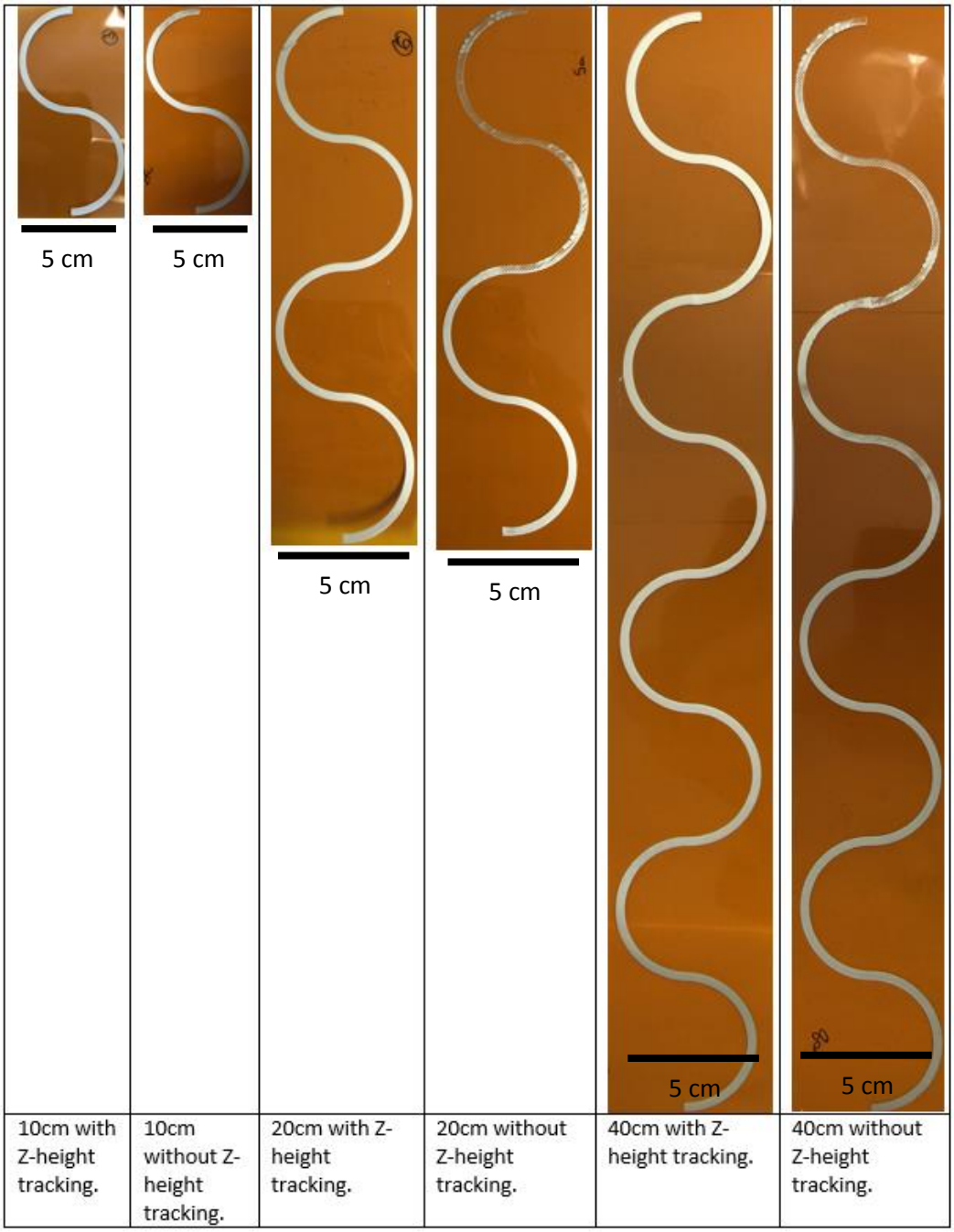

Figure 77. *Image showing 10 cm, 20 cm, and 40 cm printed samples with and without a displacement sensor.*

In each of the images without Z-height tracking inconsistencies in the printed layer are visible. This is caused by the nozzle coming into contact with the substrate due to variations in the distance between the nozzle and the substrate. The effect is not visible in the samples with Z-height tracking as the laser was used to keep the nozzle 220 µm away from the substrate.

To objectively judge the print quality, a resistance test was carried out on all of the samples. As the inks are conductive, the test gives an indication of how continuously the ink has been deposited onto the substrate. The results from the resistance tests are shown Table 24 below. All measurements were taken using a Wayne Kerr 6500B precision impedance analyser.

Table 24. *G-code results from resistance test on the samples printed with and without z-height tracking.*

Track Length (cm)	Z-Height Tracking	Sample	Track Resistance (Ω)
10	**Disabled**	A	2.619
		B	2.881
		C	15.812
	Enabled	D	0.936
		E	0.879
		F	1.073
20	**Disabled**	A	19.125 x10^6
		B	23.506 x10^6
		C	259.491
	Enabled	D	2.350
		E	2.375
		F	2.329
40	**Disabled**	A	30.177 x10^6
		B	33.386 x10^6
		C	1.855 x10^6
	Enabled	D	3.548
		E	3.139
		F	2.972

All of the 40 cm tracks without profiling, and two of the 20 cm tracks have resistances in the MΩ range, which effectively presents an open circuit. On the 10 cm tracks the average resistance, with the displacement sensor enabled, was 0.963 Ω, compared with 7.104 Ω with the displacement sensor disabled, or 7.4 times higher without the displacement sensor. The average resistance for a 20 cm track using the displacement sensor was 2.351 Ω, and for a 40 cm track was 3.220 Ω.

The print efficiency discussed earlier was found using Equation 1. The calculation found the efficiency of the print without the displacement sensor compared to the print with the displacement sensor enabled. The results in Table 25 below show the average print efficiency for a 10 cm track was 14% without the displacement sensor. For the longer tracks the print efficiency was effectively 0%.

Table 25. *Print efficiency calculations on the samples with the displacement sensor disabled compared to those with it enabled.*

Length of Track (cm)	10	20	40
Average Print Efficiency	14%	0.00%	0.00%

The results show that the performance of the printed track is significantly improved over a 10 cm distance with the displacement sensor. The tests have also shown that printing tracks over 20 cm are only feasible when using the displacement sensor. The tracks meander pattern has demonstrated this capability is not lost when printing complex designs.

5.1.5. Infill Pattern Selection for Complex Shapes

Variations in the printed layer thickness on an EL lamp can modify performance and in some cases cause failure of the material. If a solid area needs to be printed, the nozzle will pass multiple times within that area to print a continuous area of ink. There are a number of possible infill algorithms that can be selected to define the route the nozzle will take within a continuous area and this section aims to identify the most appropriate printing pattern for any shaped area. Because dispenser printing is a new technology, there are currently no standard algorithms for calculating the printing path. However, the deposition process is similar to that of 3D printers discussed earlier which already have a number of alternative algorithms available and so this would therefore be the most appropriate starting point for this new dispenser printing technology [69-71].

The primary aims of the infill algorithms used in 3D printing are to achieve a continuously filled area that has uniform thickness and that prints as quickly as possible. When using this process for dispenser printing, the surface roughness is significantly more important, in particular for multilayer applications. If the surface roughness is too great, it can cause defects in any subsequently printed layers; wasting time and material. Two of the main causes of variations in layer thickness is the infill pattern affecting the movement speed and the separation distance between the substrate and the nozzle. The motion controller is unable to keep the nozzle moving continuously at a constant speed, as the motors take time to accelerate and decelerate. These slight variations in nozzle speed can cause some parts of the print area to be thicker than others. Also minor errors in the height of the nozzle can appear when the nozzle is raised and lowered regularly during the print process, which can be reduced by an infill pattern that requires minimal movement in the Z axis.

This section selects five distinct infill patterns used in 3D printers to test with a dispenser printer in order to determine which performs best in terms of coverage, surface roughness, thickness and print time. The five infill patterns are tested with three different infill density values and four different shapes are printed as they form the building blocks of many other more complex geometries. The results are compared between different print shapes, infill patterns and density to identify the best performing infill pattern for all print shapes. In this experiment only single layers are tested to reduce the overall experimental time and the cost of deposited silver ink. It is assumed that layers printed on top of the first layer behave similarly to the first layer on polyimide film.

Each infill algorithm was selected as it potentially offered an advantage that could lead to an improvement in: the continuity of the printed layer, the surface roughness, or the print time. The

selected infill patterns with their assigned names are shown in Figure 78 below. For each pattern the route the printer nozzle would take is shown to highlight the differences between them.

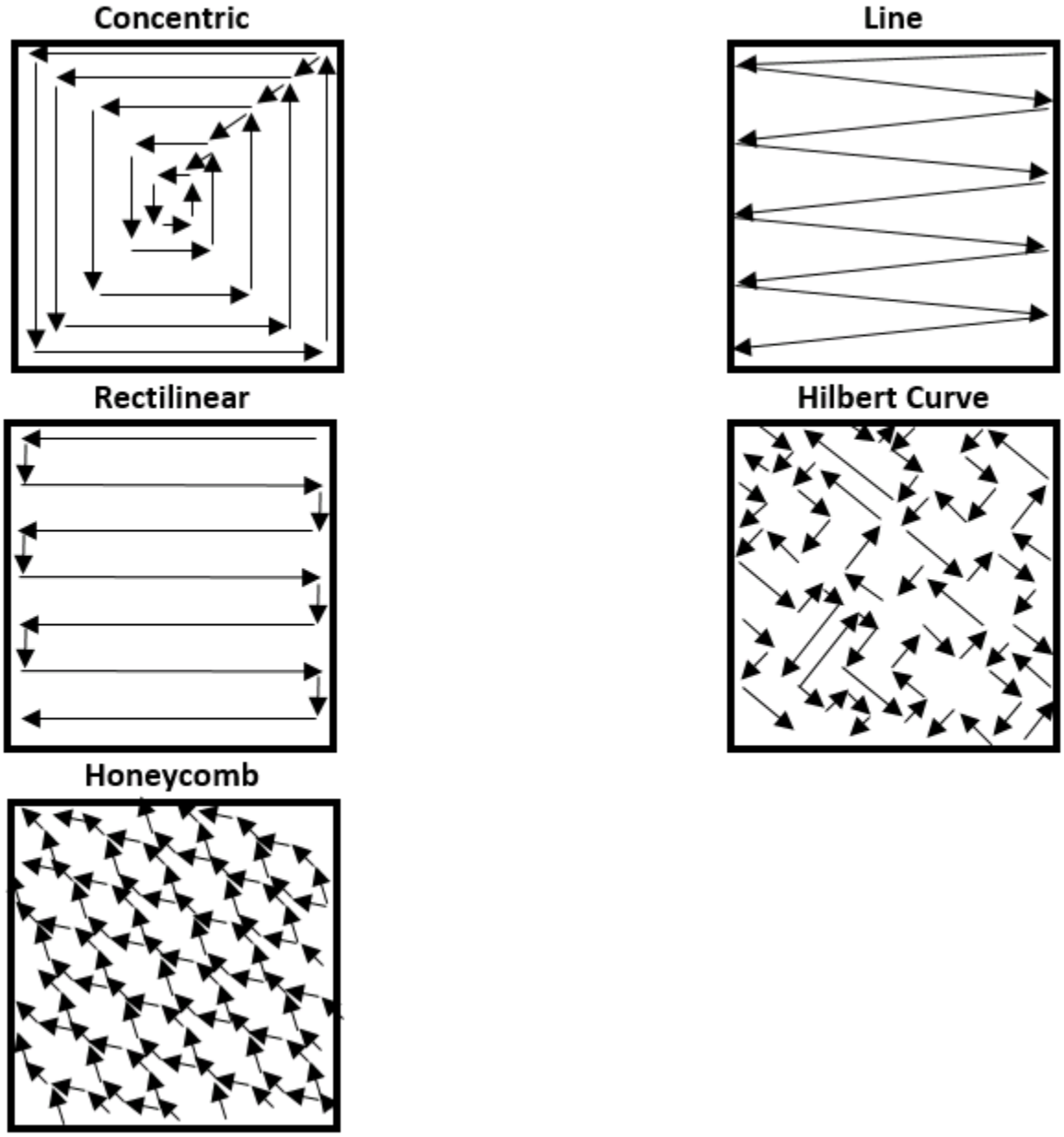

Figure 78. *Summary of selected infill patterns for testing, showing the route the printer nozzle would take for each pattern.*

The first infill pattern is referred to as 'concentric'. The nozzle moves following the perimeter anti-clockwise from the top right corner. After each continuous loop of the perimeter, the nozzle is raised and moved closer to the centre before the process repeats. Raising and lowering the nozzle aims to avoid excess material being deposited in the area where the nozzle moves towards the centre. As can be seen in later results, the raising and lowering of the nozzle appears to negatively impact the surface roughness in this area. This pattern has the disadvantage that the nozzle is frequently raised and lowered and that printing in the centre of the pattern can be difficult on more complex shapes.

The second infill pattern is referred to as ‘line’ and unlike the concentric pattern it does not involve raising and lowering the nozzle. Avoiding movement in the Z axis is beneficial as it avoids possible z-stage movement errors. The path starts in the uppermost right hand corner and crosses the print area at a defined angle until the nozzle reaches the edge of the area. The process continues working down the shape until the entire area is covered. To increase the infill density of printed lines in the shape, the angle between adjacent lines is decreased. This pattern has the disadvantage that the lines are not parallel potentially creating areas with more ink than others.

To counteract the non-parallel print path in the ‘line’ algorithm a second print algorithm, ‘rectilinear’, was tested. The rectilinear pattern is similar to the line algorithm, however rather than having adjacent print lines with differing space between them, all the print lines are parallel. This is achieved by following the perimeter of the pattern at some point to ensure all lines are parallel. This pattern has the disadvantage that there are long straight stretches with sharp corners. The printer moving stages require time to accelerate and decelerate and therefore they move more slowly at the corners on the edge of the pattern meaning more ink is dispensed at these points.

To avoid long straight areas with short sharp corners the pattern known as ‘Hilbert curve’ was tested. This pattern is a continuous fractal space filling curve that includes many sharp corners close together which should result in a more even distribution of ink over the print area. The disadvantage of this pattern is the high number of sharp corners is challenging for the moving stages to perform at speed and the pattern can create excessive vibration within the moving stages during printing which will affect their positional accuracy.

The final pattern tested is referred to as ‘honeycomb’. This is similar to Hilbert curve in that it has no long straight sections; however the angle of the corners is reduced creating less vibrations and the route the nozzle takes is simpler. The outcome is a more even distribution of ink and a faster print time.

The five printed infill patterns are shown in Figure 79 below. The samples were printed with large spacing (>1 mm) between the print lines to clearly show the pattern. All samples were printed using FabInks TC-C4007 [72] silver ink on Kapton polyimide film.

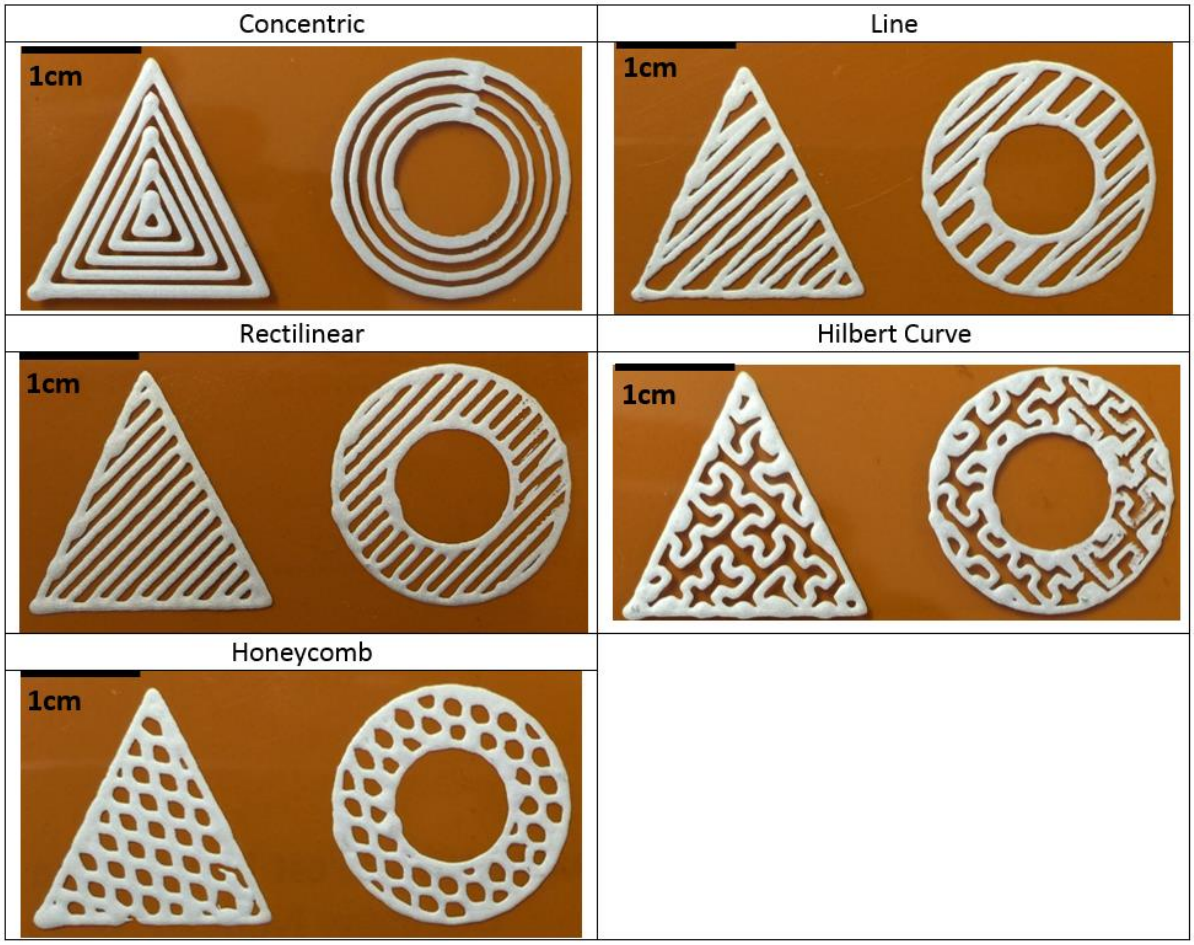

Figure 79. *Infill pattern demonstrations, printed with silver ink on Kapton polyimide film.*

The factors that affect the route the nozzle takes during printing are the infill pattern, the nozzle diameter and the infill density. When printing, the distance between adjacent lines can be adjusted to produce a print with 100% coverage. A printed track will bleed away from the initial deposit area a certain amount, depending on the ink. To save ink, print faster and to print a thin layer the defined print pattern should not pass the nozzle over the entire area. Instead small gaps should be left between adjacent lines so the ink bleeds to fill them. To calculate the print pattern, the nozzle diameter and the desired infill density are entered. The infill density defines the percentage of the total area that should be covered with ink. In this work all prints were performed with a 250 µm tapered nozzle and the infill density was tested at 30%, 50% and 70%. The effect of varying the defined infill density is shown in Figure 80 below.

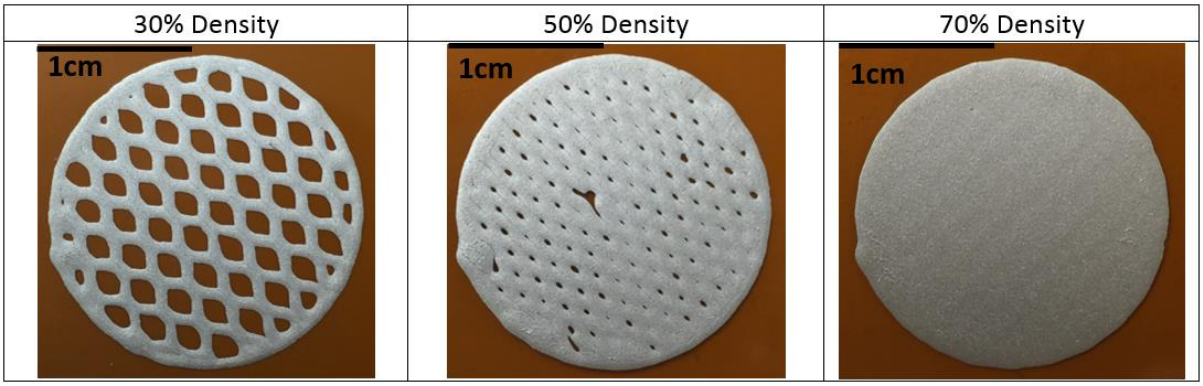

Figure 80. *Demonstration of the infill density control on a honeycomb infill pattern.*

Four shapes were chosen to test the infill patterns, a square, circle, triangle and annulus. These shapes were chosen as they are the building blocks of many other shapes with more complex geometries. The substrate selected was Kapton polyimide film as it provides a smooth surface to print on that will not significantly affect the printed patterns, thus any change can be attributed to the algorithm. The film can also withstand temperatures up to 260˚C without damage [73]. The silver ink used for all tests is FabInks TC-C4007 silver ink since conductive silver ink is widely used for printed electronics applications as a conductor. For all prints the laser displacement sensor was enabled and the print settings shown in Table 26 were used.

Table 26. *Print settings for infill pattern test samples.*

Nozzle to Substrate Separation Distance at Start (µm)	Print Speed (mm/s)	Dispense Pressure (kPa)	Vacuum Pressure (kPa)	Curing
220	10	22	1.3	120˚C 10 mins

All of the infill patterns shown in Figure 79 were tested using 30%, 50% and 70% infill density for each of the four shapes. For each printed shape the coverage, surface roughness, thickness and print time were measured and compared. The printed layer must have 100% coverage to ensure the device functions as intended; as described earlier if a dielectric layer in an electroluminescent lamp does not have 100% coverage, then the lamp will short circuit and not function. The surface roughness is also important in multilayer devices, as it is difficult to print subsequent layers if the underlying layer is rough, therefore a low surface roughness is best. A thin layer is beneficial as it reduces material usage and maintains the flexibility of the underlying material. The print time is also important for manufacturing devices, as ink typically bleeds and the longer a print takes, the more the ink will bleed away from the desired pattern.

The coverage was judged using a printed clear plastic template that had the four shapes printed onto it, each shape was divided up into 100 small squares via the template pattern thus allowing the coverage to be measured as a percentage for each shape. The surface roughness (R_a) was measured using an Alicona InfiniteFocus. For each infill pattern there were four shapes to measure, three measurements on each shape were taken, meaning a total of 12 measurements for each infill pattern. Figure 81 below shows the average of the three surface roughness measurements for each of the shapes in the group of infill patterns printed with 70% infill density. Error bars are included and calculated from the standard deviation of these results.

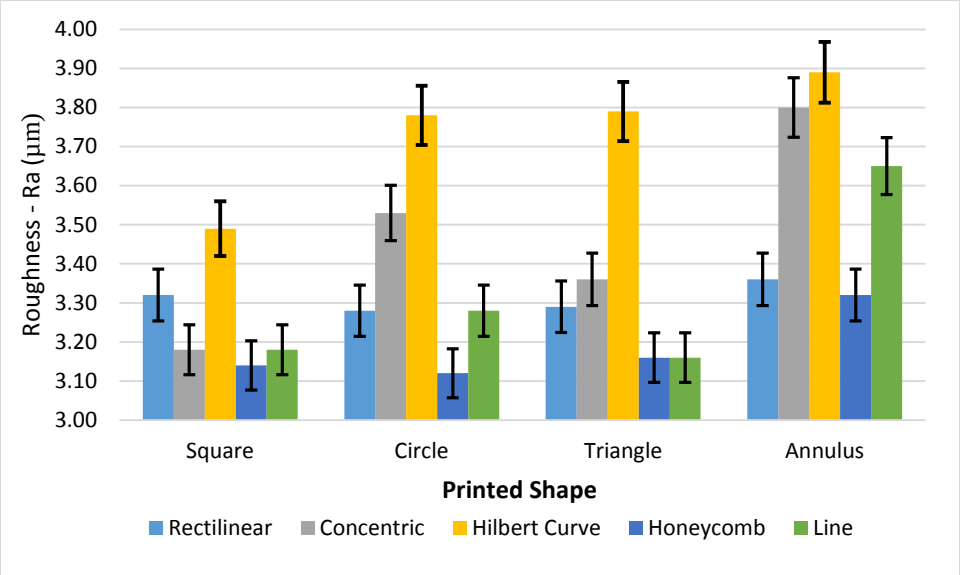

Figure 81. *Graph comparing the surface roughness for different infill patterns at 70% infill density across a range of print shapes.*

The graph shows that there are some variances in the R_a value depending on the shape, however, the aim of this work is to identify the best overall infill pattern for any shape. The Hilbert Curve pattern is clearly the worst performer in terms of surface roughness, with the highest measured surface roughness across all shapes. Both the honeycomb and rectilinear infill patterns had the most consistent low surface roughness values across all of the shapes (6.4% variance for honeycomb and 2.4% for rectilinear). The line and concentric patterns showed significant changes over the different shapes (19.5% variance for concentric and 15.5% for line). The difference between the two best performing infill patterns (honeycomb and rectilinear) was within the error bars for all shapes except circle, and therefore they can be considered to be joint best performing in terms of surface roughness. Also as the variance across the different shapes for honeycomb and rectilinear was small (6.4% and 2.4% respectively), the results from these patterns can be applied to any printed shape and are therefore applicable to all dispenser printing applications.

The thickness of each shape was measured using a Mitutoyo MDC Lite digital micrometer. The print time was measured via the printer software and covers the total time from the first ink being dispensed to the last ink dispense.

The results from the print tests are shown in Table 27 below. The times shown in the results are the total for all four shapes to be printed. To identify the optimum print pattern for multilayer devices, the data was judged, in order of priority, on the following criteria:

- 100% coverage of ink.
- Lowest surface roughness to ensure the lamp is functional.
- Lowest print thickness.
- Shortest print time.

The coverage is the most important parameter because 100% coverage in the defined areas is vital to print a functioning device, be it a simple or complex device. A simple device could be a conductive track

to power an LED, whereas a complex device would be an electroluminescent lamp and both require 100% coverage to achieve the correct functionality. A low surface roughness was the next most important parameter; the print thickness and print time were also considered as these affect the ability to print thin devices, and the cost of production, respectively.

Table 27. *Comparison of the coverage, surface roughness, thickness and print time for various infill patterns at infill densities of 30%, 50% and 70%. R_a values were measured using the Alicona Infinite Focus.*

Infill Density	Infill Pattern	Coverage (%)	Average R_a Value (µm)	Thickness (µm)	Print Time (s)
30%	Rectilinear	50	7.66	15	89.7
	Concentric	55	5.71	17	160.1
	Hilbert Curve	35	8.06	14	184.3
	Honeycomb	40	7.12	18	160.2
	Line	40	8.12	13	86.8
50%	Rectilinear	90	4.07	12	172.1
	Concentric	80	4.48	20	224.4
	Hilbert Curve	85	4.14	16	280.9
	Honeycomb	85	4.58	27	208.1
	Line	75	5.18	22	164.4
70%	Rectilinear	100	3.31	23	216.7
	Concentric	100	3.47	35	289.5
	Hilbert Curve	95	3.74	24	354.6
	Honeycomb	100	3.19	28	255.7
	Line	100	3.32	30	215.9

A number of the samples did not achieve 100% coverage and examples are shown in Figure 82 below. Only those results with 100% coverage are considered further. Those with 100% coverage are shown in Table 28 below, arranged by lowest surface roughness.

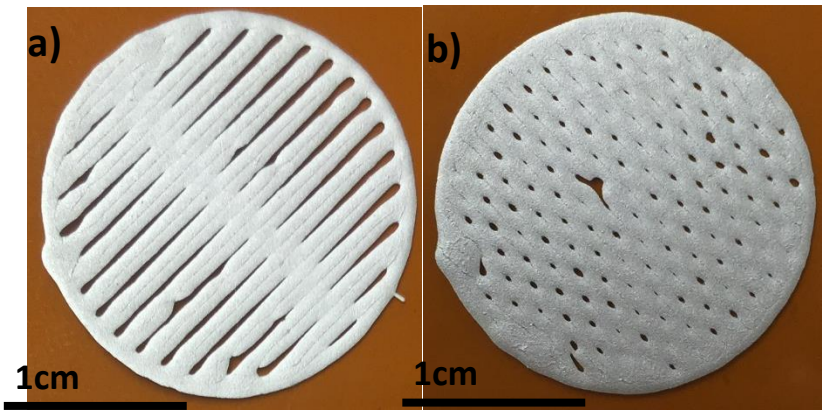

Figure 82. *Images showing printed circles with coverage less than 100%; the 50% infill density line pattern is shown in a) and the 50% infill density honeycomb pattern is shown in b).*

Table 28. *A summary of the results from Table 27 that have 100% coverage, arranged by lowest surface roughness. R_a values were measured using the Alicona Infinite Focus.*

Density	Infill Pattern	Coverage (%)	Average R_a Value (μm)	Thickness (μm)	Print Time (s)
70%	**Honeycomb**	100	3.19	28	255.7
	Rectilinear	100	3.31	23	216.7
	Line	100	3.32	30	215.9
	Concentric	100	3.82	35	289.5

As described earlier, the honeycomb and rectilinear infill patterns have the first and second lowest surface roughness respectively. The honeycomb infill pattern at 70% density offers the lowest surface roughness with 100% coverage, however the rectilinear and line infill patterns have a surface roughness only 3.8% and 4.1% higher respectively. These differences are within the error tolerance so all three patterns are considered to have an equal performance with regards to surface roughness.

As previously described, the line pattern had a variance in surface roughness of 15.5% over the four print shapes, and it is therefore not suitable to be used for all print shapes. The preliminary results earlier suggest it would perform poorly when printing an annulus shape. For this reason, the pattern is not considered a good choice for printing any shape with the dispenser.

The rectilinear infill pattern at 70% density provides the same surface roughness as the honeycomb pattern but is 18% thinner and has a 15% faster print time. The thin layer can be advantageous when trying to control printed material properties, for example a printed resistive layer or a dielectric layer in an electroluminescent lamp. In both of these cases the performance of the device is greatly affected by the layer thickness of these materials. Having a thinner printed layer allows for greater control of the material properties by printing thin single layers, or thicker layers formed from multiple thin layers. The faster print time is also advantageous when trying to avoid ink bleeding. The two optimum infill patterns are shown in Figure 83 below.

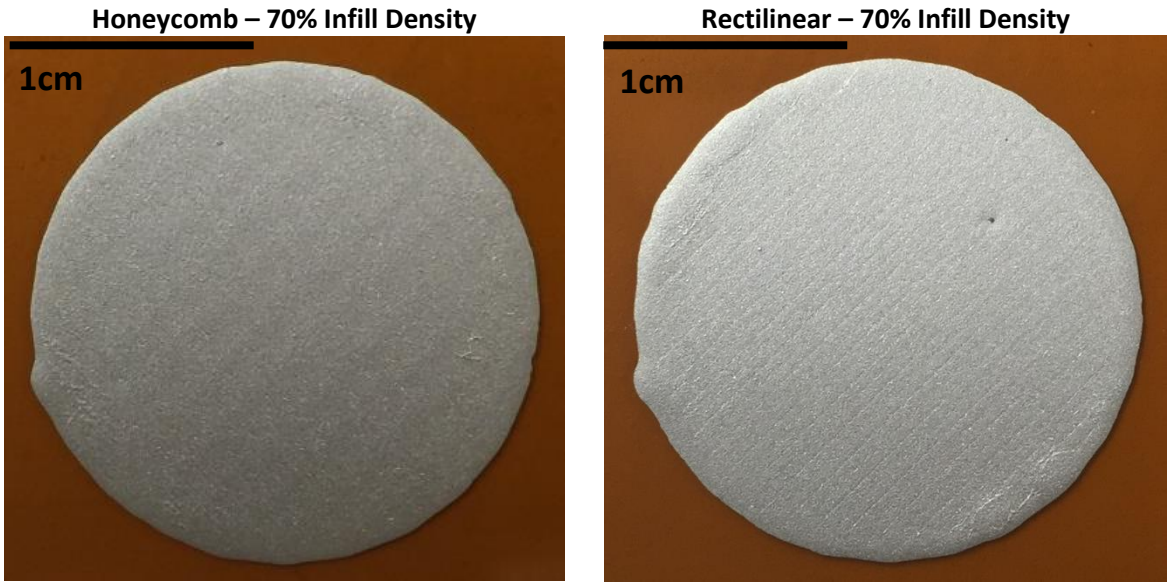

Figure 83. *A honeycomb 70% infill density and rectilinear 70% infill density print - the optimal prints from the infill pattern tests.*

For prints carried out after these tests, the rectilinear infill pattern at 70% density will be used as it offers the best compromise of surface roughness, layer thickness, and print speed.

5.2. Conclusions

The control software for the dispenser printer was considered extensively in this Chapter. The droplet mode control software was first updated to allow the Nordson dispenser controller to be used. The displacement sensor selected previously was then used to maintain a constant separation distance between the nozzle and substrate when printing in droplet mode. The new functionality was tested practically by printing three rectangular (50 x 2 mm) silver tracks for each print mode onto a woven polyester fabric. The nozzle contacted the substrate on the prints without z-height tracking. The average resistance of the tracks without z-height tracking was 5.903 Ω compared to 0.913 Ω for those tracks printed with z-height tracking enabled, a 6.4 times improvement.

Work was then undertaken to allow complex shapes to be printed using the G2 printer; the solution involved a complete redesign of the control software for the printer. Software designed for 3D printing, identified during the literature review, was used to interpret the designs into a series of movements. The upgrade allows any shape to be printed. This software was tested using a complex curved logo which was successfully printed using the new software showing the significant advances in capability.

The z-height tracking capability was then added to the continuous print mode. This functionality required significant software upgrades that could produce 3D print coordinates taking account of the changes in height of the substrate. The capability was tested as with the droplet mode; however larger curved tracks were printed. The 10 cm tracks without the z-height tracking had an average resistance 7.4 times higher than those samples with it enabled. The longer 20 and 40 cm tracks showed a resistance in the MΩ range without z-height tracking, compared to a resistance <5 Ω with it enabled, a significant improvement.

The last section of this chapter considered the effect on print quality of the that route the nozzle takes when filling a shape. Five different print route algorithms were tested at densities of 30%, 50%, and 70% across a number of print shapes representing the building blocks of more complex shapes. The results were assessed on print time, coverage of the shape, surface roughness (R_a), and layer thickness. The results have identified the honeycomb and rectilinear pathway algorithms as having the lowest surface roughness with the lowest variance between print shapes. The rectilinear pattern has been identified from these two infill patterns as having the best overall printing results with respect to printed layer coverage, surface roughness, layer thickness and printing time.

6. Dispenser Printing of Electroluminescent Lamps on Fabric

6.1. Introduction

EL lamps will be dispenser printed onto fabric using a similar structure to that discussed in section 2.3.4.3. The printed EL lamp structure used throughout this chapter including the interface is shown in Figure 84 below. The structure does not include an encapsulation layer as the prototypes do not need to be waterproof. An interface layer is included on some substrates where the high surface roughness requires it; these are typically the woven fabrics used in clothing. The interface paste is a UV curable polymer designed specifically to smooth woven fabrics to allow further layers to be printed on top. The substrates requiring an interface layer are described in section 6.2 below. Those samples printed without an interface will use the same structure with this layer removed.

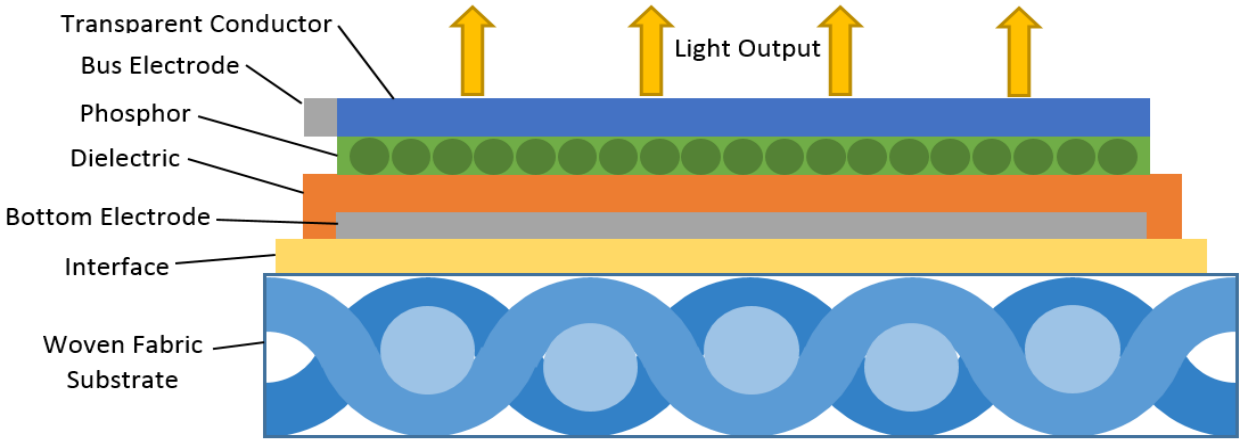

Figure 84. *EL lamp prototype structure to be dispenser printed onto fabric.*

In this chapter the fabric substrates used for printing are first considered, before a number of commercial EL drivers are compared. A series of new phosphor inks for use in EL lamps are developed. A new test pattern is then developed to test the phosphor inks and the devices are first screen-printed. Commercial inks for the transparent conductor, typically the last layer to be printed, are then tested by fabricating EL lamps with each ink and comparing them. For the ink tests the lamps were screen-printed as the work was carried out before EL lamps could be reliably dispenser printed. An investigation into the bus bar requirements for EL lamps was undertaken, where the requirement for a small track around the perimeter of the EL lamp is examined using dispenser printed test samples. An EL watch display demonstrating the improved bus bar design was then screen-printed due to the narrow tracks that were required. The initial and then improved dispenser printed EL lamps are characterised and compared to one another. Lastly a full comparison of the improved EL lamps against commercial and UoS screen-printed EL lamps was carried out.

6.2. Substrate Selection

The EL lamps will be printed onto a variety of substrates depending on the application, for example in clothing applications a blend of 65% Cotton, 35% Polyester is commonly used and is therefore a

representative test sample. When selecting a substrate, a high surface energy is generally desirable to encourage paste adhesion. Flexibility is also important due to the end application as fabrics are flexible. Two test materials have been selected as representative of common substrates used in this field, as well as two application materials stipulated by the project financing this work.

The first test material is a type of polyimide film developed by DuPont and sold under the trademark Kapton. The film can withstand temperatures up to 400 ^{o}C without damage and has a high surface energy (50 mN/m[73])making it suitable to print on. Kapton is also highly resistant to chemical attack allowing the use of solvents to clean the substrate without damaging it. In this work Kapton is used to test new materials as it offers a smooth flexible surface to print onto thereby removing many of the substrate variables associated with printing on fabric. The interface layer is not required when printing onto this substrate due to its smooth surface.

Polyester cotton has been chosen as the second test material. The fabric is formed of 65% Cotton, 35% This fabric was selected because it is widely used in clothing applications and has typical fabric properties with regards to weave, heat tolerance and texture. However, it is also difficult to print homogenous layers of material directly onto it due to its high surface roughness and loose fibres in the yarn structure, known as pilosity. To counter these problems, the interface layer described previously was printed to smooth the rough fabric surface to an acceptable level, whilst maintaining the original fabric properties where possible. The material has been tested at temperatures up to 130 ˚C without showing signs of damage.

As part of the CREATIF project, financing this work, two fabrics commonly used in architectural applications are used. The first material is a polyester woven fabric. Although a woven fabric, the surface is significantly smoother than Polyester Cotton due to the synthetic yarns used. The material is sold by Mehler under the ‘Valmex’ product range [74]. The second application material is a non-woven PVC sheet, offering an even smoother surface to print onto. The material is produced by Berger under the ‘Back-Lighttex Fr + w’ name [75]. Tests performed as part of the CREATIF project have shown these materials do not require an interface layer to be printed.

6.3. Electroluminescent Lamp Driver Circuits

EL phosphor particles require a high electric field to be applied to fluoresce. A typical EL lamp requires 100-150 V_{peak} AC, at 300-600 Hz to fluoresce at a visible brightness. A higher voltage produces a higher field, which in turn increases the overall lamp brightness. Alterations in frequency can cause small colour shifts and also alters the brightness with a higher frequency creating a higher brightness.

For this work two types of EL driver are required, the first should be a small microchip that could be integrated into a product. A fixed voltage and frequency is sufficient for this type of driver as the user will not need to manually vary the brightness of the device. The second EL driver required is a large test setup that is capable of varying the voltage between 0-400 V_{peak} and 200-2000 Hz. This system will be used to characterise the devices in the lab.

For the first EL driver there are numerous commercial drivers available that can power EL displays and could be integrated into a final device. The supply voltage is important for wearable applications as the device should be within the range that common battery types can supply. The output voltage should be around 150 V_{peak} at 400 Hz as literature shows this to be a good compromise between brightness and

lifetime [9]. The maximum lamp area defines the size and number of lamps the driver can comfortably power without reducing its lifetime.

The range of commercial drivers are compared in Appendix 1 and drivers that are discussed in this section are highlighted in red. From those highlighted in red a number of drivers will be selected to power both large area EL lamps for lighting, as well as multiple small EL lamps for communicating information to the user.

A chip best suited has been chosen for each potential application has been identified:

- Numerous small area (0.2-2 cm^2) displays for displays on portable applications – Supertex HV881 is best suited as it can drive up to 16 small displays from a single IC, making it well suited for portable applications.
- Medium area (10-250 cm^2) displays for portable applications – Supertex HV816 is best suited as it can drive a single display up to 270 cm^2 and is packaged as a small microchip making it easier to integrate into portable applications.
- Large area displays (500-1000 cm^2) for static applications – ENZ Electronics 2040 (1000) is best suited as it can drive these large displays and is supplied with all external components soldered on a PCB in a protective case.
- Very large area displays (10,000 cm^2) for static applications – ENZ Electronics E250 is best suited as it is the only driver able to power this size display and plugs directly into a mains supply. The driver is supplied with all components on a PCB in a protective case.

For the lab based test system a TTI TGA1241 signal generator and Trek PZD700 power amplifier were used to generate a voltage between 0-400 V_{peak} at frequencies ranging from 200-2000 Hz.

6.4. Ink Development and Testing

6.4.1. Phosphor Ink

As part of the CREATIF project a full spectrum of EL colours are required. The emission colour of an EL lamp is primarily controlled by the type of phosphor used and further alterations to emission colour can be achieved by filtering within the transparent conducting layer. The EL phosphor paste used to print the phosphor layer can be purchased commercially as a paste, or EL phosphor powders can be purchased and mixed with a vehicle paste. A summary of the commercially available EL phosphor pastes and phosphor powders with the required vehicle pastes is shown in Table 29 below.

Table 29. *Summary of commercially available EL phosphor pastes and phosphor powder with the required vehicle pastes.*

Phosphor Pastes (data from [76])			
Manufacturer	**Product**	**Colour**	**Max Brightness (cd/m^2) 100 V_{peak}/ 400 Hz**
Gwent	**C2101125P4**	White	85.87
Gwent	**C2070209P5**	Green	187.17
Gwent	**C2070126P4**	Orange	45.97
Gwent	**C2061027P15**	Blue	121.65
Gwent	**C2061027P13**	Blue/Green	168.97
DuPont	**8150B**	White	Data unavailable
DuPont	**8152B**	Blue/Green	Data unavailable
DuPont	**8154L**	Yellow	Data unavailable
EL Phosphor Powder (data from [43])			
Manufacturer	**Product**	**Colour**	**Max Brightness (cd/m^2) 100 V_{peak}/ 400 Hz**
Global Tungsten	**GG13/14**	Orange	18.6
Global Tungsten	**GG25**	Blue Green	76.9
Global Tungsten	**GG45**	Green	82.3
Global Tungsten	**GG65**	Blue	49.2
Global Tungsten	**GG84**	White	40.0
Vehicle for EL Phosphor Powder			
Manufacturer	**Product**	**Colour**	**NA**
Norcote	**ELG1400**	Transparent	NA
DuPont	**LuxPrint 8155**	Transparent	NA

Using EL phosphor powders with vehicles offers the advantage of having control over the ratio of phosphor powder to vehicle in the final paste. This option also allows the dielectric layer to be combined with phosphor powders. The disadvantage of using separate phosphor powder and vehicle is that the powder must be mixed thoroughly with the vehicle to ensure an even dispersion.

It was decided to screen-print the EL lamps when testing the phosphor materials, as this work was carried out before the G2 printer was finished and the UoS has significant experience with screen-printing. A set of screen designs were created to test different shaped lamps whilst also providing repeated patterns in case some lamps were faulty. The screens were designed using Tanner's L-Edit program and the final design is shown in Figure 85 below.

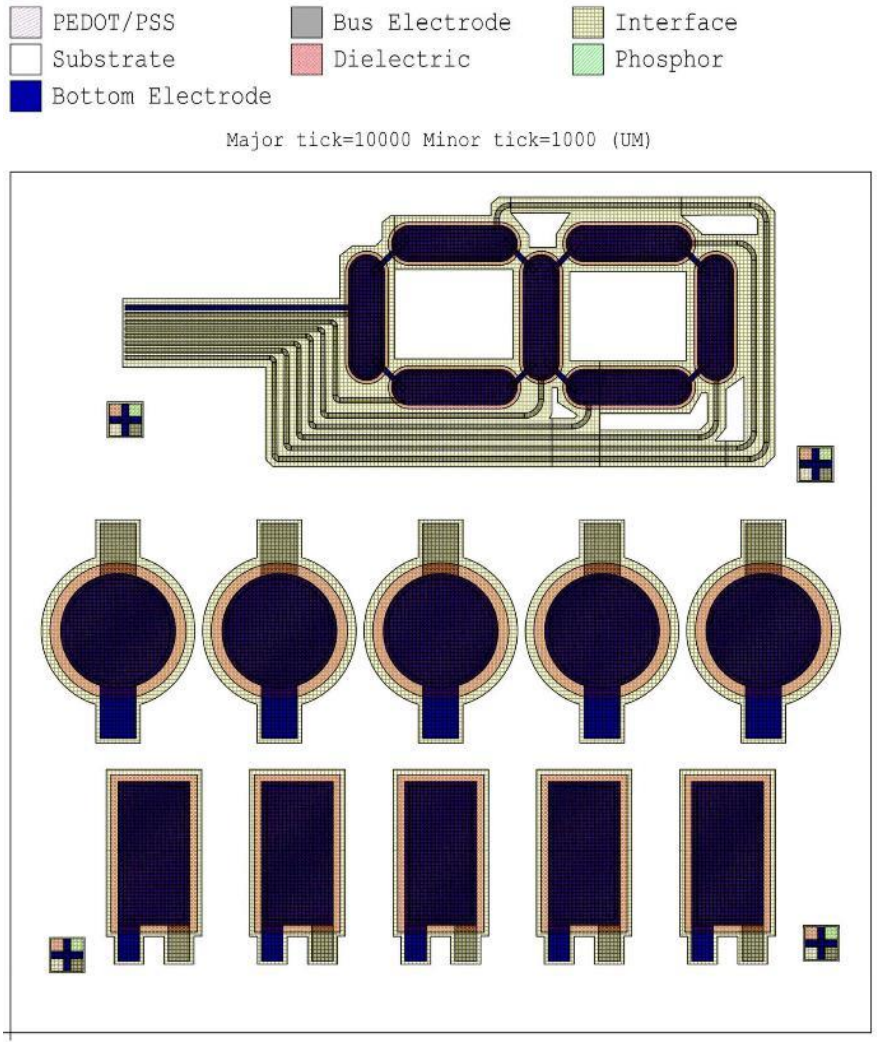

Figure 85. *Screen design to test materials for a printed EL lamp on fabric.*

The screens were produced by MCI Precision Screens. EL lamps are most commonly available in a blue-green colour and therefore this section focuses on exploring some of the other colours available. It was decided to use the Global Tungsten phosphor powders as the ratio of powder to vehicle can be controlled. The Gwent and DuPont phosphor pastes are also expensive at around £1000/kg so are only be tested if the more affordable GTP powders are unsuitable.

Of the available GTP phosphors, tests were planned for orange, dark blue, and white EL lamps. Each colour is available in a variety of sub-categories focusing on lifetime, brightness, or economy; for initial testing all powders were chosen for maximum brightness. The vehicle paste recommended by GTP was DuPont's LuxPrint 8155 [77] and the datasheet suggests a phosphor powder ratio of "55-70% by weight". During correspondence with the GTP they recommended a slightly higher ratio of powder (70%) for the dark blue phosphor powder compared to the orange and white (65%). The GPT recommended values used were used for all phosphor samples and the exact measurements are shown in Table 30 below.

Table 30. *Ratio of phosphor powder to vehicle for ELPP1, ELPP2, and ELPP3*

	ELPP1	**ELPP2**	**ELPP3**
	Orange	**White**	**Dark Blue**
Weight percentage of phosphor powder	65%	65%	70%
Weight of phosphor powder	25g	25g	25g
Weight percentage of LuxPrint 8155	35%	35%	30%
Weight of LuxPrint 8155	13.46g	13.46g	10.71g
Total weight mixed	38.46g	38.46g	30.71g

The pastes were milled using a triple roll mill. A triple roll mill is a series of motorised rollers with minimal spacing between them to encourage a uniform distribution of particles throughout the paste. The lamps were printed onto polyester cotton so all tests utilised an interface layer developed at the UoS and sold commercially as FabInk-UV-IF1004. The other layers are printed using commercially available pastes, described in Table 31 below.

Table 31. *Description of pastes used in screen-printed EL lamps for phosphor testing.*

Layer	**Paste**
Interface	FabInk-UV-IF1004
Bottom Conductor	Fabink-TC-C4001
Dielectric	Fabink-TC-D9001
Phosphor	Custom Phosphor Paste
Bus Electrode (Conductor)	Fabink-TC-C4001
Transparent Conductor	Electra Polymers ELX ITO-R

The six individually printed layers are printed sequentially to produce the EL lamp, as shown in Figure 86 below.

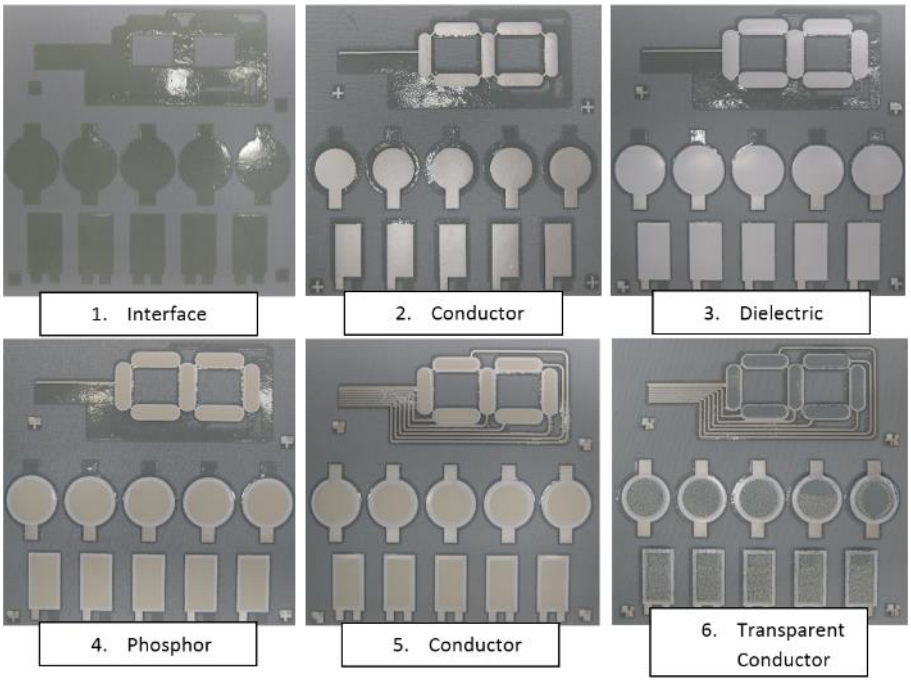

Figure 86. *Six individually printed layers built up to produce an EL display.*

All lamps were printed successfully onto a Polyester Cotton woven fabric and were illuminated using a 150 V_{peak} AC 400 Hz supply. The emitted colour was visually checked and appeared correct for the dark blue and orange lamps. However, the white lamps emitted a light blue light. The colour shift could be due to a filtering effect from the transparent conducting layer as it has a slight blue colour. The white lamp is shown emitting light blue light, along with the correct dark blue and orange lamps, in Figure 87 below. The print quality of Figure 87(a) an Figure 87(b) was poor due to incorrectly set print parameters.

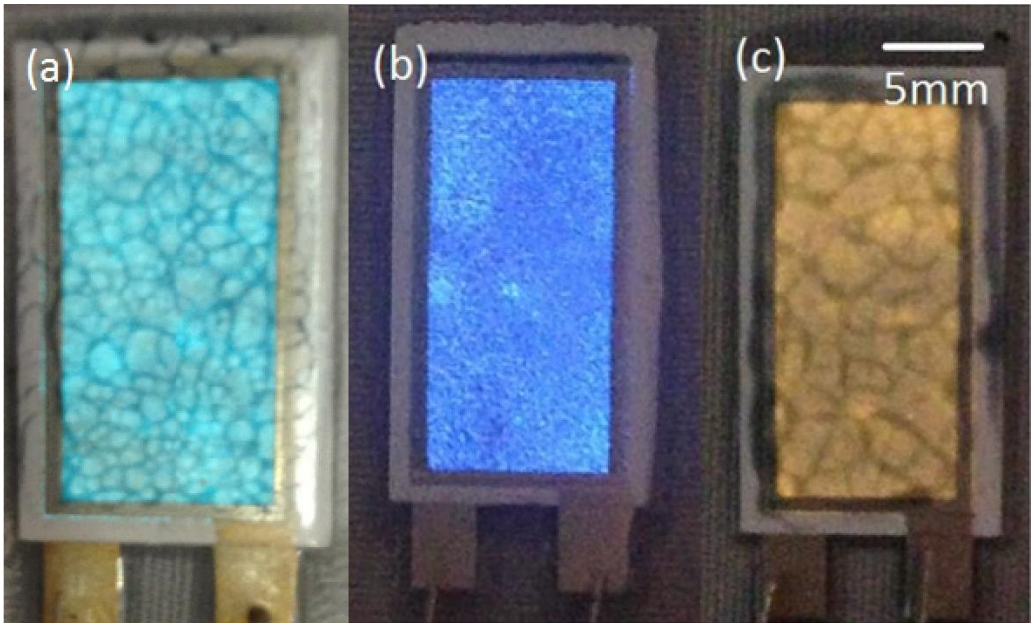

Figure 87. *Screen-printed EL lamps to test new phosphor materials: (a) 'white' phosphor (b) dark blue phosphor (c) orange phosphor*

The work in this section has successfully demonstrated a range of colours outside of the typical blue-green colour EL lamps. The demonstration has satisfied the requirement of the CREATIF project and means EL lamps can be used in potentially new applications where a range of colours are required.

6.4.2. Transparent Conductor

A transparent conductor is required to form the top electrode in the capacitor structure and to distribute the electric field equally over the EL lamp. The material used for this layer should be printable, electrically conductive, and have a high transmittance over the visible spectrum. The transmittance of a number of commercially available pastes is tested, along with an application specific test where the material's performance is checked in a practical EL lamp. Four of the transparent conducting pastes that were identified were tested and the manufacturer datasheets are summarised in Table 32 below. The last row in the table showing Indium Tin Oxide (ITO) coated PET is included as a reference as ITO was historically used for this layer in rigid EL lamps as discussed in 2.3.2. Since these tests were carried out a number of new silver nanowire pastes have become available that could offer improved performance.

Table 32. *Comparison of commercially available transparent conducting pastes, with ITO covered PET as a reference.*

Paste	Claimed Resistivity (Ω/square)	Recommended Thickness (µm)	Transparency (over 400-700 nm range)	Colour
Electra Polymers ELX ITO-R	700	12.5	>83%	Dark Blue
Agfa EL-P 3145	240	0.7	>92.5%	Dark Blue
Clevios S V3	500	0.5	No data	Dark Blue
Loctite ECI 5002 E&C	100	No data	>92%	Grey
Indium Tin Oxide coated PET	60	0.01	>92%	Transparent

Samples were obtained of all pastes listed in Table 32 for testing. In section 6.4.1 it was suggested that the transparent conducting layer could be having a filtering effect on the white phosphor making it emit a blue light. A transmittance test was performed to check whether any filtering effect was present and to what extent it affects the emitted light.

Transmittance was measured using a tungsten light source and an Ocean Optics USB2000 spectrometer. Thin layers of each of the materials listed in Table 32 were printed onto transparent polyethylene terephthalate (PET) using a stencil and squeegee. These layers were cured as per the information in the respective data sheets and all were measured as having 5 µm cured thickness. Although this is thicker than the manufacturer's recommended thickness, it is the thinnest layer that can currently be reliably produced with the dispenser printer.

Each sample had the transmittance measured five times and averaged. A reference spectrum was taken of PET without any printed layers meaning the collected results minus this reference can be assumed to be the transmittance of only the printed material. The transmittance test results are shown in Figure 88, and a reference spectrum to show the approximate colour for each wavelength is shown in Figure 89 below.

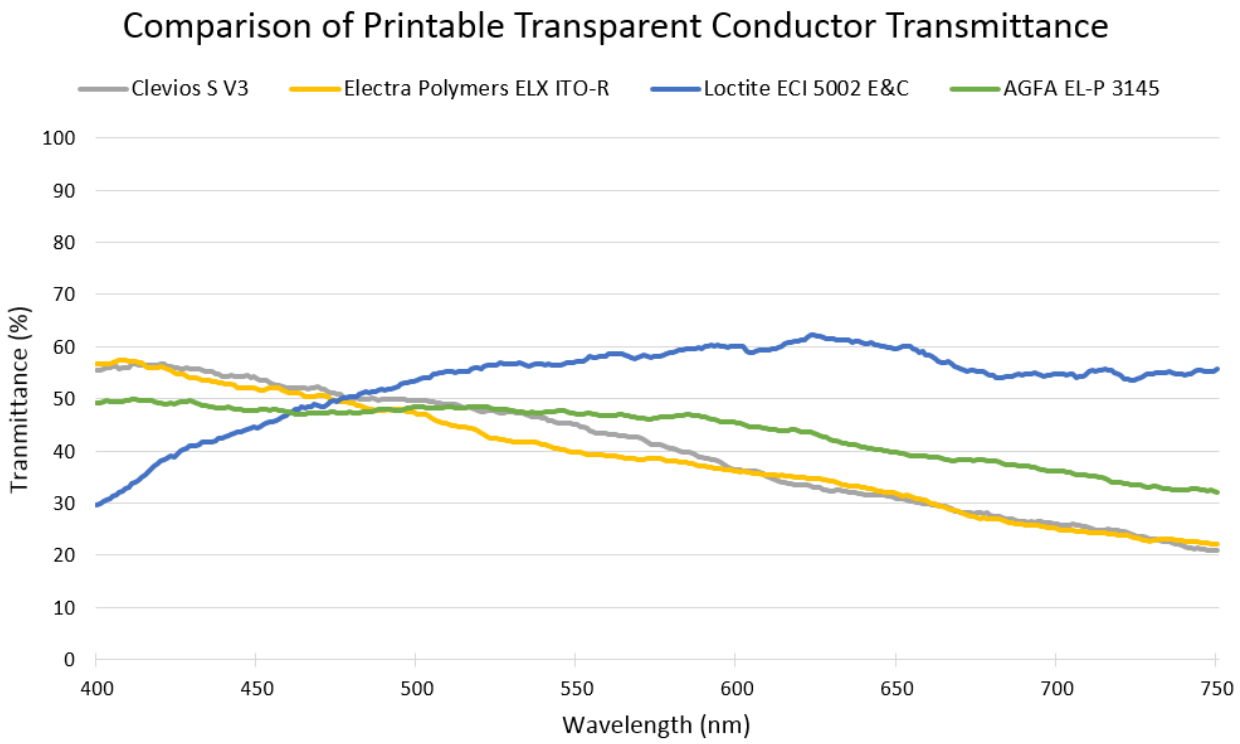

Figure 88. *Comparison of printable transparent conductor transmittance using a tungsten light source and an ocean optics spectrometer.*

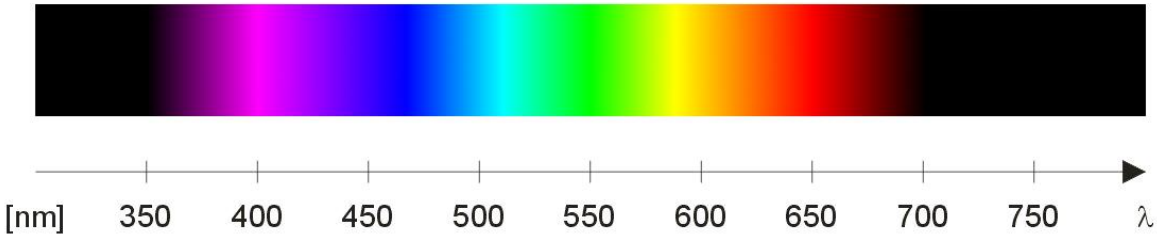

Figure 89. *Visible spectrum showing the approximate colour for each wavelength (Image from [43])*

The results show that the Clevios, Electra Polymers, and Agfa pastes all follow a similar trend of filtering out higher wavelengths and allowing a higher percentage of the blue spectrum to pass. This result was expected as these pastes are all based on the PEDOT:PSS polymer conductor which has a blue appearance. The Loctite paste differs as it is not based on the PEDOT:PSS polymer although they do not offer any further information on its composition. The Loctite paste offers good transmittance over the higher wavelengths. However, it does have a filtering effect on blue colours.

Tests were also carried out to check the practical performance of the transparent conductors in an EL lamp. Four samples were printed with identical materials and print settings, except for the transparent conducting layer, which utilised one of the four printable pastes shown in Table 32. The illuminated lamps are shown in Figure 90 below for comparison.

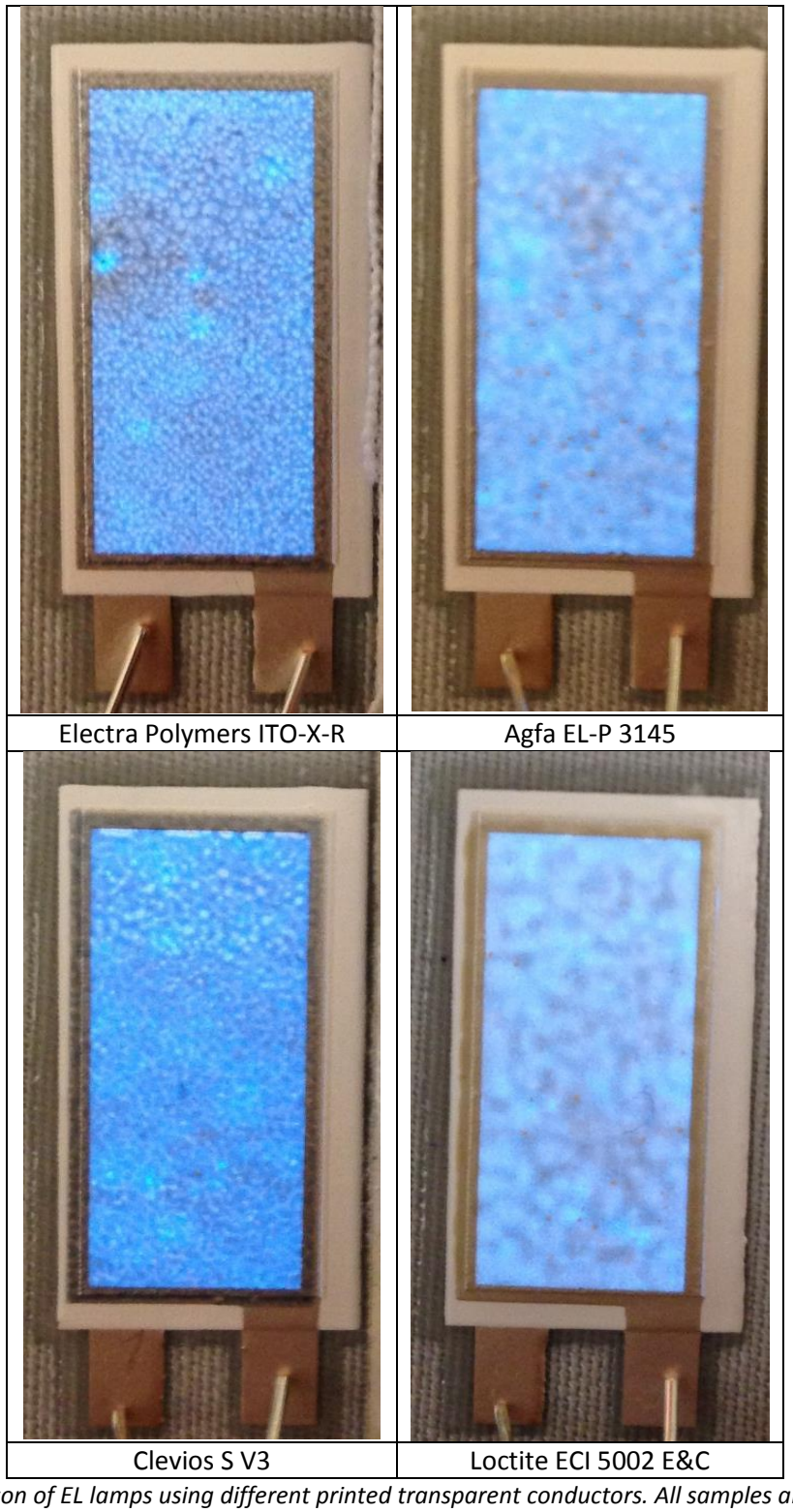

Figure 90. *Comparison of EL lamps using different printed transparent conductors. All samples are in focus and the blurry look of the emitting area is true to how it appears.*

All pastes produced working EL lamps, however it was noted that the low viscosity of the Loctite and Agfa pastes meant they showed bleeding on some samples. Although the lamps were operational, the 7 segment display did not function for these pastes as the segments had bled into one. As expected the Loctite paste showed the lightest blue, filtering the darker blue colours. In line with the transmission results, the Agfa paste also showed a slightly lighter blue colour than the Clevios and Electra Polymer pastes. The Clevios paste appeared the brightest visually, which was probably caused by the lower resistivity as shown in Table 32.

The work in this section suggests that only the Clevios and Electra Polymers paste has a viscosity sufficient to print without bleeding. Of these pastes the transmittance was virtually identical and the Clevios had a slightly lower resistance. The lower resistance will result in a brighter EL lamp and therefore the Clevios S V3 paste is used for all EL lamps in this work.

6.5. Electroluminescent Lamp Bus Bar Investigation

A traditional EL lamp design requires a high conductivity bus bar to be placed around the perimeter of the EL lamp [78]. Silver ink is commonly used for this purpose in printed EL lamps as it is a readily available ink with high conductivity and is usually also used for the bottom electrode. The high conductivity bus bar is used to evenly distribute charge to the outer edge of the lamp, reducing the distance the lower conductivity semi-transparent conductor is required to carry the charge. It was previously thought that if the bus bar did not cover the perimeter then a dimming effect would be present away from the point where the bus bar layer connects to the semi-transparent conductor.

When printing small EL lamps (<1 cm^2) the bus bar takes a significant percentage of the overall design area. An example is shown in Figure 91 below. A single segment from a seven-segment display is shown. The segment has a height of 3 mm; the bus bar track width is the minimum that can reliably be screen-printed at 350 µm. As the design includes a bus bar around the perimeter of the design a large part of the segment is non-emitting as it is covered by the opaque bus bar. This design limits the minimum size of segment that can be produced whilst maintaining visibility to the user.

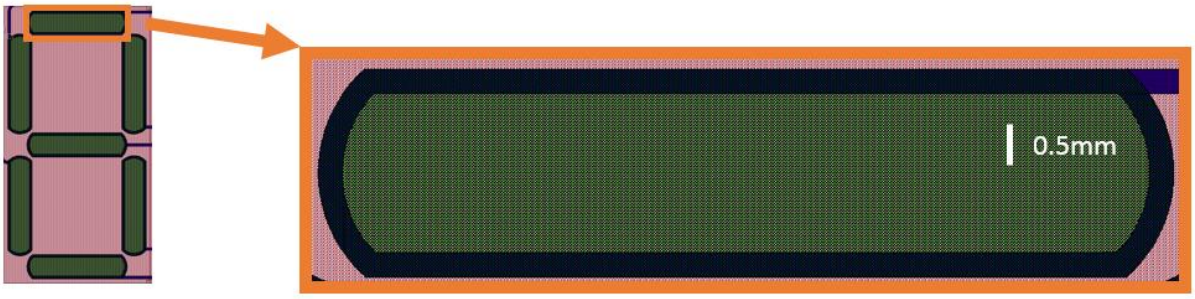

Figure 91. *A seven-segment display (left) with an enlarged single segment (right) highlighting the large percentage of the emitting area of the lamp covered by the opaque bus bar.*

A traditionally printed 3 x 3 cm EL lamp with a silver bus bar around the perimeter is shown in Figure 92 below. While the bus bar takes up a smaller percentage of the emitting area it still adds complexity and time to the print.

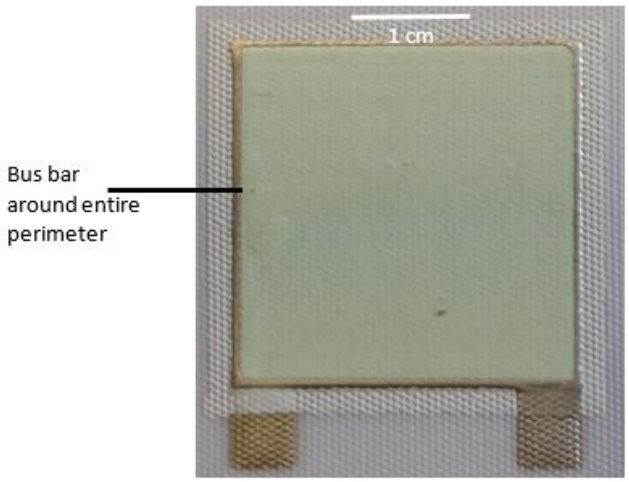

Figure 92. *3 x 3 cm dispenser printed EL lamp without the final PEDOT:PSS layer to highlight the silver bus bar around the perimeter.*

A simple COMSOL model of a rectangular EL lamp simulated the voltage drop over the transparent conducting layer. The simulation was carried out with a bus bar around the entire perimeter and with a shorter 2.5 mm bus bar. The results are shown in Figure 93 and suggest there would be a 30% voltage drop at the furthest point with the inks in use with short (<2.5 mm total length) bus bars on 1 x 2 cm EL lamp. A 30% drop in voltage is unlikely to cause a drop in brightness that is significantly noticeable to the

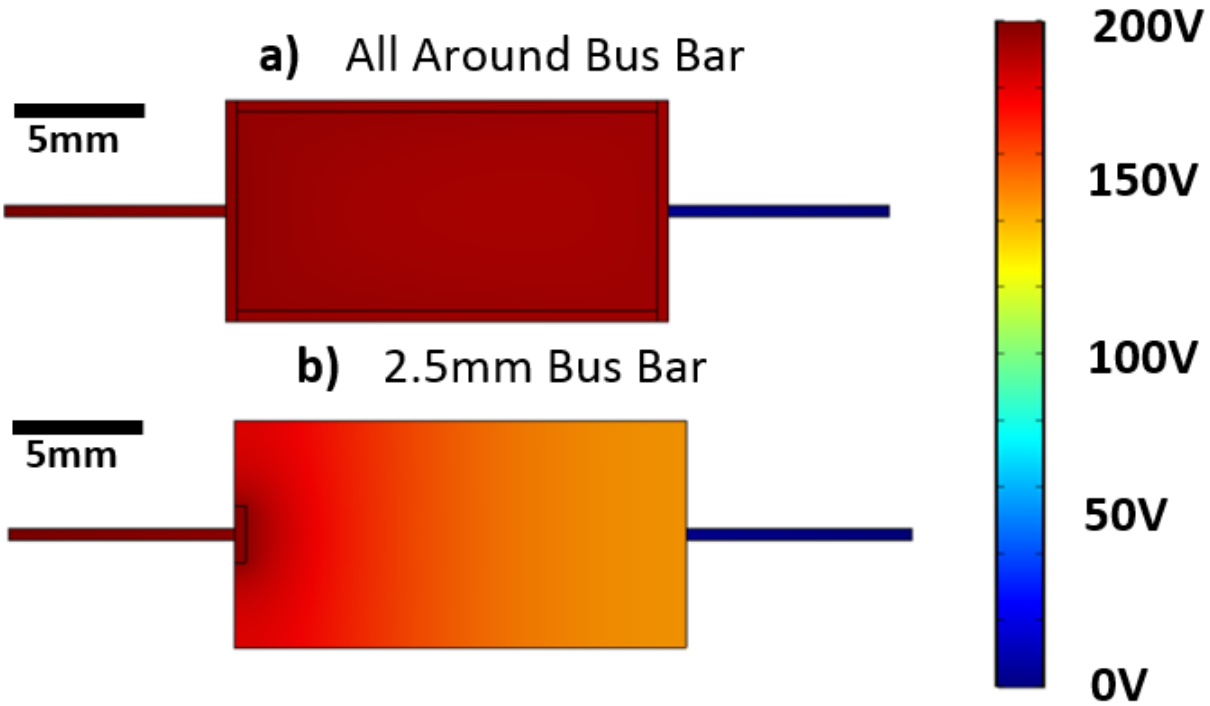

Figure 93. *Images showing the COMSOL model results for a bus bar around the entire perimeter (a) and a 2.5 mm reduced size bus bar (b).*

human eye; therefore a practical test was carried out to verify the result.

A series of EL lamps were dispenser printed to test whether the bus bar is required around the perimeter of the lamp. The emitting area of the lamps is 1 x 2 cm, with a bus bar connection only on the bottom of the rectangle. The length of the bus bar along the bottom of the lamps was varied according to Table 33. The printed EL lamps are shown in Figure 93.

Table 33. Table showing the length of the silver bus bar along the bottom of the EL lamp for each of the five samples.

Sample	(a)	(b)	(c)	(d)	(e)
Bus bar length (mm)	0.5	2.5	5	7.5	10

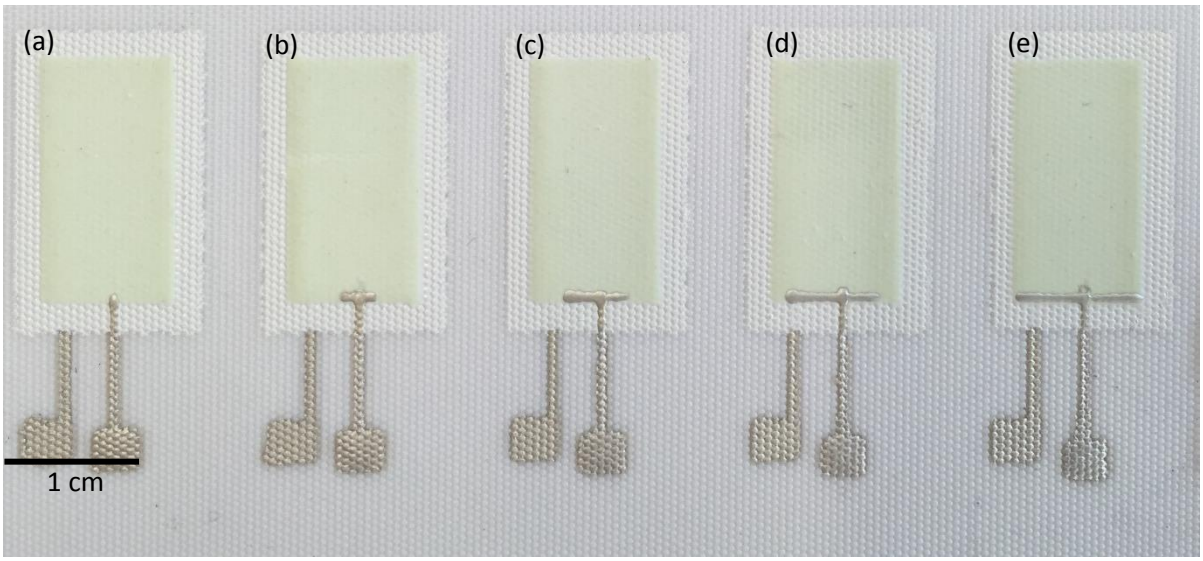

Figure 94. *Five dispenser printed EL lamps (a-e) showing bus bars along the bottom edge of 0 mm, 2.5 mm, 5 mm, 7.5 mm, and 10 mm respectively. The PEDOT:PSS layer was then printed after this image was taken.*

The lamps were tested simultaneously using a common driving circuit to allow a fair comparison and to avoid any variations in ambient light. The five EL lamps can be seen powered and unpowered in Figure 95 below.

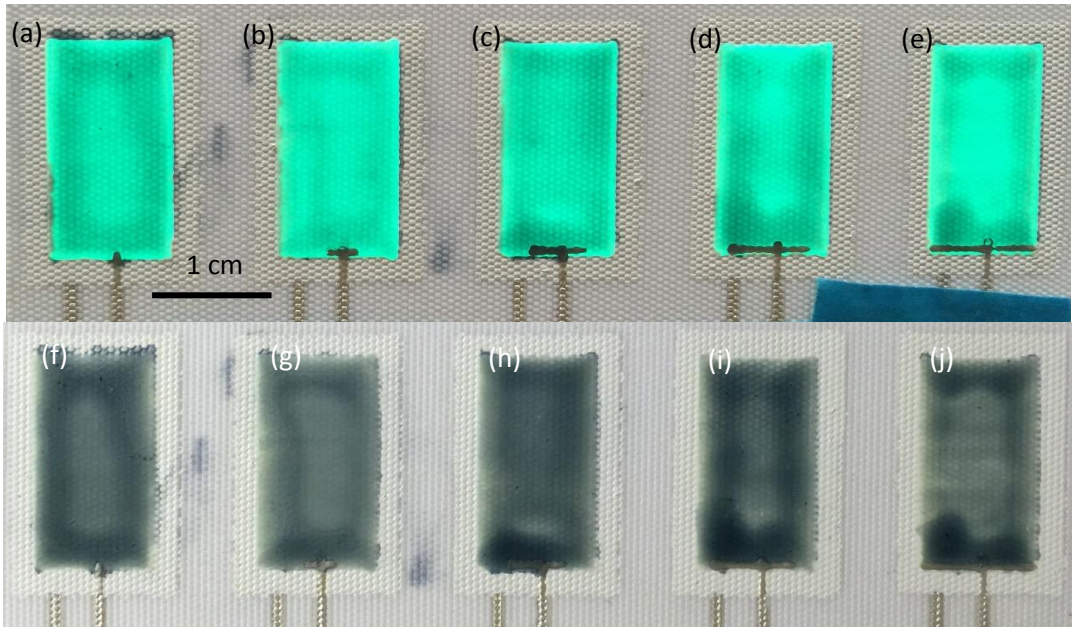

Figure 95. *Five dispenser printed EL lamps, powered (top) and unpowered (bottom).*

Figure 95 shows all of the lamps are functional and that there is no dimming away from the bus bar on the bottom edge. The slight dimming pattern towards the centre seen in Figure 95(a) can be attributed to the non-uniform PEDOT:PSS layer thickness, which is visible when unpowered in Figure 95(f). Similar patterns can be seen in some of the other samples as there was some difficulty printing the semi-transparent conducting layer.

The experiment proves that a bus bar is not required around the perimeter of an EL lamp, and a simple connection to the semi-transparent conducting layer is sufficient. The results allow smaller EL lamps to be produced because valuable space is not taken up with a bus bar around the perimeter. The smaller lamps could be used in the future to develop display screens with multiple small lamps forming pixels. Lamps printed after this work will use a reduced bus bar that is as small as possible. The exact length selected will be based on the tolerances of the print as the smaller the bus bar, the better the alignment must be to ensure there is a physical connection to the transparent conductor layer.

6.6. Demonstration of Minimal Bus Bar Design as a Screen-Printed Watch Display

In this section, the capabilities of printed EL lamps are demonstrated and the new smaller bus bar is tested in a practical device. The printed EL lamps will form a watch display screen-printed directly onto fabric. The watch display must be wearable on a wrist meaning the printed lamps and tracks must be very small. As the tracks are 400 µm wide with a 1 mm pitch they are too small to dispenser print, so screen-printing is used in this section.

Smart watches have seen significant development in recent years, with ever increasing features being included into devices being worn on the wrist. However, the appearance of watches has seen little development with the majority of watches incorporating a flexible strap attached to a rigid housing for

the electronics and display. This section demonstrates an entirely flexible EL watch display on fabric. The watch display is printed directly onto the fabric, significantly improving the ease with which displays can be integrated into existing clothing. This initial prototype assesses the feasibility of 28 printed EL displays close together on fabric to form a watch display.

The EL watch includes only the display; the control electronics are separate to simplify the design. The watch display is printed directly onto the fabric which can then be cut out into any desired shape, a diagram showing a summary of the layout can be seen in Figure 96. A limitation of the screen-printer used in this work is that the maximum print area is 15x15 cm. The watch strap needs to be longer than 15 cm to form a continuous loop around a wrist, so in this work the watch is attached to a second piece of fabric to complete the strap. This would not be a limitation if the watch were to be mass produced on a larger commercial printer.

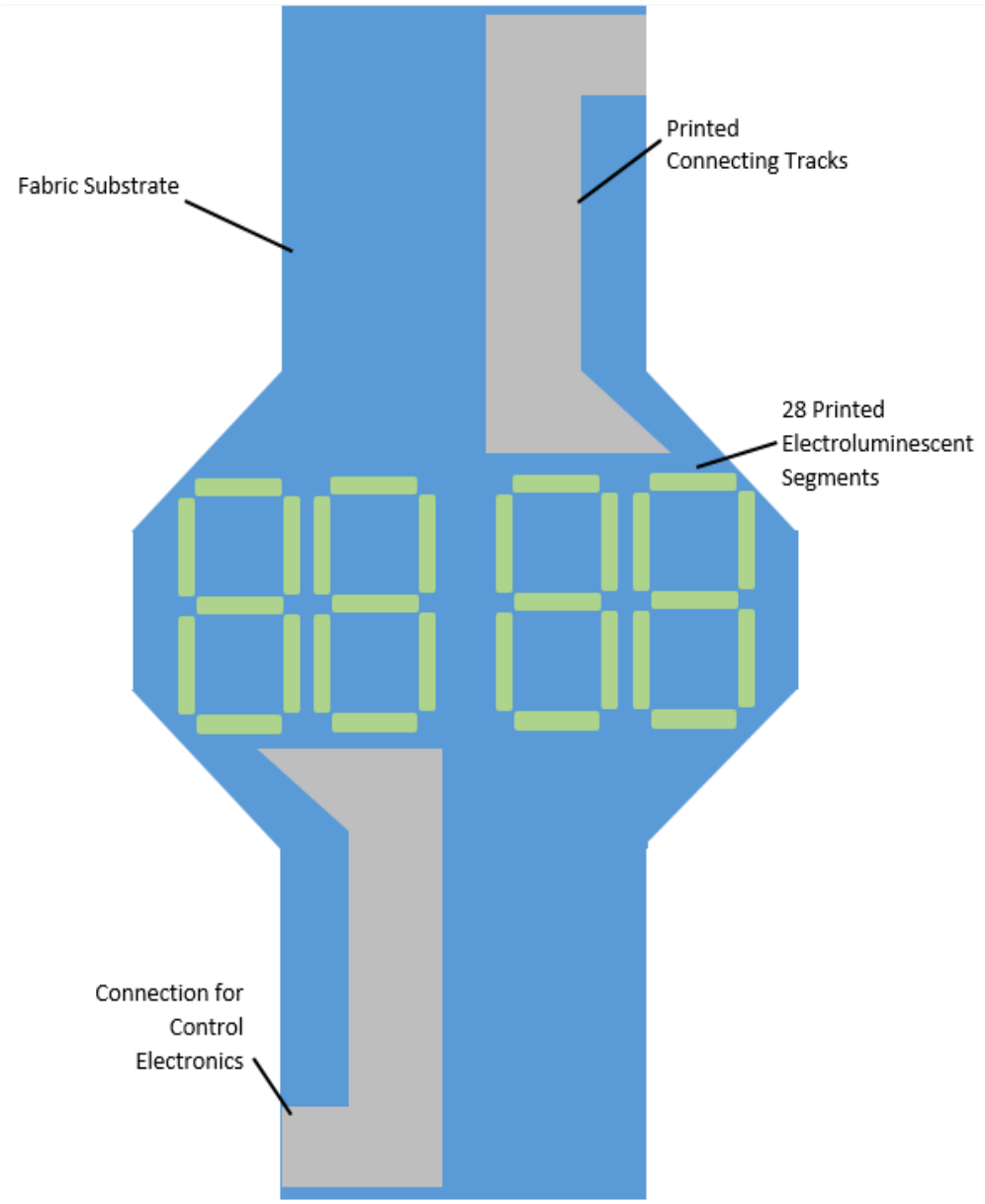

Figure 96. *Diagram of printed EL watch layout.*

The screen-printing process also places limitations on the minimum pitch of the connecting tracks. Each of the 28 EL segments used in the watch requires a separate connecting track with the overall design needing two additional tracks to power the two common bottom electrodes, meaning a total of 30 connecting tracks are needed. The tracks in this work are the narrowest with the lowest pitch successfully printed on fabric thus far at the UoS. The tracks are 1 mm pitch with 400 µm tracks. Below this thickness the tracks either bleed into each other creating short circuits or they prove unreliable during flexibility testing. Narrow tracks with a low pitch are important as it directly affects the number that can be fitted into a defined area. The screen-printed tracks are still below what is currently capable on the dispenser printer that is estimated to be a 600 µm track with 2 mm pitch

In this work it was important to fit many tracks into a small area to avoid an oversized 'watch strap' that would be visually unappealing. To aid alignment of the layers during printing triangular alignment marks are used. The dielectric also incorporates a 550 µm overlap to prevent a short circuit if there is some misalignment.

The watch display was printed a 65/35% blend polyester-cotton supplied by Klopman Srl. Figure 97 below shows an SEM cross-section of the woven polyester cotton fabric used in this work with an EL lamp printed on top of it. The EL lamp makes use of the interface layer and its smoothing properties can clearly be seen.

The difference in surface roughness (R_a) between the raw fabric surface and the fabric coated in interface was quantified using the Alicona Infinite Focus. The polyester cotton fabric on its own has a roughness of 30.7 µm, while the roughness of the same fabric with a printed interface layer was 1.5 µm. This improvement in surface roughness is sufficient when considering that the printed functional layers

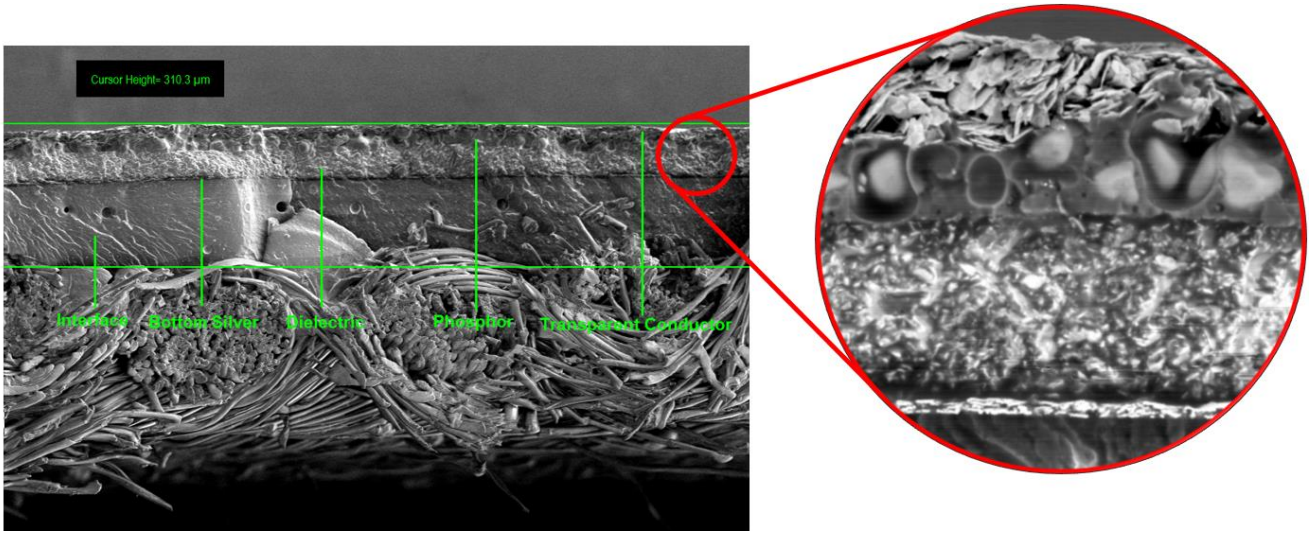

Figure 97. *EL lamp cross-section with interface layer printed onto polyester cotton, with a close up view of the printed EL lamp layers in the circle.*

are typically 10-40 microns thick. Thus the interface will allow for more consistent functional performance as well as providing encapsulation from the back of the fabric.

Using the results from section 6.5, each segment in the EL watch display was designed with a small bus bar on only one side of the segment thus maximizing the emitting area. The bus bar design improvement mean the percentage of the emitting area covered by the bus bar has been reduced from 32% to 6%.The final bus bar design used for the EL watch is shown in Figure 98 offering a visually neat

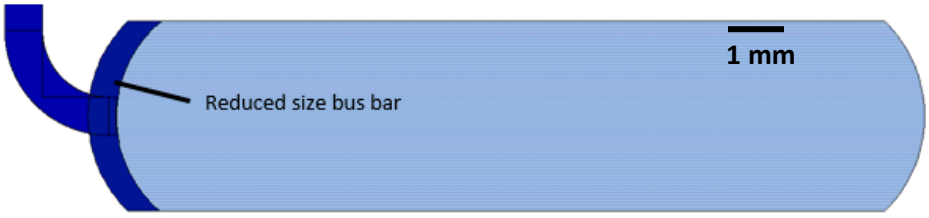

Figure 98. *Image showing the improved design of the bus bar for a single EL watch segment.*

and attractive solution.

The final EL watch design has similarities to a typical four-digit digital watch. It includes 28 individually controllable segments and has cut outs in the interface layer where no further layers are printed to maintain flexibility and breathability. The tracks incorporate an 'L' shape to allow for easier connection of the control electronics when the device is sewn onto a watch strap. The 'L' shape is required because the top and bottom ends of the fabric will not be accessible to the connecting electronics as it will be sewn down onto another fabric. The triangular patterns are alignment marks for each layer to help with the printing; they have no electrical function. The full design is shown in Figure 99.

The paste and print settings used to print each layer were based on existing research at UoS, except for the transparent conducting layer paste. The Clevios S V3 ink found to be the best performer in 6.4.2 was used for this layer. The inks and print settings for each layer are shown in Table 34 below. The print gap defines the distance between the screen and the substrate. The deposits column defines how many times the print squeegee passed over the screen; a thicker layer can be built up by performing multiple deposits. For the interface layer there are four different rows of deposits listed as there were four layers

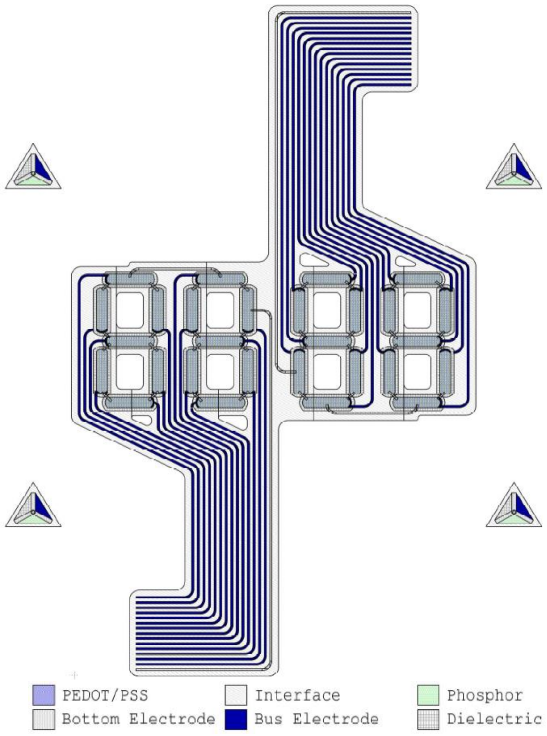

Figure 99. *Design for EL watch display showing all printed layers.*

of interface printed consecutively to build up a thick enough and sufficiently smooth layer.

Table 34. *Summary of pastes used and print settings for screen-printed EL watch display.*

Layer	Paste	Print Gap (mm)	Deposits	Curing	Pressure (kg)
Interface	Fabink-UV-IF1004	1.0	8	2 Mins UV box	5.0
		1.0	6		
		1.0	4		
		1.1	2		
Bottom Conductor	Fabink-TC-C4002	1.5	2	120°C 10 mins	5.0
Dielectric	Fabink-TC-D9001	1.7	4		6.0
Phosphor	Fabink-TC-P001	1.7	2		6.0
Bus Electrode	Fabink-TC-C4002	1.5	2		60
Transparent Conductor	Clevios SV3	2.0	1		5.0

Each layer was consecutively screen-printed onto the substrate that was mounted on an alumina tile. The alumina tile was used to ensure accurate alignment between each printed layer. Before each layer was printed the tile was pushed against four alignment pins on the screen printer. Images showing the EL watch after each layer is printed are shown in Figure 100.

Figure 100. *Images showing the EL watch after each consecutively printed layer.*

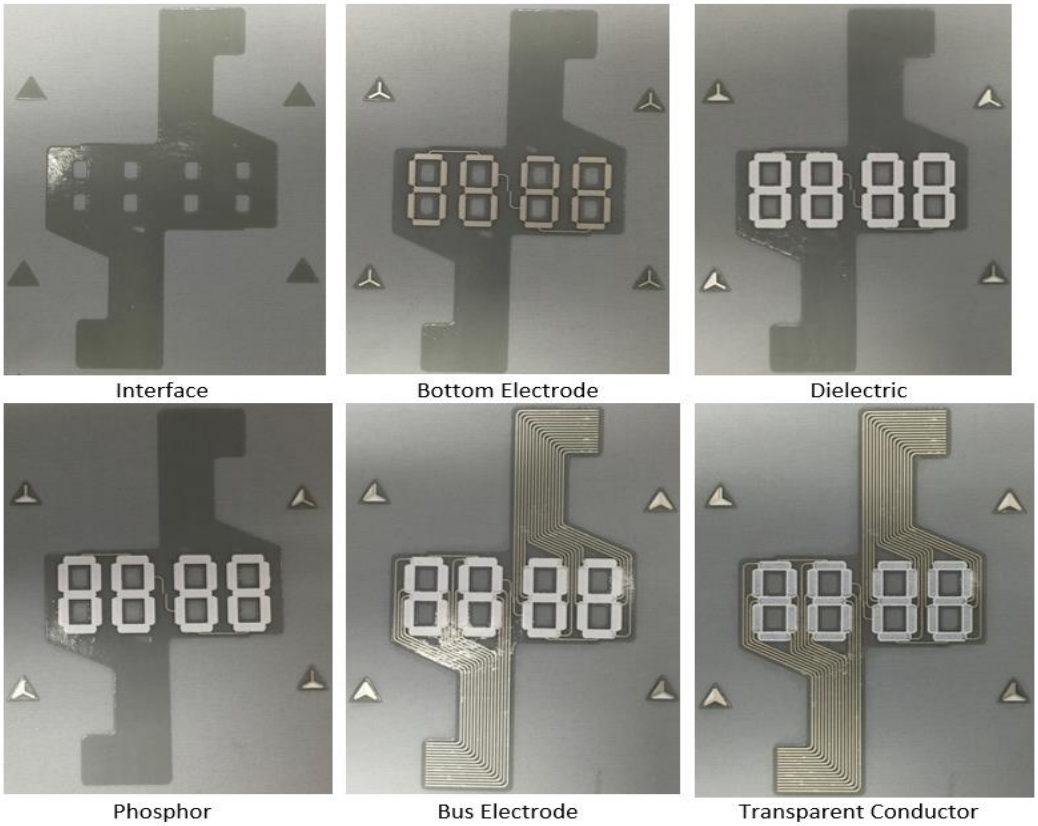

The EL watch functionality was tested, and then the luminance of the lamp was tested at a variety of driving voltages and frequencies. During functionality testing the watch was powered using two Supertex HV881 multi-segment EL drivers [79], with each driver powering two of the digits (14 segments). Software was written to control the HV881 chips using the I^2C protocol to give watch like functionality. The lab test EL driver described in section 6.3, was used for testing the lamps at various voltages and frequencies. The luminance measurements were taken using a Konica Minolta CS-100A luminance meter in a darkened room to ensure the results were not affected by ambient light.

All four watch segments were tested by showing the time as shown in Figure 101(a) below. For testing the watch was connected using a custom 3D printed connector with the correct wire pitch. However, if commercially developed the watch could be used with a bespoke zero insertion force (ZIF) connector. The watch segments were sufficiently bright to be seen in normal ambient light in laboratory conditions. Figure 101(b) shows the watch in a potential application integrated into a sleeve.

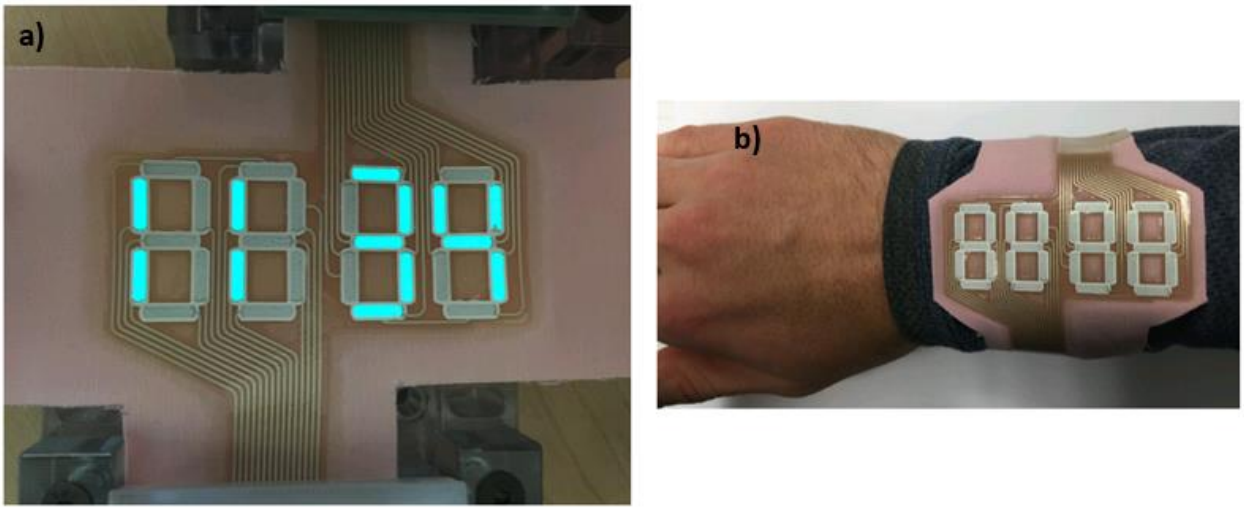

Figure 101. *a) EL watch powered using a Supertex HV881 driver and connected using a custom 3D printed connector. (b) EL watch integrated into the sleeve of a jumper.*

The EL watch display luminance was tested across a range of driving voltages and frequencies. The lab EL driver was used to drive a single segment for testing, this does not affect the brightness of the EL segment. A higher driving voltage and frequency are known to lead to a quicker degradation of the phosphor particles [9]. The luminance was measured between 50-400 V_{peak} and 200-2000 Hz driving frequency and the results are shown in Figure 102. A 150 V_{peak} voltage at 400 Hz would be typical for an EL lamp driver.

The results from the EL watch are similar to blue coloured commercial EL lamps previously tested in a published paper [80] that showed a luminance of 20.5 cd/m^2 at 200 Vpeak / 400 Hz; the EL watch demonstrates 21.8 cd/m^2 at the same voltage and frequency.

To enhance the lifetime of the EL watch, a driving voltage of 150 V_{peak} at 400 Hz was selected as it was sufficient to be easily visible in typical ambient light levels. Previous studies have suggested lifetimes of up to 10,000 hours can be achieved at these emission levels [9]. The EL watch was shown previously in Figure 101(a) under these driving conditions.

The EL watch display has successfully demonstrated the capabilities of EL with the reduced bus bar design. Without this design improvement the brightness of the watch would have been significantly reduced as a large portion of the emitting area would have been covered by the bus bar silver conductor.

6.7. Initial Dispenser Printed Electroluminescent Lamps

An initial EL lamp design was built in L-Edit to initially evaluate dispenser printing. The aim was to create

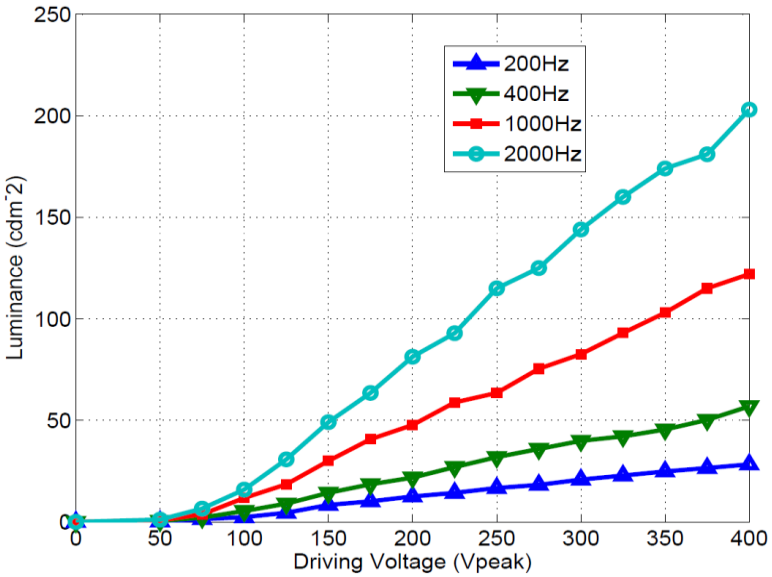

Figure 102. *Luminance data for the EL watch across a range of driving voltages and frequencies.*

a working prototype so the design has high tolerances and a simple shape. This work was carried out near the beginning of the research so only the G1 printer was functional. A basic version of both continuous and droplet printing was working but only in rectangular shapes and without z-height tracking resulting in poor layer thickness control when continuous printing. For this reason, only the thicker layers (>40 µm) were printed with continuous printing. These were the interface, dielectric and

phosphor layers. The bottom conductor, bus electrode, and transparent conducting layer were all printed with droplet printing where a better layer thickness control was achievable. The layer thickness tolerance from previous tests was estimated to be 15% for droplet mode and 25% for continuous mode printing.

The EL lamp design can be seen in Figure 103 below. The primary tolerance that can be varied is the overlap of the dielectric layer relative to the bottom conducting and transparent conducting layer. In the design below a 2 mm overlap is used which should ensure no short circuits are possible through misalignment, whereas with screen-printing a 0.3 mm overlap is typically used. As this EL lamp was printed before the work investigating the bus bar requirements, it includes a bus bar around the entire perimeter of the lamp.

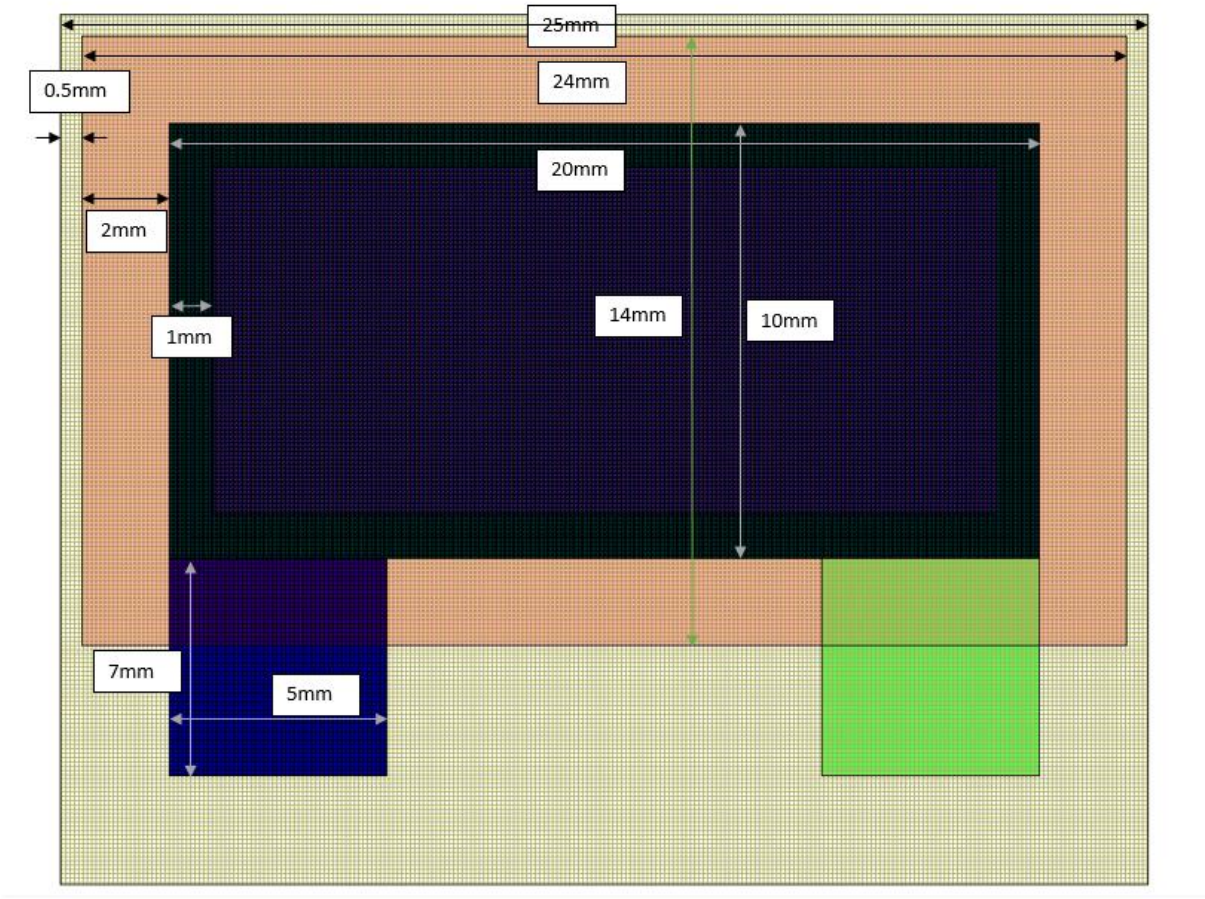

Figure 103. *EL lamp design for dispensing printing showing dimensions.*

The print settings for each layer were found using the process previously described in Figure 21. Two EL lamps were printed to test the design using the same inks shown in Table 35 below. The print settings used for each layer are also shown in Table 35 and all samples were printed using a stage movement speed of 5 mm/s. The X resolution shown in the table is the distance between deposits when droplet printing and the Y resolution is the distance between deposits for both continuous and droplet printing.

Table 35. *Ink and print settings used for each layer in the first dispenser printed EL lamp.*

Layer	Ink	Print Mode	Dispense Pressure (kPa)	Vacuum Pressure (kPa)	Dispense Time (ms)	X Resolution (mm)	Y Resolution (mm)	Curing
Interface	Fabink-UV-IF1003	Continuous	25	0.4	NA	NA	0.4	UV 2 Mins
Bottom Electrode	Fabink-TC-C4001	Droplet	40	0.8	25	0.8	0.4	120°C 10 mins
Dielectric	Fabink TC-D9001	Continuous	30	0.4	Na	NA	0.4	120°C 10 mins
Phosphor	Fabink-TC-P001	Continuous	20	0.6	NA	NA	0.4	120°C 10 mins
Bus Electrode	Fabink-TC-C4001	Droplet	40	0.8	25	0.8	0.4	120°C 10 mins
Transparent Conductor	Clevios S V3	Droplet	30	0.1	30	0.8	0.4	120°C 10 mins

The nozzle to substrate separation distance is unknown and was estimated to be 200 µm by moving the nozzle until it appeared in contact with the substrate and then moving the nozzle up 200 µm. This relies on the accuracy of the stages and the accuracy of judging when the nozzle is in contact visually. An example of the dielectric layer being continuously printed is shown in Figure 104 below.

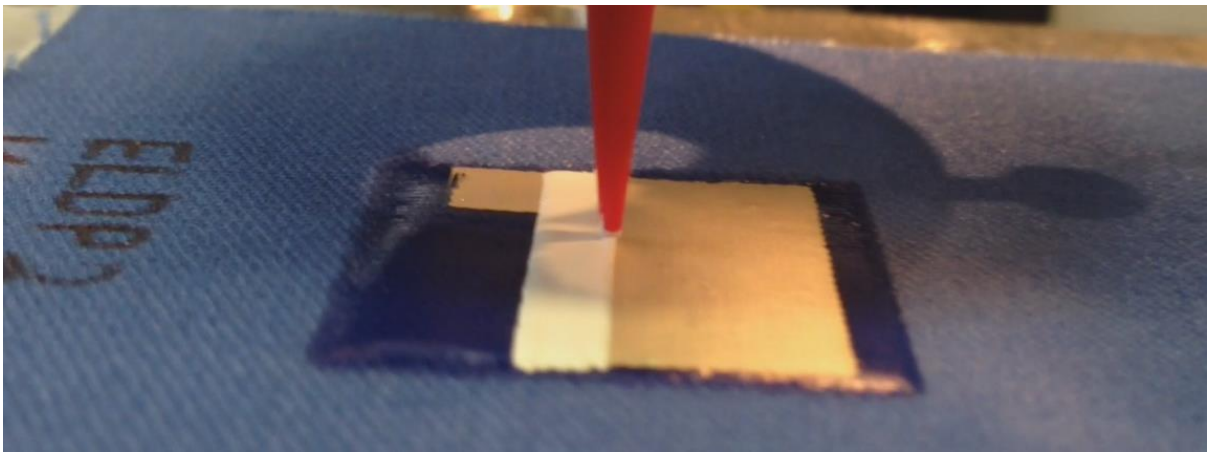

Figure 104. *Dielectric layer of EL lamp showing continuous dispenser printing.*

Upon initial testing, both lamps were functional when driven with 150 V_{peak} at 400 Hz on the lab test EL driver. The printed EL lamps are shown in Figure 105 below both unpowered in daylight and powered in a dark environment.

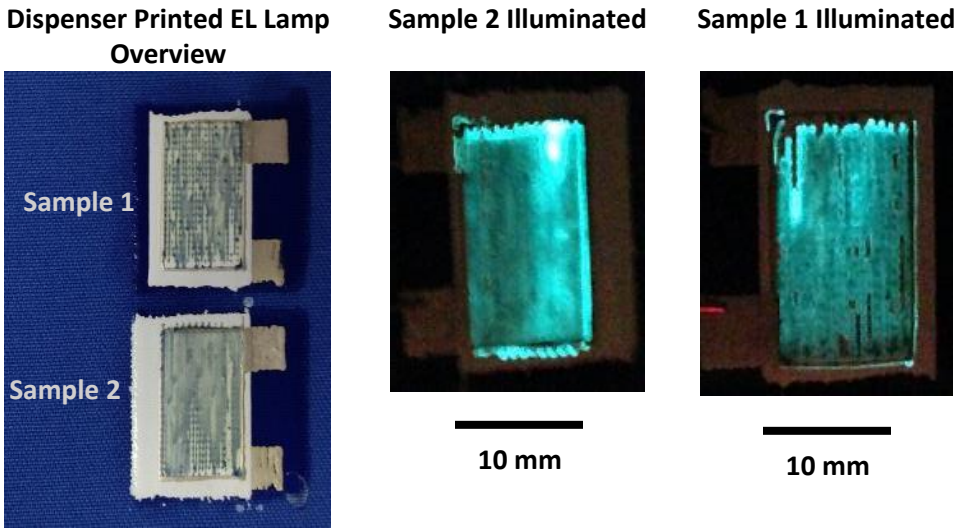

Figure 105. *Images showing (left) the two samples printed next to each other in daylight, (centre) sample 1 being driven at 150 Vpeak 400 Hz, (right) sample 2 being driven at 150 Vpeak 400 Hz.*

As can be seen from the overview image in Figure 105, the print quality of the transparent conducting layer is poor. On the transparent conducting layer the individual droplets from the print process are visible. The areas where the droplets appear smudged is due to variations in the Z height of the sample and the lack of z-height tracking causing the nozzle to touch the sample and 'smear' the ink together. The illuminated images suggest the poor print quality of the transparent conductor is affecting the light output. It is also likely that variation in the continuously printed dielectric layer will create variations in the field strength on the phosphor particles. This in turn will create further variation in brightness and is likely the cause of the bright area at the top of the illuminated photo of sample 1.

After initial tests some sparking was noted when driven, this is caused by parts of the dielectric breaking down under the applied voltage and creating a short. The typical cause of this is variation in the dielectric printed layer meaning some areas are printed too thin and the dielectric constant is not sufficiently high. After the initial function test the lamps were no longer functional meaning the luminance could not be measured. The failure is believed to be caused by a non-uniform dielectric layer that broke down under the high voltage due to the layer being too thin in some areas.

In order to analyse the quality of the print in more detail the thickness of each printed layer was measured and compared to a target thickness given in Table 36. The interface layer has a target thickness of 120 µm since this has been found in the literature to be the thickness required to obtain a smooth layer on this fabric [54]. The target thickness for the bottom conductor is based on achieving a continuous layer with all areas connected to each other. Below 10 µm the dispenser printer is unable to reliably produce uniform layers due to the undulating surface of the fabric weave, therefore a target of 10-15 µm was set. The target thickness for the dielectric material is based on achieving a breakdown voltage in excess of 500 V. The EL lamps will be tested at up to 400 V peak, therefore a minimum thickness of 30 µm based on the material datasheet will give a breakdown voltage of 500 V. The dielectric should not be excessively thick as this will result in a lower field strength on the phosphor and a less bright lamp, therefore an upper target of 45 µm was set. The target thickness for the phosphor layer is based on achieving a layer with single phosphor particles side by side and a small amount of binder material to hold them in place. If multiple phosphor particles are vertically stacked then the field

strength over them is reduced, and the emitted light from the lower phosphor particles is reabsorbed. The particles are an average diameter of 30 µm, therefore a target thickness of 40 µm was selected to allow a small amount of binder material above and below the particles. The target thickness for the PEDOT:PSS was set using the same theory behind the bottom conducting layer minimum thickness. The layer should be as thin as possible with a homogeneous coverage, based on the limitations of the dispenser printer a target thickness of 10-15 µm was set.

Sample 1 in Figure 105 was measured using a micrometer after each printed layer had been cured. One measurement in each of the four corners was taken for each layer and the average and percentage variance for each layer was calculated. The bus electrode layer is excluded from the results as the track was too narrow to get a repeatable result. The results are shown in Table 36 below.

Table 36. *Results of the thickness measurements after each layer in sample 1 had been cured.*

Layer	Target Thickness (µm)	Average Measured Layer Thickness (µm)	Variance Percentage Over Four Measurements
Interface	120	174	32%
Bottom Electrode	10-15	37	21%
Dielectric	30-45	112	37%
Phosphor	40	82	31%
Transparent Conductor	10-15	8	20%
Total (All Layers)	210-235	414	28%

The results show that the all layers, except the transparent conductor, were printed too thick. This is likely caused by a lack of z-height tracking meaning the nozzle had to be set with an excessive separation distance to ensure a continuous deposit of ink over the entire area. The variance between the measurements on each layer was also significant reinforcing this point. The variance results also show that the droplet mode has a more uniform deposit of ink than continuous printing. The droplet mode printing is not a continuous flow of ink so is less affected by variations in the separation distance.

6.8. Improved Electroluminescent Lamps

An improved EL lamp design was built incorporating the added features and research conducted. The design utilised the following new features developed as part of this work:

- Printing a large design that is 210 x 150 mm including 4 EL lamps using the G2 printer.
- Continuously printing a complex shape.
- Printing with an optimised infill pattern.
- Printing with z-height tracking to maintain a defined nozzle to substrate separation distance.
- Optimised bus bar design to reduce print time, material usage, and emitting area covered by the bus bar.

The design that was developed is larger than previously printed devices and includes four complex shaped EL lamps. A single large EL lamp was not included as the UoS does not have an EL driver capable of powering a large segment (>30 cm^2). The design is also more similar to the designs produced by the designers in the CREATIF project where multiple lamps are spread over a large area with connecting

tracks between them. The lamp was drawn in SketchUp, a 3D CAD package where each layer was created with a set thickness and placed on top of one another. The full design can be seen in Figure 106 below.

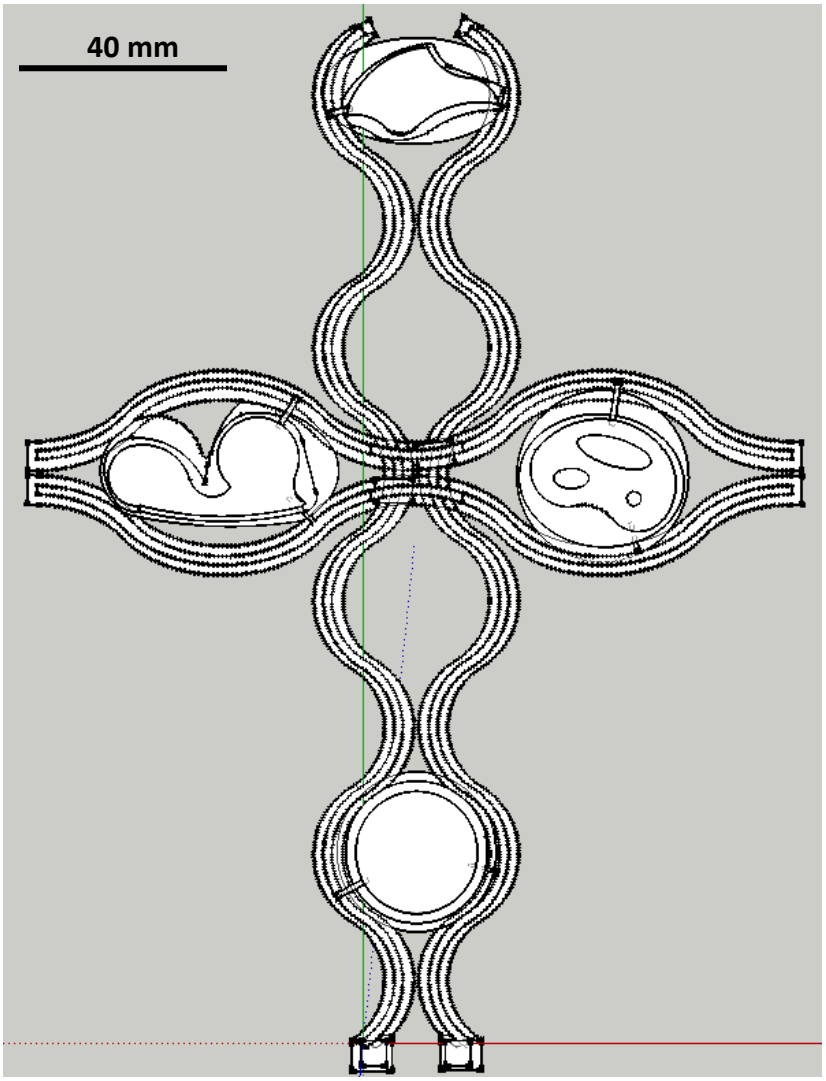

Figure 106. *Design from SketchUp for the improved EL lamp.*

Each of the EL lamps incorporates a small bus bar connection along the outer edge. This is shown in greater detail in Figure 107 for the circular EL lamp shown at the bottom of Figure 106. The figure shows the connection highlighted in a red circle made up of a 2 mm diameter track extending 2.5 mm into the emitting area of the EL lamp. The same design was repeated on the other three EL lamps and covers 15 times less of the emitting area than a bus bar around the entire perimeter.

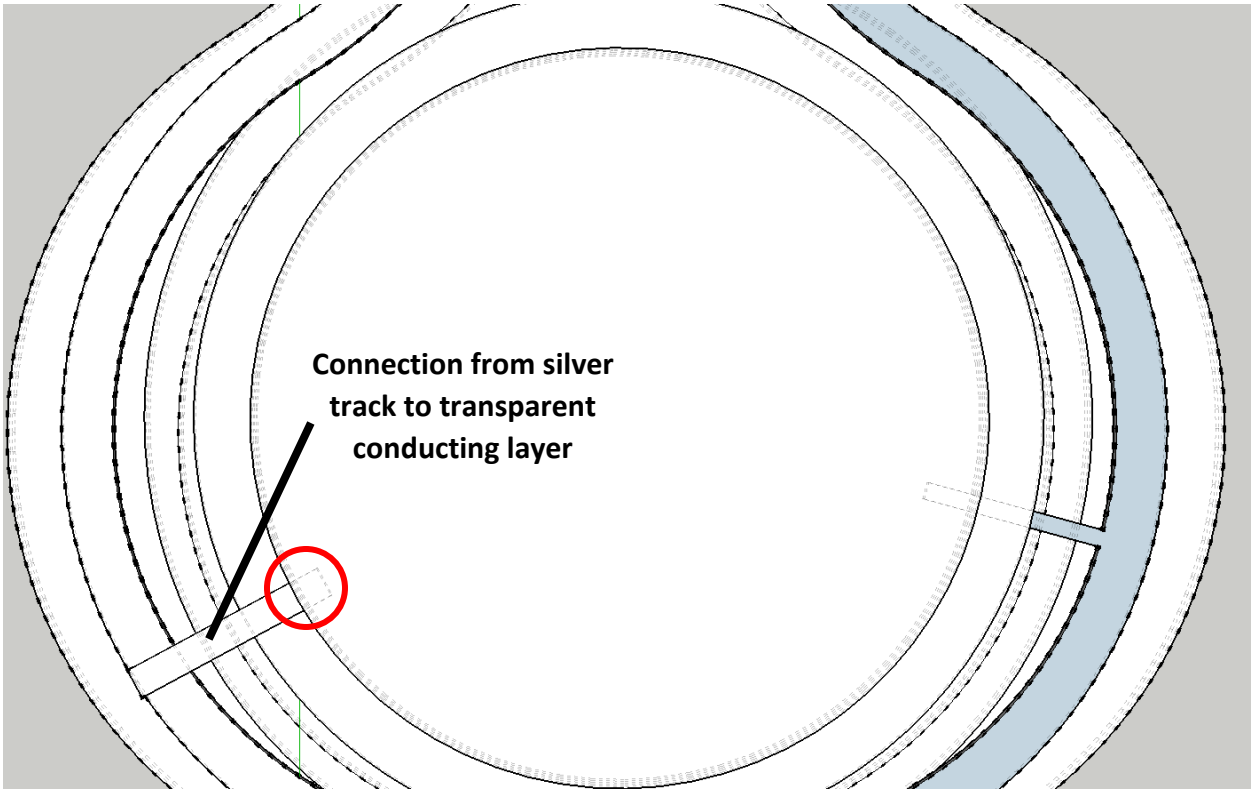

Figure 107. *SketchUp design close up view of bottom circular EL lamp, highlighting the bus bar connecting the silver track to the transparent conducting area.*

The design also includes a complicated 'crossover' in the middle. This involves silver tracks crossing other tracks in order to connect to the lamps in a visually attractive way. In Figure 106 there are four silver tracks and they are connected as follows:

- Left vertical track – Positive terminal.
- Right vertical track – Negative terminal.
- Top horizontal track – Positive terminal.
- Bottom horizontal track – Negative terminal.

To achieve these connections, the 'crossover' section in the middle includes two extra sections of silver and dielectric. This is shown in greater detail in Figure 108 where the extra silver and dielectric deposits of inks have been coloured for clarity. The dielectric was printed at the end followed by an extra silver layer to provide the connection on top of the dielectric. Where present the dielectric layer prevents a connection being formed between the silver tracks allowing a positive and negative terminal connected track to cross.

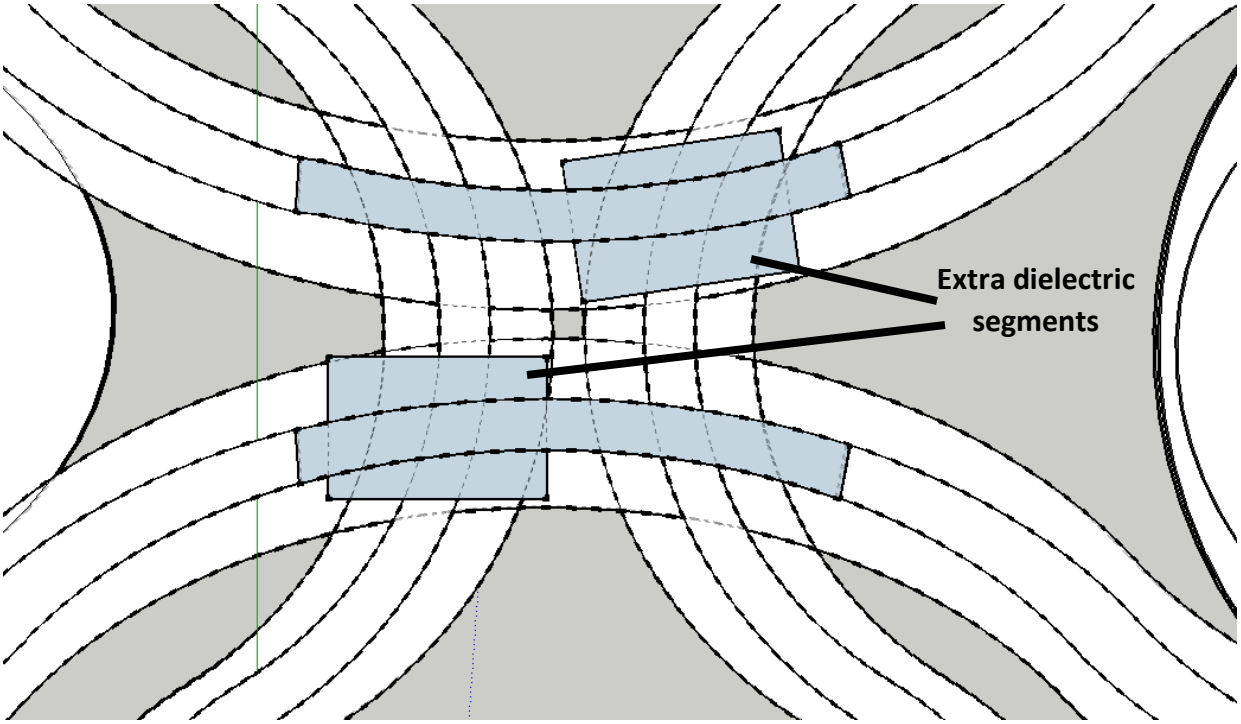

Figure 108. *Close-up view of 'crossover' section of tracks in the improved EL lamp highlighting the extra dielectric segments.*

The lamp was printed using the inks and settings shown in Table 37. The inks for each layer are the same as the initial EL lamp described in the previous section. The dispense pressures were found using the experimental process described in Figure 21. All layers were printed continuously at 10 mm/s stage movement speed and the optimum infill pattern (rectilinear at 70% density) found previously was used for all layers. An initial profile of the substrate was taken and then, after each layer, the ink thickness was measured and entered into the printer software to raise the nozzle the defined amount. No interface layer was required as this lamp was printed onto the Berger CREATIF fabric described in section 6.2. The printed sample is shown unpowered after the final layer was cured in Figure 109(a) and powered at 150 V_{peak} 400 Hz in Figure 109(b).

Table 37. *Summary of inks and print settings used for the improved EL lamp.*

Layer	Ink	Dispense Pressure (kPa)	Vacuum Pressure (kPa)	Curing
Bottom Electrode	Fabink-TC-C4001	20	1.1	120°C 10 mins
Dielectric	Fabink-TC-D9001	40	0.8	120°C 10 mins
Phosphor	Fabink-TC-P001	30	0.8	120°C 10 mins
Bus Electrode	Fabink-TC-C4001	20	1.1	120°C 10 mins
Transparent Conductor	Clevios S V3	8	0.1	120°C 10 mins

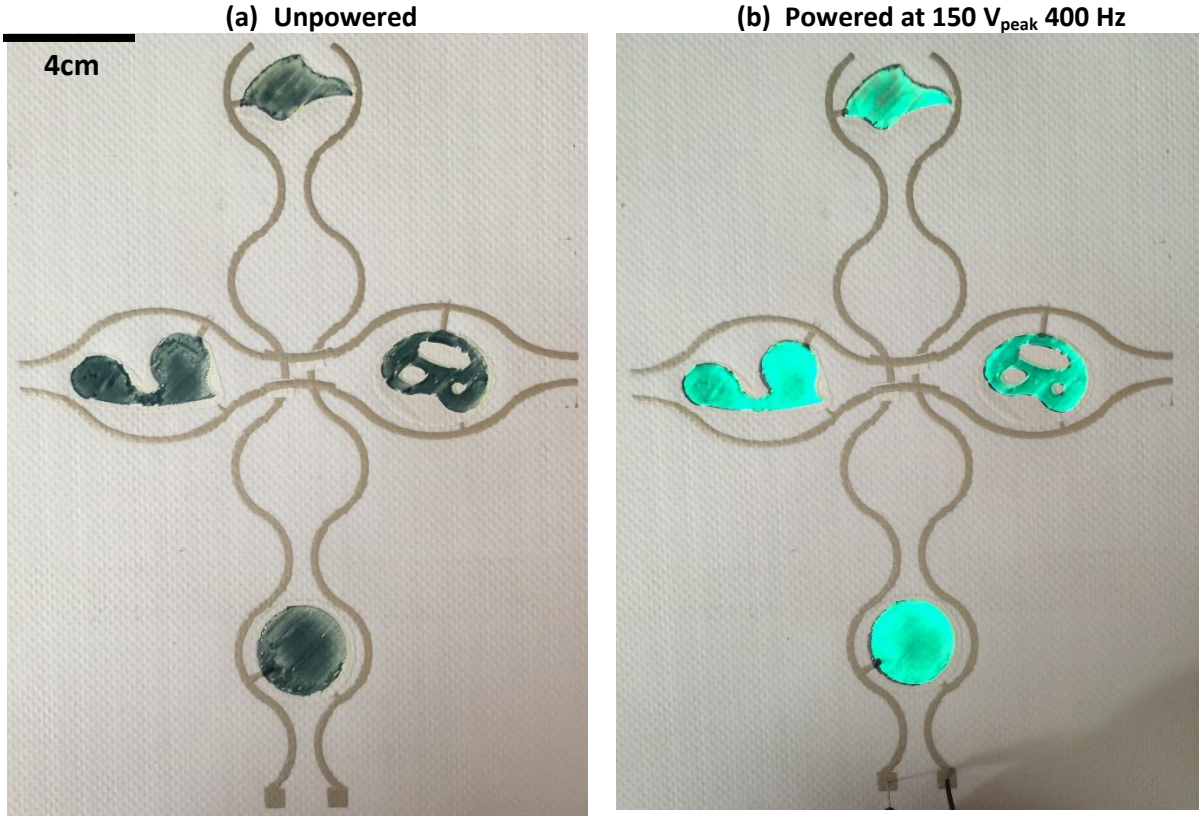

Figure 109. *Improved EL lamp (a) unpowered after the final layer was cured, (b) powered by the lab EL test driver.*

All four of the EL lamps are fully functional showing that all parts of the design including the track 'crossover' were successful. The PEDOT:PSS ink used for the transparent conducting layer is challenging to print as it has a relatively high surface tension and therefore does not coalesce as easily as the other inks. The print lines are more visible after curing leading to a non-uniform surface. This will affect the field distribution, which will in turn affect the light output.

In order to characterise the lamps luminance an experiment was planned that would test driving voltages in the 0-400 V_{peak} range and driving frequencies of 200-2000 Hz. This range of voltages and frequencies is commonly referenced in literature. The lab EL driver is not capable of driving this device at the higher voltages and frequencies as the emitting area was too large, corresponding to a capacitance that was too large for the amplifier. Upon initial tests this became apparent through a warning on the Trek amplifier.

To allow for a full set of results to be collected a smaller single EL lamp (1x2 cm) was printed using exactly the same materials, print settings, and processes as the EL lamp in Figure 109. The bus bar connection was printed having the same area as the improved EL lamp in Figure 109 to ensure the sample was representative. The smaller test sample is shown after each printed layer and powered at 150 V_{peak} 400 Hz in Figure 110. When viewed closely, the EL lamp shows the pattern of the fabric weave, which is due to the height variance of the weave causing changes in the field strength over the EL phosphors.

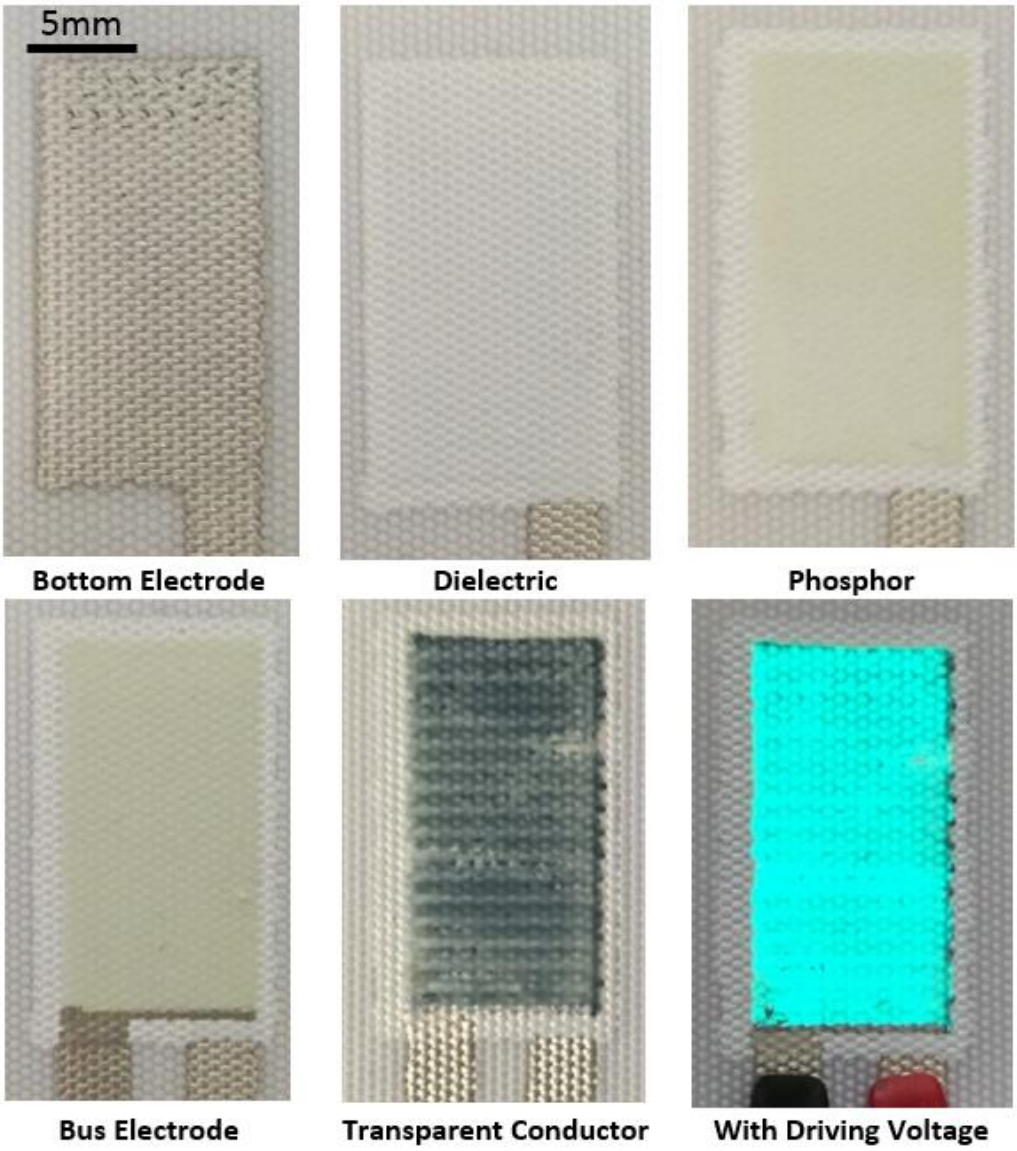

Figure 110. *1x2 cm EL lamp printed to use with the lab EL driver to measure the luminance.*

To quantify the brightness of the dispenser printed EL lamps, a Konica Minolta CS-100 was used to record luminance. The colour co-ordinates were also given by this equipment and the data was recorded. A similar technique was used by Wang et al. [81]. The lamp was driven using the lab EL driver from 50-400 V_{peak}, and frequencies of 200 Hz, 400 Hz, 1000 Hz and 2000 Hz. The results can be seen in Figure 111 below.

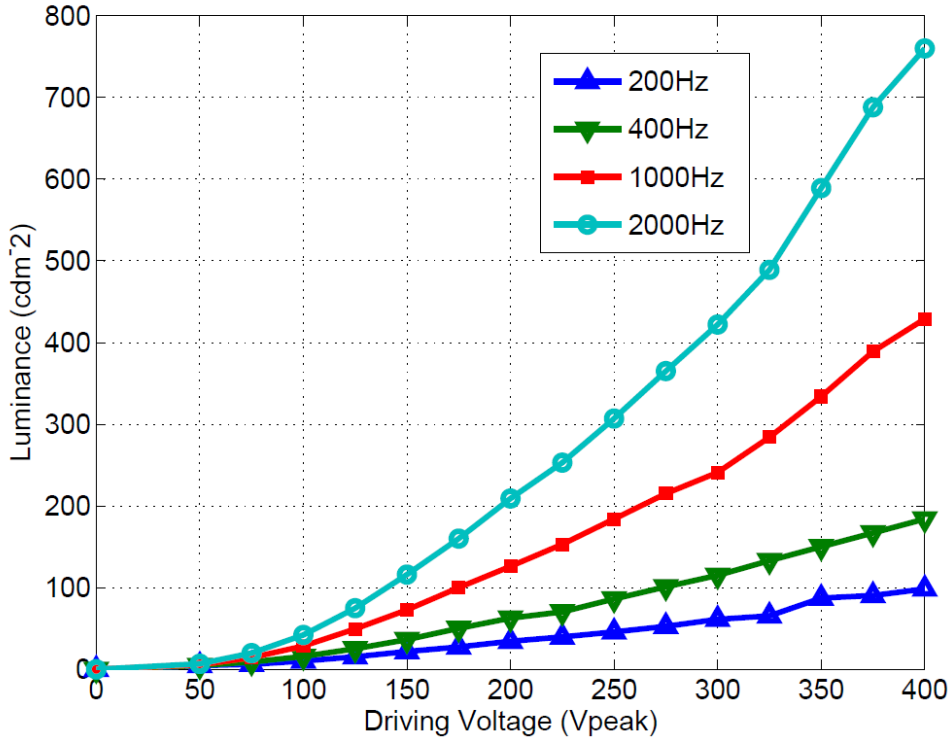

Figure 111. *The luminance of the 1 x 2 cm EL lamp at various driving voltages and frequencies.*

As was expected the graph shows the luminance increases with greater driving voltages, and also with higher driving frequencies. These results are compared to commercial EL lamps in section 6.10 to give context to this data.

A colour shift based on the driving frequency was also noticed during testing across different frequencies. The phenomenon has previously been explained by Jayaraj [82]. The colour shift is significant and could be useful in some design applications with colour offering a second level of communication beyond the lamp being on or off. The colour shift is shown on a CIE 1931 colour space chromacity diagram in Figure 8. The data shows a shift towards a lower wavelength of blue light at higher driver frequencies.

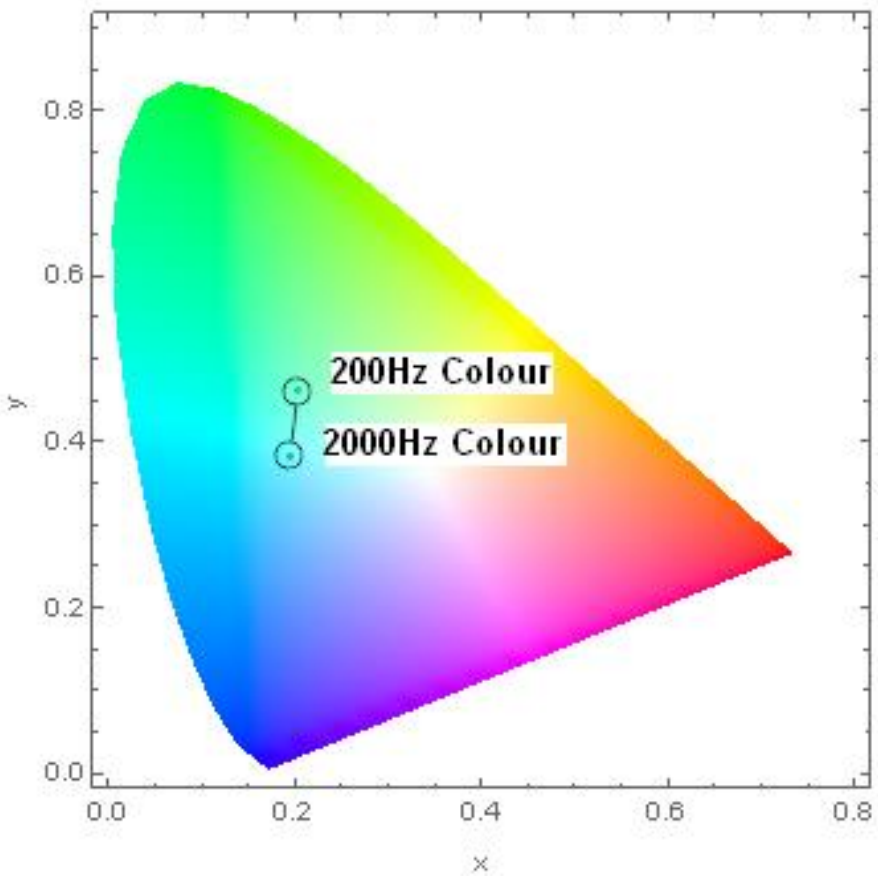

Figure 112. *CIE 1931 colour space chromacity diagram showing the colour shift of a dispenser printed EL lamp based on driving frequency.*

After each layer was cured the thickness of the printed layer was measured in all four corners as in the initial EL lamp. The same target thicknesses were used as in the earlier section and the results are shown in Table 38 below.

Table 38. *Results of the thickness measurements after each layer in the 1x2 cm improved EL lamp had been cured.*

Layer	Target Thickness (µm)	Average Measured Layer Thickness (µm)	Variance Percentage Over Four Measurements
Bottom Electrode	10-15	12	8%
Dielectric	30-45	97	12%
Phosphor	40	53	11%
Transparent Conductor	10-15	14	7%
Total (All Layers)	90-115	176	28%

The measured layer thicknesses are within the target thickness range for the bottom conductor and transparent conductor layers. The dielectric is significantly thicker than the minimum thickness. The single layer was printed thicker in an attempt to ensure there was at least 30 µm of dielectric ink in all areas, to prevent the breakdown voltage being exceeded. The thicker dielectric layer will cause a reduced field strength to be present over the phosphor, resulting in a lower luminance. However, a 30 µm layer must be present in all areas and this is difficult to achieve due to the surface roughness of the

woven fabric. The phosphor layer was also printed 33% thicker than the target thickness. This was caused by variations in the height of the underlying dielectric layer, meaning more ink was dispensed in some areas than others.

The sample was also viewed under an SEM. A technique was developed where the samples are cooled in liquid Nitrogen for 15 minutes leaving them brittle. The samples were then fractured using a sharp blade to reveal the structure in the centre of a lamp. This technique is preferred over simply cutting the samples as this crushes the printed layers resulting in poorly representative images. The results from the SEM revealed that layer thicknesses varied with the weave of the fabric. The SEM cross-section can be seen in Figure 113. Distinct layers are visible and it can be seen how the consecutive layers smooth the weave of the fabric to provide an overall smooth surface.

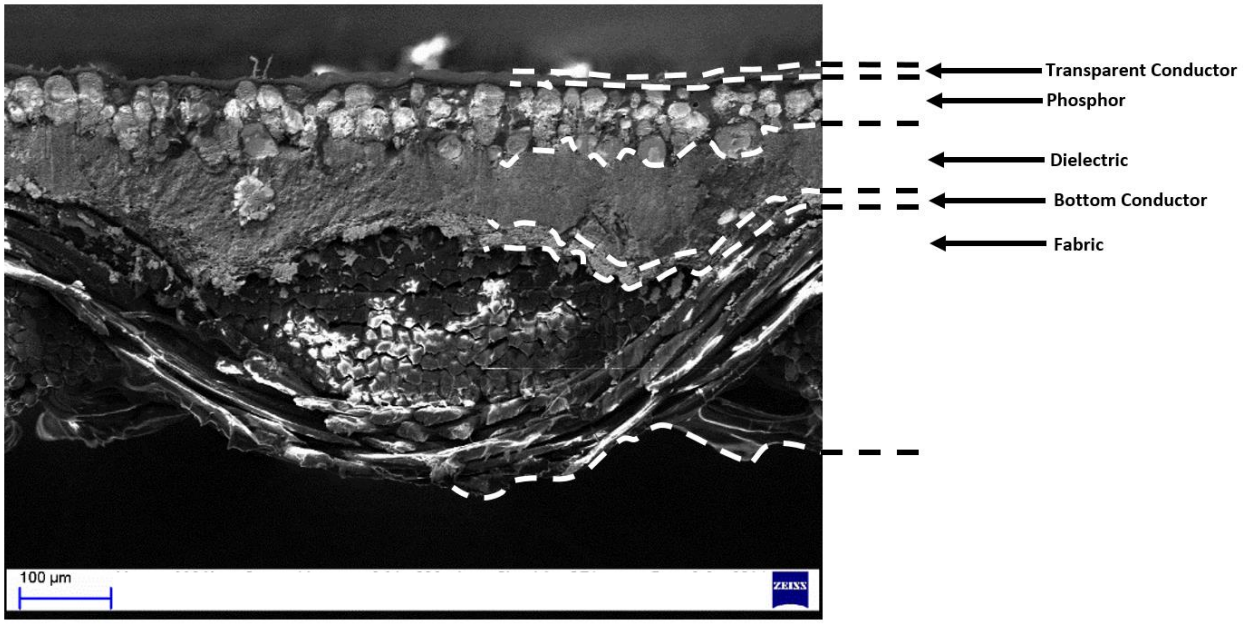

Figure 113. *SEM image showing the cross-section of the 1x2 cm improved EL lamp.*

6.9. Comparison of Initial and Improved Dispenser Printed Lamps

The initial and the two improved EL lamps were compared in terms of printed layer thickness, variance of the printed layer and visual appearance both unpowered and powered. Clearly the larger improved EL lamp has a far more advanced design that would give greater options to the end user in terms of appearance.

The thickness and variance in thickness of the printed layers is shown in Table 39 below with the interface layer excluded from the comparison as it was only required on the initial EL lamp substrate. The results for thickness show that all layers were closer to the target thickness, with two of the layers falling within the target thickness range. The variance was also significantly reduced for all layers in the improved EL lamp, showing that the layers were printed more uniformly. This improvement is believed to be caused by the z-height tracking ensuring the nozzle remains a set distance above the substrate.

The increase in transparent conducting thickness will result in a more even distribution of ink over the top of the EL lamp and will ensure the entire area of phosphor emits light. The reduction in phosphor and dielectric layer thicknesses will also result in a higher luminance for a given voltage/frequency.

Table 39. *Comparison of layer thickness and variance for the initial and 1x2 cm improved EL lamp.*

		Initial EL Lamp		1x2 cm Improved EL Lamp	
Layer	**Target Thickness (µm)**	**Average Measured Layer Thickness (µm)**	**Variance Percentage Over Four Measurements**	**Average Measured Layer Thickness (µm)**	**Variance Percentage Over Four Measurements**
Bottom Electrode	10-15	37	21%	12	8%
Dielectric	30-45	112	37%	97	12%
Phosphor	40	82	31%	53	11%
Transparent Conductor	10-15	8	20%	14	7%
Total (All Layers)	90-115	239	28%	176	28%

The initial and 1x2 cm EL lamp were then compared visually as there is no luminance data for the initial lamp. Both lamps are shown powered and unpowered in Figure 114 below. In the unpowered images of the EL lamps it is apparent that the ink is more evenly distributed in the improved EL lamp despite the weave of the fabric being visible. In the top left of the unpowered initial EL lamp, the silver appears to have a section missing where the nozzle came into contract with the sample, whereas on the improved EL lamp both silver connectors were printed successfully. The differences in bus bar design are also apparent as the improved EL lamp includes a single thin track along the bottom of the emitting area as opposed to a much larger bus bar around the entire perimeter on the initial EL lamp.

The images showing the two lamps powered (at 150 V_{peak} 400 Hz) offer the best insight into the quality of the lamps. The initial EL lamp had the photo taken in a darkened room making it appear brighter. Even with this enhancement it is clear that the EL lamp is not as bright as the improved 1x2 cm EL lamp. The homogeneity of the emitted light is also worse in the initial lamp as there are sections of the display that are not illuminated. This is likely caused either by a non-uniform transparent conducting layer or by short circuits through the dielectric layer that ultimately led to the device failing.

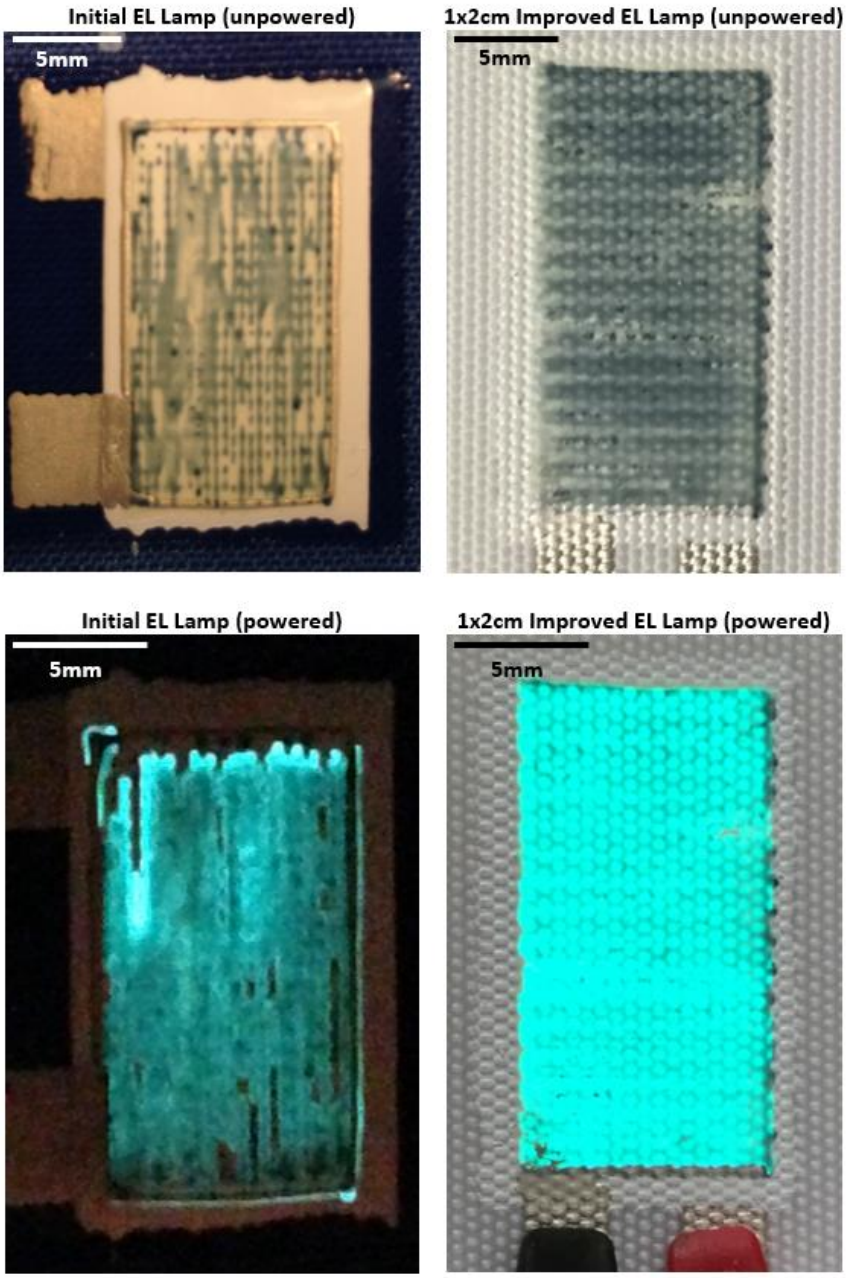

Figure 114. *Images of the initial and improved 1x2 cm EL lamps both unpowered and powered at 150 V_{peak} 400 Hz.*

6.10. Comparison of Improved Dispenser Printed, Screen-Printed and Commercial Electroluminescent Lamps

In order to compare the improved EL lamp to the state of the art a further two comparisons are made in this section. The improved dispenser printed EL lamp is first compared to a screen-printed EL lamp onto the same substrate with the same ink. It is then compared to a number of commercial EL lamps.

Screen-printed EL lamps were produced in the same dimensions as the dispenser EL lamp to allow comparison to a commonly used printing technique. The lamps were fabricated using the same settings

as the EL watch. The same inks were used for both the dispenser and screen-printed lamps and the same measurement technique was used to record the luminance data. A graph comparing the luminance data for the dispenser and screen-printed EL lamps over a range of driving voltages and frequencies can be seen in Figure 115.

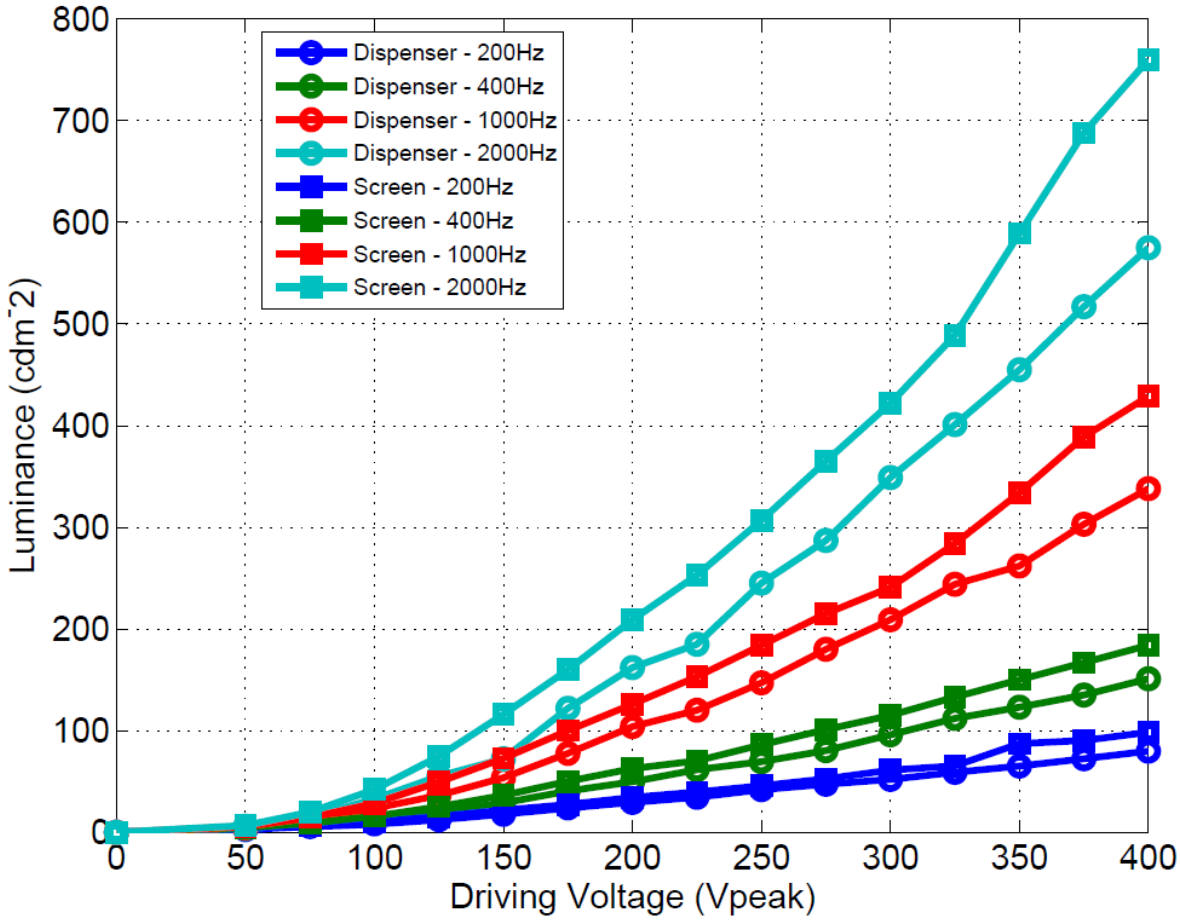

Figure 115. *Comparison between the improved dispenser and screen-printed EL lamp both with dimensions 1 cm by 2 cm over a range of driving voltages and frequencies.*

While the layer thickness and surface roughness of the printed layers were different for the screen-printed EL lamp, the graph allows some conclusions to be made. The primary conclusion is that dispenser printing is a viable technology for the production of EL lamps on fabric showing little noticeable difference in visible luminance at 400 Hz, the most common drive frequency of commercial EL drivers.

The results show that the screen-printed lamps are brighter – on average they have a 25% higher luminance, with an error of ±5% due to variations in luminance over the EL lamp surface. The difference can be attributed to the screen-printer currently having finer control of layer thickness than the dispenser printer. This is visible when comparing the thickness of the dielectric layer, which is 64 µm for the screen-printed EL lamp compared to 97 µm for the dispenser printed EL lamp. The thinner dielectric layer will result in a stronger field strength over the phosphor particles for a given drive voltage, causing a higher luminance.

The printed EL lamps on fabric were then compared to a range of commercially available EL lamps. These commercial lamps are all screen-printed onto a polyurethane film thus avoiding issues surrounding surface roughness of the substrate. The lamps tested were a range of sizes, as shown on the graph legend. However, the luminance is related to the field strength, which is the same for all of the lamps, therefore they are comparable. The light distribution is approximately uniform across the surface of the lamp. However, three measurements for each voltage were taken and the measurements were then averaged.

The lamps were tested at 400 Hz as it is the most commonly used driving frequency for commercial EL drivers. The lab EL driver described earlier was used for all of the lamps and results are shown in Figure 116 below.

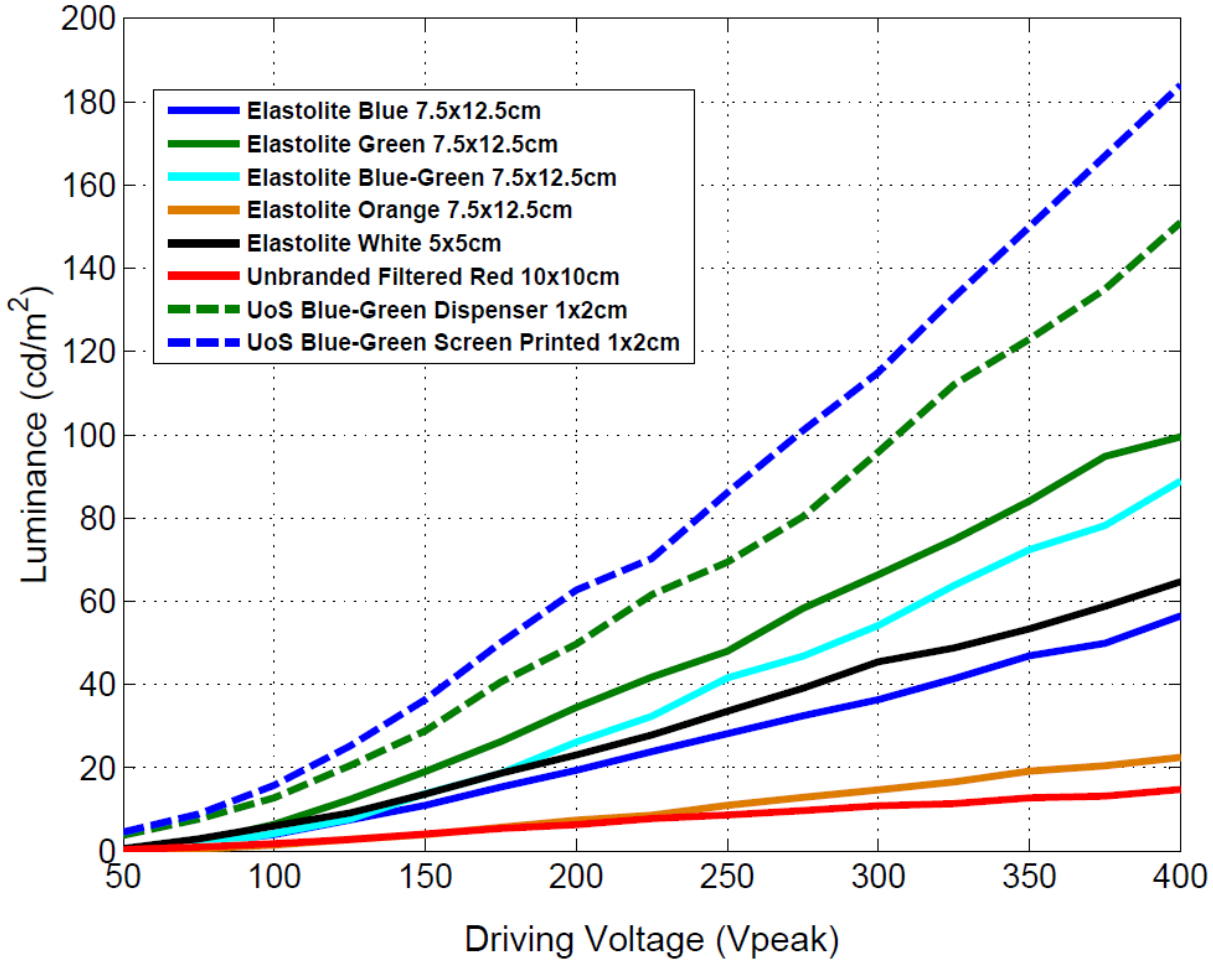

Figure 116. *Comparison of UoS dispenser and screen printed EL lamps, with a range of commercial EL lamps. All sizes in the legend are in inches.*

The results show that the two UoS printed lamps on fabric are brighter than any of the commercial EL lamps. The University of Southampton (UoS) dispenser printed EL lamp has a luminance 1.5 times higher on average than the best of the commercial EL lamps. The results are an indicator of good performance, however it is not possible to draw any firm conclusions as the materials, structure, or manufacturing

processes of the commercial lamps is unknown. The higher luminance is likely to be caused by better control and design of the EL lamps layer thickness and superior inks used to produce the UoS lamps.

The luminance of the UoS EL lamps is also significantly better than the recently published stretchable EL devices Wang et al [81], with a luminance approximately four times that of the device in that paper at 1KHz, 300Vpeak.

6.11. Closure

The requirements for the substrate of an EL lamp were initially considered, identifying Kapton and polyester cotton as suitable test substrates along with two further test fabrics required for the CREATIF project applications. The Kapton was used throughout this chapter as a smooth test sample, while the polyester cotton was used initially for fabric tests, before the CREATIF project required that their fabric samples were used for later work.

A review of the available commercial EL drivers was undertaken and a recommendation of a suitable driver for four different applications was made. The most relevant to this work was the driver recommended for numerous small area EL lamps, the Supertex HV881. This driver was used later in the chapter to drive the EL watch. The lab EL driver was also described as this is used to test all the EL lamps across a range of frequencies and voltages.

The available inks were investigated for the phosphor and transparent conducting layers. A comparison of commercially available phosphor pastes and powders was produced, with the aim of showing the available colours that could be produced. A number of sample materials were obtained and three colours of EL lamp were screen-printed onto woven fabric using a custom screen design. The tests show that, as well as the standard blue-green colour commonly associated with EL, a dark blue and an orange are possible. The white phosphor appeared visually closer to a blue EL lamp so was discounted.

The transparent conducting layer was considered in detail, with four commercial pastes being compared. The pastes were tested for transparency. The Loctite paste produced the best result, with a transmittance of 50-60% over a broad spectrum, but the print quality was very poor so it was not considered further. Of the remaining three inks the Clevios S V3 ink was the best performer in the practical tests so this ink was used for all future prints.

The requirement for a silver bus bar around the perimeter of the lamp was then examined. A COMSOL model suggested that the voltage drop over the sample would be approximately 30% with a small 2.5 mm bus bar compared to one around the entire perimeter. These results suggested a practical test was warranted. A test involving varying lengths of bus bar showed that with the chosen Clevios PEDOT:PSS sufficiently carried the electric charge with only a minimal 0.5 mm bus bar. This development meant much smaller EL lamps could be printed due to the requirement for a track around the entire perimeter no longer being in place.

To demonstrate the smaller bus bar design, a screen-printed EL watch display was designed. The display includes 28 individual EL segments that were smaller than would have been previously possible. Each segment has a small curved bus bar around the edge of one side of the segment. The watch display represents the first time printed EL lamps have been combined to form a watch display on fabric and was reported on by numerous news and blog websites.

The initial dispenser printed EL lamps were also characterised. Each lamp was 2 x 1 cm with a 2 mm dielectric overlap and was printed with a combination of droplet and continuous printing due to the limited layer thickness control when continuous printing. The two lamps that were demonstrated had the thickness measured after each printed layer. They were briefly functional but both quickly failed before luminance measurements could be taken. The failure was likely caused by the non-uniform dielectric layer being printed too thin in some areas and breaking down under the high voltage. The thickness measurements also showed a poor correspondence to the target thickness ranges with a high variance for each layer caused by the lack of z-height tracking.

A complex design representing an improved EL lamp was then demonstrated. The design included four individual curved lamps and had a track 'crossover' section in the centre. The design was printed using the optimum infill pattern (rectilinear at 70% density) found earlier in the thesis. The print also utilised z-height tracking to maintain a defined nozzle to substrate distance. The lamp was fully functional but was too large to be powered across the necessary voltages and frequencies by the lab EL driver so a similar smaller EL lamp was printed and characterised.

The initial and improved EL lamps were compared, showing a significant improvement in layer thickness control. The overall print quality was also improved with lower variances in thickness and a more uniform deposit of ink on the transparent conducting layer. The lamp appeared to be significantly brighter visually.

The luminance of the improved dispenser printed EL lamp was then shown to be comparable to those which are screen-printed, with screen-printing being an average of 25% higher. The UoS printed fabric EL lamps were also compared to commercial EL lamps and the experiment showed they had a higher luminance than any of the commercial lamps on polyurethane. While a direct comparison is not possible due to the uncontrolled factors, such as the layer thickness of the commercial EL lamps, it does show that dispenser printing is a viable fabrication technology for EL lamps.

7. Conclusions

The work in this thesis demonstrates the development of a novel dispenser printing process for fabricating EL lamps. In order to achieve these complex multilayer structures novel advancements in z-height tracking, bus bar design, control software and infill pattern have been made.

The hardware used in the dispenser printer was considered with many displacement sensors reviewed and three laser triangulation sensors tested by profiling a printed EL lamp. The tests highlighted the difficulties some of the sensors faced in sensing transparent layers, due to the angle of the incident laser. The Keyence LK-G10 sensor was selected for future use. The G2 profilometer was compared to a commercially built system by Alicona and the results suggested that the G2 system was not sensing the semi-transparent PEDOT:PSS layer, and was in fact measuring the opaque phosphor layer below.

The z-height tracking software was tested using droplet mode printing of silver tracks onto woven polyester fabric. The results showed the average resistance of the tracks printed with z-height tracking is 6.4 times lower than the resistance of the tracks printed without it. The z-height tracking with continuous mode printing was then tested with larger shapes and the results showed that 20 cm and 40 cm silver tracks can only be successfully printed if z-height tracking is enabled. The shorter 10 cm tracks also showed the resistance was 7.4 times lower with z-height tracking enabled.

The effect of the infill pattern on print quality was also investigated by reviewing five infill patterns across three densities on four shapes. The shapes were the building blocks of other more complex shapes so are representative. The results showed that rectilinear at 70% density was the best performing in terms of coverage, surface roughness, print time and layer thickness.

A review of the bus bar design was also conducted, using a simulation that showed a 30% voltage drop for a short 2.5 mm bus bar compared to a bus bar around the perimeter of 1x2 cm EL lamp. The results warranted further investigation, so a series of EL lamps were printed with bus bars varying from 1 mm to 10 mm. The results showed no noticeable difference in brightness so a novel bus bar design was developed that means significantly more of the emitting area is used.

Significant time was spent developing the control software for the dispenser printer. The improvements were z-height tracking for both droplet and continuous mode printing and a capability to print any shape continuously rather than the rectangles to which the printer had previously been limited. The enhanced control software was demonstrated by printing an interface layer of a popular logo involving many complex curves.

Once a number of advancements to the print process had been made, improved dispenser printed EL lamps were fabricated. The improved lamps were in a complex shape, printed with the optimum infill pattern and had z-height tracking enabled. The comparison between the initial and improved EL lamps showed much better reliability and layer thickness control of the improved EL lamps with the layer thickness variance reduced by more than half.

The improved dispenser printed EL lamps were then compared to screen-printed EL lamps produced at the UoS, along with screen-printed commercial lamps. The dispenser printed EL lamp far outperformed the commercial EL lamps, with a luminance on average 1.5 times higher than the equivalent coloured commercial EL lamp. The dispenser printed EL lamp had a luminance slightly lower than the UoS screen-

printed EL lamp due to its thinner dielectric layer. The UoS EL lamps also compared favourably to previously published stretchable EL lamps, with a luminance four times higher.

To ensure suitable dispenser printing pressures can be found reliably a simulation model of the dispenser syringe was built, allowing the volume of ejected ink to be simulated for specific dispenser settings. The simulation was used to identify the optimum dispense pressure to achieve a target volume of dispensed ink. The simulation was tested with both an interface and silver ink and the optimum dispense pressure was found for both inks. The simulation was compared to an experimental method that gave the same results faster so the experimental method was selected for subsequent use in this work.

Work was also undertaken to analyse the base plate uniformity relative to the nozzle on the G2 printer. Minimising the variation over the plate is essential when trying to maintain a separation between nozzle and substrate. The results showed there was a variation in excess of 2 mm over the plate and a series of repairs were undertaken reducing this to 0.7 mm. However, the significant variation means z-height tracking is still essential.

In conclusion, this thesis has presented a number of improvements in the dispenser printing process. The improved EL lamps show that dispenser printing is now a viable method to produce high quality EL lamps with luminance comparable to other printing technologies and outperforming a number of commercial products and previously published devices.

Future work should be undertaken to improve the speed of profiling a substrate and the quality of the profile by incorporating a wide beam laser displacement sensor into the printer. Curing the devices using a heater attached to the dispenser printer could also be investigated to remove the need to move the substrate to a curing oven in between layers. Lastly, a number of new inks for EL lamps have been released in the latter months of this PhD, particularly silver nanowire inks, that could be tested as a replacement to the difficult to print PEDOT:PSS based inks currently used for the transparent conducting layers.

8. References

1. Calvert, P., *Inkjet printing for materials and devices.* Chemistry of materials, 2001. **13**(10): p. 3299-3305.
2. Larson, C., B. Peele, S. Li, S. Robinson, M. Totaro, L. Beccai, B. Mazzolai, and R. Shepherd, *Highly stretchable electroluminescent skin for optical signaling and tactile sensing.* Science, 2016. **351**(6277): p. 1071-1074.
3. Wang, J., C. Yan, K.J. Chee, and P.S. Lee, *Highly Stretchable and Self-Deformable Alternating Current Electroluminescent Devices.* Advanced Materials, 2015. **27**(18): p. 2876-2882.
4. *CREATIF - EU FP7 Project*. Date Accessed: 12 June 2014; Available from: http://www.creatif.ecs.soton.ac.uk/.
5. Lanz, T., A. Sandström, S. Tang, P. Chabrecek, U. Sonderegger, and L. Edman, *A light–emission textile device: conformal spray-sintering of a woven fabric electrode.* Flexible and Printed Electronics, 2016. **1**(2): p. 025004.
6. Sloma, M., D. Janczak, G. Wroblewski, A. Mlozniak, and M. Jakubowska, *Electroluminescent structures printed on paper and textile elastic substrates.* Circuit World, 2014. **40**(1): p. 13-16.
7. Hu, B., D. Li, O. Ala, P. Manandhar, Q. Fan, D. Kasilingam, and P.D. Calvert, *Textile-Based Flexible Electroluminescent Devices.* Advanced Functional Materials, 2011. **21**(2): p. 305-311.
8. Ireland, T. and J. Silver, *Studies on the Orientation of ACEL ZnS: Cu Particles in Applied AC Fields.* ECS Journal of Solid State Science and Technology, 2014. **3**(3): p. R25-R32.
9. Bredol, M. and H. Schulze Dieckhoff, *Materials for powder-based AC-electroluminescence.* Materials, 2010. **3**(2): p. 1353-1374.
10. Tao, X., *Wearable electronics and photonics*. 2005: Elsevier.
11. Deflin, E., V. Koncar, and A. Weill, *Bright optical fiber fabric: A new flexible display.* Textile Asia, 2002. **33**(5): p. 25-28.
12. Cochrane, C., L. Meunier, F.M. Kelly, and V. Koncar, *Flexible displays for smart clothing: Part I-Overview.* Indian Journal of Fibre and Textile Research, 2011. **36**(4): p. 422.
13. Ghahremani Honarvar, M. and M. Latifi, *Overview of wearable electronics and smart textiles.* The Journal of The Textile Institute, 2016: p. 1-22.
14. Vozzi, G., A. Previti, D. De Rossi, and A. Ahluwalia, *Microsyringe-based deposition of two-dimensional and three-dimensional polymer scaffolds with a well-defined geometry for application to tissue engineering.* Tissue Engineering, 2002. **8**(6): p. 1089-1098.
15. Kipphan, H., *Handbook of print media: technologies and production methods*. 2001: Springer Science & Business Media.
16. Gilleo, K., *Rheology and surface chemistry for screen printing.* Screen Print Magaz, 1989: p. 128-132.
17. Hobby, A., *Screen-Printing for the Industrial User*. 1997, DEK Printing Machines Ltd.
18. Pan, J., G.L. Tonkay, and A. Quintero, *Screen printing process design of experiments for fine line printing of thick film ceramic substrates.* Journal of Electronics Manufacturing, 1999. **9**(3): p. 203.
19. Soukup, R., A. Hamacek, and J. Reboun. *Organic based sensors: Novel screen printing technique for sensing layers deposition*. in *Electronics Technology (ISSE), 2012 35th International Spring Seminar on*. 2012.
20. Wei, Y., R. Torah, K. Yang, S. Beeby, and J. Tudor, *Screen printing of a capacitive cantilever-based motion sensor on fabric using a novel sacrificial layer process for smart fabric applications.* Measurement Science and Technology, 2013. **24**(7): p. 075104.

21. Wei, Y., R. Torah, K. Yang, S. Beeby, and J. Tudor, *A screen printable sacrificial fabrication process to realise a cantilever on fabric using a piezoelectric layer to detect motion for wearable applications.* Sensors and Actuators A: Physical, 2013. **203**: p. 241-248.
22. Yang, K., R. Torah, S. Beeby, and J. Tudor, *Flexible and washable conductive textile achieved by screen printing for smart fabric applications.* 2013.
23. Numakura, D. *Advanced Screen Printing "Practical Approaches for Printable & Flexible Electronics"*. in *Microsystems, Packaging, Assembly & Circuits Technology Conference, 2008. IMPACT 2008. 3rd International*. 2008.
24. Soukup, R., A. Hamacek, and J. Reboun. *Advanced screen printing for the fabrication of organic humidity sensors*. in *Electronic System-Integration Technology Conference (ESTC), 2012 4th*. 2012.
25. Wargo, C., *Characterization of Conductors for Printed Electronics.* NanoPChem.
26. Ujiie, H. *State of Art of Inkjet Textile Printing: Status Report 2012*. in *NIP & Digital Fabrication Conference*. 2012. Society for Imaging Science and Technology.
27. Cummins, G. and M.P. Desmulliez, *Inkjet printing of conductive materials: a review.* Circuit World, 2012. **38**(4): p. 193-213.
28. Angelo, P.D., *Inkjet-printed light-emitting devices: applying inkjet microfabrication to multilayer electronics*. 2013, University of Toronto.
29. Crump, S.S., *Modeling apparatus for three-dimensional objects*. 1994, Google Patents.
30. Robotics, S. *Fab@Home Model 3 Research Platform*. 2014 Date Accessed: 03 March 2015; Available from: http://www.seraphrobotics.com/FAH3_specs_quote.pdf.
31. Intertronics. *Preeflow Eco-Pen*. Date Accessed: 29 Sep 2016; Available from: http://www.intertronics.co.uk/products/preeflow_precision_dispensing.htm.
32. EFD, N. *Ultimus V Brochucre*. Date Accessed: 29 April 2014; Available from: http://www.nordson.com/en-us/divisions/efd/Literature/Brochures-Data-Sheets/Dispensers/Air-powered/Nordson-EFD-Ultimus-Brochure.pdf.
33. EnvisionTEC. *3D-Bioplotter*. Date Accessed: 29 Sep 2016; Available from: http://envisiontec.com/3d-printers/3d-bioplotter/.
34. Wright, P.K., D.A. Dornfeld, A. Chen, C.C. Ho, and J.W. Evans, *Dispenser printing for prototyping microscale devices.* Trans. of NAMRI/SME, 2010. **38**: p. 555-561.
35. Ho, C.C., J.W. Evans, and P.K. Wright, *Direct write dispenser printing of a zinc microbattery with an ionic liquid gel electrolyte.* Journal of Micromechanics and Microengineering, 2010. **20**(10): p. 104009.
36. Raja, S., *The systematic development of Direct Write (DW) technology for the fabrication of printed antennas for the aerospace and defence industry*. 2014, © Sandeep Raja.
37. Chen, A., D. Madan, P. Wright, and J. Evans, *Dispenser-printed planar thick-film thermoelectric energy generators.* Journal of Micromechanics and Microengineering, 2011. **21**(10): p. 104006.
38. King, C.N., *Electroluminescent displays.* Journal of Vacuum Science & Technology A, 1996. **14**(3): p. 1729-1735.
39. Theodore, J.J., *Electroluminescent device*. 1960, Google Patents.
40. Institute, M.A. *All the Time in the World, London Heathrow*. Date Accessed: 8 May 2014; Available from: http://mediaarchitecture.org/all-the-time-in-the-world-london-heathrow/.
41. Systems, P. *Example EL Displays*. Date Accessed: 8 May 2014; Available from: http://thefutureofthings.com/3212-new-transparent-electroluminescent-displays/.
42. Ono, Y.A., *Electroluminescent displays*. Vol. 1. 1995: World Scientific.
43. Phosphors, G.T. *Electroluminescent Phosphor - Technical Information Bulltetin*. Date Accessed: 25 April 2014; Available from: http://www.globaltungsten.com/en/products-services_phosphor.htm.

44. Arlt, G. and D. Hennings, *Dielectric properties of fine-grained barium titanate ceramics.* Journal of Applied Physics, 1985. **58**(4): p. 1619-1625.
45. Dang, Z.-M., L. Wang, H.-Y. Wang, C.-W. Nan, D. Xie, Y. Yin, and S.C. Tjong, *Rescaled temperature dependence of dielectric behavior of ferroelectric polymer composites.* Applied Physics Letters, 2005. **86**(17): p. -.
46. Materials, D.M. *Material for Printed Electronics - Technical Information*. Date Accessed: 25 April 2014; Available from: http://www2.dupont.com/MCM/en_US/tech_info/products/printed_electronics.html.
47. Szepesi, Z., W. Lehmann, and D. Leksell, *Preparation and characteristics of white EL display panels.* Journal of Electronic Materials, 1978. **7**(4): p. 515-524.
48. Ahn, B.Y., D.J. Lorang, and J.A. Lewis, *Transparent conductive grids via direct writing of silver nanoparticle inks.* Nanoscale, 2011. **3**(7): p. 2700-2702.
49. Wang, X., L. Zhi, and K. Müllen, *Transparent, conductive graphene electrodes for dye-sensitized solar cells.* Nano letters, 2008. **8**(1): p. 323-327.
50. Heikenfeld, J. and A. Steckl, *Low-Cost Display Technology Utilizing Thick Dielectric Electroluminescent (TDEL) Devices on Glass Substrates.* 2001.
51. Bharathan, J. and Y. Yang, *Polymer electroluminescent devices processed by inkjet printing: I. Polymer light-emitting logo.* Applied Physics Letters, 1998. **72**(21): p. 2660-2662.
52. Gaver, W., J. Bowers, A. Boucher, A. Law, S. Pennington, and N. Villar. *The history tablecloth: illuminating domestic activity*. in *Proceedings of the 6th conference on Designing Interactive systems*. 2006. ACM.
53. Park, S.M., K.S. Cho, and K.H. Chung, *Electroluminescent fabric embedding illuminated fabric display*. 2013, Google Patents.
54. Yang, K., R. Torah, Y. Wei, S. Beeby, and J. Tudor, *Waterproof and durable screen printed silver conductive tracks on textiles.* Textile Research Journal, 2013. **83**(19): p. 2023-2031.
55. Rabe, M., E. Lempa, and C.M. Steinem, *Electroluminescent textile and method for the production thereof*. 2012, Google Patents.
56. Wood, V., M.J. Panzer, J. Chen, M.S. Bradley, J.E. Halpert, M.G. Bawendi, and V. Bulović, *Inkjet-Printed Quantum Dot–Polymer Composites for Full-Color AC-Driven Displays.* Advanced Materials, 2009. **21**(21): p. 2151-2155.
57. SigmaKoki. *SGSP26-50 Motorised Stage Web Catalogue*. Date Accessed: 29 April 2014; Available from: http://www.products-sigmakoki.com/en/catalog/gno.aspx?pnoname=SGSP26-(XY)&ccode=W9015&dcode=&gnoname=SGSP26-50(XY).
58. Technology, A. *Arcus NEMA 23 Motor Data Sheet*. Date Accessed: 23 February 2015; Available from: http://www.arcus-technology.com/products/stepper-motors/nema-23/.
59. Engineering, M. *Musashi ML-808 FX COM-CE Datasheet*. Date Accessed: 23 February 2015; Available from: http://www.musashi-engineering.co.jp.e.cn.hp.transer.com/products/099_3-1-1-12.html.
60. Ho, C.C., *Dispenser Printed Zinc Microbattery with an Ionic Liquid Gel Electrolyte*. 2011, University of California, Berkeley.
61. de Vos, M., R. Torah, S. Beeby, and J. Tudor. *Functional Electronic Screen-printing – Electroluminescent Lamps on Fabric*. in *Eurosensors*. 2014.
62. *M-DVRT - Microminiature Displacement Sensor Datasheet*. Date Accessed: 17 March 2015; Available from: http://files.microstrain.com/M-DVRT-Microminiature-Data-Sheet.pdf.
63. *Tech Note - Precise Non-Contact Displacement Sensors*. Date Accessed: 17 March 2015; Available from: http://www.micro-epsilon.com/download/products/T001--en--precise-non-contact-sensors.pdf.

64. *optoNCDT - Laser Triangulation Displacement Sensors Catalogue*. Date Accessed: 17 March 2015; Available from: http://www.micro-epsilon.com/download/products/cat--optoNCDT--en.pdf.
65. *LK-G10 Laser Displacement Sensor Datasheet*. Date Accessed: 17 March 2015; Available from: http://www.keyence.co.uk/products/measure/laser-1d/lk-g3000/models/lk-g10/index.jsp.
66. *LK-G32 Laser Displacement Sensor Datasheet*. Date Accessed: 17 March 2015; Available from: http://www.keyence.co.uk/products/measure/laser-1d/lk-g3000/models/lk-g32/index.jsp.
67. Danzl, R., F. Helmli, and S. Scherer. *Focus variation–a new technology for high resolution optical 3D surface metrology*. in *Proceedings of the 10th international conference of the Slovenian society for non-destructive testing*. 2009.
68. Ranellucci, A., *Slic3r*. 2014.
69. Ding, D., Z. Pan, D. Cuiuri, and H. Li, *A tool-path generation strategy for wire and arc additive manufacturing.* The International Journal of Advanced Manufacturing Technology, 2014. **73**(1): p. 173-183.
70. Hayasi, M.T. and B. Asiabanpour, *Machine path generation using direct slicing from design-by-feature solid model for rapid prototyping.* The International Journal of Advanced Manufacturing Technology, 2009. **45**(1): p. 170-180.
71. Jin, G., W. Li, C. Tsai, and L. Wang, *Adaptive tool-path generation of rapid prototyping for complex product models.* Journal of manufacturing systems, 2011. **30**(3): p. 154-164.
72. *Smart Fabric Inks Ltd*. Date Accessed: 1 Feb 2016; Available from: http://www.fabinks.com/.
73. Katco. *Kapton Polyimide Film*. Date Accessed: 2 February 2016; Available from: http://www.katco.eu/uk/site__1344/.
74. Technologies, M. *Technical Datasheet - Valmex*. 2014 Date Accessed: 17 March 2015; Available from: http://www.mehler-texnologies.com/de/produktuebersicht/Brochueren/VALMEX_facade_2014-08.pdf.
75. Berger. *Technical Datasheet - Back-Lighttex Fr + w*. 2013 Date Accessed: 17 March 2015; Available from: http://www.seri-deco.fi/images/Materiaalien%20tekniset%20tiedot_kortit/Berger%20Lighttex%20FR%20w.pdf.
76. *Gwent Group - Electroluminescent Material Overview*. Date Accessed: 21 May 2014; Available from: http://www.gwent.org/gem_data_sheets/polymer_systems_products/electroluminescent_display_materials/electroluminescent_brochure.pdf.
77. *DuPont LuxPrint 8155 Phosphor Vehicle*. Date Accessed: 1 Feb 2016; Available from: http://www2.dupont.com/MCM/en_US/assets/downloads/prodinfo/8155.pdf.
78. *Processing Guide for DuPont Luxprint EL Inks*. Date Accessed: 22 May 2014; Available from: http://www.dupont.com/content/dam/assets/products-and-services/electronic-electrical-materials/assets/datasheets/prodlib/EL_Processing_Guide.pdf.
79. Inc., S. *Electroluminescent (EL) Backlight Driver ICs*. Date Accessed; Available from: http://www.supertex.com/pdf/misc/el_driver_ics_SG.pdf.
80. de Vos, M., R. Torah, and J. Tudor, *Dispenser Printed Electroluminescent Lamps on Textiles for Smart Fabric Applications.* Smart Materials and Structures 2015.
81. Wang, J., C. Yan, K.J. Chee, and P.S. Lee, *Highly Stretchable and Self-Deformable Alternating Current Electroluminescent Devices.* Advanced Materials, 2015. **27**(18): p. 2876-2882.
82. Jayaraj, M. and C. Vallabhan, *A study of the white electroluminescence in ZnS: Cu, Pr, Cl phosphors.* Journal of Physics D: Applied Physics, 1989. **22**(9): p. 1380.
83. (Durel), R.C., *DUREL Backlight IC Driver Product Selector Guide*.

84. Micrel. *Micrel EL Drivers Summary*. Date Accessed: 23 April 2014; Available from: http://www.micrel.com/index.php/products/power-management-ics/lighting-displays/el-drivers.html.
85. Electronics, E. *EL Drivers Summary*. Date Accessed: 23 April 2014; Available from: http://www.enz.ch/pages/en/el-drivers.php.
86. Corporation, J.C. *EL Inversters Summary*. Date Accessed: 23 April 2014; Available from: http://www.jkllamps.com/inverter/elinverters.

9. Appendix 1 – Summary of EL Drivers

Table 40. *Rogers Corp. (Durel) EL Drivers (data from [83])*

Model	Supply Voltage (V_{DC})	Output Voltage (V_{pk-pk})	Lamp Frequency (Hz)	Max Lamp Area (cm^2)	External Components	Comments
D307A	4.5 – 5.5	350 - 400	330 - 430	180	10 - 12	
D355B	1.0 – 7.0	110 – 220	230 – 390	40	1 – 2	Enabled by input low
D356B	1.0 – 7.0	110 – 220	230 – 390	40	1 – 2	Enabled by input high
D371A	2.0 – 6.5	160 – 220	190 – 330	65	1 – 4	
D372A	2.0 – 6.5	160 – 220	236 – 330	80	3 – 5	
D381B	2.0 – 7.0	150 – 220	230 – 310	80	1 – 4	
D391A	2.0 – 7.0	170 – 220	280 – 350	80	1 – 4	
D504B (20 lead QFN)	2.1 – 7.0	170 – 220	280 – 350	4 x 20	2 – 6	Controls 4 lamps using I^2C

Table 41. *Micrel EL Drivers (data from [84])*

Model	Supply Voltage (V_{DC})	Output Voltage (V_{pp})	Lamp Frequency (Hz)	Max Lamp Area (cm^2)	External Components	Comments
MIC4826	1.8 – 5.5	160	60 - 1000	19	6	
MIC4827	1.8 – 5.5	180	60 – 1000	19	6	
MIC4830	1.8 – 5.5	180	60 – 1000	25	6	
MIC4832	1.8 – 5.5	220	60 – 1000	19	6	Low noise chip.
MIC4833	2.3 – 5.8	220	100 – 1500	2 x 25	8	Drives two EL panels.
MIC4834	2.3 – 5.8	220	100 – 1500	2 x 19	6	Drives two EL panels.

Table 42. *Supertex EL Drivers (data from [79])*

Model	Supply Voltage (V_{DC})	Output Voltage (V_{pp})	Lamp Frequency (Hz)	Max Lamp Area (cm^2)	External Components	Comments
HV816	2.7 – 5.5	360	100-1000	270	14	External MOSFET for boost converter
HV823	2 – 9.5	180	330-450	150	6	
HV825	1 – 1.6	112	400-2000	20	7	No output regulation
HV830	2 – 9.5	200	220 - 280	160	7	
HV833	1.8 – 6.5	180	240 - 300	80	6	
HV857	1.8 – 5.0	190	200 – 1000	32.25	5	
HV859	1.8 – 5.0	210	200 - 1000	32.25	8	
HV860 (12 lead QFN)	2.5 – 4.5	220	150 - 500	32.25	8	
HV858	1.73 – 6.58	190	200 - 1000	3 x 6.45	5	Drives 3 EL panels using logic inputs
HV881 (32 lead QFN)	1.8 – 5.5	145 – 195	200 – 1000	16 x 1.94	11	Drives 16 EL Panels using I^2C

Table 43. *ENZ EL Drivers (data from [85])*

Model	Supply Voltage (V_{DC})	Output Voltage (V_{pp})	Lamp Frequency (Hz)	Max Lamp Area (cm^2)	External Components	Comments
E040 Range	6 – 24	120 - 360	400 – 1000	200	0	Driver in complete package 2.5 x 2 x 1 cm
2040 (500) Range	6 – 24	100 – 320	400 – 1000	500	0	Driver in complete package 10 x 3 x 4 cm
2040 (1000) Range	12 – 24	100 – 320	400 – 1000	1,000	0	Driver in complete package 15 x 21 x 5 cm
E250	110 – 240 VAC	40 – 400	300 – 750	10,000	0	Driver in complete package 2.5 x 2 x 1 cm

Table 44. *JKL Lamp EL Drivers (data from [86])*

Model	Supply Voltage (V_{DC})	Output Voltage (V_{pp})	Lamp Frequency (Hz)	Max Lamp Area (cm^2)	External Components	Comments
NDL-102	3 – 5.5	220 – 340	500 – 600	30	0	Driver in complete package 2.2 x 2.1 x 1.4 cm
NDL-104	3 – 5.5	220 – 340	500 – 600	40	0	Driver in complete package 2.2 x 2.1 x 1.4 cm
NDL-106	3 – 5.5	220 – 340	500 – 600	80	0	Driver in complete package 2.2 x 2.1 x 1.4 cm
NDL-206	3 – 5.5	220 – 340	500 – 600	100	0	Driver in complete package 2.4 x 2.4 x 1.9 cm
NDL-208	3 – 5.5	220 – 340	500 – 600	140	0	Driver in complete package 2.4 x 2.4 x 1.9 cm
NDL-217	3 – 5.5	220 – 340	500 – 600	170	0	Driver in complete package 2.4 x 2.4 x 1.9 cm